INFORMATION TO USERS

This manuscript has been reproduced from the microfilm master. UMI films the text directly from the original or copy submitted. Thus, some thesis and dissertation copies are in typewriter face, while others may be from any type of computer printer.

The quality of this reproduction is dependent upon the quality of the copy submitted. Broken or indistinct print, colored or poor quality illustrations and photographs, print bleedthrough, substandard margins, and improper alignment can adversely affect reproduction.

In the unlikely event that the author did not send UMI a complete manuscript and there are missing pages, these will be noted. Also, if unauthorized copyright material had to be removed, a note will indicate the deletion.

Oversize materials (e.g., maps, drawings, charts) are reproduced by sectioning the original, beginning at the upper left-hand corner and continuing from left to right in equal sections with small overlaps.

ProQuest Information and Learning
300 North Zeeb Road, Ann Arbor, MI 48106-1346 USA
800-521-0600

CONFORMAL OPTICAL DESIGN

by

David James Knapp

A Dissertation Submitted to the Faculty of the

COMMITTEE ON OPTICAL SCIENCES (GRADUATE)

In Partial Fulfillment of the Requirements
For the Degree of

DOCTOR OF PHILOSOPHY

In the Graduate College

THE UNIVERSITY OF ARIZONA

2002

UMI Number: 3073240

ProQuest Information and Learning Company
300 North Zeeb Road
P.O. Box 1346
Ann Arbor, MI 48106-1346

THE UNIVERSITY OF ARIZONA ®
GRADUATE COLLEGE

As members of the Final Examination Committee, we certify that we have read the dissertation prepared by David James Knapp

entitled Conformal Optical Design

and recommend that it be accepted as fulfilling the dissertation requirement for the Degree of Doctor of Philosophy

Jose Sasian	Date 12/09/02
John Greivenkamp	Date 12/09/02
James P. Mills	Date 12/09/02
	Date
	Date

Final approval and acceptance of this dissertation is contingent upon the candidate's submission of the final copy of the dissertation to the Graduate College.

I hereby certify that I have read this dissertation prepared under my direction and recommend that it be accepted as fulfilling the dissertation requirement.

Dissertation Director, Jose Sasian — Date 12/14/02

STATEMENT BY AUTHOR

This dissertation has been submitted in partial fulfillment of requirements for an advanced degree at The University of Arizona and is deposited in the University Library to be made available to borrowers under rules of the Library.

Brief quotations from this dissertation are allowable without special permission, provided that accurate acknowledgment of source is made. Requests for permission for extended quotation from or reproduction of this manuscript in whole or in part may be granted by the copyright holder.

SIGNED: 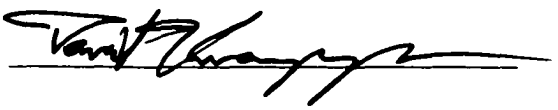

ACKNOWLEDGEMENTS

I would like to thank Major Andy Keipert for being a mentor to me while I was in high school. His excitement about optical technology was contagious.

I would like to acknowledge my employer, Raytheon Missile Systems, whose support of higher education has made this effort possible.

Many current and former coworkers have provided insight, support, or good jokes along the way: Rick Juergens, Paul Manhart, Scott Sparrold, Joel Williams, Rich Pfisterer, Holden Chase, Elka Koehler, Scott Ellis, David Markason, John Tesar, Tom Mitchell, Tony Lin, Kevin O'Shea, and Craig Shott. Special thanks go to Jim Mills for his guidance and encouragement during my exploration of conformal optics technology.

My wife, parents, and in-laws have given me a great amount of love and support throughout this process. It is an undeserved blessing to be related to them.

I would like to thank my advisor Jose Sasian for his feedback and advice.

DEDICATION

This dissertation is dedicated to my wife, Jessica

and my parents, Jim and Alice.

Table of Contents

TABLE OF FIGURES **8**
ABSTRACT **11**
CHAPTER 1- Introduction **13**
Introduction 13
Scope of Dissertation 15
History of Conformal Optics 16
Conformal Optics in the Literature **38**
Prior Art Summary **40**
Conventional Windows and Domes **41**
Conformal Shapes **42**
Aerodynamic Benefit of Conformal Shapes 42
Benefit of Increased Field of Regard 44
Increased Aberrations of Conformal Optics 45
Aberrations of Conformal Surfaces 46
Initial Design Considerations 48
Resources for Conformal Optical Design 54
Solution Forms **55**
ARTICULATING ELEMENTS 55
The Arch 55
Counter-rotating Phase Plates 57
Aberration Generators 63
FIXED CORRECTOR ELEMENTS 64
OTHER TYPES OF CORRECTION 65
Deformable Mirror 65
Requirements for Deformable Mirror Correction 68
Software Correction 69
Surface Types **70**
Design Tools **74**
Optical Design Program 74
Computer Workstation 75
Local and Global Optimization 75
Damped Least Squares 77
Surface Conversion Macros 77
Analysis Tools 78
Direct Solve Tools 78
Summary **86**
CHAPTER 2- Wassermann-Wolf Equations **88**
Introduction 88
Introduction to the Wassermann-Wolf Equations 89
Ingredients of the Wassermann-Wolf Equations **93**
Wassermann-Wolf Equations **97**
Steps in Wassermann-Wolf Solution **99**
Defining Ray Fans 100
Abbe Sine Condition **104**
Finite conjugate case 111
Cardinal Points **113**
Application to the Wassermann-Wolf Equations 118
Aperture Stops and Pupils **121**
Summary **127**

Chapter 3- Generalized Aspheric Design Equations **128**
Introduction 128
Review of the Wassermann-Wolf equations 129
Asymmetric Case 131
Derivation of Generalized Aspheric Design Equations 133
Wassermann-Wolf Equations as a Special Case of the Generalized Equations **150**
Steps in Solving Generalized Asphere Design Equations **152**
Aperture Filling Functions 155
Abbe Sine condition revisited 158
Summary 167
CHAPTER 4- Examples **169**
SINGLET 170
Conventional Design **170**
Differential Design **178**
Conformal Dome 187
Conformal Dome 188
Window with Wedge 191
Conventional Approach **191**
GAP Approach **193**
Cylindrical Windows 196
Mustang Camera 205
Summary 213
CHAPTER 5- Discussion **214**
Accomplishments 215
Problems Areas that Benefit from Generalized Equations 217
Summary 217
CHAPTER 6- Conclusions **218**
Summary 218
Suggestions for Future Work 221
Improving GAP **221**
Exploring Solution Space **222**
Conclusion 223
APPENDIX A- GAP Macro **224**
APPENDIX B- Wassermann-Wolf Macro **232**
REFERENCES **238**

TABLE OF FIGURES

Figure 1. Conformal Optical Surfaces....13
Figure 2. Conformal Patents Timeline....17
Figure 3. Illustration of toric corrector from US Patent #4,291,848....19
Figure 4. Illustration of gradient index dome from US Patent #4,245,890....20
Figure 5. Illustration of holographic corrector from US Patent #4,384,759....21
Figure 6. Illustration of distortion corrector from US Patent #4,840,465....22
Figure 7. Illustration of Piezoelectric corrector from US Patent #5,220,159....23
Figure 8. Illustration of fixed corrector from US Patent #5,368,254....24
Figure 9. Illustration of Dynamic Aberration Corrector from US Patent #5,526,181....25
Figure 10. Illustration of Torus Window from US Patent #5,914,821....26
Figure 11. Illustration of Translating Cylinders from US Patent #5,946,143....27
Figure 12. Illustration of Static and Dynamic Correctors from US Patent #6,018,424....28
Figure 13. Illustration of Arch Corrector from US Patent #6,028,712....29
Figure 14. Illustration of Two Stage Aberration Corrector from US Patent #6,091,548 . 30
Figure 15. Illustration of Dynamic Aberration Generator from US Patent #6,091,548 ... 30
Figure 17. Illustration of Deformable Mirror from US Patent #6,201,230....32
Figure 18. Illustration of Asymmetric Arch from US Patent #6,310,730....33
Figure 19. Illustration of Zernike Corrector from US Patent #6,313,951....34
Figure 20. Illustration of Risley Prisms from US Patent #6,343,767....35
Figure 21. Illustration of Toroidal Arch in X-Z Plane from US Patent #6,356,396....37
Figure 22. Illustration of Toroidal Arch in Y-Z Plane from US Patent #6,356,396....37
Figure 26. Relative Drag of Elliptical Forebody....44
Figure 27. Increased FOR Possible with a Conformal Dome....45
Figure 28. Hemispherical dome limits FOR....45
Figure 31. Significant zernike aberrations of a fineness ratio (F) 1.5 elliptical dome....47
Figure 32. Front end and back end distinction....49
Figure 33. Dome dimensions....50
Figure 34. Dome aberration vs. Index of Refraction....51
Figure 35. Dome thickness vs. aberration....52
Figure 36. Dome aberration vs. Aperture ratio....52
Figure 38. Important Resources in Conformal Optical Design....55
Figure 39. Arch Corrector in X-Z view and Y-Z view....57
Figure 40. Gimbal motions....57
Figure 43. Counter-rotated prisms point to 0 degree look angle....62
Figure 44. Identical prism orientation points to maximum look angle....62
Figure 47. Fixed Corrector....65
Figure 48. Layout of a Conformal System with a Deformable Mirror....67
Figure 49. System at 40° Look Angle....67
Figure 52. Fixed Corrector Example Layout....72
Figure 53. Solution Space....77
Figure 54. Surface conversion is a useful tool in the design process....79
Figure 56. Wavefront Aberration Plot of Wassermann-Wolf System....81
Figure 57. Wassermann-Wolf approach does not work with decentered elements....82

Figure 59. New design equations handle asymmetry 84
Figure 61. Layout of a typical system 90
Figure 62. Object Space Ray Fan 91
Figure 63. Image space ray fan 92
Figure 65. R, R_z and R_y 95
Figure 66. Ray intercept at first aspheric surface 96
Figure 67. Ray intercept at second aspheric surface 97
Figure 68. Rays propagating through the optical system 98
Figure 69. Singlet created with Wassermann-Wolf Equations 101
Figure 70. Beam Expander 102
Figure 74. Plano-conic singlet with coma 105
Figure 75. Double aspheric singlet with no coma 106
Figure 76. Sine condition for an infinite conjugate 107
Figure 77. Plot of height to sine theta ratio 107
Figure 78. Wave aberration plot for singlet with coma 108
Figure 80. Wave fans and spot diagram for singlet with no coma 110
Figure 82. Angle definition for Abbe Sine Condition 113
Figure 83. Front and rear focal points 114
Figure 84. Front and rear principal planes 115
Figure 85. First and second nodal points 116
Figure 86. Principal Planes in Paraxial Approximation 116
Figure 87. Abbe Sine Condition Leads to Curved Principal Surfaces 117
Figure 88. Principal Surfaces for Infinite Conjugate Sine Condition 117
Figure 89. Steps in using Code V macro 121
Figure 90. WW Algorithm works on a centered ray bundle 122
Figure 91. Location of the aperture stop will define pupil locations 123
Figure 92. Oversize on-axis ray fan 124
Figure 93. Corrector designed to make front end afocal 125
Figure 94. +/- 10° field of regard and +/- 4° field of view 125
Figure 97. Planes tangent to the optical axis 130
Figure 98. Ray fan in object space 131
Figure 99. Tangent plane in image space shows desired conjugate ray fan 131
Figure 100. Layout of asymmetric system with desired ray bundle conjugates 132
Figure 101. Ray bundle at object space tangent plane 133
Figure 102. Desired ray bundle at image space tangent plane 133
Figure 103. Layout of system 134
Figure 104. Skew ray intersecting a surface. 135
Figure 105. Snell's law 136
Figure 106. Passage of an oblique ray through two adjacent surfaces 139
Figure 107. Ray trace to first tangent plane 140
Figure 108. Ray refracted at first surface 141
Figure 109. Ray refracted at second surface into rest of optical system 142
Figure 110. Y-Z view of first surface intersection 144
Figure 111. Intersection of a ray with a surface 152
Figure 112. Layout of Asymmetric system 155

Figure 113. Tracing a single fan of rays creates a contour line on the two aspheric surfaces 157
Figure 114. A ray fan in a different slice plane will trace out another contour line on the two aspheric surfaces 157
Figure 115. Examples of aperture filling functions. Rays are launched along the lines. The ideal aperture filling function fills in the aperture such that it is a solid color. I.e. the ray bundle samples the aperture to a very large density. In practice, one has to compromise due to computational limitations on the number of rays that may be traced in a reasonable amount of time. 158
Figure 116. Direction cosines and coordinates at aspheric tangent planes 159
Figure 117. Rays in a plane passing through the axis of symmetry 160
Figure 118. A cylindrical element will add anamorphic power 162
Figure 119. The preferred conjugate bundle in image space may be rotationally symmetric in image space. 162
Figure 120. A slice plane containing a ray and the optical axis 163
Figure 121. A ray contained in the Slice plane. 164
Figure 129. Wavefront Aberration and Spot Diagram of Plano-Conic Singlet 175
Figure 131. Double Aspheric BK-7 Singlet 177
Figure 132. OSC for Aspheric-Aspheric BK7 Singlet 178
Figure 133. Initial Lens Setup 179
Figure 134. N*k steps are calculated, but only N steps are used in the curve fit. 180
Figure 136. Result of Wassermann-Wolf Program used to create a singlet (300 * 3000 sag points calculated for each surface, but 300 points are used in the curve fit) 182
Figure 137. Offense Against the Sine Condition is Substantially Less for New Design. This chart also verifies the operation of the algorithm to prove that the Abbe Sine condition is met. 183
Figure 139. DLS vs. Differential Design Performance 185
Figure 141. Layout of Conformal Dome 189
Figure 142. Layout of Dome after WW Macro 190
Figure 143. Wave Aberration Plot of system created with 100,000 rays 190
Figure 144. Wave Aberration Plot of system created with 10,000 rays 191
Figure 145. System with perfect lens added 191
Figure 148. Adding a tilted plane parallel plate 193
Figure 150. Design Supports Large FOV 195
Figure 151. Before application of the GAP program 197
Figure 153. After application of the GAP program 200
Figure 154. Exit pupil map of wavefront aberration minus power 201
Figure 156. Reduced aperture of 1", a 10° field, and a perfect lens 203
Figure 157. Spot diagram across field 204
Figure 158. Wavefront aberration across field 204
Figure 159. Location on Vehicle 206
Figure 161. X-Y Cross-Section of Layout 209
Figure 162. System after execution of the GAP macro 210
Figure 163. Wave aberration fans and spot diagram 211
Figure 164. F/2 system with 5° full field of view 211
Figure 165. Wave fans and spot diagrams for full bandwidth and full field of view 212

ABSTRACT

Optics with external surfaces that deviate from conventional forms to better satisfy the needs of a host platform are known as conformal optics. These external surfaces generate significant amounts of aberration that may be compensated with additional corrector elements.

This dissertation introduces a new tool for the design of correctors for non-rotationally symmetric optical systems. This is accomplished through the derivation of two new differential equations using an approach similar to that of Wassermann and Wolf. The new aspheric design equations are derived without the assumption of axial symmetry and may be used to precisely control a ray bundle. Solving the new design equations produces the surface profiles of two aspheric optical surfaces which make a non-rotationally symmetric system aplanatic. The aplanatic system may contain tilted and decentered elements, or optical elements without rotational symmetry before and after the two aspheric surfaces. As coma and spherical aberration can be significant in conformal windows, these equations are powerful for producing starting points and developing a design.

To validate the new equations, they were implemented in a Code V® macro called the Generalized Aspheric design Program (GAP). This macro is used in the design of a variety of non-rotationally symmetric optical systems to create a diffraction limited field of view. These include a system with an elliptical dome with a decentered inside surface, a system containing cylindrical elements, and a system with a toroidal conformal window. In all cases, GAP is able to directly generate corrector surfaces. For comparison,

the classical Wassermann-Wolf equations were also implemented in a Code V macro for the design of rotationally symmetric systems.

"No one can possibly achieve any real and lasting success or 'get rich' in business by being a conformist. "
J. Paul Getty (1892 - 1976) US oil man
In "International Herald Tribune," 10 Jan 1961.

CHAPTER 1- Introduction

Introduction

Conformal optical systems are characterized as having external optical surfaces that are optimized for non-optical system requirements. This typically implies blending smoothly with a host platform to achieve an optimum shape.

Conformal optical systems have tremendous potential. When applied to missile design, they hold the promise of greatly enhanced electro-optical missiles that can fly farther and faster with a larger payload. Aircraft can be stealthier and have less drag, which makes them more survivable. The key to this improvement is the use of exterior optical surfaces that conform to the performance needs of the host platform. This might take the form of an ogive missile dome or a window blended with an aircraft mold line. Figure 1 shows several types of conformal surfaces including a missile dome, a canopy, and a window for a sensor.

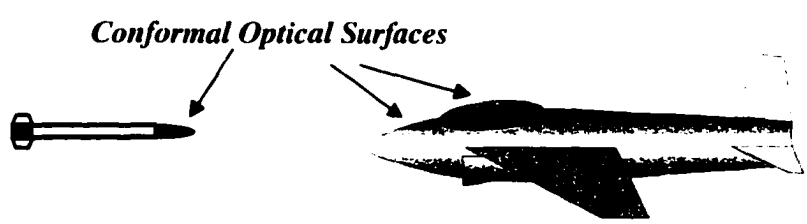

Figure 1. Conformal Optical Surfaces

The improved performance comes with some design challenges. Specifically, conformal optics present difficulties in design, fabrication, and test.

First, the design of conformal optical systems is challenging because conformal windows and domes usually induce large amounts of aberration. This aberration can vary significantly with gimbal look angle in the field of regard* (FOR). In a passive correction approach, the aberration is compensated by utilizing one or more aspheric corrector elements. In an active correction approach, one uses a dynamic aberration generator in the optical system to generate aberrations conjugate to those induced by the conformal window or dome. This approach requires additional mechanisms and control electronics to actuate the dynamic aberration generator.

Second, the fabrication of conformal optical systems is challenging because of the aspheric surfaces found in conformal optical systems. The traditional optical fabrication method of grinding a sphere and polishing in the aspheric departure is usually inappropriate for making conformal optical windows and domes or their corrector optics. Typically, the surfaces must be manufactured to a high degree of precision using techniques such as single point diamond turning[1], chemical vapor deposition with replication[2], deterministic microgrinding[3], and magnetorheological polishing[4].

Third, the testing of conformal optics is challenging because of the inherent difficulty of testing aspheric surfaces. Aspheric surfaces in conformal optical systems typically have large amounts of departure that is out of the dynamic range of a standard

* The field of regard (FOR) is the maximum seeker look angle measured relative to the boresight position.

interferometer[†]. Alternate techniques must be used such as null optics[5], Shack-Hartmann wavefront testing[6], or profilometry[7].

Scope of Dissertation

Success in developing a conformal optical system requires mastery of all three aspects of conformal optics: design, fabrication, and test. This dissertation focuses on the design aspect. It shows that the combination of solution form, surface types, and design tools are an effective means of approaching the design of this class of optical systems. Furthermore, this dissertation presents a new tool for the design of systems that are not rotationally symmetric. In particular, this tool corrects a conformal optical system to remove spherical aberration and satisfy the Abbe Sine Condition to remove coma. The foundation for this tool is a novel set of generalized design equations that are derived using an approach similar to that used in the Wassermann-Wolf equations, but without the assumption of axial symmetry of the optical system. The generalized design equations allow one to control a ray bundle very precisely by defining the surfaces of a corrector element. The corrector element refracts an incident bundle of rays into a desired distribution. The solution from the equations can be used as-is, or be used as a starting point for further interactive design. Examples are shown of applying the equations to various problems including a conformal window, and a prism. The new tool yields a direct means of determining effective design variables and creating a finite field of view that is aberration free.

[†] The deviation of a corrector shape from a base sphere can often be on the order of inches rather than waves.

History of Conformal Optics

One could argue that all optical systems up to the present have been conformal in some fashion. Indeed, the success of an optical system can be measured by how well it conforms to a set of design constraints. A pair of binoculars cannot be arbitrarily heavy, or cost more than the buyer is willing to pay. A consumer camera must take acceptable pictures and use a standard film size. In the present usage, "conformal optics" has come to mean that the optical system incorporates a window or dome that departs significantly from sphericity in order to better conform to the needs of the host platform. As a result, better overall system performance is obtained than would ordinarily be possible using conventional windows or domes.

Conformal optical systems are well suited for military applications. This is due to the fact that the most stressing operational requirements tend to be for military purposes. Many missiles and fighter jets must fly at several times the speed of sound while retaining excellent aerodynamic performance. Even minor improvements in drag can significantly increase system effectiveness and survivability. Due to the utility of conformal optics for military systems, much of the early work in conformal optics is not well documented in the open literature. Perhaps the best source of historical information is found in the patent literature. The following is a review of the patents relating to conformal optics.

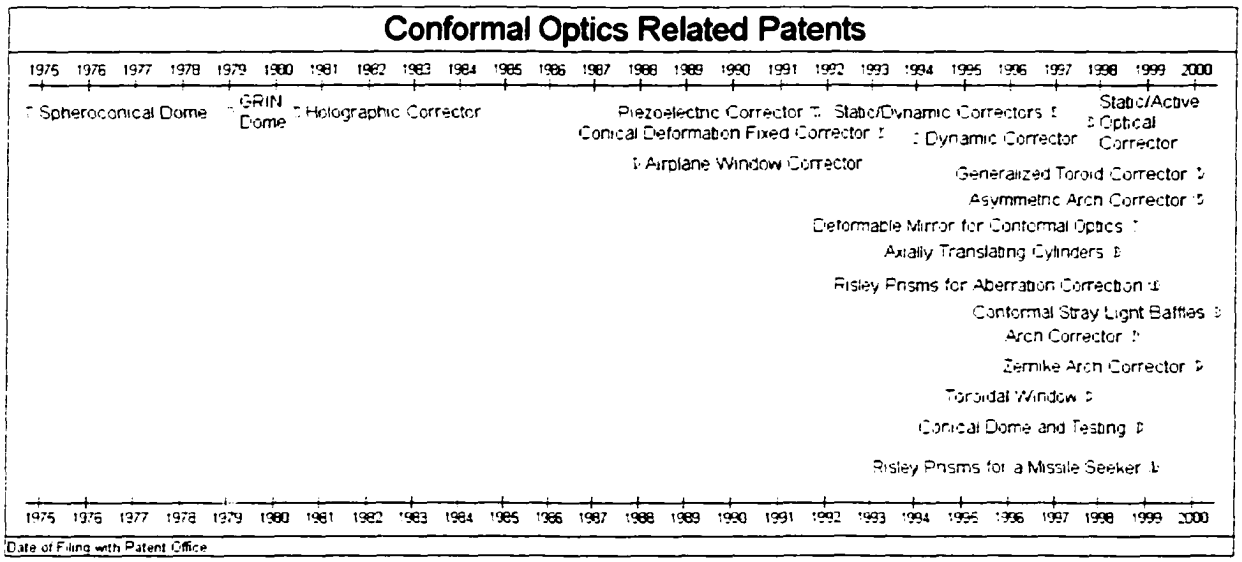

Figure 2. Conformal Patents Timeline

The timeline in Figure 2 shows the progression of conformal optics related patents with respect to the date that they were filed. Each of these inventions will be discussed in greater detail. The dates of submission range from the mid 1970s to the present. The period of most sustained interest in conformal optics technology is in the late 1990s time frame, which corresponds to the duration of the Precision Conformal Optics Technology Program.[8] The patents describe a range of solution forms for conformal optical systems. These include methods of increasing the FOR of a missile seeker by using a spheroconical dome, an aerodynamically improved window shape in the shape of a section of a torus, articulating lens elements for correction, and various forms of optical correctors. Also included is a method for testing a conformal dome, a method for using a deformable mirror, and a baffle for blocking stray radiation.

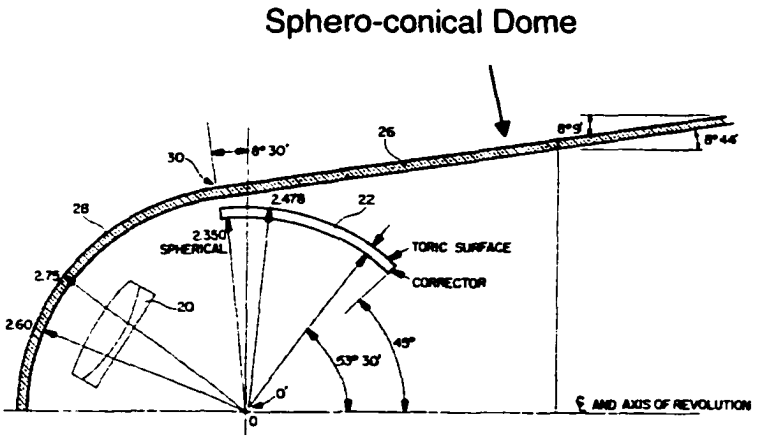

Figure 3. Illustration of toric corrector from US Patent #4,291,848

The earliest example from the US Patent Office of a conformal dome for an electro-optical (EO) guided missile is found in US Patent #4,291,848, filed on September 13, 1974 by Keith Clark. The dome in this document is a sphero-conical missile dome with a capability to extend the FOR out to 135° using two spherical-toric corrector lenses. The spherical-toric lenses are positioned such that the seeker objective looks through them when viewing the conical portion of the missile dome. This patent is significant in that it shows how one may obtain an increase in the FOR by using a non-hemispherical dome. This early invention also shows how corrective optics may be used to maintain image quality when looking through portions of the dome that break from spherical symmetry. A drawback to this implementation is that the imaging discontinuity between the toric corrector/conical portion of the dome and the hemispherical portion of the dome can create double images when the seeker is looking through both portions of the dome simultaneously and a corresponding loss of resolution.

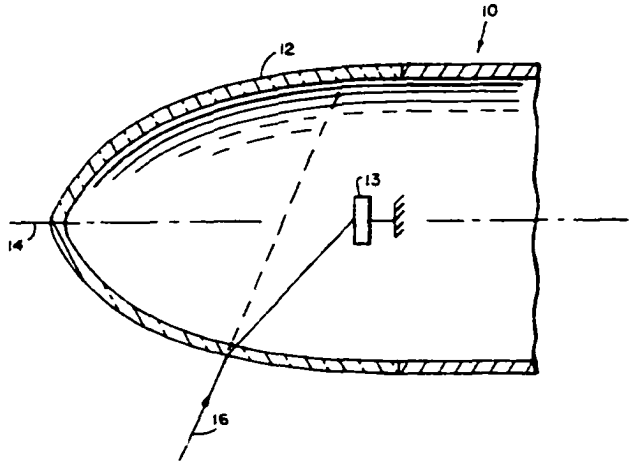

Figure 4. Illustration of gradient index dome from US Patent #4,245,890

The next example of a conformal dome is in US Patent #4,245,890 filed on January 2, 1979. An illustration from this patent is shown in Figure 4. In the patent, Hartman and Guenther describe an ogive dome made from a gradient index (GRIN) glass to make it optically equivalent to a spherical dome. The level of correction attained by this technique is claimed to be sufficient for a non-imaging semi-active laser (SAL) seeker type of optical system. In a SAL, one conventionally uses a quad-cell detector to detect the centroid of the energy focused by the optical system. As the spot size does not need to be minimized, the permissible magnitude of aberrations is much higher than in an imaging seeker. In practice, limited material choices and manufacturing technology make this design not as attractive as other designs which utilize additional optics behind the dome to achieve correction.

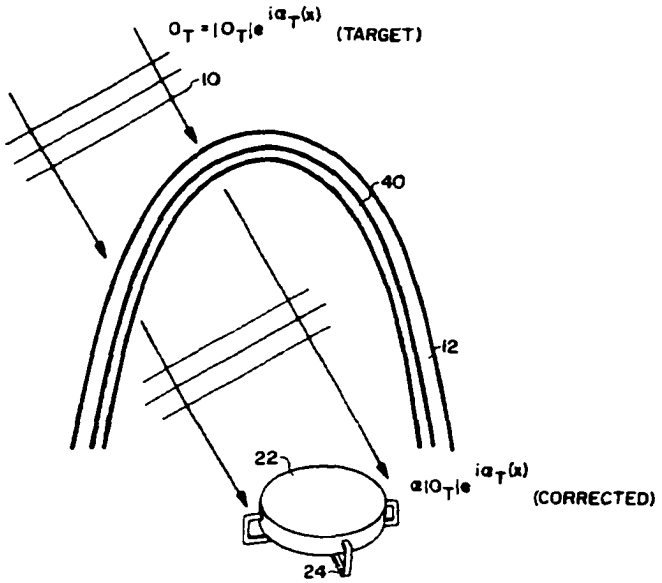

Figure 5. Illustration of holographic corrector from US Patent #4,384,759

In US Patent #4,384,759 filed on June 3, 1980, Ferrante shows how a holographic corrector may be constructed such that the combination of the hologram and conformal dome produces a corrected wavefront. In the illustration from the patent shown above, an incident wavefront (10) is transmitted through the dome (12) where it is corrected by the holographic corrector (40). This invention appears to be limited in spectral bandwidth due to the chromatic variation of the hologram. Additionally, the various orders of the hologram can contribute to increased background signal at the detector.

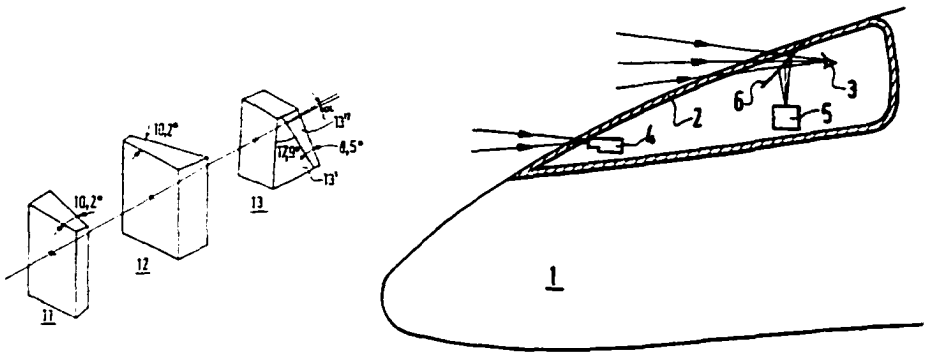

Figure 6. Illustration of distortion corrector from US Patent #4,840,465

In US Patent #4,840,465 filed on November 19, 1987, Loy, Perrin et al. describe the use of a set of distortion compensating elements to make the views identical through two different parts of an aircraft window (2). This is achieved through the use of three prisms (11,12,13) which are shown in the figure above. This invention is important in that it describes a means of correcting aberrations arising from a non-axisymmetric window. The drawback of this approach is that it requires three separate prisms to achieve a limited amount of correction.

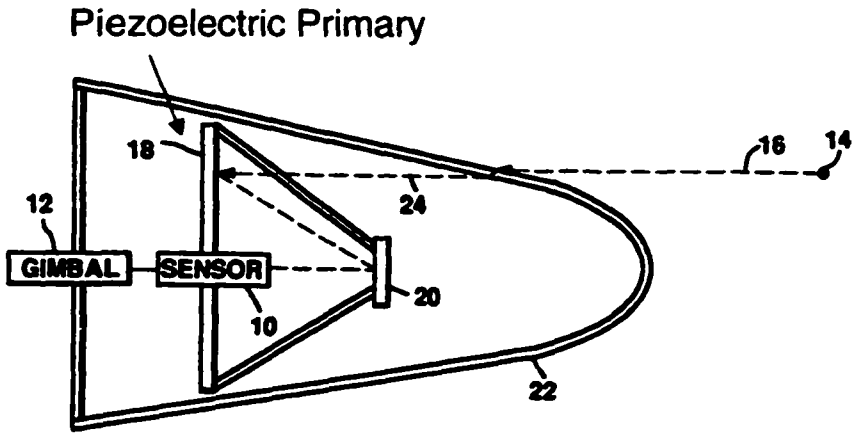

Figure 7. Illustration of Piezoelectric corrector from US Patent #5,220,159

In US Patent #5,220,159 filed on September 23, 1991, Friedenthal introduces the concept of a deformable mirror as a primary mirror in an optical system to dynamically correct conformal dome aberrations. Friedenthal describes using a piezo-electric reflector that is actuated by high voltages to deform at the different azimuthal positions of the sensor. This invention is particularly noteworthy in that it introduces the concept of correcting aberrations through actively changing the optical system in response to the viewing angle through the dome. In comparison to a passive approach, this method of correction requires a source of power and electronics to drive the mirror. This patent introduces the concept of contouring the inside surface of the conformal optical element to decrease the aberrations that the rest of the system must correct. In many conformal optical systems, the inside surface of the window or dome is an important design variable.

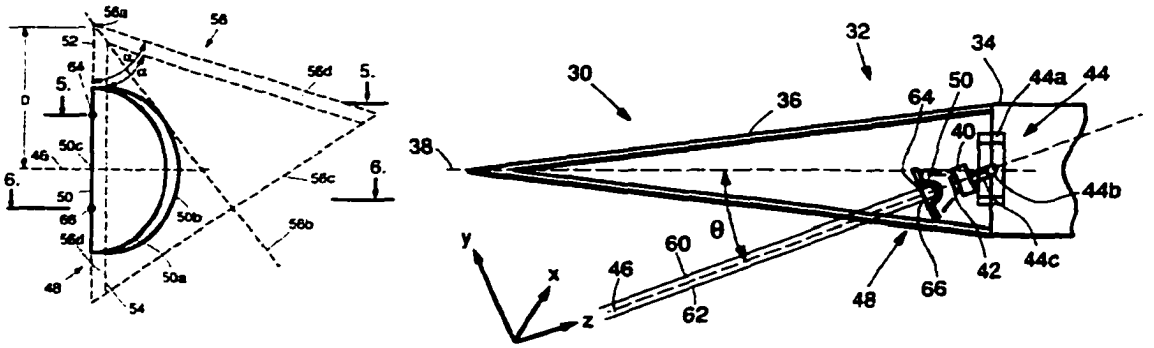

Figure 8. Illustration of fixed corrector from US Patent #5,368,254

In US Patent #5,368,254 filed on March 16, 1993, Wickholm shows a means of correcting conical and ogival domes using a fixed corrector to reverse the conical deformation. This is shown in Figure 8. The corrector (50) is mounted to the camera (40) and moves with the camera on the gimbal. The corrector compensates for aberration at a particular look angle through the dome. Performance falls off as the camera points at other look angles. This invention is limited in that the system does not have very good performance when pointing at low look angles through the dome. Furthermore, there is a limit on system performance as the aberration induced by the fixed corrector is constant with respect to look angle and cannot correct the varying aberrations of looking through different portions of the dome.

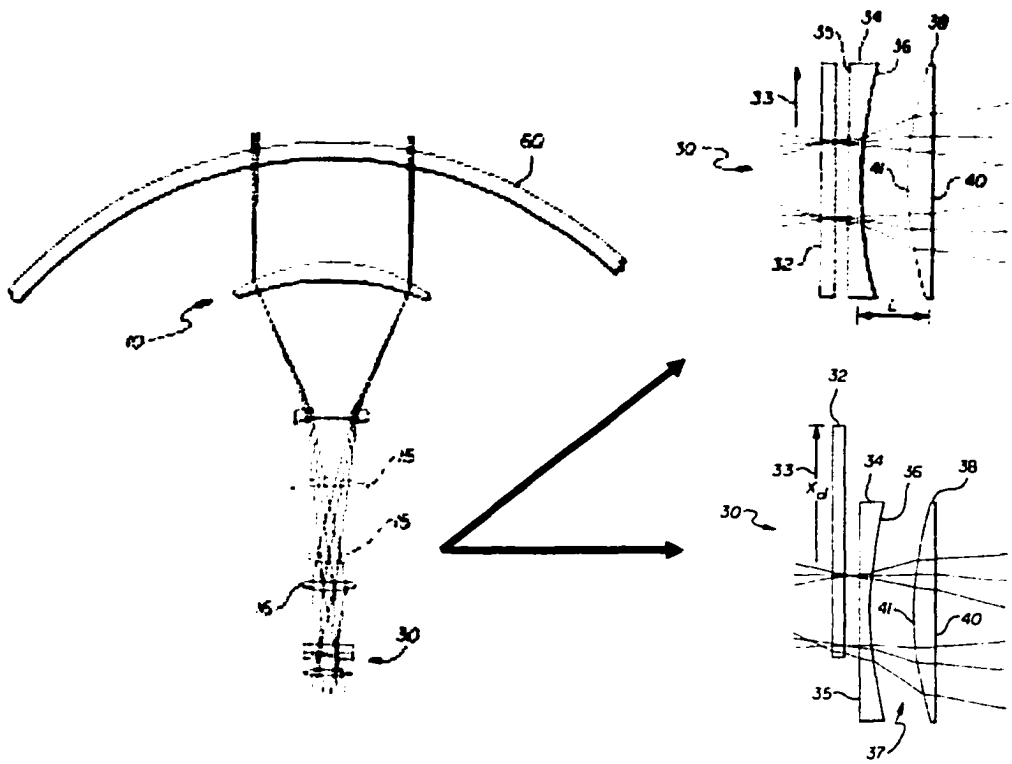

Figure 9. Illustration of Dynamic Aberration Corrector from US Patent #5,526,181

In US Patent #5,526,181 filed on December 22, 1993, Kunick, Chen et al., teach the use of a dynamic aberration corrector consisting of a non-axisymmetric corrector plate and cylindrical lenses to correct the aberrations from a conformal window. The corrector plate (33) is decentered to induce coma. The cylindrical lenses are of equal and opposite powers. Astigmatism is induced by varying the spacing and/or rotation of the cylindrical lenses. The active aberration generator comprised of the cylinders and corrector plate can be used in an optical train to compensate aberrations induced by a conformal window (60). This patent is significant in that it introduces the concept of

rotating, decentering, and translating elements to compensate the aberrations from the conformal window. Like all active correction methods, this invention requires the use of control electronics to dynamically change the positioning of the elements with a change in look angle. This can add cost and complexity to the optical system.

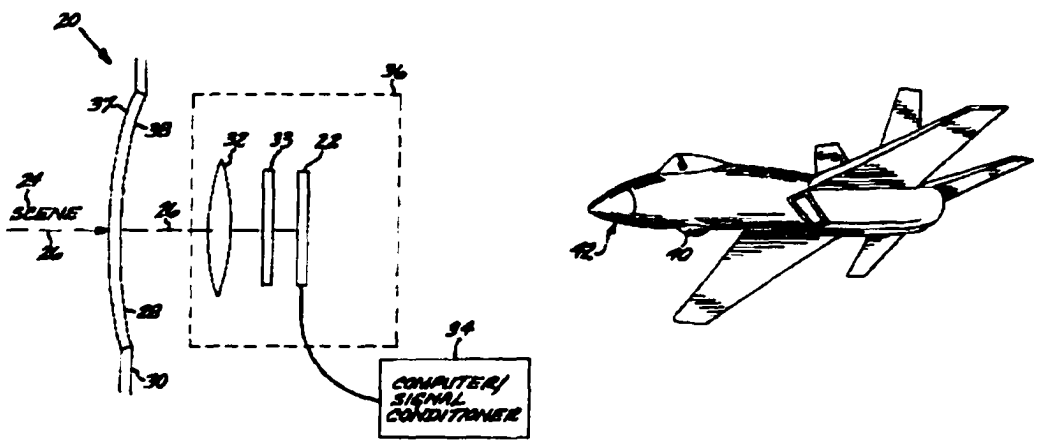

Figure 10. Illustration of Torus Window from US Patent #5,914,821

In US Patent #5,914,821 filed on October 6, 1997, Chen, Hart et al. show how a toroid can be used as a shape for a conformal window. The toroid is described as being beneficial in terms of aerodynamics and reduced aberrations compared to other conformal shapes. The window (37) is shown in the figure above in front of the imaging system (36) and also shown mounted on an airplane (40). No method of correction is provided in this patent.

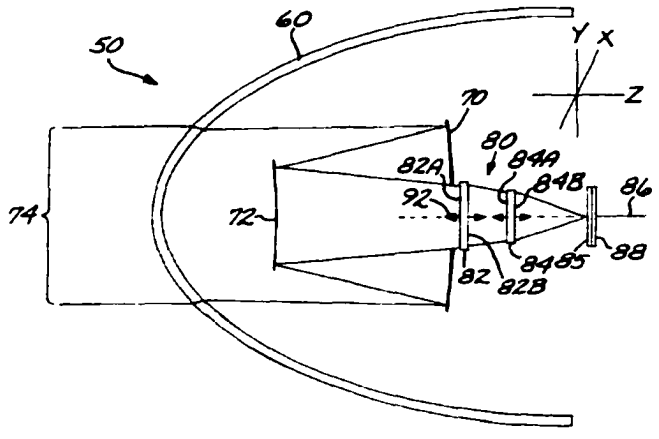

Figure 11. Illustration of Translating Cylinders from US Patent #5,946,143

In US Patent #5,946,143 filed on May 5, 1998, Whalen shows how one may generate astigmatism using an axially translating cylinder approach. This forms the basis of a dynamic corrector used to correct astigmatism from a conformal dome. This is shown in Figure 11. In this figure, the conformal dome (60) is followed by a reflective telescope. The two cylinders (82,84) follow the secondary and translate in axial position. This invention is well suited for conformal shapes that have astigmatism as the dominant aberration.

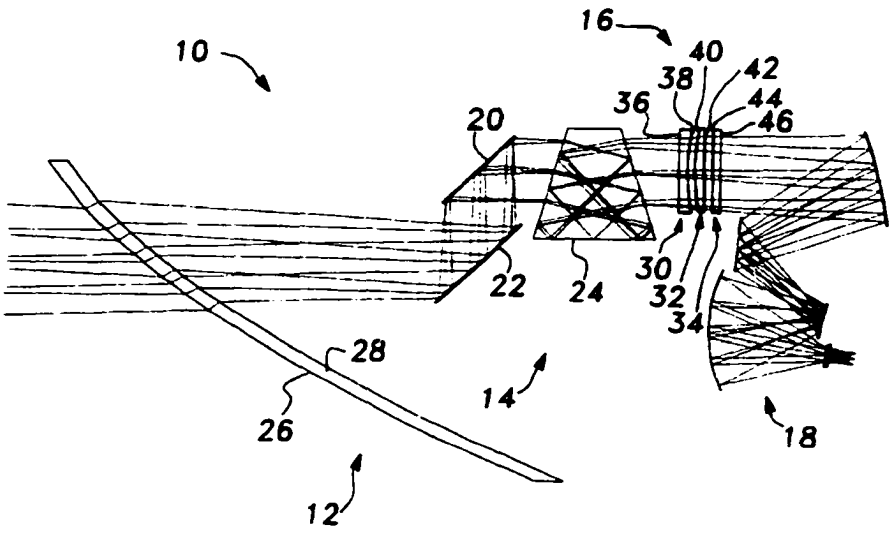

Figure 12. Illustration of Static and Dynamic Correctors from US Patent #6,018,424

In US Patent #6,018,424 filed on December 11, 1996, Morgan and Cook present a means of correcting a conformal window using a static and dynamic corrector. The inside surface of the conformal window (28) is contoured to reduce higher order aberrations. The aberration generator (16) corrects for focus and astigmatism over the FOR. The aberration generator has elements that may be rotated and axially translated to generate the astigmatism and focus. Two or more of the surfaces in the aberration generator are contoured with a certain degree of cylindrical power in order to generate on-axis astigmatism. The aberration generator is followed by an imaging system (18). This invention illustrates the usefulness of using a combination of passive and active aberration correction. It also provides a design form that uses a three mirror anastigmat (TMA) in the conformal optical system.

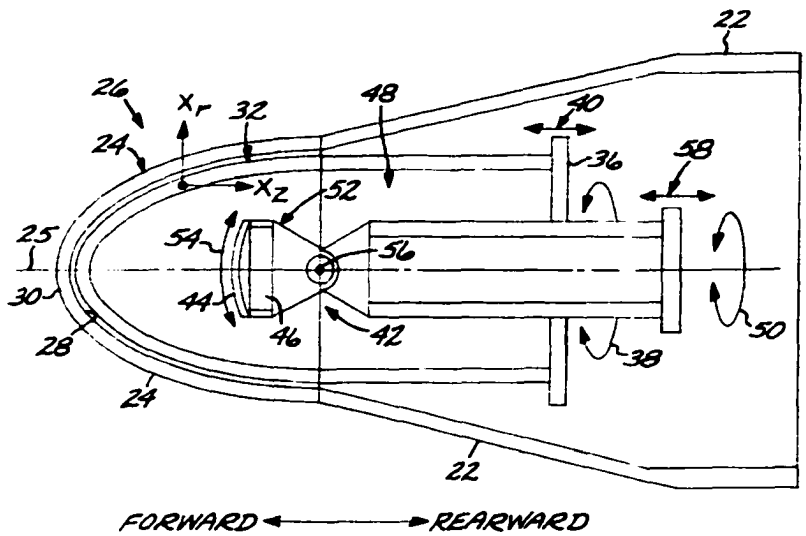

Figure 13. Illustration of Arch Corrector from US Patent #6,028,712

In US Patent #6,028,712 filed on September 30, 1998, McKenney, Sparrold, et al. introduce the concept of an arch corrector for a conformal dome. The arch corrector (32) is a bilaterally symmetric thin strip of material that is mounted behind the conformal dome (24) to the roll gimbal (50). The arch moves in azimuth with the imaging system (42). This patent is significant in that it shows how a bilaterally symmetric optical element, an arch, may be used to correct aberrations from an axially symmetric aspheric dome. This correction approach can only be used in a roll-nod type of gimbal, as the arch must move with the roll motion.

This patent introduces the concept of using a gimbal with the ability to vary the distance between the imaging system (42) and the dome. This additional degree of freedom allows line of sight error and focus to be corrected through opto-mechanical movements.

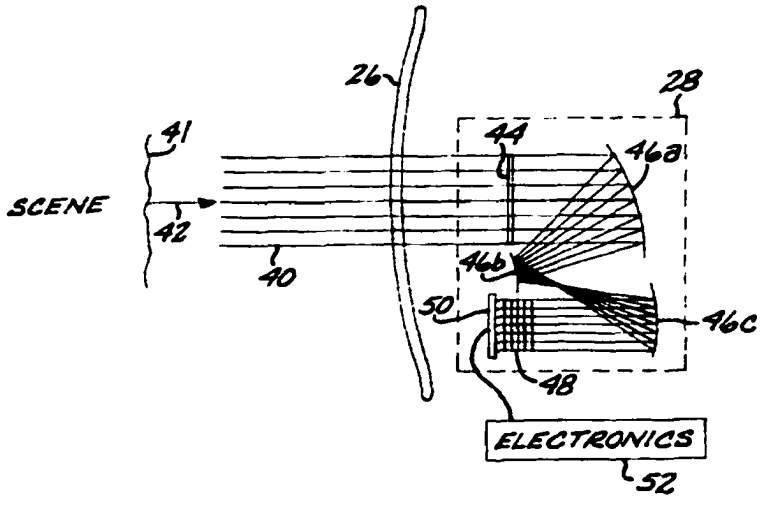

Figure 14. Illustration of Two Stage Aberration Corrector from US Patent #6,091,548

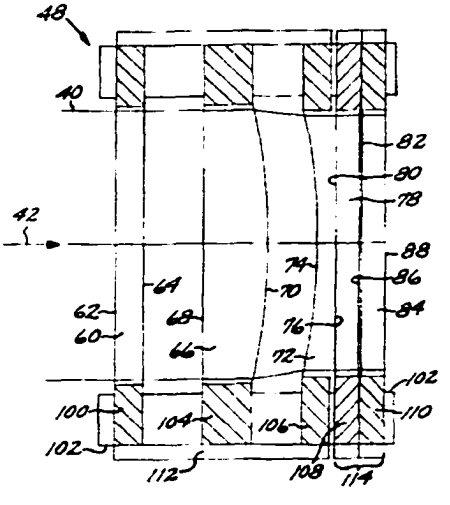

Figure 15. Illustration of Dynamic Aberration Generator from US Patent #6,091,548

In US Patent #6,091,548 filed on October 1, 1997, Chen shows a two stage aberration correction approach. Aberrations from a wavefront (41) passing through a conformal window (26) are first corrected with a static corrector (44) to remove aberrations that are constant with look angle. The wavefront then passes through a relay system (46) into the dynamic aberration generator (48). The dynamic aberration generator

corrects astigmatism, defocus, and coma. This invention continues with the concept of using a combination of active and passive optical correction. It suffers many of the limitations of other active correction schemes in terms of increased cost and complexity.

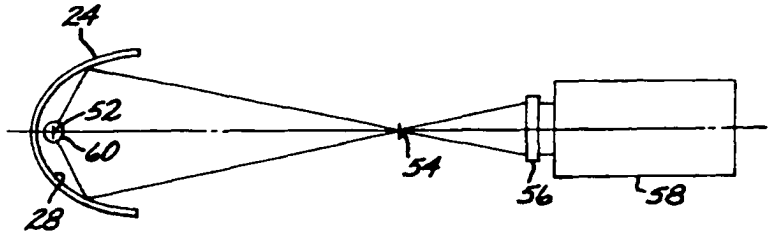

Figure 16. Illustration of Conic Dome from US Patent #6,180,938

In US Patent #6,180,938 filed on November 5, 1998, Crowther, McKenney, et al. invented a conformal dome that is significantly easier to test. Essentially, the complexity is reduced by contouring the inside surface of the dome such that a simple reflective test can be used. The outside surface (24) may be a general aspheric profile. A layout of the test setup is shown above. Light from a remote focus of the dome (54) may be directed to the inside surface of the dome where it is reflected to the near focus (52). An interferometer (58) with a reference sphere (56) may be used to provide light at the remote focus. A ball bearing (60) may be used to reflect the light at the near focus in order to create a double pass test. This patent illustrates a simple and powerful method of testing a conformal dome. However, it does not provide a method for testing the outside surface of the dome. Furthermore, the designer is limited to a conic inside surface in order to use this test technique.

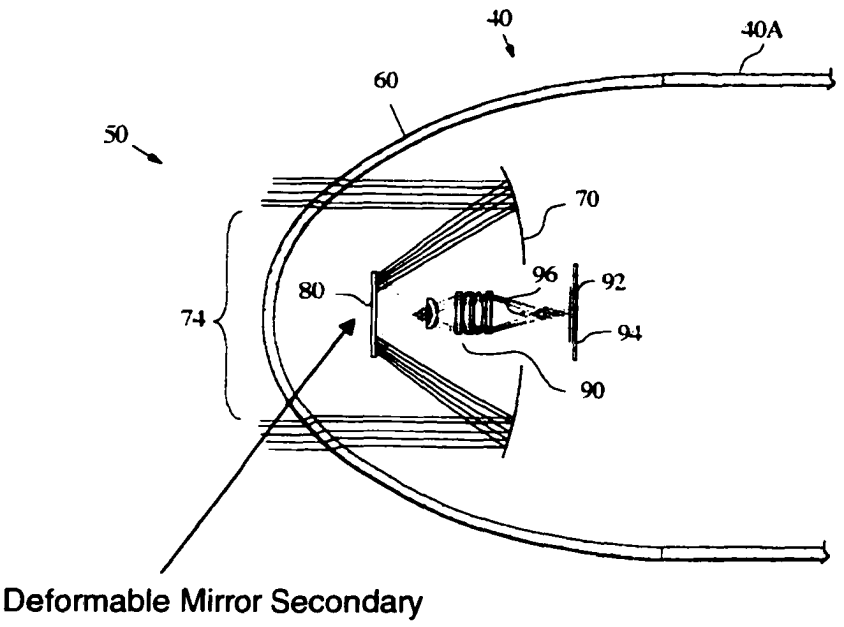

Figure 17. Illustration of Deformable Mirror from US Patent #6,201,230

In US Patent #6,201,230 filed on September 30, 1998, Crowther, McKenney et al. describe the use of a deformable mirror to correct aberrations from a conformal dome. The deformable mirror (80) is shaped as a function of the look angle through the dome to correct dynamic aberrations. The mirror may be further deformed to correct for variations due to thermal changes and optical tolerances. A layout of a system with a deformable mirror is shown in Figure 17. The deformable mirror (80) is a secondary mirror in the catadioptric system that also includes a primary mirror (70) and relay lens group (90). A conformal dome (60) is shown with a non-spherical axially symmetric shape. Friedenthal's US Patent #5,220,159 used a piezo-electric mirror to correct conformal dome aberrations. Crowther's patent generalizes the use of deformable mirrors to encompass many of the new mirrors that became commercially available including the MEMS mirror by Okotech. Deformable mirrors are powerful aberration generators in that

a relatively low mass of material is moved to change the aberrations. In comparison, many of the other active correction schemes required the movement of relatively large elements to produce aberrations.

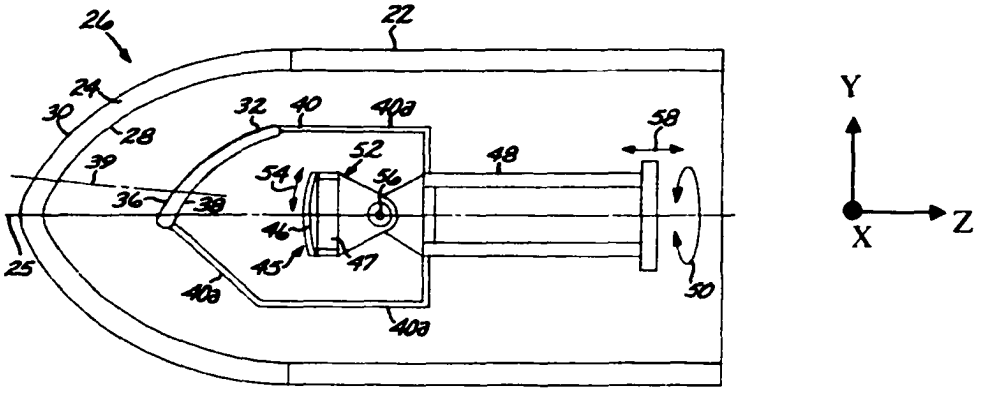

Figure 18. Illustration of Asymmetric Arch from US Patent #6,310,730

In US Patent #6,310,730 filed on February 1, 2000, Knapp and Sparrold expand on the arch corrector by introducing a variant of an arch with an asymmetric form. Specifically, this arch increases performance by removing the need to be double plane symmetric. In other words, a conventional arch is symmetric about the Y-Z plane and the X-Z plane. The asymmetric arch is only symmetric about the Y-Z plane. In addition to the slightly increased performance, the asymmetric arch reduces the number of stray light paths, lowers the mass on the roll gimbal, and decreases the cost of fabrication. These benefits come at the cost of reduced gimbal range in the nod motion (54).

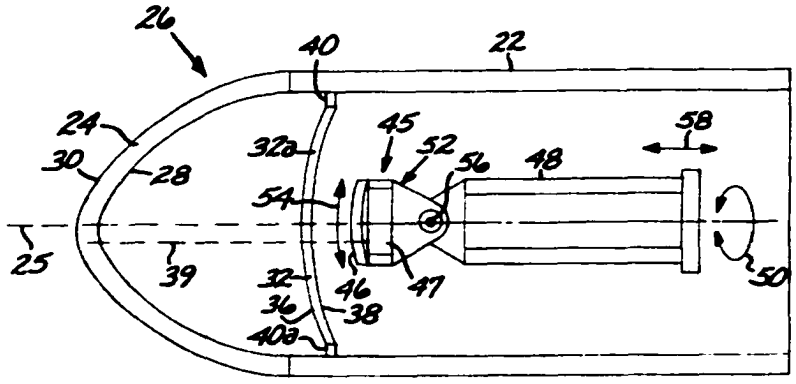

Figure 19. Illustration of Zernike Corrector from US Patent #6,313,951

In US Patent #6,313,951 filed on February 1, 2000, Manhart, Knapp et al. further enhance the design forms for a conformal corrector. They describe using Zernike polynomials to contour the surfaces of a corrector. The corrector may be fixed in place relative to the conformal window (26) as shown in Figure 19. The Zernike polynomials allow the corrector to represent a form suitable for correcting aberrations from a non-rotationally symmetric window. Alternatively, the corrector may be mounted on a roll gimbal and take the form of an arch corrector with single or double plane symmetry. This patent also describes how the correctors may be fabricated by means of etching the Zernike profiles into a base spherical substrate. The Zernike corrector form is effective for a large number of asymmetric window shapes. The limitation of this invention is that large deviations from the base axisymmetric surface are nontrivial to fabricate and test.

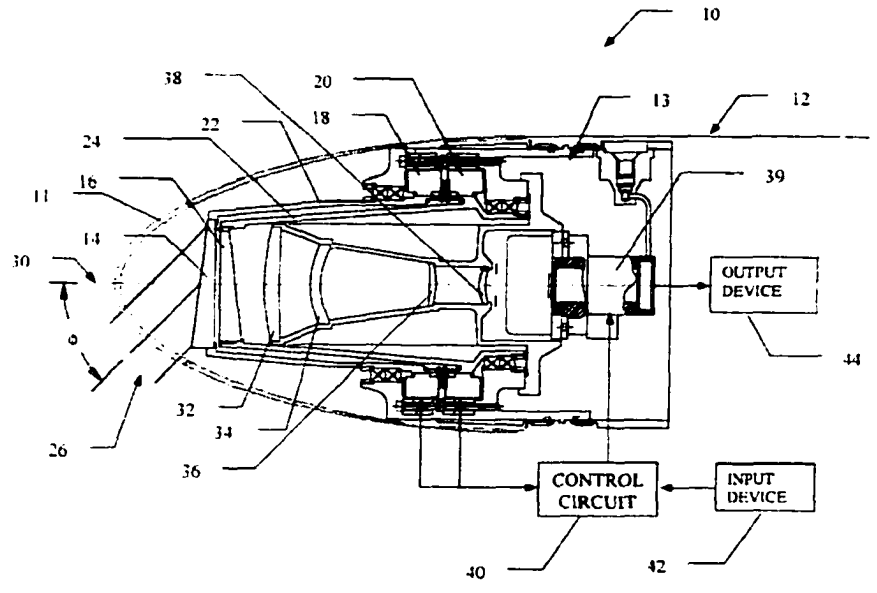

Figure 20. Illustration of Risley Prisms from US Patent #6,343,767

In US Patent #6,343,767 filed on March 3, 1999, Sparrold, Mills, et al. teach the use of contoured Risley prisms to provide simultaneous beam steering and aberration correction for a missile seeker. By themselves, the Risley prisms (14, 16) are a means of changing the look angle of an imaging system. Each prism deviates light by a certain angle phi. When the prisms are counter-rotated about the z axis (30) with respect to each other, the prism deviations cancel and the net deviation through both prisms is zero. When the prisms are rotated to the same position as shown in Figure 20, the prism deviations add to produce a net deviation that is double that of one prism. Rotating the prisms in opposite directions produces a change in the beam in missile seeker elevation (a nodding motion in the Y-Z plane). Rotating the prisms together produces a change in seeker azimuth, a rotation about the Z axis.

By contouring the prisms with a non-axisymmetric profile, aberrations are generated as a function of the rotation difference between the two prisms. The contoured

Risley prisms are shown to be an effective means of correcting the aberration from a conformal dome (16). A body fixed imaging system is placed behind the prisms.

In US Patent #6,344,937 filed on March 3, 1999, Sparrold, Mills, et al. describe the contoured Risley prisms in a more general sense for aberration correction and beam steering. Specifically, the use of the prisms is broadened beyond the previous patent's use of the prisms in a missile seeker.

Both patents describe fabrication of the contoured Risley prisms through laser etching, micromachining, and photolithography.

These patents are significant in that they illustrate a means of combining active aberration correction with gimbal motion. In comparison to other active correction schemes, this patent does not require a computer to dynamically calculate the aberration required for a particular look angle. A drawback to this invention is that it requires an investment in gimbal and gimbal control software development.

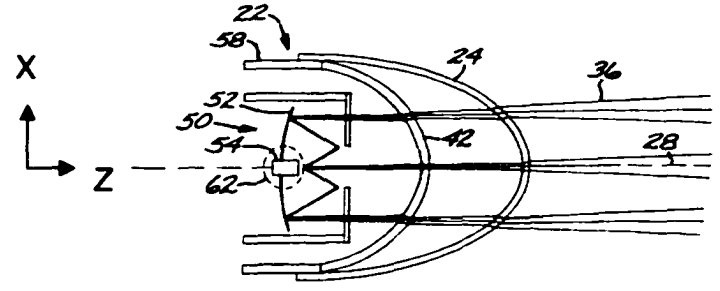

Figure 21. Illustration of Toroidal Arch in X-Z Plane from US Patent #6,356,396

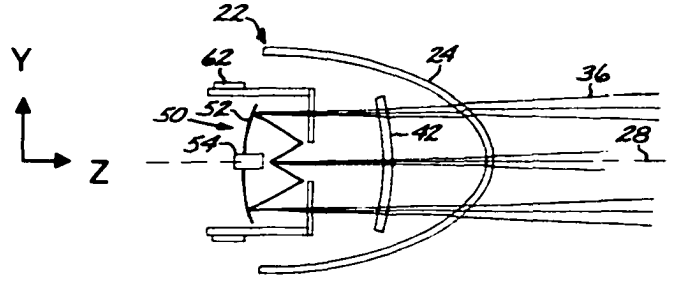

Figure 22. Illustration of Toroidal Arch in Y-Z Plane from US Patent #6,356,396

In US Patent #6,356,396 February 1, 2000, Chen, Fry, et al. describes a variant of a conformal corrector consisting of a generalized torus. As with the Zernike corrector, the toroidal corrector (42) may be mounted to a roll gimbal to serve as an arch corrector for a conformal missile dome (24). A layout of this configuration is shown in the figures above. A telescope is mounted to the gimbal behind the arch to image the corrected wavefront. The toroidal corrector may also be fixed in position relative to a conformal window and used to correct aberrations from non-axisymmetric window shapes. This patent illustrates the usefulness of a toroidal arch corrector for correcting dome aberrations. This invention suffers from the limitations of the other arch patents in that it is not well suited for asymmetric conformal shapes and would be difficult to manufacture.

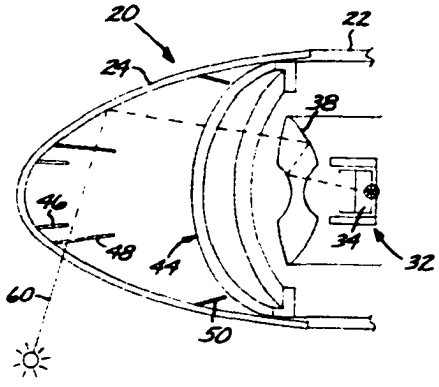

Figure 23. Illustration of Baffles from US Patent #6,462,889

In US Patent #6,462,889 filed on June 22, 2000, Jackson shows how one may use rotationally symmetric stationary baffles to block stray radiation in conformal domes. A layout of such a system is shown above. Conformal domes have the problem that light (60) from outside the field of view can pass through the dome and in a single reflection on the inside surface pass directly into the imaging system (38). This makes the missile seeker susceptible to countermeasures such as flares or other bright light sources like the sun. This problem can be solved through the use of rotationally symmetric baffles (46,48,50) to block the paths of unwanted radiation light. The baffles take the form of a frustoconical tube, a shape like a lampshade, to minimize the obscuration of light in the field of view. This invention shows an excellent solution to the stray light problem created by conformal domes. The limitations of this invention are the increase in vignetting from the baffles, and the potential for the baffles to detach from the dome during hard acceleration or extreme thermal variations during flight.

Conformal Optics in the Literature

There is also a substantial amount of information that has been written on conformal optics in journals, theses, and dissertations.

Fischer explored correcting conformal domes using binary optics.[9] Fischer noted previous attempts made to control aberrations using gradient index conformal domes, and multilayer domes. Fischer found these previous attempts to be impractical due to manufacturing considerations. The binary optical corrector was shown to provide modest correction for a small aperture ratio and waveband.

Sparrold first described the concept of an arch corrector element for conformal domes.[10] Sparrold also examined a fixed corrector, but found it not as effective as the arch. Sparrold further conducted a broad exploration of the correction capabilities of an arch element.[11]

Novak characterized first-order properties of conformal domes and described the change in aberrations with respect to gimbal look angle. Novak further provided several designs for correcting dome aberrations.[12]

Chen described using a toroidal conformal aircraft window.[13] This shape was shown to allow excellent fields of regard and relatively low aberrations.

Crowther analyzed the aberrations of conformal domes.[14] He used a Zernike polynomial decomposition of the wavefront passing through a conformal dome at various look angles.

Palusinksi and Sasian described a method of aberration generation using laterally translating phase plates.[15] Mills described a method of correcting dome aberrations using

counter-rotating phase plates.[16] This work was further described by Sparrold.[17] Mitchell showed how axially translating phase plates could be used to generate aberration.[18]

Whalen described correcting variable astigmatism using axially translating cylindrical elements.[19] This technique was used in a toroidal conformal window demonstration. Marushin described the design, fabrication, and test of the window demonstration.[20]

Ellis analyzed the aberration properties of ellipsoidal domes.[21] Ellis investigated the first and third order properties for different dome fineness ratios, thicknesses, and indices of refraction. Astigmatism and coma were found to be the dominant aberrations.

Lerner developed several surface types useful for conformal optical design.[22,23] Specifically, he found that an implicit x-y-z polynomial surface and a truncated parametric Taylor polynomial were better aspheric surface representations than the standard explicit asphere.

Chase investigated optical design with Non-Uniform Rational B-Splines (NURBS).[24] NURBS are of interest in optical design due to their complex hull property and ability to attain complex forms.

Mills described the design, fabrication, and test of the world's first conformal optical imager.[25] A fineness ratio 1.0 CaF_2 ellipsoidal dome was corrected using a single aspheric fixed corrector.

Prior Art Summary

As of October 20, 2002 there were at least 20 patents relating to conformal optics.[‡] These patents describe solution forms that are appropriate for missile seekers, airborne sensors, and other applications that require imaging through a conformal window. Two of the patents concern deformable elements. Four of the patents concern tilting and decentering elements for aberration generation. Two of the patents concern contoured Risley prisms. Four of the patents concern a specific new type of conformal dome. The articles, theses, and dissertations on conformal optics also provide a broad sampling of information on conformal optical design. As with much of the literature, performance of one solution relative to another can be difficult to gauge. An overall synthesis of the solution forms and methodology for conformal optical design can be useful for making sense of the point solutions. The next section will therefore describe the fundamentals of conformal design, starting with a comparison with conventional optics, initial design considerations, and moving into a discussion of solution forms, surface types, and design tools. [26]

[‡] Of the 20 patents in conformal optics reviewed, it is interesting that Raytheon holds 16 of them.

Conventional Windows and Domes

Before looking at conformal windows and domes, it is insightful to look at ordinary windows and domes.

Conventional electro-optical systems use only two types of outer elements, flat windows and hemispherical domes. Optically, this makes the optics much easier to design. In the case of a perfect flat window, collimated light traverses a plane parallel element without inducing aberrations. Consequently, one may gimbal an imaging system behind the flat window without having to correct for FOR dependent aberrations. Figure 25 shows a perfect lens gimballing behind a plane parallel window. One can move the gimbal point farther away from the window without any optical effect except for a larger optical footprint on the window. In the case of a perfect hemispherical dome, the gimbal point is fixed at the dome center of curvature. At this position, the dome induces symmetric aberrations that are invariant with look angle. The dome acts identically to a fixed concentric outer element. Figure 24 shows a perfect lens gimballing behind a concentric hemispherical dome.

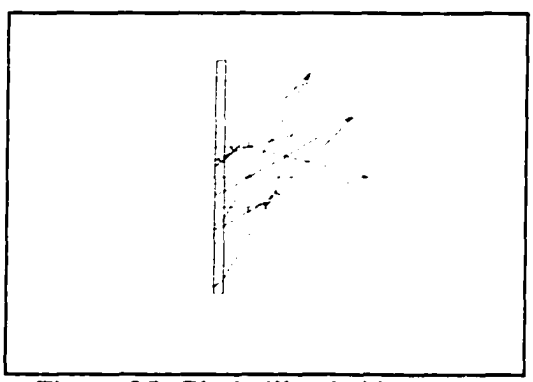

Figure 25. Gimballing behind a flat window

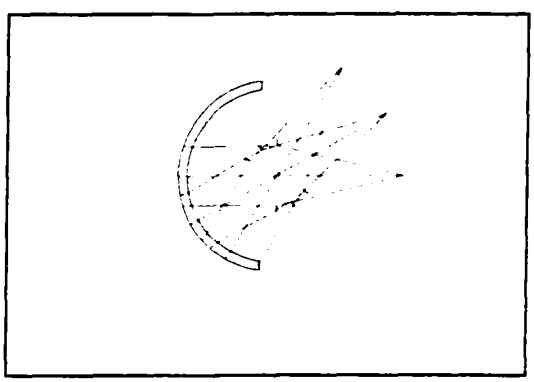

Figure 24. Gimballing behind a hemispherical dome

Unfortunately, flats and hemispheres are not the best window shapes for optimum aerodynamic performance. In the case of a missile, a hemispherical dome can double the nose drag compared to an optimum low-drag shape. The poor aerodynamic performance of conventional windows and domes drives one to a conformal shape for increased performance.

Conformal Shapes

Aircraft Forward Looking InfraRed (FLIR) pods and missiles are two types of systems that can benefit greatly from an improved leading edge optical shape. One such candidate shape is the ellipse.

Aerodynamic Benefit of Conformal Shapes

The ellipse is a conic surface that can be elongated along the axis of symmetry. As its length-to-diameter ratio (fineness ratio) increases, the drag caused by the ellipse goes down. Figure 26 shows the drag reduction possible for various elliptical fineness ratios. [§] For reference, the hemisphere has a fineness ratio of 0.5.[27]

[§] Fineness ratio is defined as the ratio of nose length (L) to nose diameter (D). This ratio will be abbreviated as F. (F=L/D)
Note that F is not an abbreviation for F-number. F-number will be abbreviated as F/2 for an F-number 2 system.

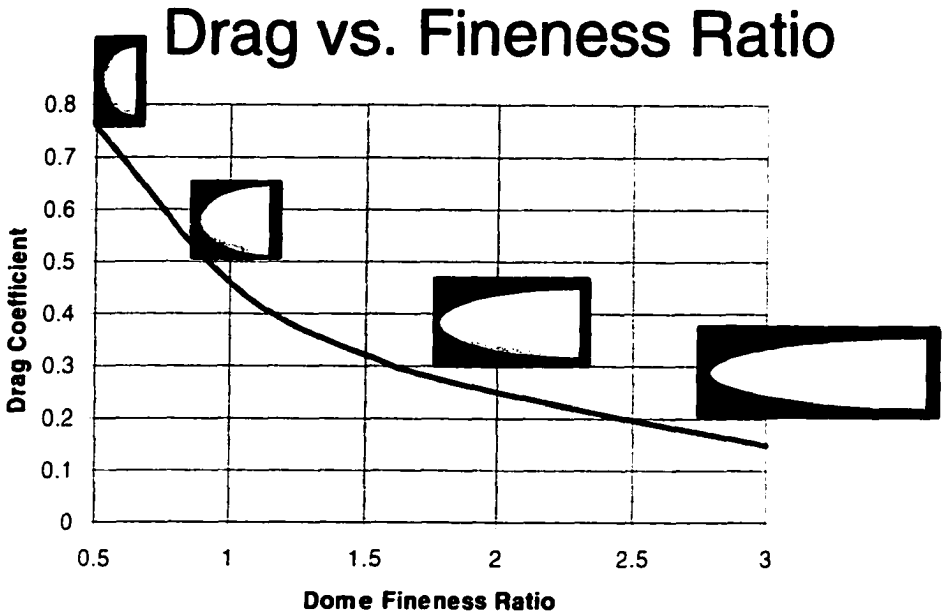

Figure 26. Relative Drag of Elliptical Forebody

Clearly, there is a definite aerodynamic benefit in going to a conformal surface. The designer may tune a design to trade off design complexity with increased aerodynamic performance. In contrast, conventional shapes restrict the options of a designer. In a gimbaled system, a conventional dome requires the gimbal point to be about the dome center of curvature. For a given clear aperture diameter, conventional optical design essentially locks the aeronautical engineer into a hemispherical dome, take it or leave it.

Benefit of Increased Field of Regard

A further advantage in using conformal optical surfaces is the potential to have larger unvignetted fields of regard (FOR) than a conventional window or dome. For example, hemispherical domes limit the unvignetted FOR to less than +/- 90°, whereas conformal surfaces can result in unvignetted FOR's exceeding 90°. This is due to the fact that a conformal window element may wrap around the imaging system. Figure 27 shows a conformal dome with a large unvignetted FOR. Figure 28 shows a hemispherical dome with a vignetted field of view at a 90° look angle.

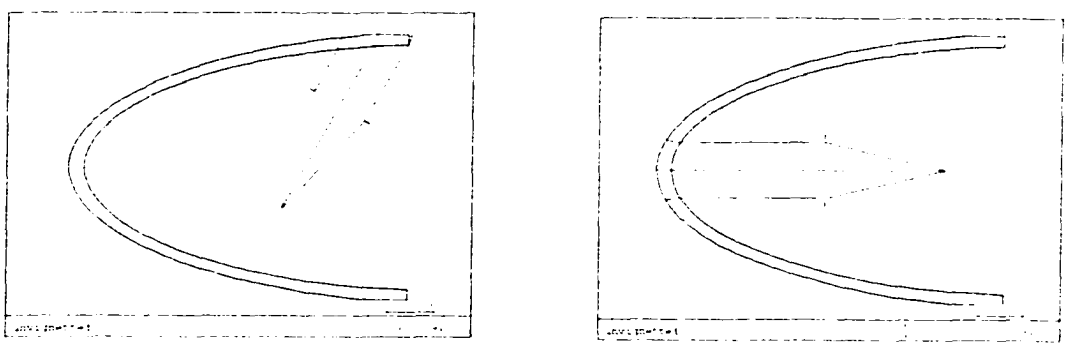

Figure 27. Increased FOR Possible with a Conformal Dome

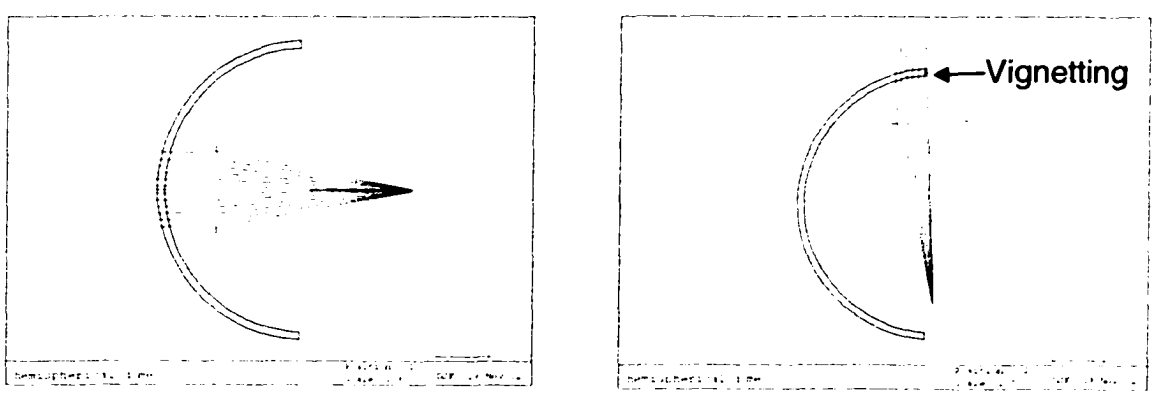

Figure 28. Hemispherical dome limits FOR

Conformal shapes may be designed to wrap around a gimbaled imaging system and provide clear aperture in directions unobtainable with non-segmented conventional optics.

Increased Aberrations of Conformal Optics

The benefits of decreased drag and improved FOR come at a price. Conformal surfaces create aberrations that vary with off-axis look angle. A missile seeker with a conformal dome is shown in Figure 29 and in Figure 30. The seeker has a telescope mounted on a gimbal that moves independently of the dome so that it may be pointed at a target of interest away from the missile axis (look angle). As the telescope gimbals away from boresight (0 degree look angle), the symmetry is broken and the section of the dome that the telescope looks through changes.

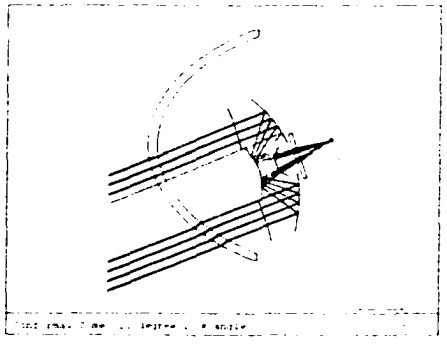

Figure 29. Conformal Dome and telescope at 20 degree look angle.

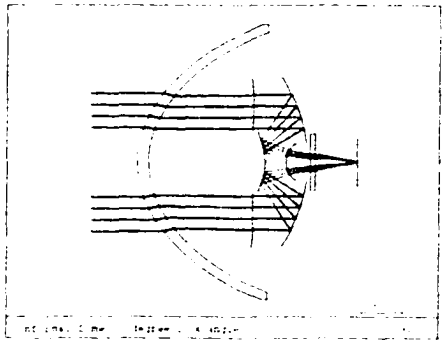

Figure 30. Conformal Dome and telescope at 0 degrees look angle

The symmetry break leads to aberrations that can be on the order of 10's to 100's of waves in magnitude.[28]

Aberrations of Conformal Surfaces

At this point, it is insightful to examine quantitatively the aberrations induced by a conformal surface. Aberrations of conformal windows and domes are conveniently characterized by decomposing the wavefront at the exit pupil into Zernike polynomials. Zernike polynomials are a complete orthogonal set of polynomials over a unit circle. This insures that the decomposition is unique with regard to the values of the various Zernike polynomials. Furthermore, the orthogonality guarantees that the wavefront residual after a fit of lower order Zernike terms will solely be composed of higher order Zernike terms.[29] To ascertain performance over a gimbaled imager's FOR, the coefficients of the various Zernike terms may be plotted versus the gimbal look angle. From this, one may identify important aberrations and gauge the level of correction that needs to be attained.

As an example, Figure 31 shows a plot of three Zernike aberrations versus FOR for a perfect lens gimballing behind an elliptical dome. The gimbal has a half angle range of 40 degrees from boresight to the edge of the FOR. The aperture ratio** is 0.27.

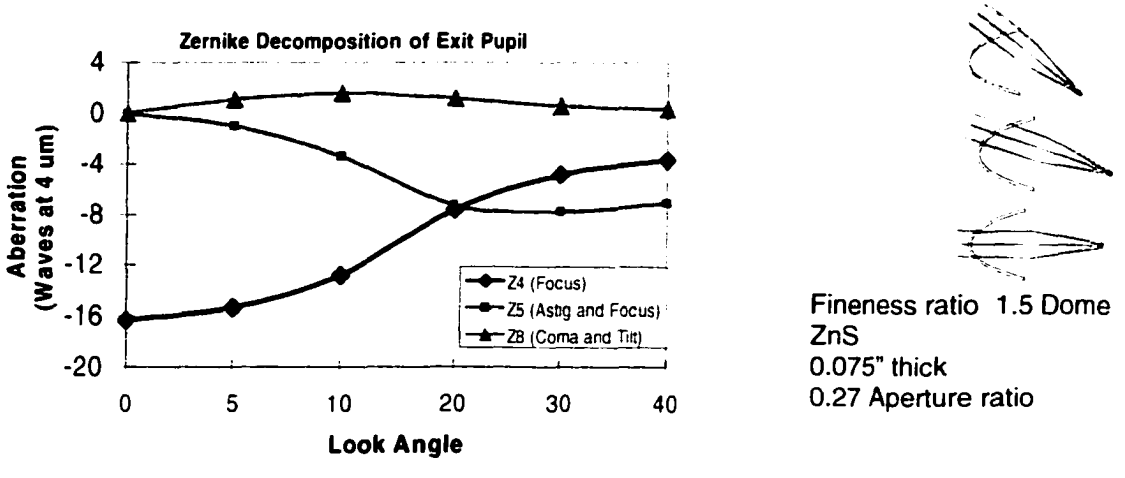

Figure 31. Significant zernike aberrations of a fineness ratio (F) 1.5 elliptical dome

** The aperture ratio is defined as the ratio of the imaging system pupil diameter to the clear aperture diameter of the dome or window.

Clearly, this uncorrected conformal dome has a significant amount of aberration with a large amount of variation versus look angle. Other conformal surfaces will similarly induce large amounts of aberrations that change with the look angle of the gimbal. The freedom to arbitrarily shape a conformal element introduces the greatest challenge: the need to correct the large amount of induced aberration.

A conformal window yields an additional complexity in that the variation in aberrations from the window is not necessarily symmetric about boresight. In other words, a change in 10 degrees of gimbal elevation may not induce the same change in aberration as a 10 degree change in gimbal azimuth.

Initial Design Considerations

To begin designing with a conformal window or dome, a distinction should be seen between the front end and back end of a conformal optical system. The front end is composed of the dome or window and any other elements upstream from the imaging system. Aberrations from the front end vary with look angle. The variation may be minimized by adding corrective optical elements in the front end. The back end of the conformal optical system is generally an imaging system that contributes fixed aberrations with respect to gimbal look angle. See Figure 32.

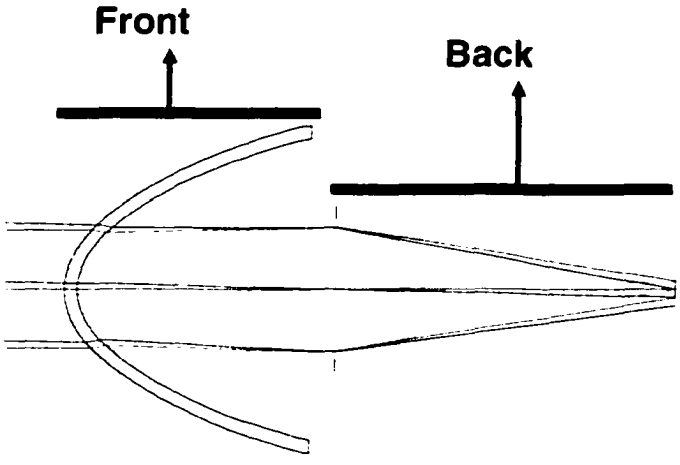

Figure 32. Front end and back end distinction

If the aberrations of a gimbaled conformal optical system are plotted versus look angle, the back end of the system will contribute constant aberrations versus look angle. The conformal window or dome will contribute a variation of aberrations with look angle. One may optimize the front end of a conformal system separately from the back end and then perform a final combined optimization. For the sake of clarity, the examples for this section utilize a perfect lens to represent the imaging system. One may of course substitute in any number of well-known imaging systems such as reflective telescopes,

refractive triplet, or other less-than perfect lenses. An exception to the front end/back end distinction is where an active aberration generator is used in the imaging system to dynamically compensate aberrations arising from the front end. In this case, the aberration contribution from the back end will vary with respect to look angle. The design goal in this case would be for the combination of the aberrations from the back end and the front end to be minimized below a tolerable level. As with other types of optical design, conformal design comes with a set of trade-offs. Among these are the surface formula, fineness ratio in one or more cross-sections, material type, thickness, and aperture ratio.

To yield general insight into a conformal dome's aberration behavior, a case study is shown using an elliptical dome and a perfect lens. A perfect lens was used to stand in for the imaging optics. The general layout for the study is shown in Figure 33.

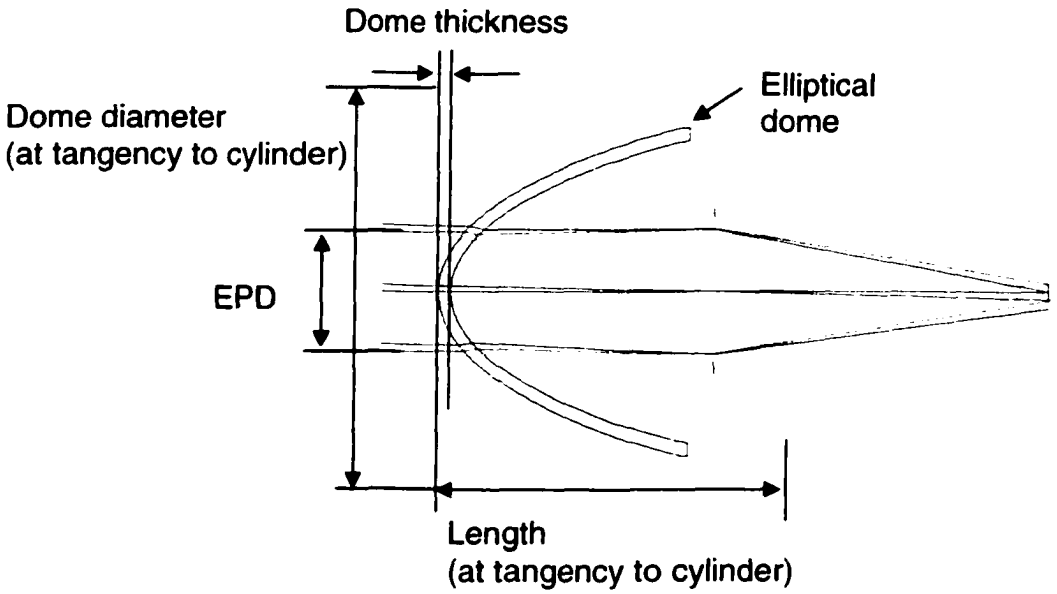

Figure 33. Dome dimensions

No corrective optimization was performed in the case study. Merely, the peak to valley amplitude of astigmatism and coma across the FOR was recorded for each change in parameter. Dome fineness ratio, index, thickness, and aperture ratio are examined. The system wavelength is set at 4 microns.

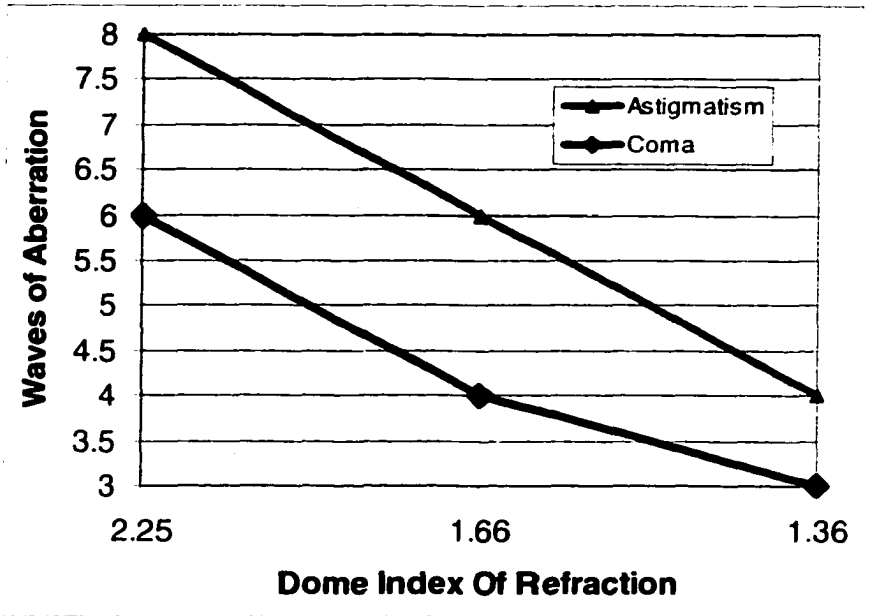

F 1.5 ZnS (n=2.25), ALON (n=1.66), MgF_2 (n=1.36) Domes

Figure 34. Dome aberration vs. Index of Refraction

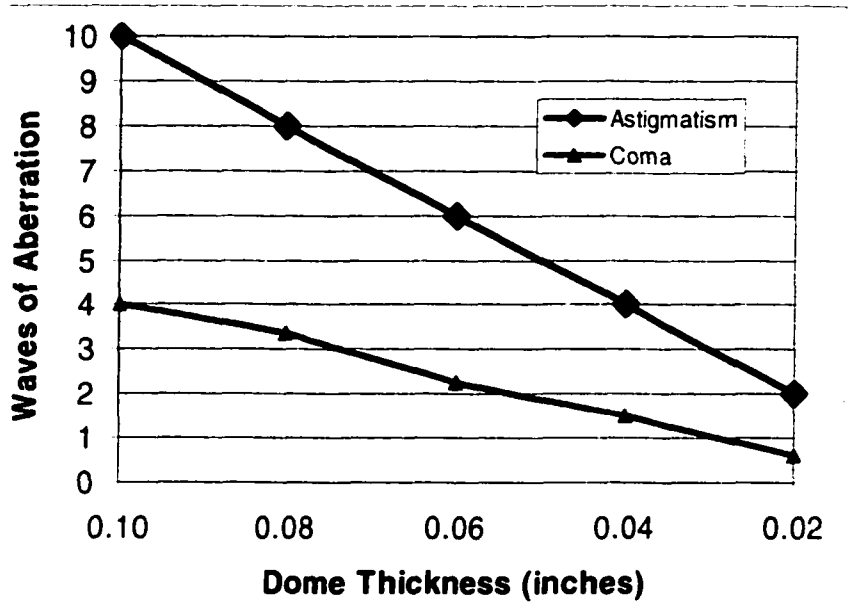

Figure 35. Dome thickness vs. aberration

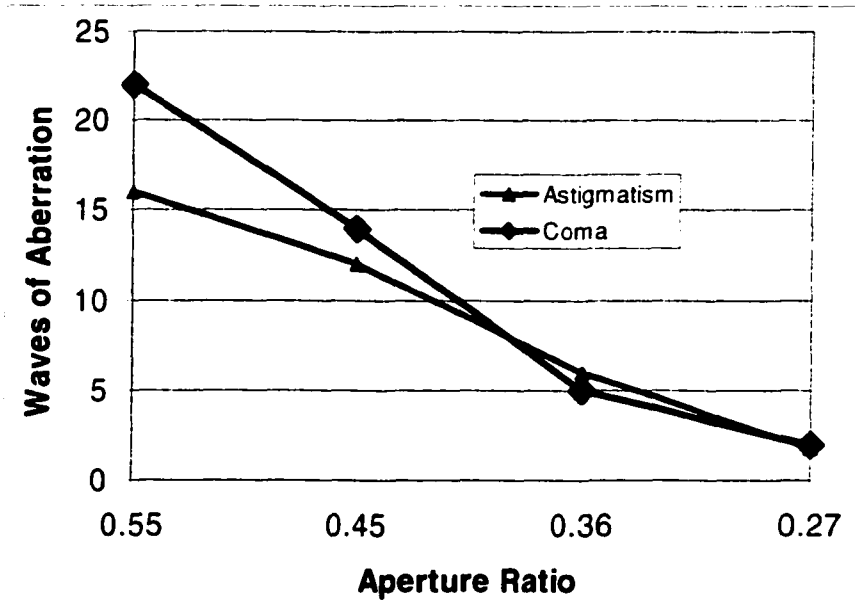

Figure 36. Dome aberration vs. Aperture ratio

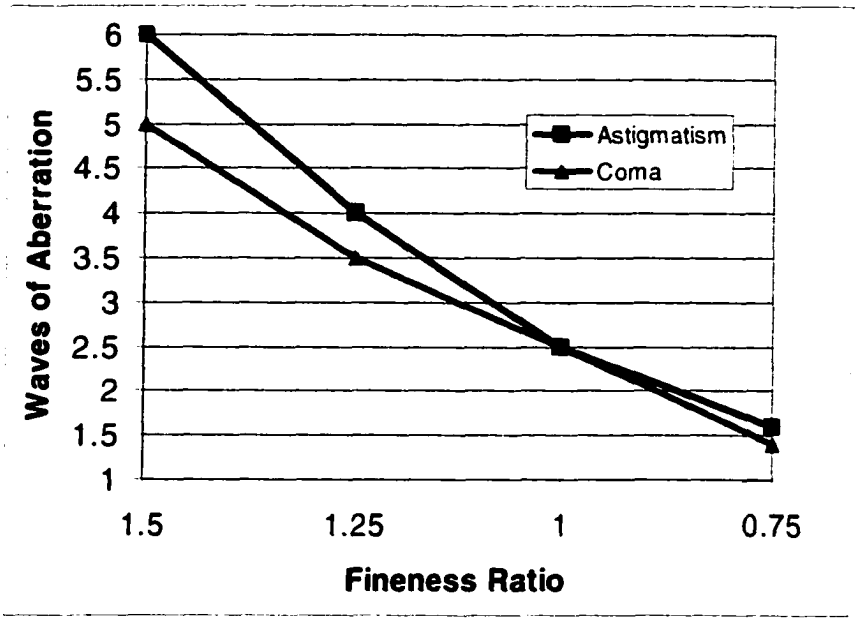

Figure 37. Dome aberration vs. Fineness ratio

Several lessons may be learned from these graphs. Each parameter has a significant effect on the peak-to-valley amplitude of the aberrations across the FOR. The peak to valley amplitude is associated with the qualitative difficulty of correcting a particular conformal dome. The optical designer is therefore well advised to include these parameters in the trade space. The dome fineness ratio should be no higher than is necessary for aerodynamic considerations. Low index dome materials are preferred. Dome thickness should be driven thin for optical and thermal shock considerations, but be thick enough to withstand pressures and particle impacts incident upon it. The value for the aperture ratio (EPD to dome diameter) should be balanced between energy collection requirements and ease of correction.

After the initial window or dome parameters are established, one moves into the detailed design phase.

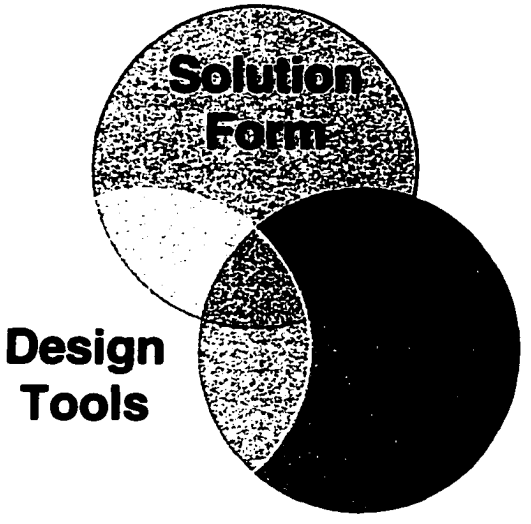

Figure 38. Important Resources in Conformal Optical Design

Resources for Conformal Optical Design

Many resources can be used in the detailed design phase. Figure 38 shows three important categories. First, there are several solution forms available for correcting conformal aberrations. These have various tradeoffs in terms of design complexity, required gimbal type, and performance. Second, there are many surface types available for modeling a conformal optical system. Not all surface types are appropriate for every solution form. Appropriate surface type selections will be discussed along with the solution form that they are typically used with. Third, there are several optimization tools and direct solution tools that are used to arrive at a finished design.

Solution Forms

To design a conformal optical system, the designer must start with a basic solution approach. As will be shown, surface types are closely linked with different solution forms. The solution forms developed so far can be separated into the following categories:

A. Articulating optical correcting elements

B. Fixed corrector elements

C. Deformable correcting elements

D. Image based software correction.

ARTICULATING ELEMENTS

The Arch

The arch element is an aspheric element whose parameters are free to vary in non-axially symmetric directions.[30] It is placed immediately behind a conformal dome to introduce balancing amounts of aberration such that the residual aberrations are constant with look angle.[31 32]

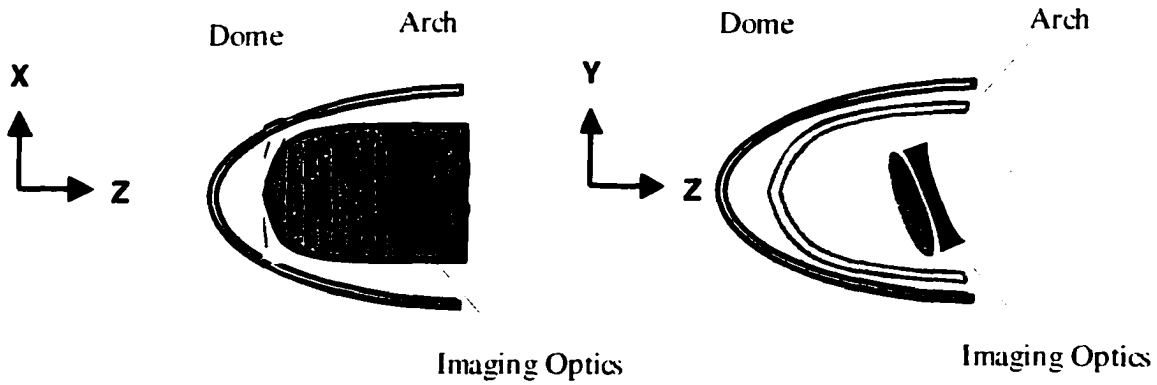

Figure 39. Arch Corrector in X-Z view and Y-Z view

The imager behind the arch is designed to correct out the remaining spherical aberration and focus.

A roll-nod gimbal is needed with the arch and imager. As the name implies, this type of gimbal has two motions, roll and nod. The gimbal uses the roll motion to change azimuth about the missile axis and a nod motion to change elevation. See Figure 40.

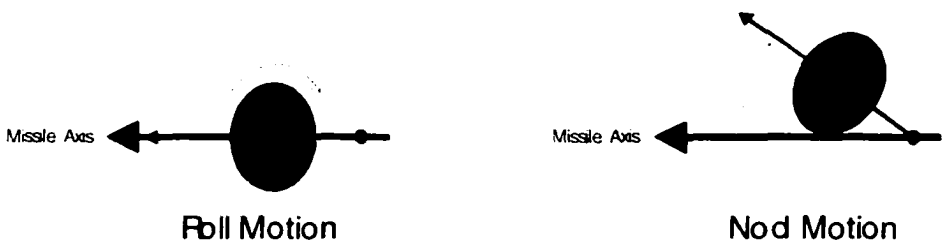

Figure 40. Gimbal motions

The arch remains fixed with nod and rolls with the gimbal. Due to the fact that it rolls with the gimbal, the arch can be designed with bilateral symmetry. This extra degree of freedom results in arch corrector elements that outperform their axisymmetric brethren.[33] The arch can be used in conjunction with other corrective elements for added effect. In the initial design stages, global optimization can be used successfully to find

candidate arch forms to correct a given conformal dome shape. The anamorphic asphere equation and the Zernike polynomial equations work well for modeling the arch.[34]

Counter-rotating Phase Plates

This method of correction relies on a pair of aspheric surfaces to correct the aberrated wavefront from the conformal element[35]. Each surface is allowed to rotate independently about the optical axis. Each surface is defined by a thickness function T:

$$T_1(r,\theta) = T_1(x,y) = c + t(r,\theta)$$

$$T_2(r,\theta) = T_2(x,y) = c - t(r,\theta)$$

Equation 1

where c is the base thickness and t is the deviation from the base thickness. See Figure 41.

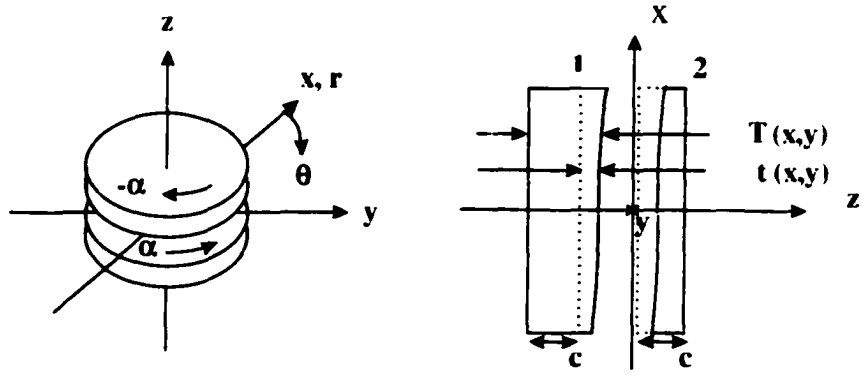

Figure 41. Phase plates

The deviation functions t are identical for each surface but opposite in sign. At an initial angle with respect to each other of $\alpha = 0$, the plates are aligned such that the net thickness across both plates is 2c:

$$T_1(r,\theta)+T_2(r,\theta)=2\cdot c$$

Equation 2

The surfaces at this position will therefore induce a constant OPD across a wavefront passing through both plates. However, as the plates are counter-rotated with respect to each other, an aberration is induced into the wavefront. Mills[36] approximated the optical path difference (OPD) across the two plates with a small counter-rotation as:

$$OPD(r,\theta,\alpha)\approx 2\alpha\cdot(n-1)\cdot\frac{\partial}{\partial\theta}\cdot t(r,\theta)$$

Equation 3

Here n is the index of refraction and α is the counter-rotation angle. Essentially, the wavefront deformation induced by the surfaces is proportional to the derivative of the surface profile and proportional to the relative rotation of the plates with respect to each other. If the surface profile is described by a Zernike polynomial, the wavefront can be described by a related Zernike polynomial.[37] Table 1 lists the first nine Zernike Polynomials.

Term	Name	Zernike Polynomial
Z1	Piston	1
Z2	y Tilt	$r\cos(\theta)$
Z3	x Tilt	$r\sin(\theta)$
Z4	Focus	$2r^2-1$
Z5	Astigmatism	$r^2\cos(2\theta)$
Z6	Astigmatism	$r^2\sin(2\theta)$
Z7	Coma (3^{rd})	$(3r^3-2r)\cos(\theta)$
Z8	Coma (3^{rd})	$(3r^3-2r)\sin(\theta)$
Z9	Spherical, 3^{rd}	$6r^4-6r^2+1$

Table 1. Zernike Polynomials

Surface Zernike Term	Surface Description	Resulting OPD after both elements counter-rotate by α	Wavefront Zernike Term
Z3	$a[r\sin\theta]$	$2a(n-1)\sin\alpha[r\cos\theta]$	Z2
Z2	$b[r\cos\theta]$	$-2b(n-1)\sin\alpha[r\sin\theta]$	Z3
Z6	$d[r^2\sin2\theta]$	$2d(n-1)\sin2\alpha[r^2\cos2\theta]$	Z5
Z5	$e[r^2\cos2\theta]$	$-2e(n-1)\sin2\alpha[r^2\sin2\theta]$	Z6
Z8	$f[(3r^3-2r)\sin\theta]$	$2f(n-1)\sin\alpha[(3r^3-2r)\cos\theta]$	Z7
Z7	$g[(3r^3-2r)\cos\theta]$	$-2g(n-1)\sin\alpha[(3r^3-2r)\sin\theta]$	Z8
Z11	$i[r^3\sin3\theta]$	$2i(n-1)\sin3\alpha[r^3\cos3\theta]$	Z10
Z10	$j[r^3\cos3\theta]$	$-2j(n-1)\sin3\alpha[r^3\sin3\theta]$	Z11

Table 2. Wavefronts produced by surfaces with Zernike contours

Table 2 lists pairs of related Zernike polynomials. The first column lists the Zernike term that contours a surface. The second column lists the polynomial corresponding to that Zernike term. The third column lists the wavefront optical path difference (OPD) after a wavefront passes through two phase plates contoured by the Zernike term of the first column. The fourth column lists the Zernike term that corresponds to the wavefront OPD. The Zernike polynomial terms can be added to yield a composite effect on the wavefront.

Figure 42 shows the aberration induced by two plates contoured with a Z6 Zernike term as the plates counter-rotate with respect to each other.

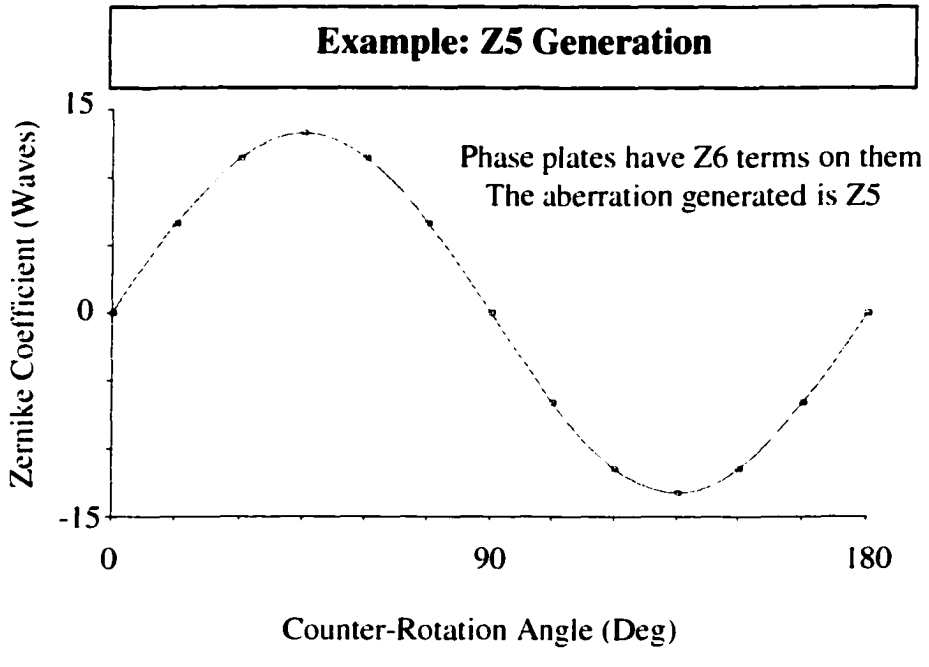

Figure 42. Z5 generated by plates contoured with Z6

In the context of conformal optics, phase plates are used as aberration generators. The aberration from the plates is matched to the conjugate aberration from a conformal dome or window. The rotational position of the plates with respect to each other is

adjusted for each look angle through the conformal element. The net aberration through the conformal element and plates is ideally set to be constant across all positions.

Additionally, one may contour a pair of Risley prisms with Zernike surfaces to change look angle and generate aberration with prism rotation. Devices of this nature are called Zernike wedges or Zernike prisms. After the Zernike wedges, fixed imaging optics are used. See Figure 43 and Figure 44.

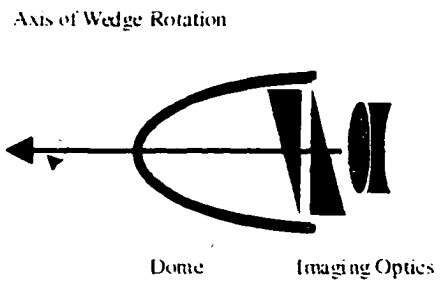

Figure 43. Counter-rotated prisms point to 0 degree look angle

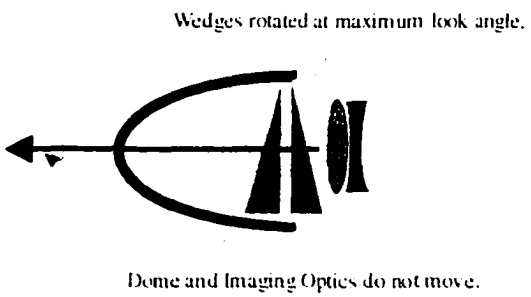

Figure 44. Identical prism orientation points to maximum look angle

Zernike wedges act essentially like a roll-nod gimbal. When both prisms are rotated in the same direction, the look angle changes in azimuth about the missile boresight. When the prisms are rotated in opposite directions, the look angle changes in elevation.

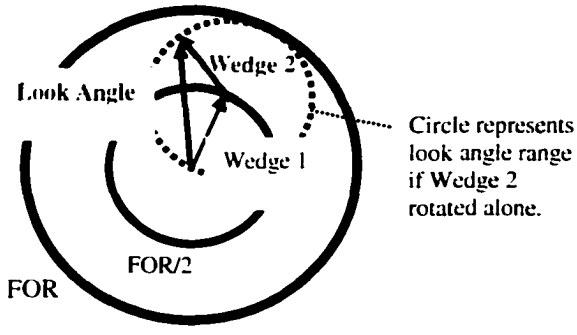

Figure 45. Deviations of Prisms combine to give field of regard (FOR)

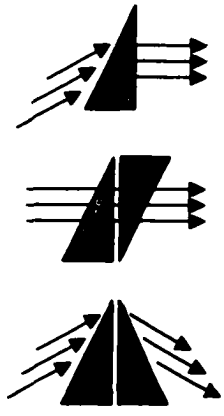

Figure 46. Prisms change look angle

Aberration induced by the prisms is a function of elevation and is constant across azimuth. An axisymmetric conformal dome may be used with a pair of Zernike wedges. However, a bilaterally symmetric conformal window should be used with a fixed corrector element such that the aberration properties for a given look angle is axisymmetric.

Aberration Generators

A conformal optical system incorporating an active aberration generator uses a set of one or more moving optical elements to generate aberration in response to a change in the gimbal look angle. The contoured Risley prisms are one example of an aberration generator.

Other types of aberration generators may be targeted to specific aberrations. For astigmatism generation, one may counter-rotate cylindrical elements or vary the spacing between them.[38,39] A constant amplitude astigmatism that changes in orientation may be created by rotating a cylindrical element about the optical axis. For spherical aberration generation, one may vary the air space between two plates contoured with equal but opposite magnitudes of a spherical aberration profile.[40] For coma generation, one may decenter a corrector plate relative to the optical axis.[41] Astigmatism and coma may also be generated by tilting or decentering a lens element. The focal length may be varied by displacing an element with optical power along the optical axis. The back focal distance may be varied by altering the axial location of the image plane.

Aberration generators are powerful due to the fact that they may be set independently from the front end of the optical system. The disadvantage of an aberration generator is that the additional actuators add to the cost and complexity of the optical system.

FIXED CORRECTOR ELEMENTS

Fixed correctors are elements that are rigidly positioned behind the conformal optic.[42,43] The combination of the two, dome and corrector, yields the optical equivalent of a conventional dome. For example, Figure 47 shows a conformal missile dome and a fixed corrector.

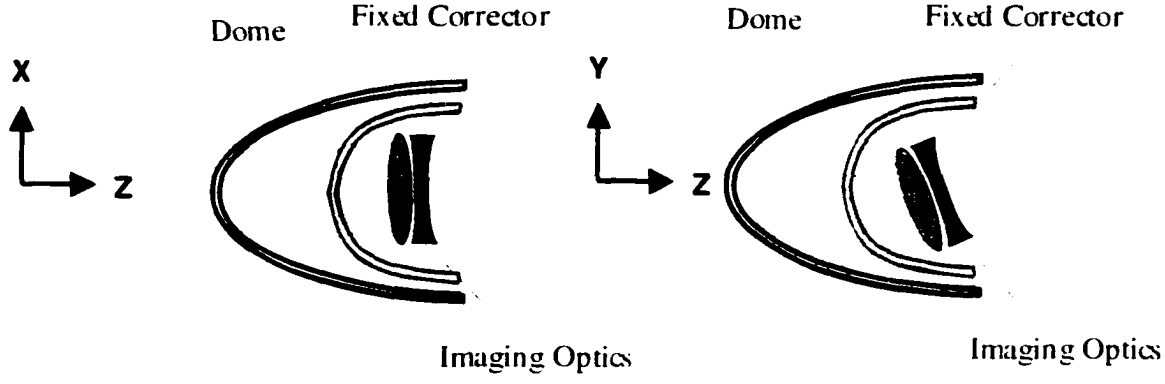

Figure 47. Fixed Corrector

The fixed corrector compensates all the look angle dependent aberrations. Like the conformal dome, the fixed corrector is axisymmetric. The imaging system corrects the remaining spherical aberration and defocus. This imaging system can be mounted on either a roll-nod or an azimuth elevation gimbal. One may deduce that the gimbal position and shape of the conformal element will determine the symmetry of the corresponding fixed corrector. Fixed axisymmetric correctors can be represented in optical design programs with an even polynomial asphere, odd and even ordered polynomial asphere, superconic, and extended spline surface types. The fixed corrector also works well with the NURBS[44] and Z polynomial surfaces.[45]

One may use more than one fixed corrector. With two correctors, different materials can be used to improve color correction and athermalization.

In some cases, it is possible to replace a conventional window or dome with a conformal optic and fixed corrector combination without changing the rest of the imaging system. Such a system can be very advantageous in terms of retrofitting existing systems to conformal domes for enhanced performance.

OTHER TYPES OF CORRECTION

Deformable Mirror

One can use a deformable mirror in an imaging system to dynamically correct aberrations from the conformal window. Deformable mirrors are essentially reflective surfaces that are electromechanically manipulated to produce desired surface profiles. In the case of a conformal system, the deformable mirror can be used to create aberrations to compensate for those induced by a conformal window or dome.

Figure 48 shows the layout of an example conformal optical system with a deformable mirror. The dome is a fineness ratio 1.5 MgF_2 dome. The secondary mirror was modeled with a Zernike surface with zoomed polynomial parameters to simulate a deformable element. The primary mirror is an F/0.75 parabola. The system wavelength was set at 4 microns and the field was set at zero. This monochromatic system could be considered a beam director for a laser.

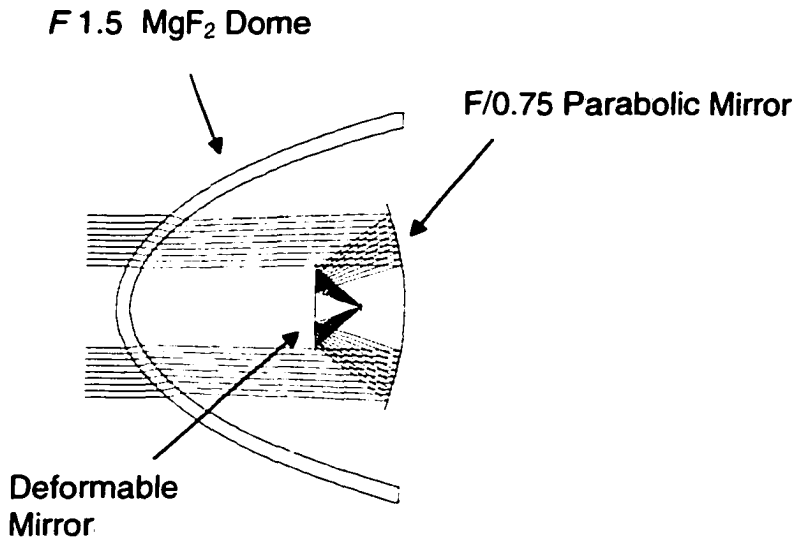

Figure 48. Layout of a Conformal System with a Deformable Mirror

The telescope was allowed to rotate through a FOR of 40 degrees. Increasing degrees of freedom were allowed for the deformable mirror to simulate additional actuators and the capability of the mirror to represent higher orders of a Zernike polynomial profile. The system was then re-optimized in Code V®.

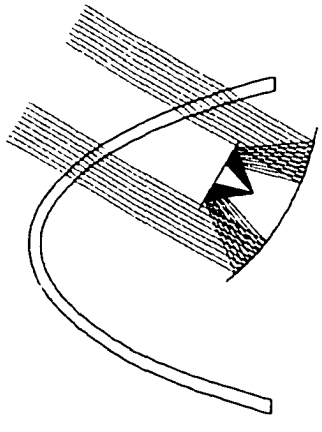

Figure 49. System at 40° Look Angle

The next chart shows a plot of RMS spot size versus look angle. The top line shows the system spot size with a non-deformable secondary flat mirror. The next line shows the decrease in spot size with the secondary allowed to translate along the optical axis. Similarly, the next lines show how higher orders of allowed deformation of the secondary contribute to a drop in RMS spot size. For comparison, the diffraction limited spot size for this wavelength and F/# is also shown.

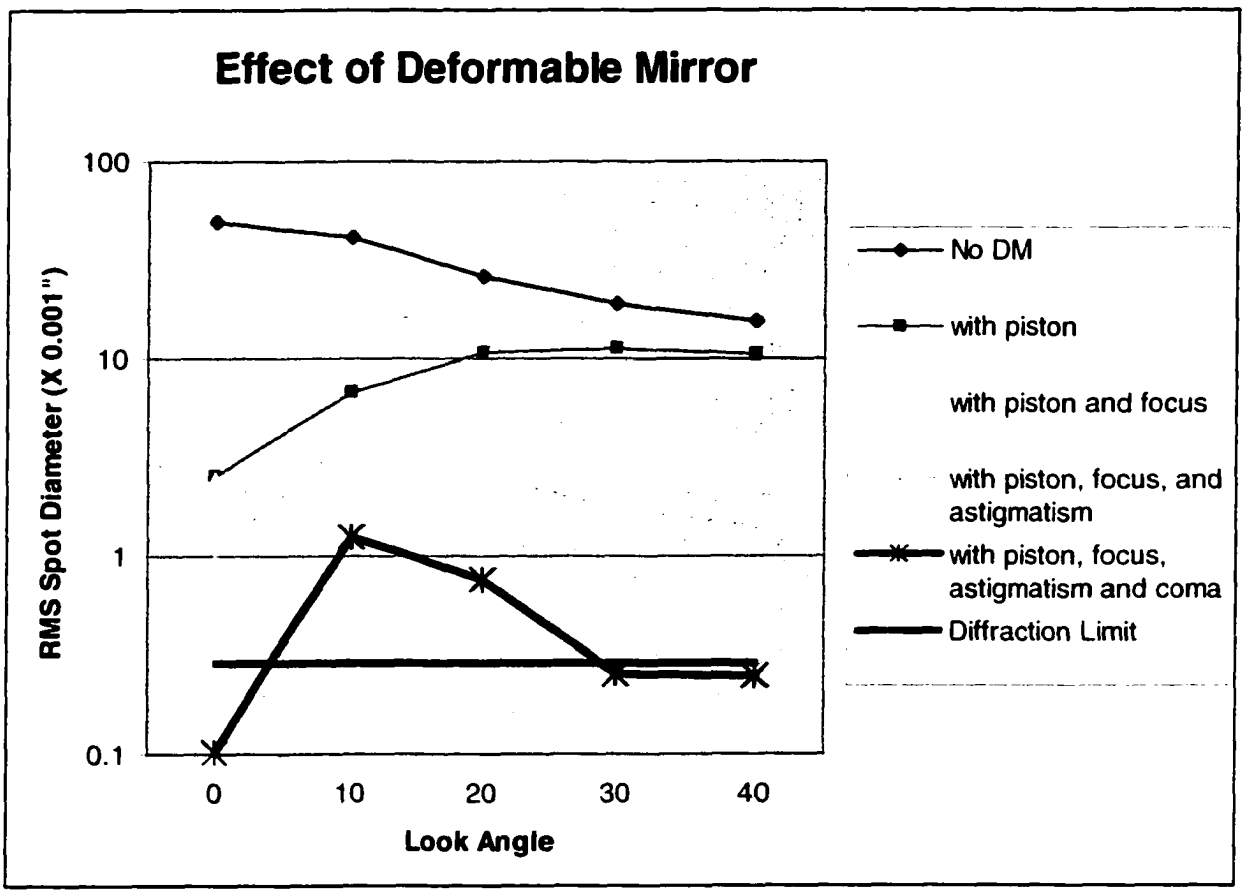

Figure 50. Spot Size vs. Look Angle

Clearly, a deformable mirror provides a great deal of leverage in correcting the aberrations.

Requirements for Deformable Mirror Correction

There are two requirements for using deformable mirrors for dynamic aberration correction. First, the range of aberration correction needed must be within the dynamic range of the deformable mirror. Deformable mirrors have a finite number of independent actuators that are used to distort the reflective surface. Each actuator has a limited range of motion and response time. The reflective surface is limited in how far it can stretch. The electronics driving the deformable mirror have a finite bandwidth. All these factors constrain the spatial and temporal range of correction of the deformable mirror. Additional corrector elements may be used in a conformal system to bring the aberration down to a level that the deformable mirror can control.

Second, the wavefront incident on the deformable mirror must be known. Traditionally, adaptive optical systems use a wavefront sensor to measure the aberrated wavefront at the mirror. In the case of conformal optical deformable mirror systems, one may only be concerned with correcting aberrations from the conformal window or dome. In that case, a wavefront sensor may be dispensed with in exchange for a sensor to detect gimbal look angle. As the aberrations from the conformal window are effectively deterministic, all that is needed is a software lookup table to set the mirror deformation corresponding to the current look angle.

Generally, passive methods of correction such as aspheric corrector elements are preferred over active methods of correction such as deformable mirrors due to increased complexity and cost. As deformable mirrors drop in price, they may find greater usage.

Software Correction

One might also correct optical aberrations with image processing.[46] Conformal optical systems present a great challenge for software correction. The amount of aberration that must be corrected is typically in the tens to hundreds of waves. Furthermore, this aberration is non-shift invariant with respect to field angle and gimbal look angle. Noise on the image plane, limited computing power on many platforms, and requirements on electro-optical system response times add additional challenge to software based aberration correction.

Surface Types

A second aspect of conformal dome design is the use of advanced surface types. Surface types are a great enabler in conformal dome design. Better performing optical systems can result from surface types with adequate degrees of freedom to describe the proper corrector shape.

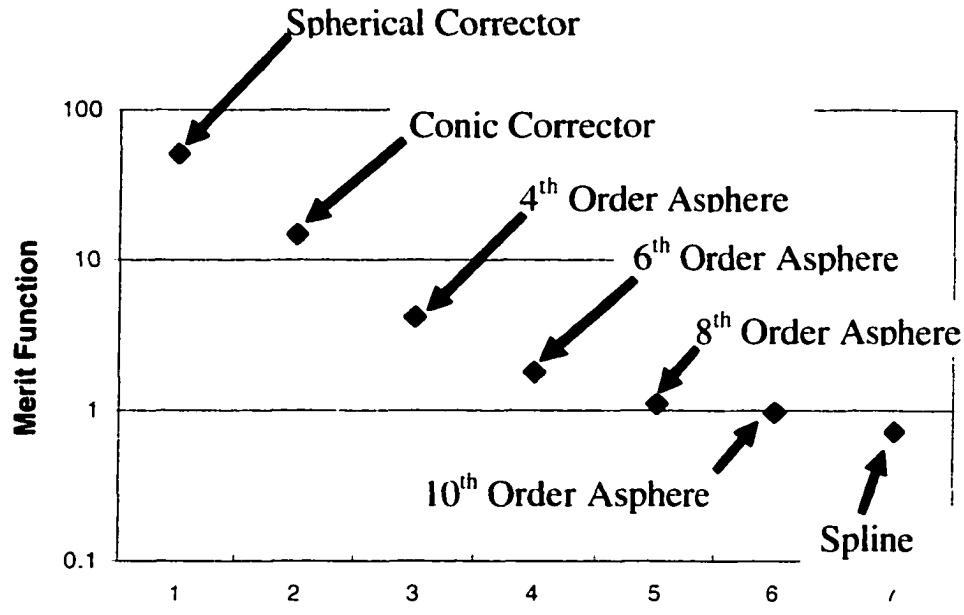

Figure 51. Improvement of correction with new degrees of freedom

An example of this is shown in Figure 51. A simple conformal optical system consisting of an equithickness F 1.5 elliptical dome, a fixed corrector, and a perfect lens was optimized with increasingly higher polynomial orders allowed on the fixed corrector. The Code V default merit function was used with equal weighting across the 40° FOR. For each configuration, the system was optimized and the merit function value was recorded. Initially, the corrector started out as an all-spherical element. Next, the two surfaces on the corrector were converted into conics. The conic term was frozen and

higher orders of the even polynomial were unleashed. Improvements to the system bottomed out at the 10th order polynomial. Freeing higher ordered terms resulted in minimal improvements. Conversion of the corrector surfaces to splines resulted in an improvement in performance beyond the even ordered aspheres. A layout of the system used in the optimization is shown below.

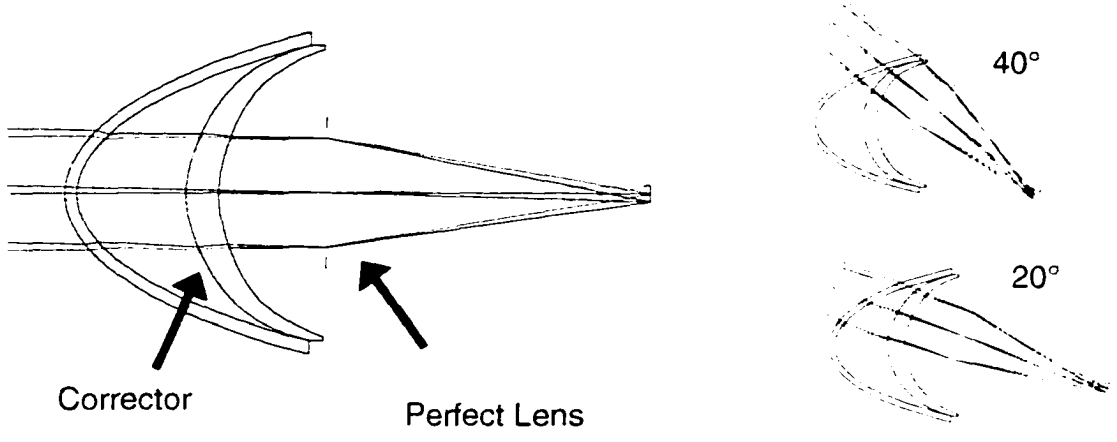

Figure 52. Fixed Corrector Example Layout

From this example, one can conclude that a conformal optical system will not perform to its full potential if the surface representation does not have a sufficient number of degrees of freedom. It is therefore very important to select a surface formula that has effective design parameters.

Louis Henri Sullivan once said that "Form follows function."[47] In the case of conformal dome design, it might be said that the formula follows the function. As was previously mentioned, the choice of solution form often has implications for the surface types that must be used. For example, one must naturally use formulas that are rotationally symmetric in the case of a fixed corrector solution. In some instances, the surface representation allows one to have insight about the optical properties of the solution form as in the case of the Zernike Wedges. Table 3 lists some of the common surface types used in conformal dome design.

Surface Types	Notes
Even ordered polynomial	Excellent starting surface type due to speed.
Splines	One may convert to a spline later in the design process to obtain a final boost in performance. Useful surface representation for the inside dome surface.
NURBS	Useful due to convex hull property and ability to model complex shapes.[48]
Anamorphic asphere	Useful with arch solution form.
Zernike surfaces	Useful with arch and Zernike wedge solution forms.
Odd polynomial	Good for correcting domes with odd terms.
X-Y Polynomial	Useful with arch solution form.

Table 3. A few surface types

There is still much room for improvements in surface types. In the past, application of new surface types has led to better conformal system performance. As new conformal window and dome shapes are used, there will undoubtedly be a need for specialized surfaces that are well matched to correct their aberrations. Furthermore, there are a number of advanced surface types that have already been developed, but are not widely used since the implementations of the surfaces are not always widely shared with the community. Finally, improvements in the optimization speed of existing surfaces can

also greatly improve the conformal design surface through making optimization with a surface practical. A silver bullet surface type can be useless if the optimization cycle associated with it is greater than the patience of the designer.

Design Tools

After the solution form and its surface representation have been chosen, the detailed design of a conformal optical system begins. There are a variety of tools available to assist the designer.

Optical Design Program

Modern optical design programs such as Code V, Zemax®, and OSLO® can be used to create a working conformal optical system. Several factors should be considered when selecting a design program for conformal optics:

- How well does it handle tilted and decentered surfaces?
- How easy is it to write macros for custom analysis and design?
- How well does it handle user defined surfaces?
- How well does it handle zoomed systems? (Zoom positions are used to model different look angles.)
- Do the default analysis functions adequately cover zoomed systems?
- Is there a base of conformal design macros available?
- Is there a good set of advanced surface types built into the program?
- How many variables are allowed for each surface?
- How available is the program?

Conformal optical designs have been successfully created with Code V, Zemax, and OSLO. The preference of one program over another can be the result of individual weighting factors assigned to the answers to the questions above.

Computer Workstation

Conformal optical design can require a fast computer. Several factors contribute to this requirement. First, in a gimbaled system, one must optimize across a sampling of look angles in the FOR. Second, many of the solution forms make use of surfaces with many parameters. In the latter stages of a design, there can be many free variables. Third, the break in symmetry from conformal optical surfaces typically requires that full ray bundles are traced. Fourth, the aspheric surfaces in the system can require a high density sampling of rays to adequately model the system performance.

Advances in the speed and memory of personal computers have made conformal optical systems design significantly more practical.

Considering that the tracing of rays in an optical system may be done in parallel, there is an opportunity to vastly improve conformal design and stray light analysis through networked computing or massively parallel processing.

Local and Global Optimization

The goal of lens optimization routines is to find the values of the free system variables that give the best performance for a given set of constraints. Design problems are often compared to looking for the lowest point in a mountainous landscape. In this analogy, latitude and longitude correspond to design parameters that may be varied such as a lens thickness and curvature. Elevation corresponds to the performance of the design as a function of the two design parameters, where a lower elevation corresponds to a better design. A design problem with n design parameters becomes an n+1 dimensional

landscape. The entire landscape represents the solution space, the range of possible configurations. In the analogy, constraints show up as forbidden regions of the landscape.

Figure 53. Solution Space

Optimization is much like hiking down the terrain in the direction of maximum descent. A local optimization routine walks the design downhill from its initial drop-off point to the first pit or valley it finds. The position where the design rests is a local minimum. However, this position may not be the absolute lowest possible elevation in the entire landscape. In the search for better performance, a designer may change the free parameters, revise constraints, manually change design parameters, or amend the performance criteria. This has the effect of altering the terrain such that a new direction of downhill travel opens up. The process may then repeat itself with a local optimization of this new starting position.

By comparison, a global optimization routine is like systematically dropping off hikers across a landscape at different samplings of latitude and longitude. Local optimization is used by each hiker to obtain the closest minimum in elevation. The positions of the lowest points are recorded as more hapless hikers are systematically

dropped off. This process repeats itself until it is stopped or the entire design space is sampled.

Damped Least Squares

One of the most common local optimization routines is Damped Least Squares (DLS) optimization [49]. This algorithm minimizes an error function defined by $\sum_i W_i \cdot (z_i - t_i)^2$. For the ith parameter, W_i is a weighting factor, t_i is the target parameter value, and z_i is the actual computed parameter value. The merit function can encompass anything from ray targets to surface curvatures to MTF performance. The error function parameters chosen by the lens designer define the system figure of merit and the idealized behavior of the system. A DLS algorithm iteratively changes the values of system variables until a local merit function minimum is reached. The designer can typically adjust the change in each parameter (the step size) to avoid instabilities in the optimization process.

Surface Conversion Macros

Surface conversion macros can be very advantageous for switching surface types without impacting the performance of the nominal design. For instance, one may begin an optical design with a standard polynomial asphere for speed and simplicity. Later in the design process, one may convert to a surface type with additional degrees of freedom. Flexibility in switching surfaces allows one to find the surface type most suited to a particular application. Figure 54 shows how one may start with an even polynomial

asphere surface type and then progress to using other surface formulas using conversion tools.

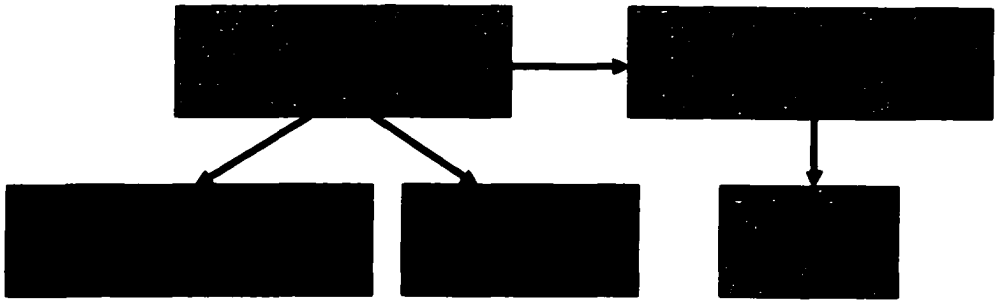

Figure 54. Surface conversion is a useful tool in the design process

Analysis Tools

Standard analysis tools familiar to the optical designer retain their usefulness in conformal design. These tools include spot diagrams, ray aberration curves, energy on detector calculation, Zernike wavefront decomposition, and graphical aberration field plots. The new twist with conformal design is that it becomes useful to plot many of the standard analyses versus the gimbal look angle.

Direct Solve Tools

Direct solve tools can be beneficial for quickly generating conformal dome designs. The generated designs may perform well enough to be the final design, or they may serve as a starting point for further refinement. The best example of this type of tool is one that implements the Wassermann-Wolf equations. The Wassermann-Wolf equations can be numerically solved to generate a fixed corrector that exactly corrects for

spherical aberration and coma at boresight. One extremely useful feature of the Wassermann-Wolf equations is that the centered axisymmetric optical system upstream and downstream from the corrective optic is completely arbitrary. Trotta found that this allows one to use the equations to generate corrective optics for a variety of different domes. [50]

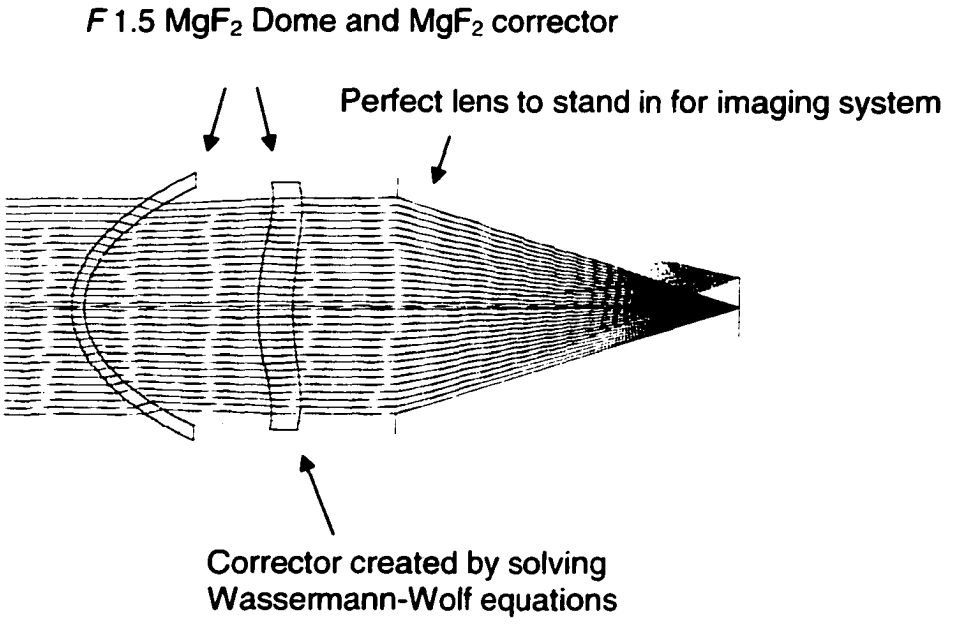

Figure 55. System created with Wassermann-Wolf aplanatic solve approach

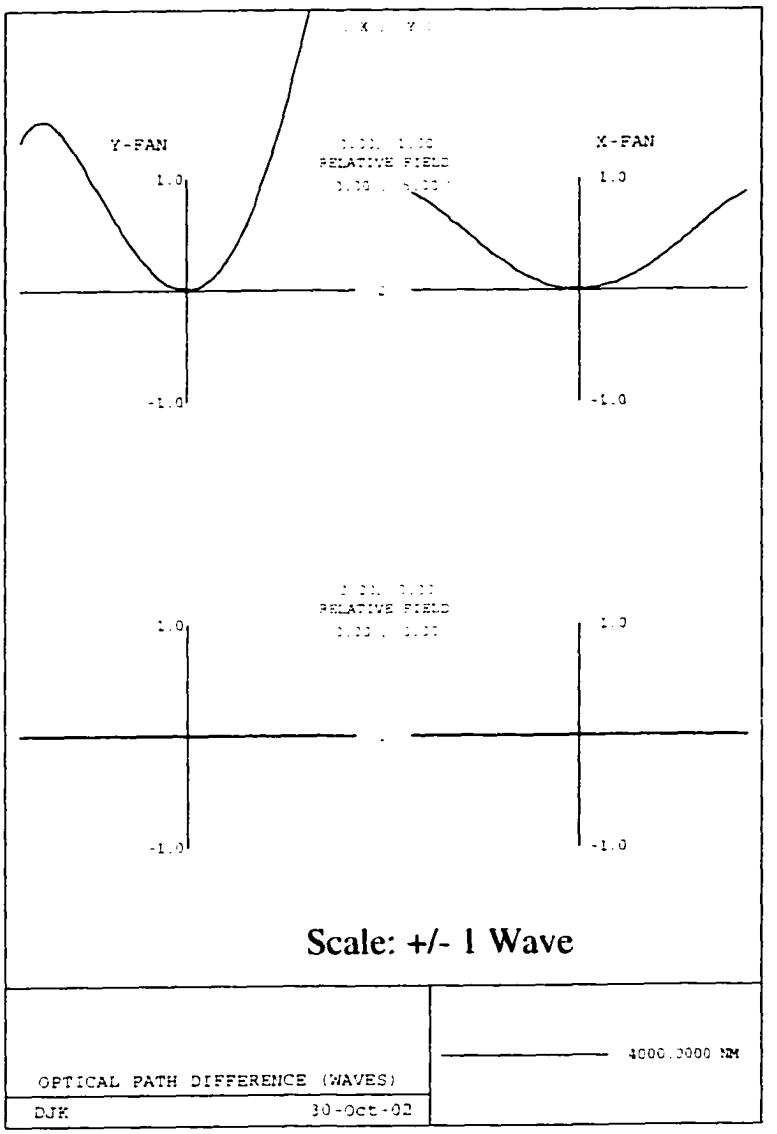

Figure 56. Wavefront Aberration Plot of Wassermann-Wolf System

One of the deficiencies of the Wassermann-Wolf direct solve tool is that it does not work for systems containing non-axisymmetric or tilted/decentered optical elements. The new aspheric design equations developed in this dissertation correct this deficiency

and allow the generation of a fixed corrector for systems with arbitrary symmetry or tilted/decentered components.

An example illustrates the deficiency of the Wassermann-Wolf equations to handle non-symmetric elements. Shown in Figure 57 is the equal thickness fineness ratio 1.5 MgF_2 dome decentered by 0.03". Solving the Wassermann-Wolf equations for this configuration yields a system with poor performance; see Figure 58. Using the new design equations on the same system yields an acceptable system.

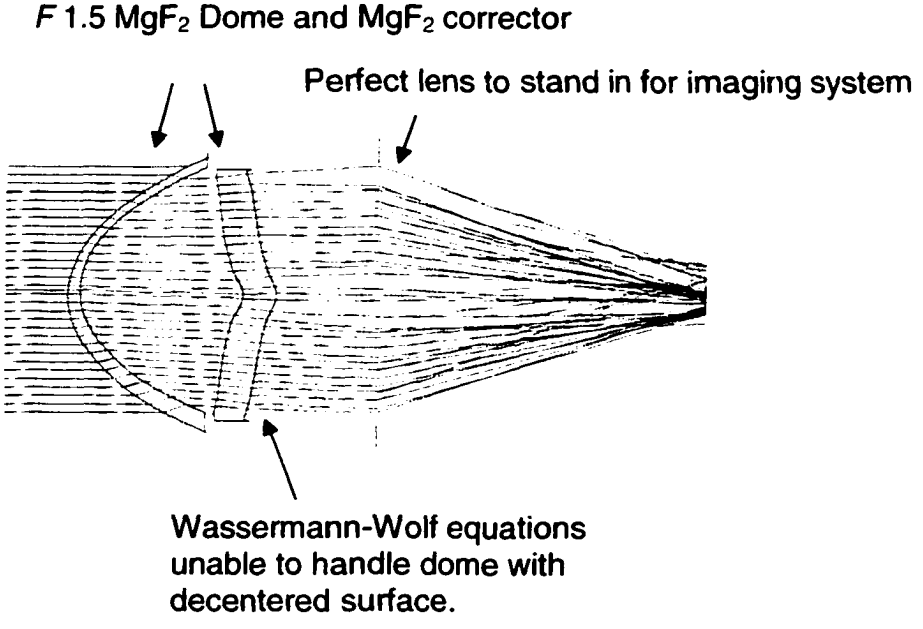

Figure 57. Wassermann-Wolf approach does not work with decentered elements

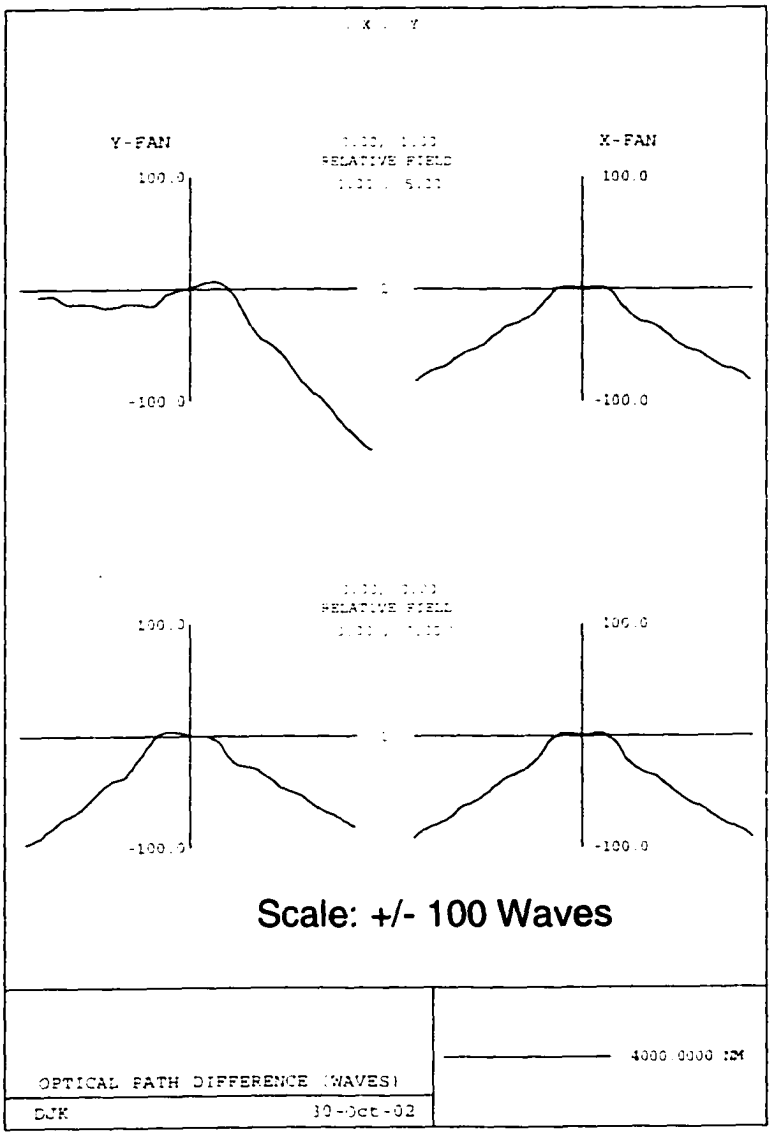

Figure 58. Wavefront Aberration Plot of System in Figure 57

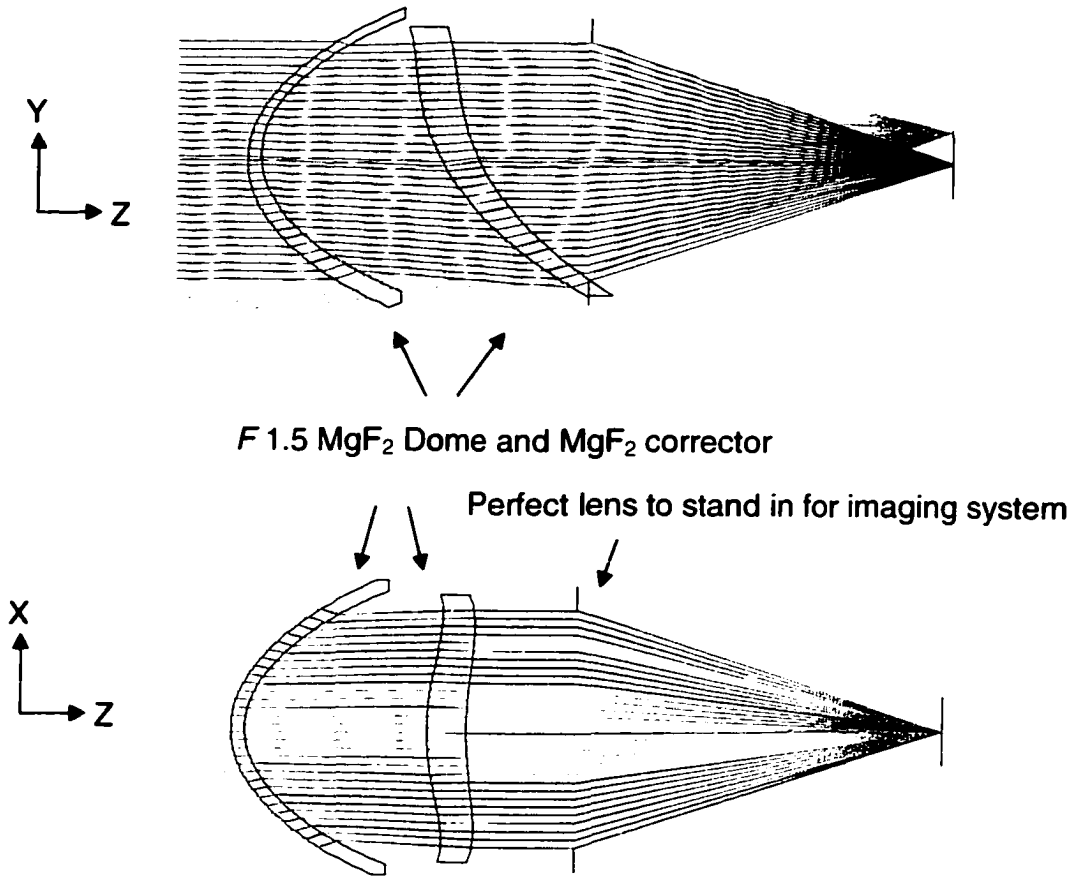

Figure 59. New design equations handle asymmetry

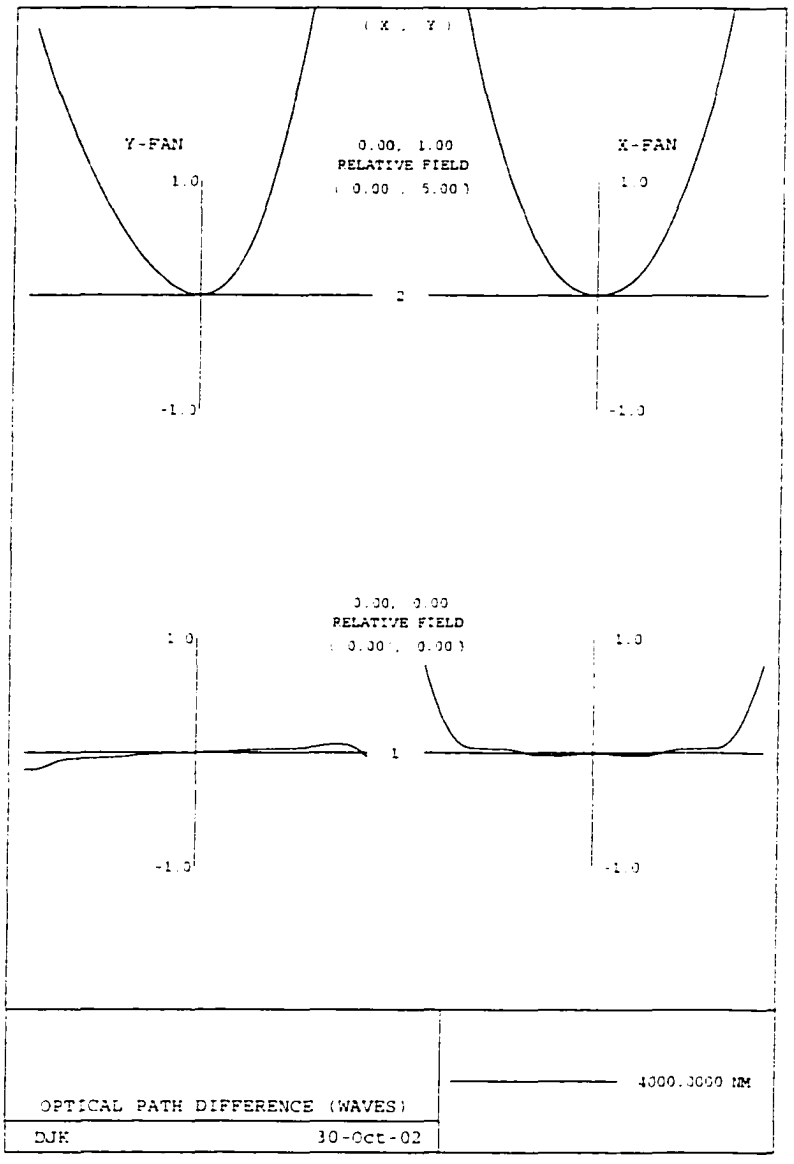

Figure 60. Wave Aberration Plot of System in Figure 59
SCALE: +/- 1 Wave

With the new design equations, tilted and decentered elements can be placed in the system. The wave aberration at the zero degree field in Figure 60 can be diminished further with a higher accuracy solution of the new design equations.

The Wassermann-Wolf equations and the Code V macro implementing them are covered in greater detail in Chapter 2. The new design equations created for this dissertation are covered in greater detail in Chapter 3.

Summary

This chapter reviewed the prior art in conformal optical design and synthesized an overall approach to conformal optical design. As much of the early work in conformal optics is not available in the open literature, the best source of information was found to be in the patent literature. The patent literature showed a variety of solutions for conformal optics. These solutions included dynamic aberration generators, deformable mirrors, fixed corrector elements, GRINs, and holograms. The patent literature presents point solutions, but does not necessarily instruct one in the methodology of conformal optical design. Therefore, the second half of Chapter 1 established a methodology for conformal optical design. Initial design considerations were given. These included the front end/back end distinction and the effect of materials, fineness ratio, aperture ratio, and thickness.

Beyond the initial considerations, three categories of resources are valuable in conformal optical design. These categories are solution forms, surface types, and design tools. Solution forms represent the general approach that the designer takes to correcting aberrations. A variety of forms are already known including articulating elements such as an arch corrector, pairs of counter-rotating contoured Risley prisms, fixed correctors, and deformable mirrors. Surface types are the formulas used to model the solution form. Conformal optical systems are unique in that they often require highly aspheric systems with strange contours that are not always adequately modeled with even ordered aspheric polynomials. Exotic surface types such as splines and anamorphic aspheres provide useful degrees of freedom. Design tools are required to develop a solution form. These

tools run the gamut from the conventional to the unusual. Tools include commercial optical design software, fast computers, optimization, and standard optical analyses. Other tools include surface conversion macros and direct solve methods. In a direct solve method, one generates the surfaces of a corrector element by solving a pair of equations. For rotationally symmetric systems, the Wassermann-Wolf equations may be used to remove coma and spherical aberration through the automatic design of a fixed corrector element. These equations break down for asymmetric systems, and are therefore not useful for conformal systems containing non-rotationally symmetric optics. At the end of Chapter 1, a new tool was previewed that allowed the direct solution of a fixed corrector for a system containing asymmetric optics.

"Someone told me that each equation I included in my book would halve the sales. I did put in one equation, Einstein's famous equation, E = MC squared. I hope that this will not scare off half of my potential readers. "
Stephen Hawking
A Brief History in Time

CHAPTER 2- Wassermann-Wolf Equations

Introduction

In Chapter 1, direct solution algorithms were described as an effective tool for generating the surface profiles of a corrector optic. As part of this dissertation, the Wassermann-Wolf equations were implemented into a Code V macro. An implementation of the Wassermann-Wolf algorithms in Code V has not been widely available, although the algorithm is implemented in OSLO and as privately developed functions.

Understanding the Wassermann-Wolf equations is useful for two reasons. First, the Wassermann-Wolf equations are valuable for the design of axially symmetric systems. They provide a means of creating corrector optics to precisely control a tangential ray fan. Second, the Wassermann-Wolf equations are derived using a similar approach to that used to create the generalized aspheric design equations in Chapter 3. The Wassermann-Wolf equations operate on a special case with a ray fan contained in the Y-Z plane and with centered rotationally symmetric optics. The new equations in Chapter 3 operate on a general case with a ray bundle comprised of rays are not necessarily in the Y-Z plane, and optics that may contain surfaces that are non-rotationally symmetric or that are tilted and decentered.

Introduction to the Wassermann-Wolf Equations

In 1948, G.D. Wassermann and E. Wolf published a paper on the theory of aplanatic aspheric systems.[51] An aplanatic system is corrected for spherical aberration, and coma. In the paper, they introduced a numerical solution for achieving exact aplanatism for a centered axisymmetric system with an arbitrary number of surfaces. Aplanatism is achieved through the design of two neighboring aspheric surfaces such that a fan of rays passing through the system meets the Abbe Sine Condition. The aspheric surface profiles are designed by solving a pair of coupled differential equations. Any number of centered axisymmetric surfaces may be before or behind the aspheric surfaces. Figure 61 shows the location of the aspheric surfaces relative to the rest of the system.

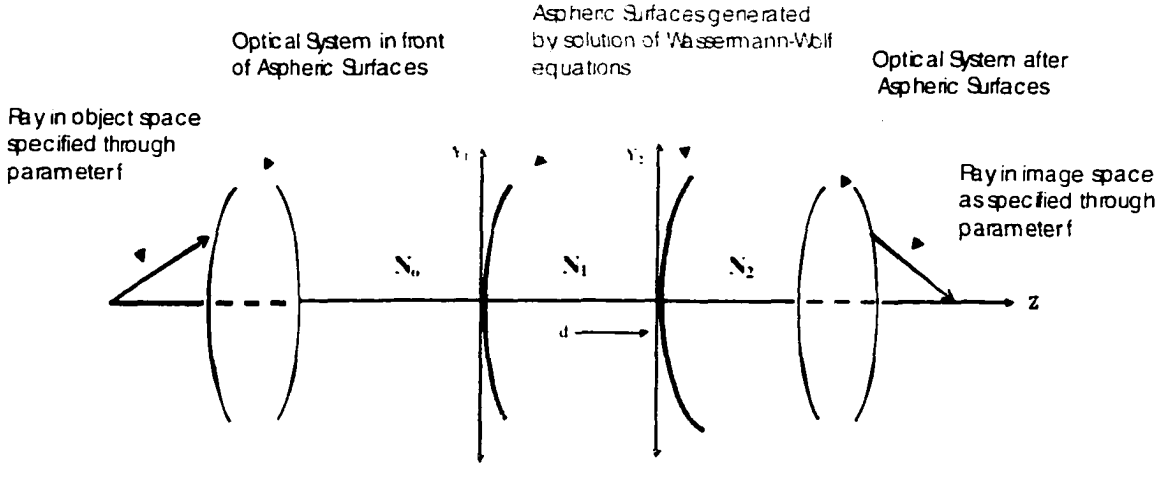

Figure 61. Layout of a typical system

The designer is free to specify the location of the neighboring aspheric surfaces in the optical system, the thickness between them, and the indices of refraction. Furthermore, the designer must specify a parameterized fan of rays in object space. Each

ray in the fan is traced through the optical system to the tangent plane of the desired location of the first aspheric surface generated by the Wassermann-Wolf equations. At this tangent plane, the height of intercept and angle with respect to the z axis is recorded. This is shown in Figure 62. N_0 and N_1 are the indices of refraction immediately before and after the aspheric surface. U_0 and h_1 are the variables corresponding to the angle and height, respectively for ray f.

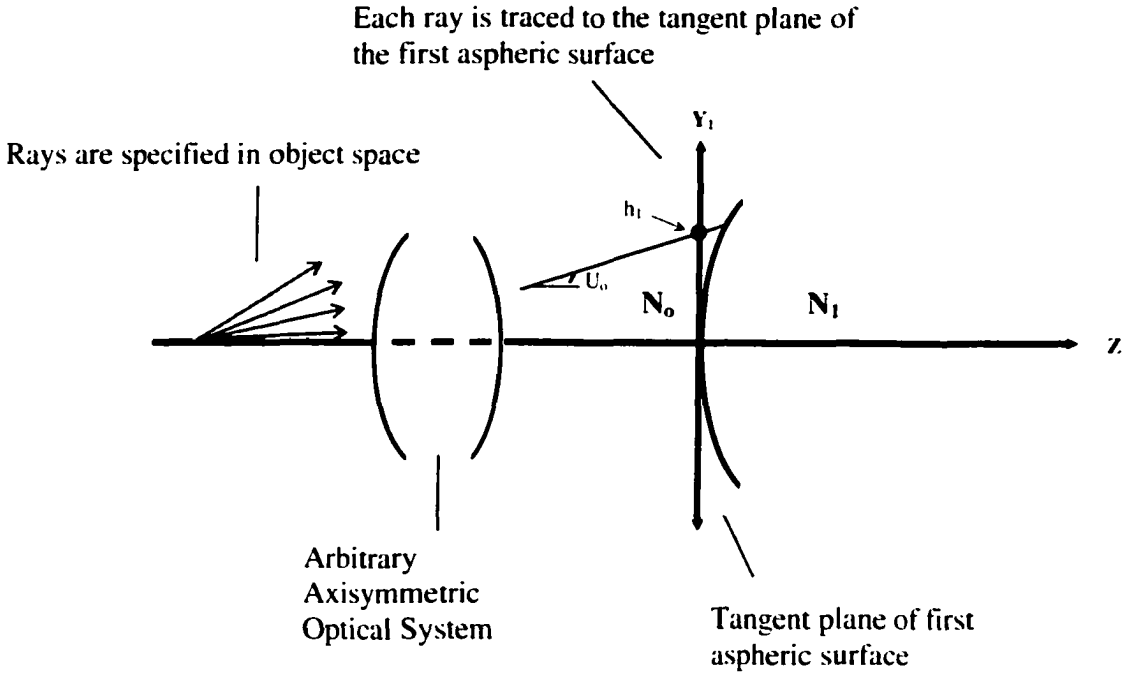

Figure 62. Object Space Ray Fan

Similarly, the designer must specify a desired parameterized set of rays in image space. Each ray in the fan is reverse traced to the tangent plane of the second aspheric surface. Once again, at the tangent plane the angle with respect to the z axis and height of intercept is recorded. This is shown in Figure 60. U_2 and h_2 are the angle and height of image ray f at the second tangent plane, respectively for ray f. There is a one-to-one

correspondence between a specified ray in object space and a specified ray in image space. The designer is essentially defining the input ray fan in the system and the desired ray fan that he or she wants the input rays to become. N_2 is the index of refraction immediately after the second aspheric surface.

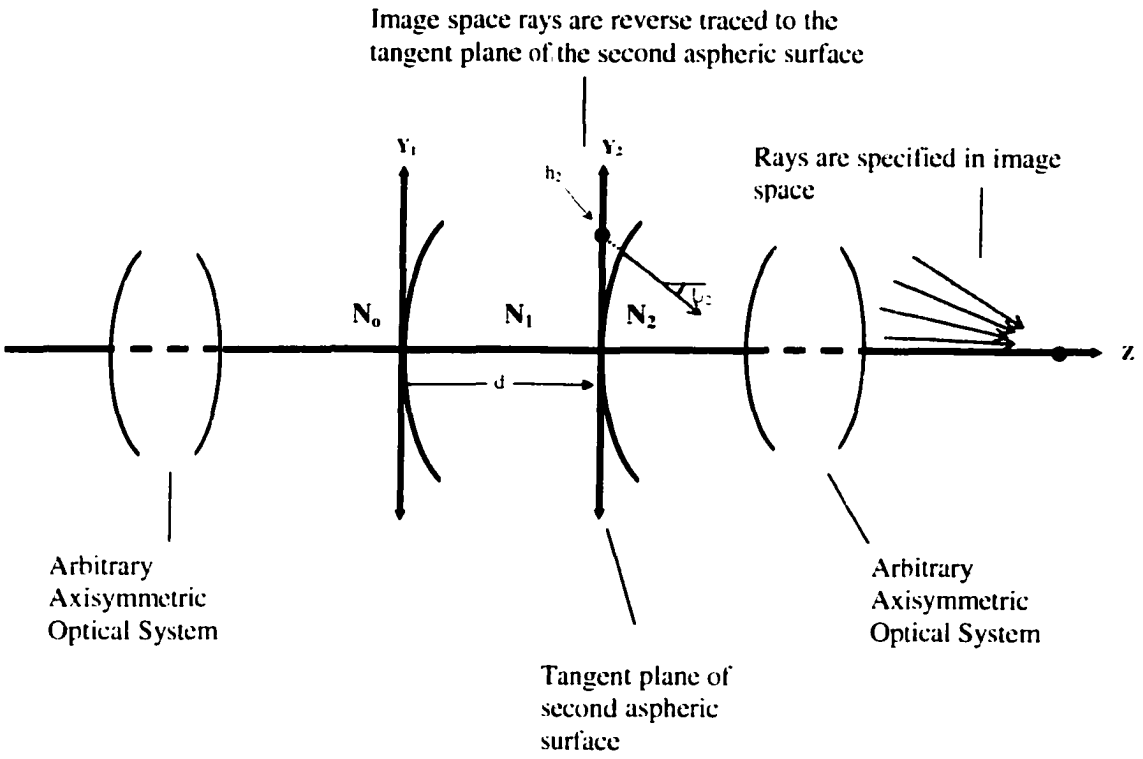

Figure 63. Image space ray fan

As will be discussed in greater detail later, the designer may define the object and image space rays such that they meet the Abbe Sine Condition. This makes the system aplanatic.

In the specific case where no additional surfaces exist after the second aspheric surface, specifying the ray fan in image space directly gives one the angle of each ray and allows a simple calculation to determine the height at the second tangent plane.

By means of forward tracing the parameterized fan of rays emanating from the object point, a relation is determined of the form:

$$U_{o'} = U_{o'}(f), \quad H_1 = H_1(f)$$

Equation 4

Similarly, reverse tracing the ray fan emanating from the image point to the tangent plane of the second aspheric surface will determine a relation of the form:

$$U_2 = U_2(f), \quad H_2 = H_2(f)$$

Equation 5

Ingredients of the Wassermann-Wolf Equations

It is necessary to understand the constituent variables and expressions in the equations. Consider the passage of a ray through the axisymmetric optical system containing two adjacent aspheric surfaces separated by a distance d as shown in the next figure.[52] The aspheric surfaces have profiles as yet to be determined, but possess the property of refracting the ray shown in object space into the desired ray in image space.

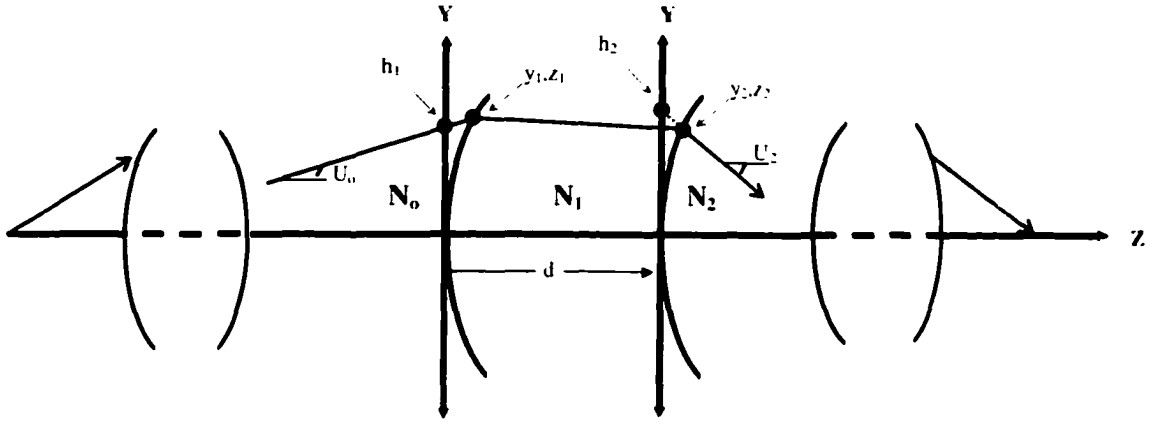

Figure 64. Design of two aspheric surfaces to attain Aplanatism

As before, the object space ray has an angle and height of incidence at the first aspheric surface tangent plane of U_0 and h_1 respectively. At the point of intercept with the first aspheric surface, the object space ray will have coordinates y_1, z_1. Similarly, reverse ray tracing the image space ray to the second aspheric surface tangent plane gives an angle and height of U_2 and h_2. At the point of intercept with the second aspheric surface, the image space ray will have coordinates y_2, z_2.

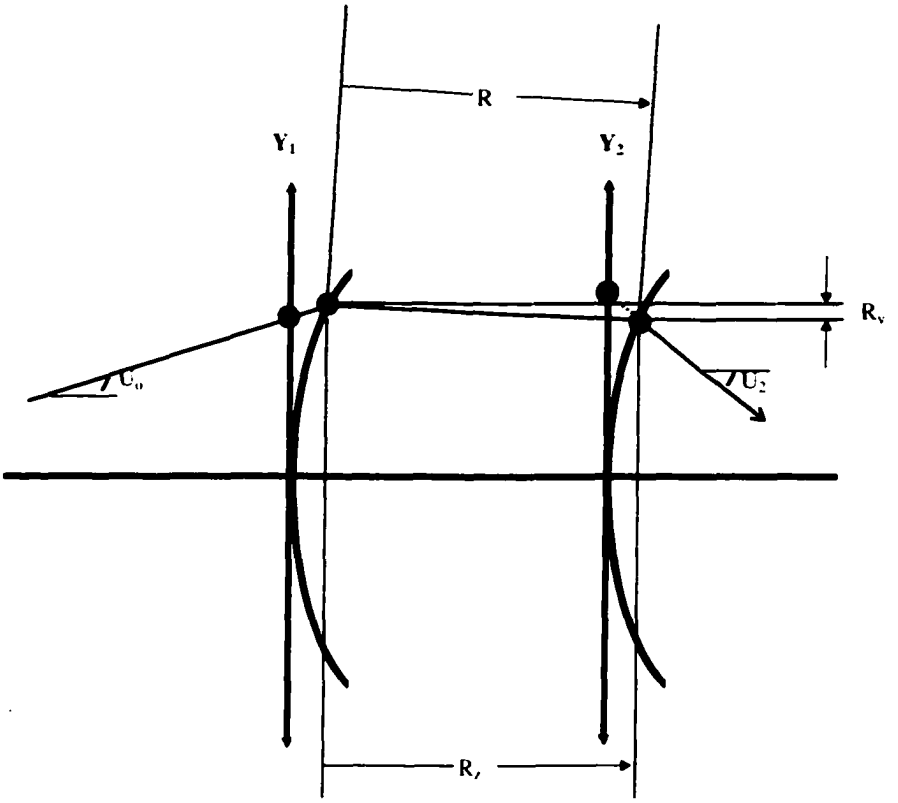

Figure 65. R, R_z and R_y

Let

$$R_y = y_2 - y_1 \quad \text{and} \quad R_z = d - z_1 + z_2 \quad \text{and} \quad R = \sqrt{R_y^2 + R_z^2}$$

Equation 6

R is the distance in real units that the ray traverses in the space between the first aspheric surface and the second aspheric surface. From R, R_y, and R_z, the ray angle in this space may be calculated.

The angle of the ray as it progresses from the first aspheric surface to the second aspheric surface is given by:

$$\sin U_1 = \frac{R_y}{R} \quad \text{and} \quad \cos U_1 = \frac{R_z}{R}$$

Equation 7

Looking more closely at the first aspheric surface shows a relationship between the incident angle of the ray, the height at the tangent plane, and the y,z coordinates of the ray on the aspheric surface.

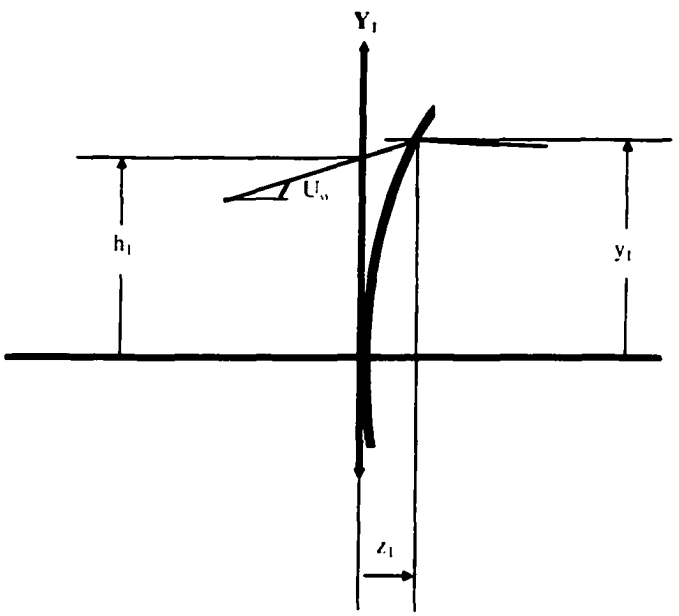

Figure 66. Ray intercept at first aspheric surface

The y intercept is therefore given by:

$$y_1 = h_1 + z_1 \tan U_1$$

Equation 8

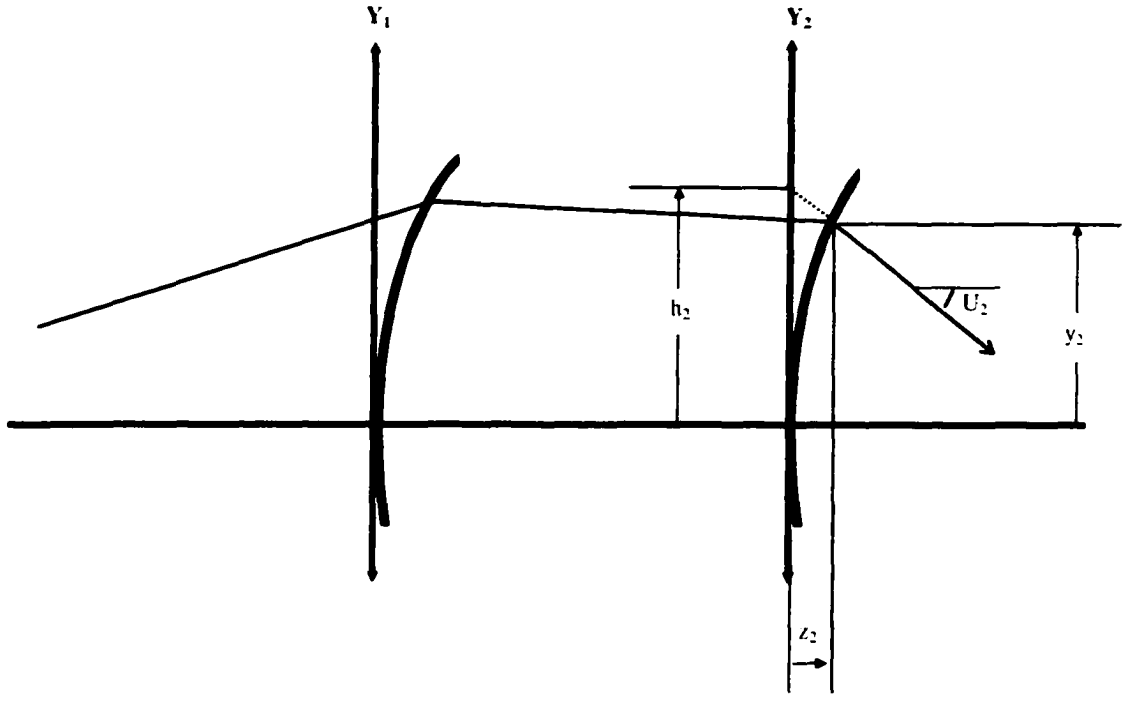

Figure 67. Ray intercept at second aspheric surface

Similarly, a relationship may be determined for the y coordinate of the ray at the second aspheric surface.

$$y_2 = h_2 + z_2 \tan U_2$$

Equation 9

The previous two relations are important in that they relate the sag of the aspheric surfaces to the y intercept points on the surface. Generally, the ray angles and heights at the tangent planes are known. (They are determined from tracing the object space and image space rays.) If the surface sags at the point of intercept may be determined in some fashion, the relations allow one to solve for the y coordinate at that sag z.

Wassermann-Wolf Equations

Up to this point, relations have been created for a single ray traversing through the optical system. Each ray is part of a fan described by an equation with a parameter f that is varied to select the ray. The relations that have been created for a single ray are identical for every ray in the fan.

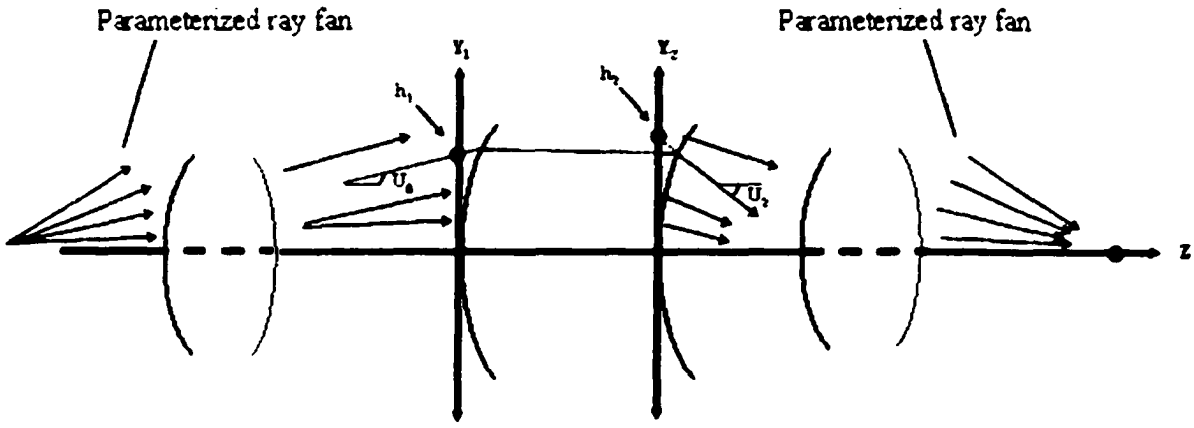

Figure 68. Rays propagating through the optical system

Using Snell's law and the relations shown in this chapter, Wassermann and Wolf derived a pair of differential equations to describe the slope of the aspheric surfaces with respect to a change in the ray parameter f. The aspheric surfaces are designed such that each object space ray is refracted[††] by the first surface toward the second surface where it is refracted into a corresponding ray in the image space ray fan. The net effect is that the ray fan in object space becomes the desired ray fan in image space.

[††]With minor modifications, these equations may also be used to design two reflective surfaces. Reference: G. Wassermann and E. Wolf, "On the Theory of Aplanatic Aspheric Systems," Proc. Phys. Soc. 62B, 1949.

The Wassermann-Wolf equations are:[53]

$$\frac{dz_1}{df} = -\left[\frac{N_1 R_z - N_0 R\cos U_o}{N_1 R_y - N_o R\sin U_o} + \tan U_o\right]^{-1} \left(\frac{dh_1}{df} + z_1 \frac{d\tan U_o}{df}\right)$$

Equation 10

and

$$\frac{dz_2}{df} = -\left[\frac{N_1 R_z - N_2 R\cos U_2}{N_1 R_y - N_2 R\sin U_2} + \tan U_2\right]^{-1} \left(\frac{dh_2}{df} + z_2 \frac{d\tan U_2}{df}\right)$$

Equation 11

These equations define the change in sag of the aspheric surfaces with respect to a change in the ray parameter f. Solving these two differential equations numerically yields the profiles of the two desired aspheric surfaces to bring the ray fans together. The numerical process is typically an integration step by step over f to solve for each z_1, z_2, y_1, and y_2 beginning at the known starting point of the gut ray and proceeding to the top of the ray fan. This may be done using a standard numerical method such as Runge-Kutta integration.[54] The result are two sets of Y-Z values corresponding to the zone and sag along the aspheric surface. These values must be curve fit to a functional form such as a polynomial series so that the surface may be used in an optical design program.

Steps in Wassermann-Wolf Solution

1. Forward trace ray to first tangent plane starting from the optical axis (f=0) and moving out.
2. Store data in array for h_1 and u_0 of ray
3. Reverse trace ray to second tangent plane starting from the optical axis (f=0) and moving out.
4. Store data in array for h_2 and u_2 of ray
5. Solve Wassermann-Wolf equations using information from the ray just traced. Finite differences are used to calculate $\frac{dh_1}{df}$, $\frac{dh_2}{df}$, $\frac{d\tan U_1}{df}$ and $\frac{d\tan U_2}{df}$. (Solution is initiated at known aspheric sag values such as $y_1=0$, $z_1=0$ and $y_2=0$, $z_2=0$.) A method such as the Runge-Kutta method may be used.
6. The results from step 5 are two z values corresponding to points on the two aspheric surfaces. These z values are then related to corresponding y values using the equations: $y_1 = h_1 + z_1 \tan U_1$ and $y_2 = h_2 + z_2 \tan U_2$.
7. The y, z values for the two surfaces are added to the list of calculated y,z points for the surfaces and used as a seed value for the next iteration.
8. Steps 1-7 are repeated as necessary until the edge of the aperture is reached.
9. Finally, a curve fit of y,z values to a surface representation is performed. This can be a spline or a polynomial fit.

Defining Ray Fans

The Wassermann-Wolf equations give one complete control over a single tangential ray fan. The solution created by solving the Wassermann-Wolf equations is dependent on how that ray fan is defined.

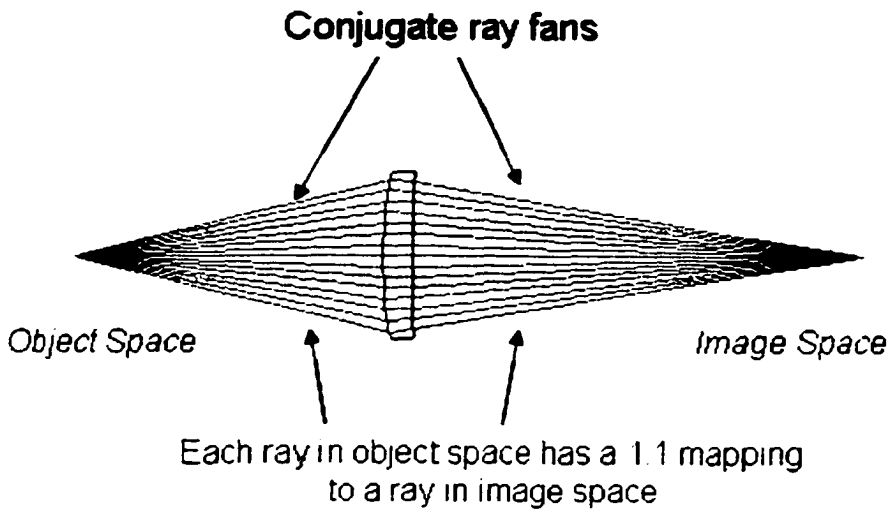

Figure 69. Singlet created with Wassermann-Wolf Equations

For instance, one may define collimated outgoing ray fans such that they are identical to the collimated incident ray fans, but scaled. Solving the Wasserman-Wolf equations in this case creates a beam expander as shown in Figure 70. Residual on-axis aberration is due to the accuracy of the technique used to solve the Wassermann-Wolf equations. The aberrations present in the beam expander are shown in Figure 71 One may also create a collimator by defining a ray fan that originates at a near object point and is focused at an infinite image point. This is shown in Figure 73.

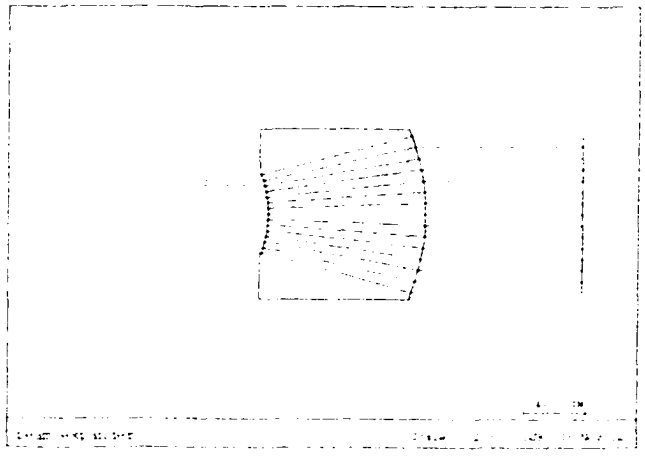

Figure 70. Beam Expander

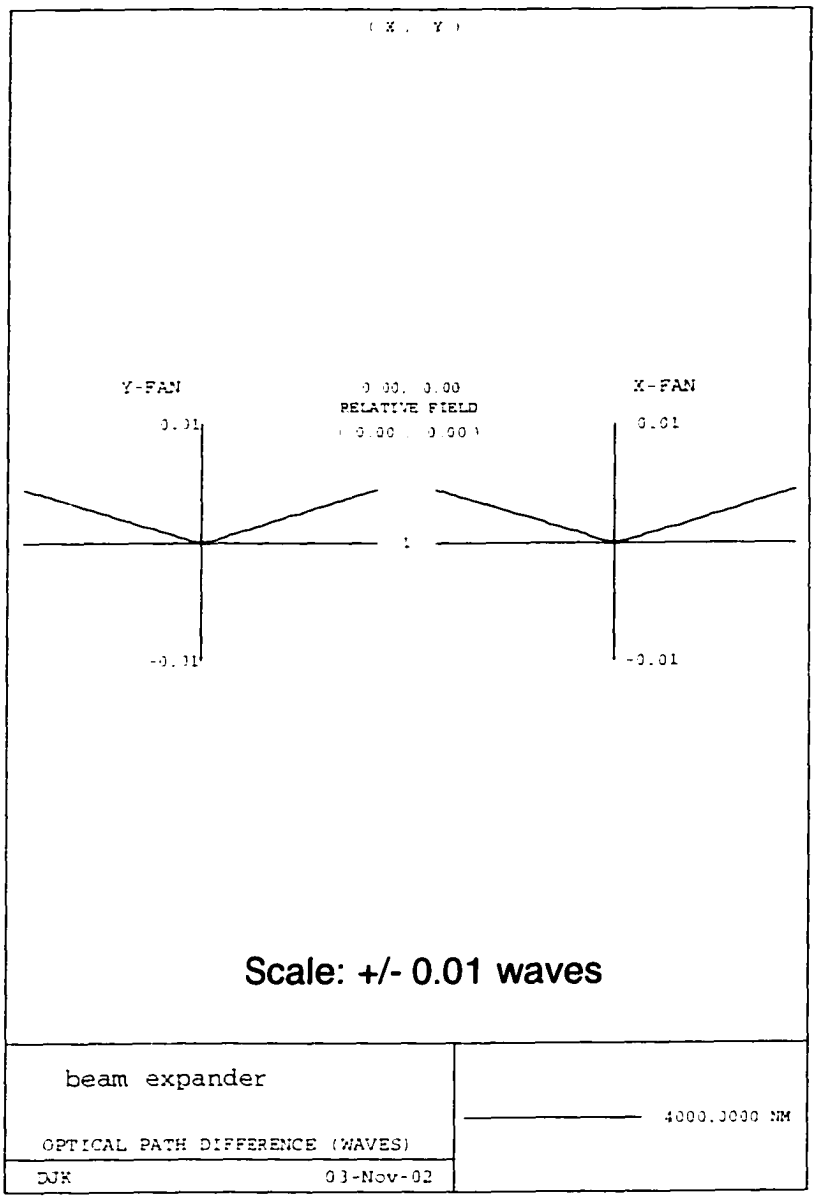

Figure 71. Wave Aberration Plot of Beam Expander shown in Figure 70

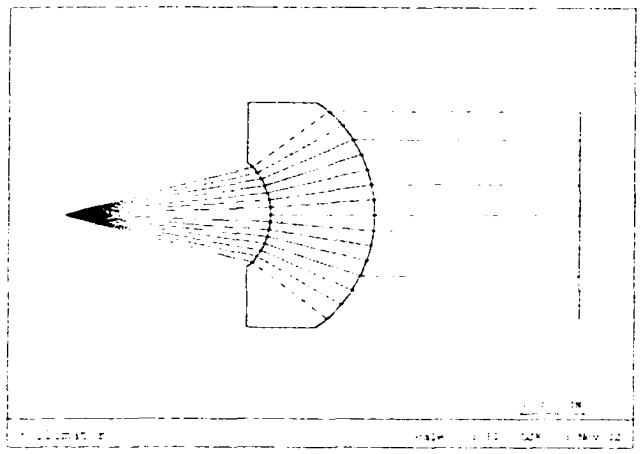

Figure 73. Collimator created with W-W equations

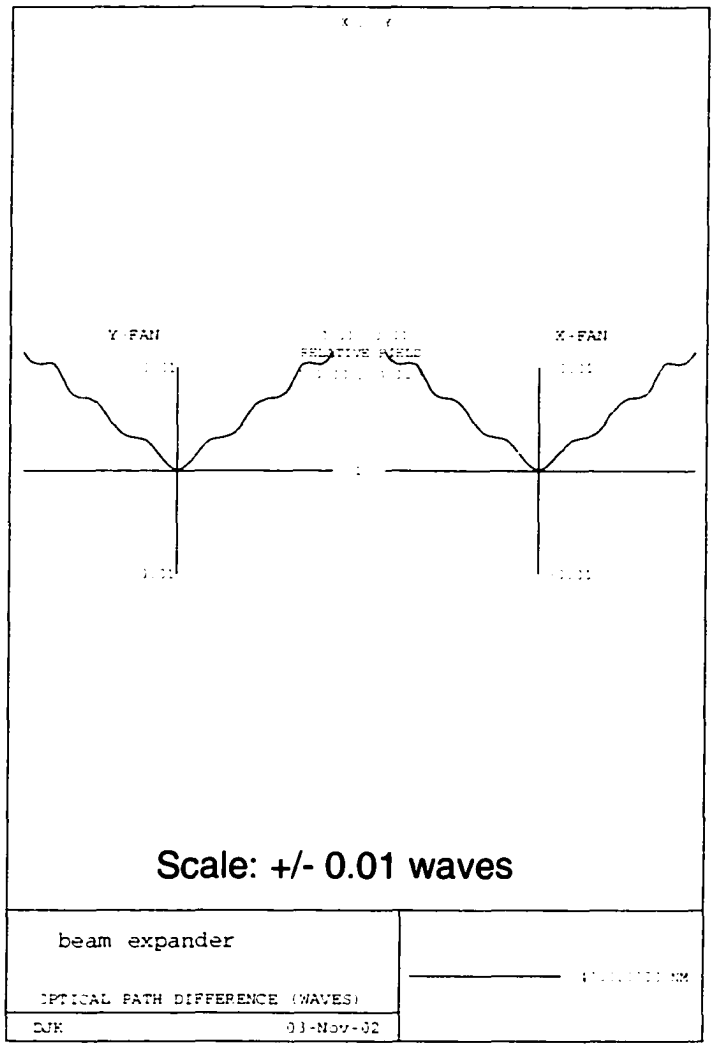

Figure 72. Wave Aberration Plot of Beam Expander shown in Figure 71

Abbe Sine Condition

One extremely useful way of defining the ray fans is to define them such that they satisfy the Abbe Sine Condition. Solving for this condition corrects coma. If spherical aberration is also corrected, this is all that is needed to create a finite field of view. A system created in this way can also serve as an excellent starting point to correct other aberrations.

The Abbe Sine Condition was described by Ernst Abbe in 1872. Abbe was a German mathematician and physicist who worked for Carl Zeiss to create the Zeiss Optical Works in 1866. This company designed and fabricated high performance optical systems, particularly microscopes. Abbe studied the theoretical foundations of imaging and was therefore able to design many microscope objective designs based upon calculations rather than trial and error.[55] In his studies, Abbe noticed that coma could be considered a change in magnification with aperture. Consequently, setting a condition for constant magnification over the aperture of an objective would remove coma.[56] Figure 74 shows a lens with a high amount of coma and the effect that it has on magnification with respect to aperture.

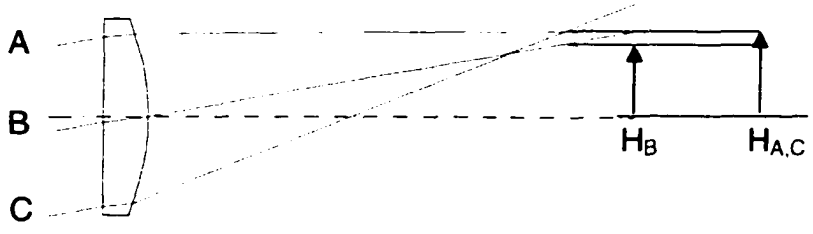

Figure 74. Plano-conic singlet with coma

Rays A and C which pass through the top and bottom of the lens respectively cross at image height $H_{A,C}$. Ray B goes through the center of the stop and is at an image height of H_B at the z position where rays A and C cross. The height difference shows a change in magnification with respect to aperture.

In comparison, a singlet with no coma will have rays A, B, and C cross at the same height. Both lenses have the same f-number, focal length, wavelength, and are also corrected for spherical aberration.

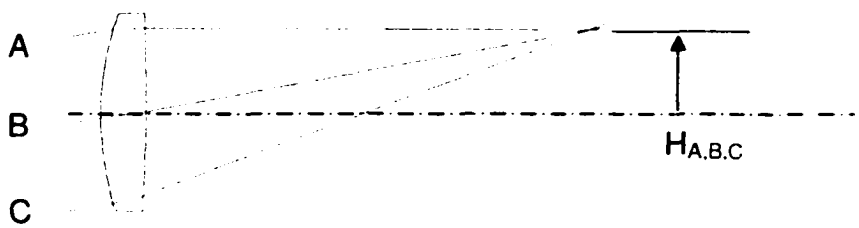

Figure 75. Double aspheric singlet with no coma

The difference between these two lenses is their conformance to the Abbe Sine Condition. For an infinite conjugate, the Abbe Sine condition is given by: [57]

$$focal\_length = \frac{h}{\sin(\theta')}$$

Equation 12

In Equation 12, θ' is the angle of a given marginal ray in image space; h is the height in object space. If the ratio is not constant for all rays incident on the lens from an object at infinity, the lens violates the Abbe Sine Condition.

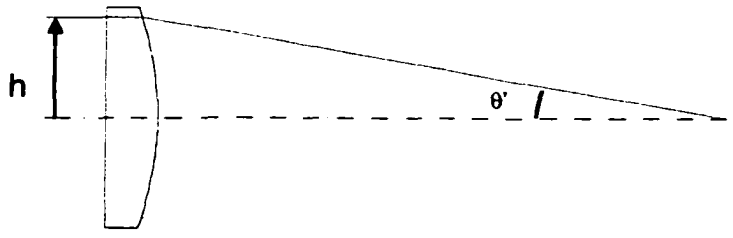

Figure 76. Sine condition for an infinite conjugate

The ratio of the incident ray height to the sine of the ray angle in image space may be plotted across the aperture for the two singlets. The singlet with no coma maintains a constant ratio across the aperture. In contrast, the singlet with coma has a ratio that is equal to the paraxial focal length only for rays near the optical axis.

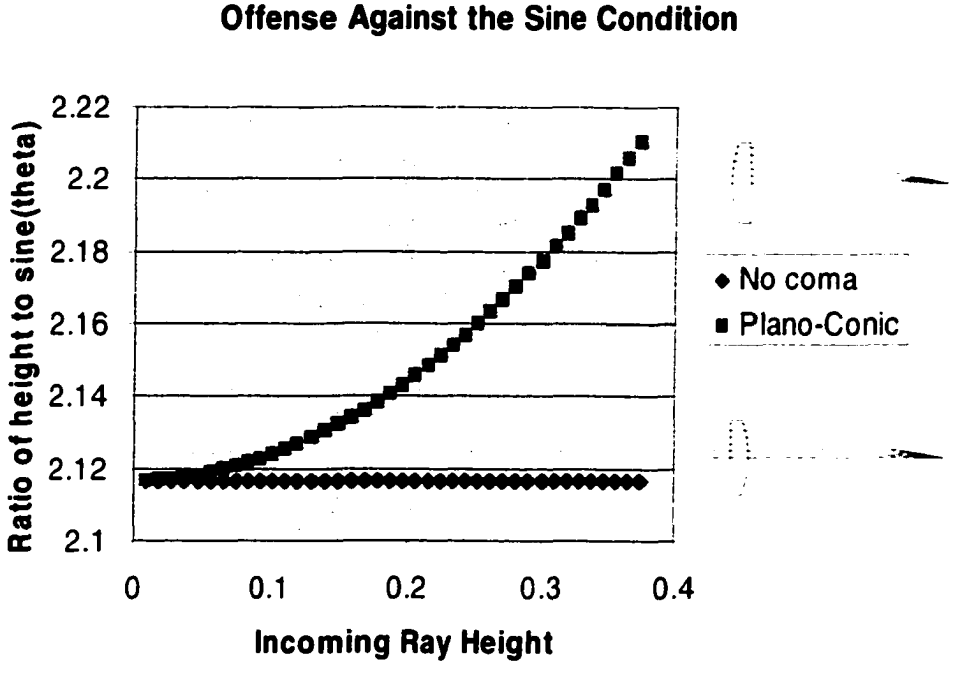

Figure 77. Plot of height to sine theta ratio

The lens with coma shows a significant deviation from the sine condition. One may examine the wave fan and spot diagram for the lens with a 10° field. The spot diagram at the 10° field shows the characteristic comet-like shape indicative of coma.

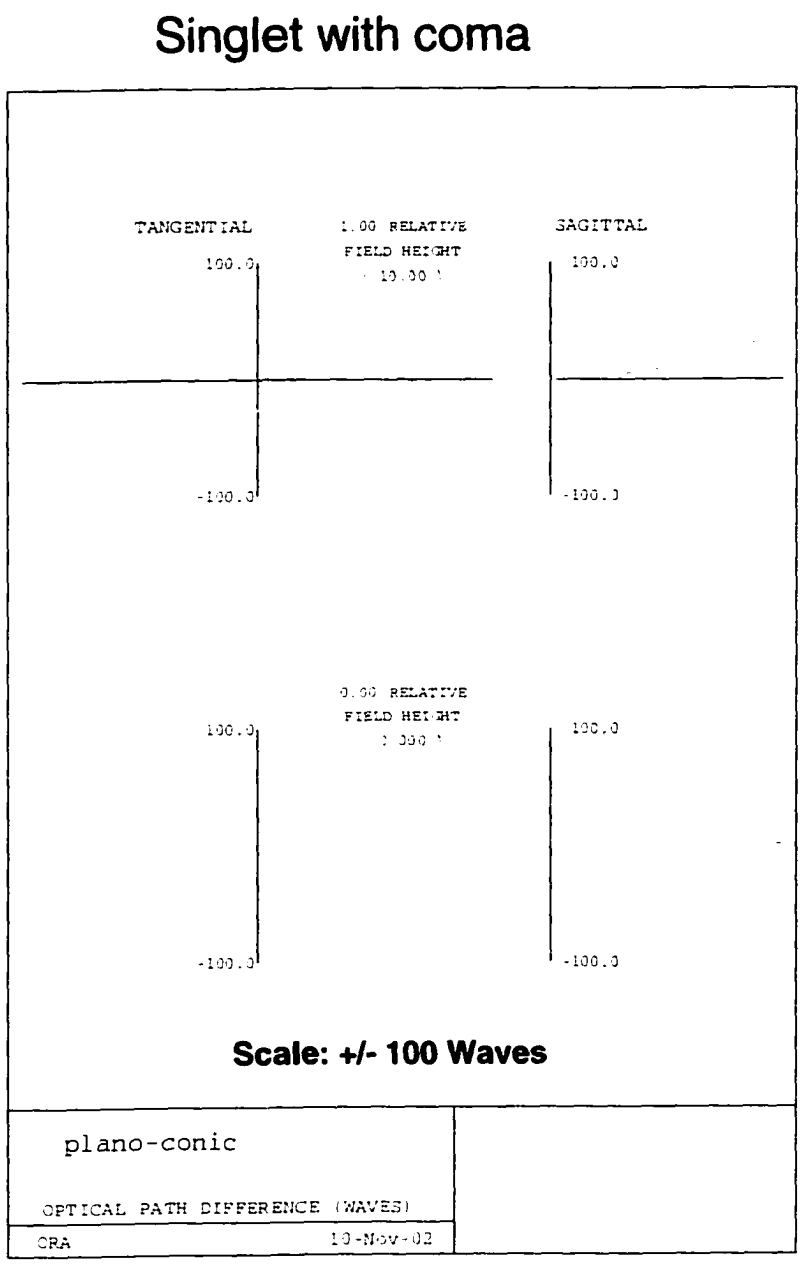

Figure 78. Wave aberration plot for singlet with coma

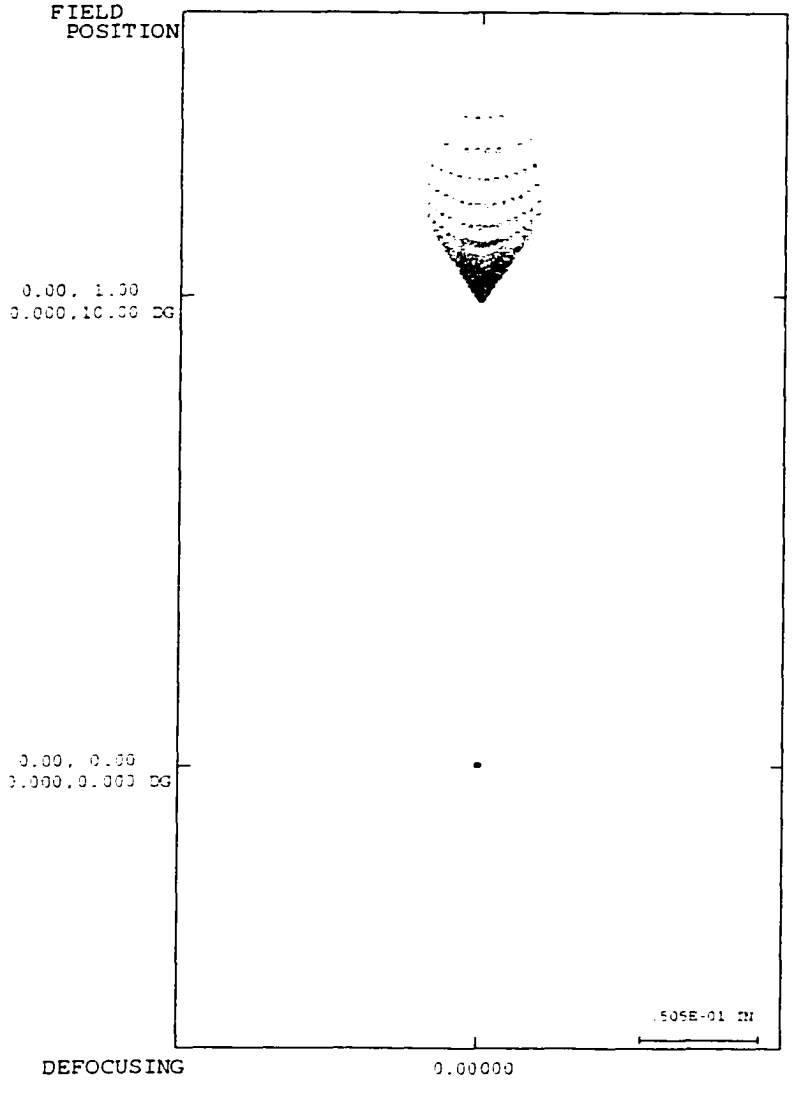

Figure 79. Spot Diagram for Singlet with Coma

As may be expected, the lens with no coma meets the sine condition. As this lens is also corrected for spherical aberration, this lens is aplanatic. The aberration content at high field angles is dominated by field curvature and astigmatism. The RMS spot size of the lens that meets the sine condition is smaller than the lens with coma, 0.0075 inches

vs. 0.039 inches. The centroid of the lens with coma is skewed away from the chief ray by 440 microns. The lens without coma is skewed away from the chief ray by only 0.8 microns.

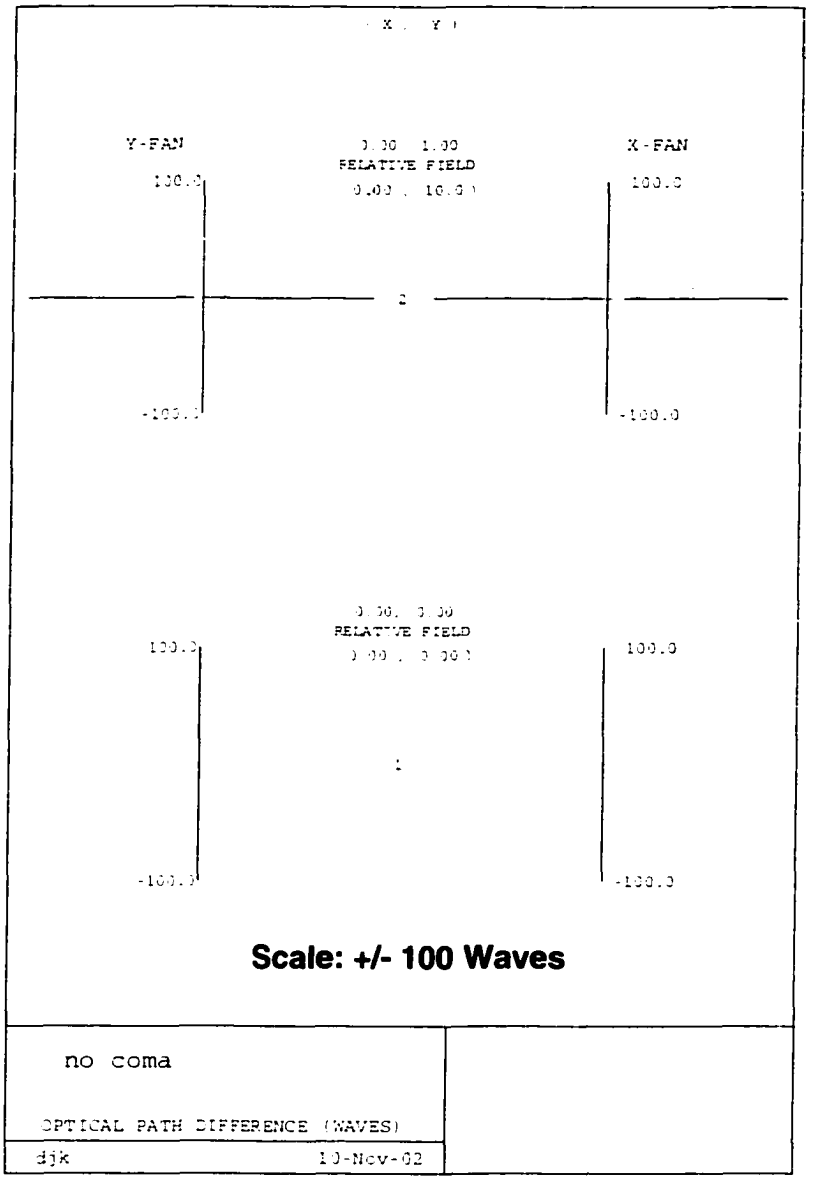

Figure 80. Wave fans and spot diagram for singlet with no coma

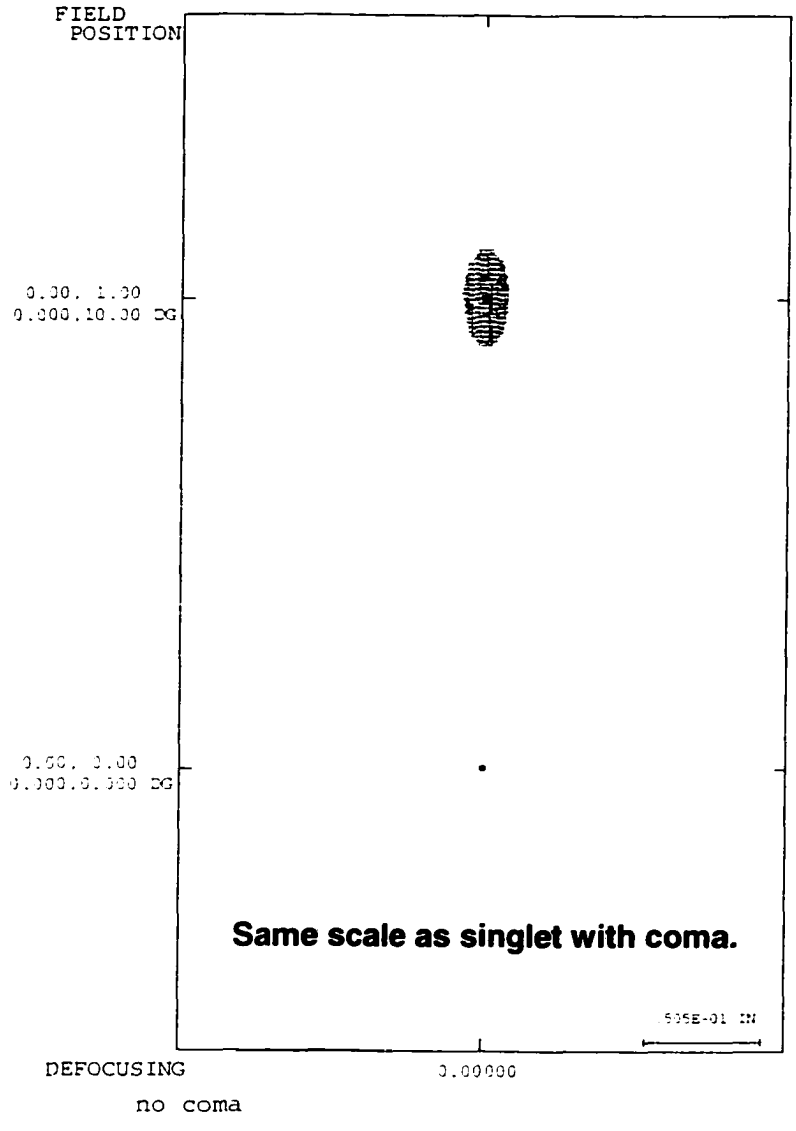

Figure 81. Spot Diagram for Singlet with No Coma

One may calculate the highest half- angle that each singlet makes before the geometrical spot size is at the threshold of being larger than the diffraction limited spot size. The lens with coma has a maximum half field angle of 0.05°. The lens without coma has a maximum half-field angle of 0.75°. Assuming that this half-angle describes

the edge of a diffraction limited imagery patch centered on the optical axis, the lens without coma has a patch with an area 225 times larger than the lens with coma!

Finite conjugate case

For a finite conjugate case, the Abbe Sine condition may be obtained by setting the paraxial magnification equal to the marginal magnification.[58]

For paraxial rays, the approximation sin(θ)=θ may be used. The paraxial magnification is given by:

$$m = \frac{n \cdot \theta}{n' \cdot \theta'}$$

Equation 13

Where n and n' are the refractive indices of the media containing the incident and refracted rays respectively, and θ and θ' are the slopes of the incident and refracted marginal rays.

The marginal magnification is given by:

$$M = \frac{n \cdot \sin\theta}{n' \cdot \sin\theta'}$$

Equation 14

Setting the marginal magnification equal to the paraxial magnification leads to the Abbe Sine Condition:

$$m = \frac{n \cdot \theta}{n' \cdot \theta'} = \frac{n \cdot \sin\theta}{n' \cdot \sin\theta'}$$

Equation 15

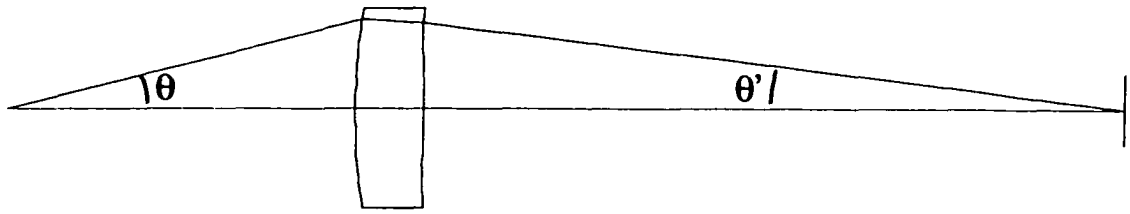

Figure 82. Angle definition for Abbe Sine Condition

To meet the Abbe Sine Condition, the magnification $\frac{n \cdot \sin(\theta)}{n' \cdot \sin(\theta')}$ of the optical system for each marginal ray should stay constant. As with the infinite conjugate case, obeying this condition makes the lens aplanatic.

Cardinal Points

It is instructive to look at the Abbe Sine Condition with respect to the cardinal points of the optical system. The cardinal points of an optical system originate from paraxial optics. In paraxial optics, the small angle approximation is made wherein tan(θ) and sin(θ) are both replaced by θ. (Sine θ ≅ Tangent θ ≅ θ) As a consequence of this approximation, one may define the first order behavior of any complex centered optical system with a set of cardinal points.[59] The first order behavior of an optical system describes the size and location of an image for a given object location.

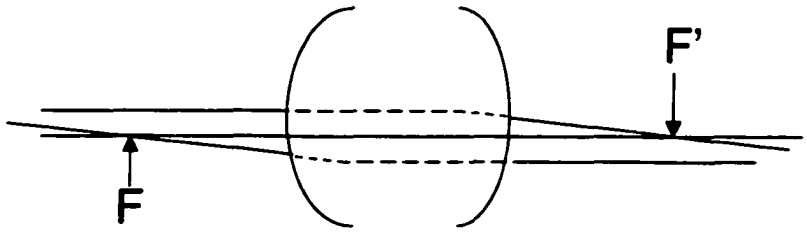

Figure 83. Front and rear focal points

Two cardinal points are the front and rear focal points, F and F'. The front focal point F may be located by reverse tracing a paraxial marginal ray from a point image at infinity. The location where the ray crosses the optical axis in object space is the front focal point. Similarly, the rear focal point F' may be located by tracing a paraxial marginal ray from a point object at infinity and noting the location where it crosses the axis in image space.

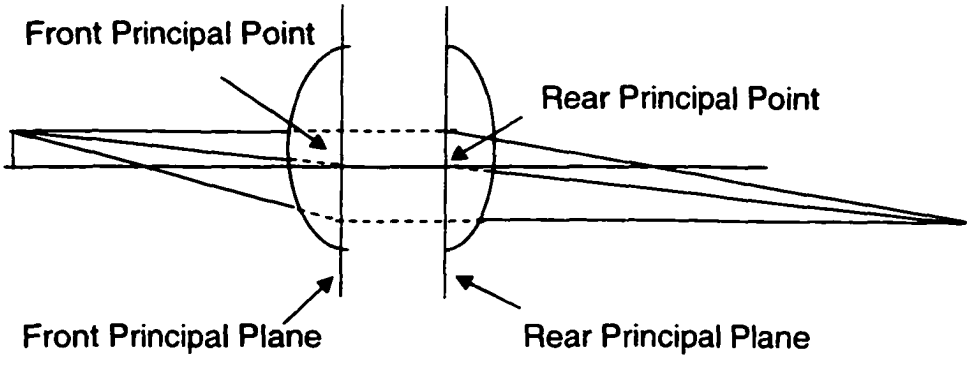

Figure 84. Front and rear principal planes

The next two cardinal points are the front and rear principal points, which arise out of the principal planes. The front and rear principal planes are defined as the conjugate planes in an optical system of unit transverse magnification. That is, a ray that intersects the front principal plane at height h will emerge from the rear principal plane at height h. The intersections of the principal planes with the optical axis are the front and rear principal points. Additionally, the distance from the rear principal point to the rear focal point is equal to the rear focal length of the system.

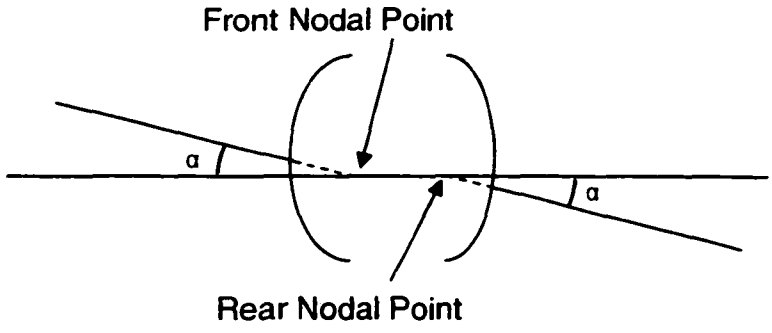

Figure 85. First and second nodal points

The final two cardinal points are the front and rear nodal points. These are defined as the points in the optical system of unit angular magnification. In other words, a ray that enters the front nodal point at some angle alpha, will emerge from the optical system from the rear nodal point at the same angle alpha. If the object space and image space are of the same index of refraction, the nodal points will coincide with the principal points.[60]

Figure 86. Principal Planes in Paraxial Approximation

In a real optical system, rays will deviate from the paraxial approximation. In particular, the principal planes will no longer be conjugate. A ray entering the front principal plane at a given height may leave from the rear principal plane at a different height. However, if the optical system satisfies the Abbe Sine Condition for a given pair of conjugate points, the principal planes become spherical surfaces centered about those

object and image points.[61] In this configuration, the heights are measured from the spherical principal surfaces. Each ray intersecting the front spherical principal surface has a 1:1 mapping onto the rear spherical principal surface. In other words, the height of the ray at the front principal surface will leave the rear principal surface at the same height. See Figure 87. Note that an optical system that satisfies the Abbe Sine Condition for one pair of conjugate object and image points might not satisfy the condition for a different pair of conjugate points along the axis. In that case, the ray entering the first principal surface will no longer emerge at the same height from the second principal surface.

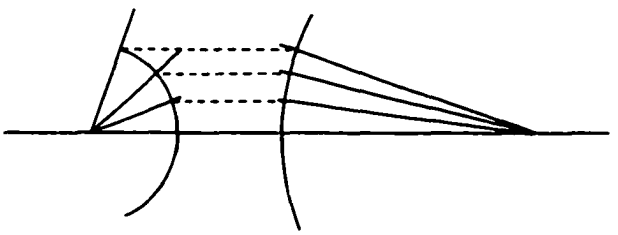

Figure 87. Abbe Sine Condition Leads to Curved Principal Surfaces

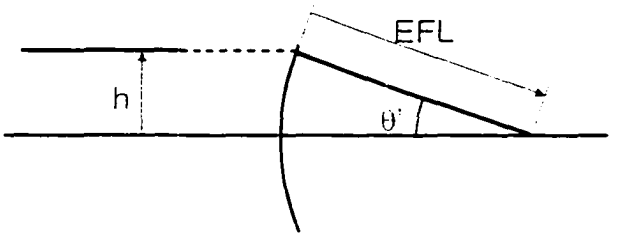

Figure 88. Principal Surfaces for Infinite Conjugate Sine Condition

If a system meets the Abbe Sine Condition for an object at infinity, the rear principal plane becomes curved about the rear focal point.

$$focal\_length = \frac{h}{\sin(\theta')}$$

Equation 16

Several key aspects of the Abbe Sine Condition may be summarized. First, satisfaction of the Abbe Sine Condition is necessary and sufficient to remove coma in a nominal design that has also been corrected for spherical aberration. Coma is defined as a variation of magnification with aperture. The Abbe Sine Condition defines a constant magnification with aperture. Second, coma deviates the centroid of a spot away from the chief ray by a substantial amount compared to a lens with no coma. Third, coma limits the unaberrated field of view of a lens. Removing coma and spherical aberration creates an aberration-free region around the center of the field. Beyond this region, other aberrations such as field curvature and astigmatism will start to limit the field of view. Four, the Abbe Sine Condition prescribes that the principal planes be spherical surfaces centered about the object and image points. Five, the Abbe Sine condition stipulates a 1:1 mapping between the principal surfaces. In the paraxial case, the principal planes are defined as conjugate planes of unit magnification. A paraxial ray piercing the front principal plane at height h leaves the rear principal plane at the same height h. In the non-paraxial case, the Abbe Sine Condition defines a pair of principal surfaces curved about the object and image points. A real ray emanating from the object point will pierce the front principal surface at a given height. The ray will leave the rear principal surface

at that same height. Each point on the front principal surface will map to a point on the rear principal surface.

Application to the Wassermann-Wolf Equations

The Abbe Sine Condition is a very powerful tool for controlling coma. It is particularly interesting in that it reduces aberrations for off-axis image points using only an on-axis ray fan. Using the Abbe Sine Condition to define ray fans for the Wassermann-Wolf equations creates a dynamic duo in correcting aberrations.

The Wassermann-Wolf equations are of broad interest due to their ability to design two neighboring aspheric surfaces for an arbitrary centered optical system. In 1957, the Wassermann-Wolf method was extended by Evelyn Vaskas to remove the neighboring surface requirement.[62] She showed that for k surfaces in between the aspheric surfaces, k+2 differential equations are needed to solve for the aspheric profiles.

In 1995, Pat Trotta applied the Wassermann-Wolf equations to the solution of conformal optical systems.[63] Trotta demonstrated that the Wassermann-Wolf equations are very effective for creating a fixed corrector for a conformal missile dome. Trotta's work was subsequently incorporated into OSLO. In Trotta's OSLO implementation, two neighboring aspheric surfaces in a system may be updated each optimization cycle with profiles generated by the Wassermann-Wolf equations.

A similar design capability did not exist in Code V. Hence, the Wassermann-Wolf equations were implemented into a Code V macro for this dissertation. The design

goal of the macro was to allow for the design of axisymmetric conformal dome fixed correctors.

The Code V macro follows the steps previously outlined for the solution of the Wassermann-Wolf equations.

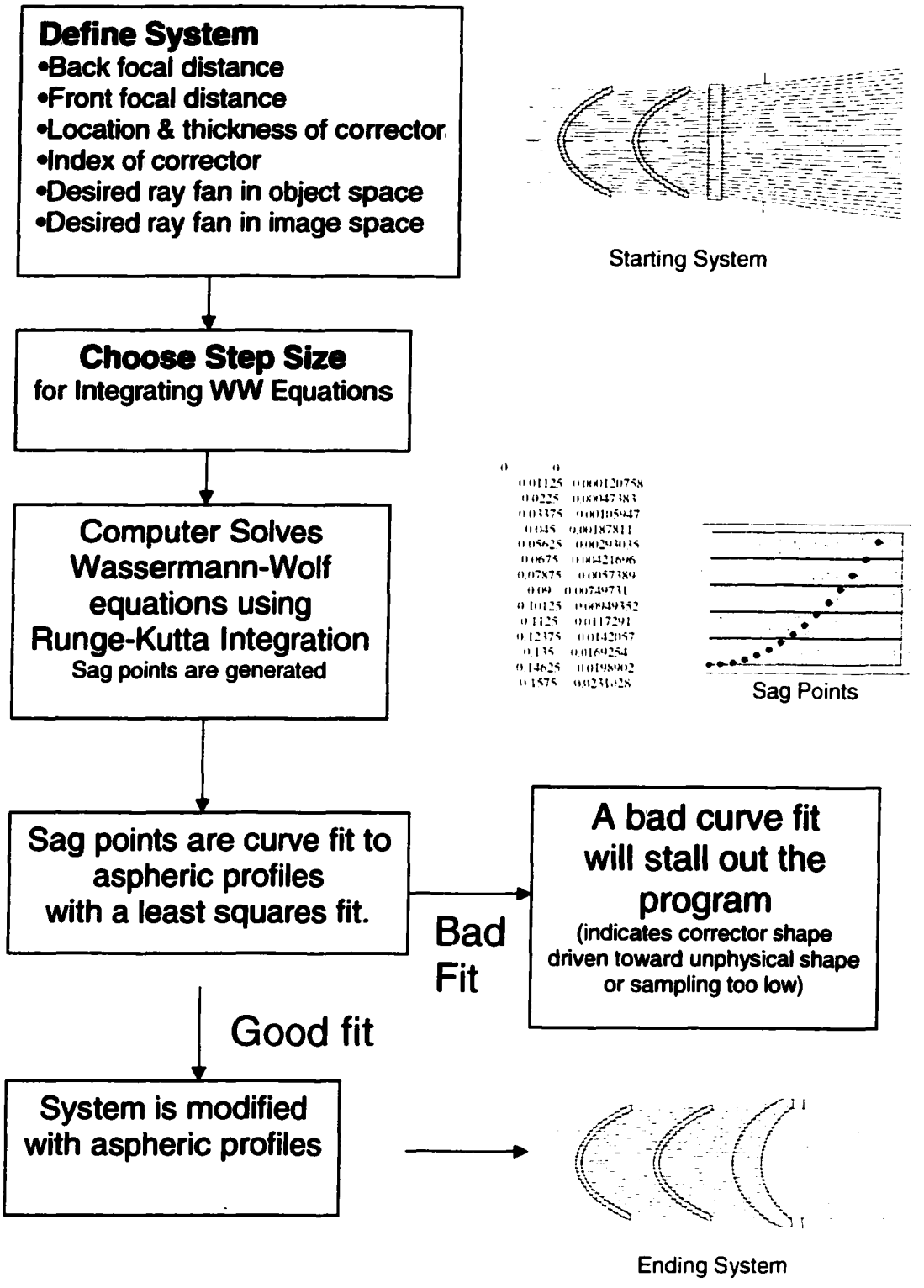

Figure 89. Steps in using Code V macro

Aperture Stops and Pupils

When adding a field of view to an optical system designed using the Wassermann-Wolf equations, it is necessary to select an aperture stop in the system. The aperture stop is defined as the limiting clear diameter in the optical system which defines the extent of the imaging bundle reaching an on-axis image point. By definition, the chief ray from a field point crosses the optical axis at the aperture stop. The entrance pupil is defined as the image of the aperture stop in object space. The chief ray crosses the optical axis in object space at the axial location of the entrance pupil. The exit pupil is defined as the image of the aperture stop in image space. The chief ray also crosses the optical axis in image space at the axial location of the entrance pupil.

An initial system on which the Wassermann-Wolf algorithm is used does not necessarily have an aperture stop defined. The Wassermann-Wolf operates on a single fan of rays emanating from an on-axis object point and the desired conjugate ray fan in image space. The extent of these ray fans must be defined. However, the axial location of the aperture stop may be left indeterminate as it may be located at any point along the ray fan.

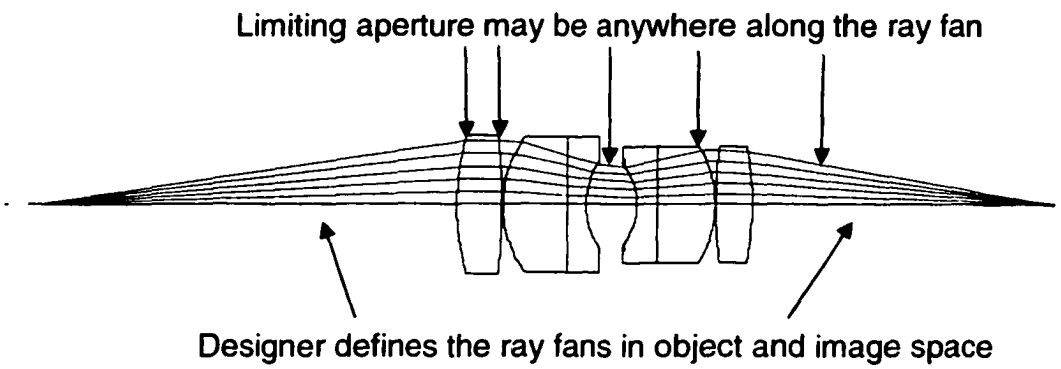

Figure 90. WW Algorithm works on a centered ray bundle

After the Wassermann-Wolf algorithm is used to create an aspheric element, one may define an aperture stop and add field points to the system. As Figure 91 illustrates, the location of the aperture stop will have an effect on the size and location of the pupils. All three of the systems shown have identical on-axis ray bundles.

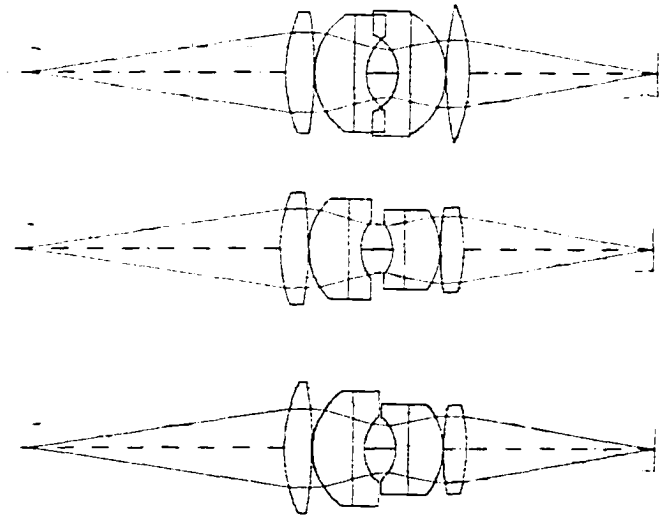

Figure 91. Location of the aperture stop will define pupil locations

The Wassermann-Wolf algorithm will only generate the profiles of the aspheric surfaces up to the extent of the ray bundle defined. The surface profile of the surfaces beyond the footprint of the on-axis bundle essentially becomes an extrapolation of the surface that was fit to the points. Ray bundles from off-axis points may impinge on the surfaces at the extrapolated points with unpredictable results. For this reason, it is generally wise to define an oversize on-axis wave fan to be used for the Wassermann-Wolf equations. After the aspheric surfaces have been generated, the system may be stopped down to the desired entrance pupil size.

This may be demonstrated with a conformal dome design. In the example shown in Figure 92, the goal is to create a fixed corrector for a fineness ratio 1.5 conformal dome. The ray bundle is made oversized and the Wassermann-Wolf equations are used to define the corrector profile.

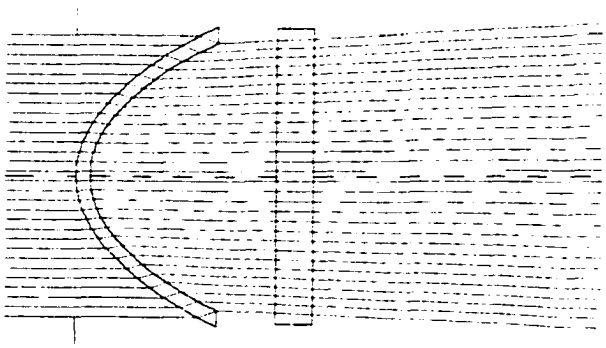

Figure 92. Oversize on-axis ray fan

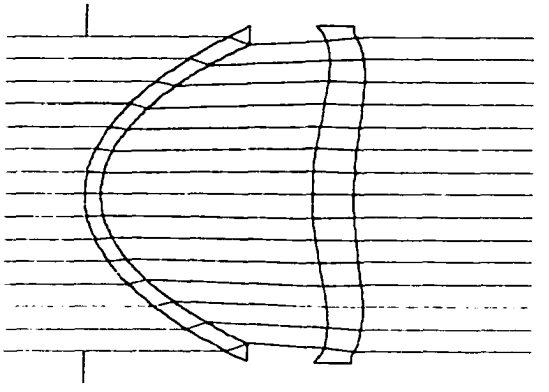

Figure 93. Corrector designed to make front end afocal

After the corrector has been created, the actual stop of the system may be defined and a perfect lens used to simulate the imaging system behind the front end. The perfect lens may be given a field of view and rotated within a field of regard. As there is ample corrector area defined, no problems arise from the off-axis ray bundles.

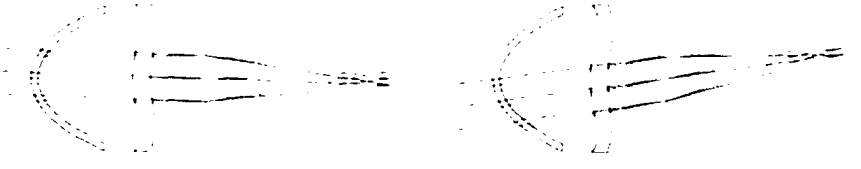

Figure 94. +/- 10° field of regard and +/- 4° field of view

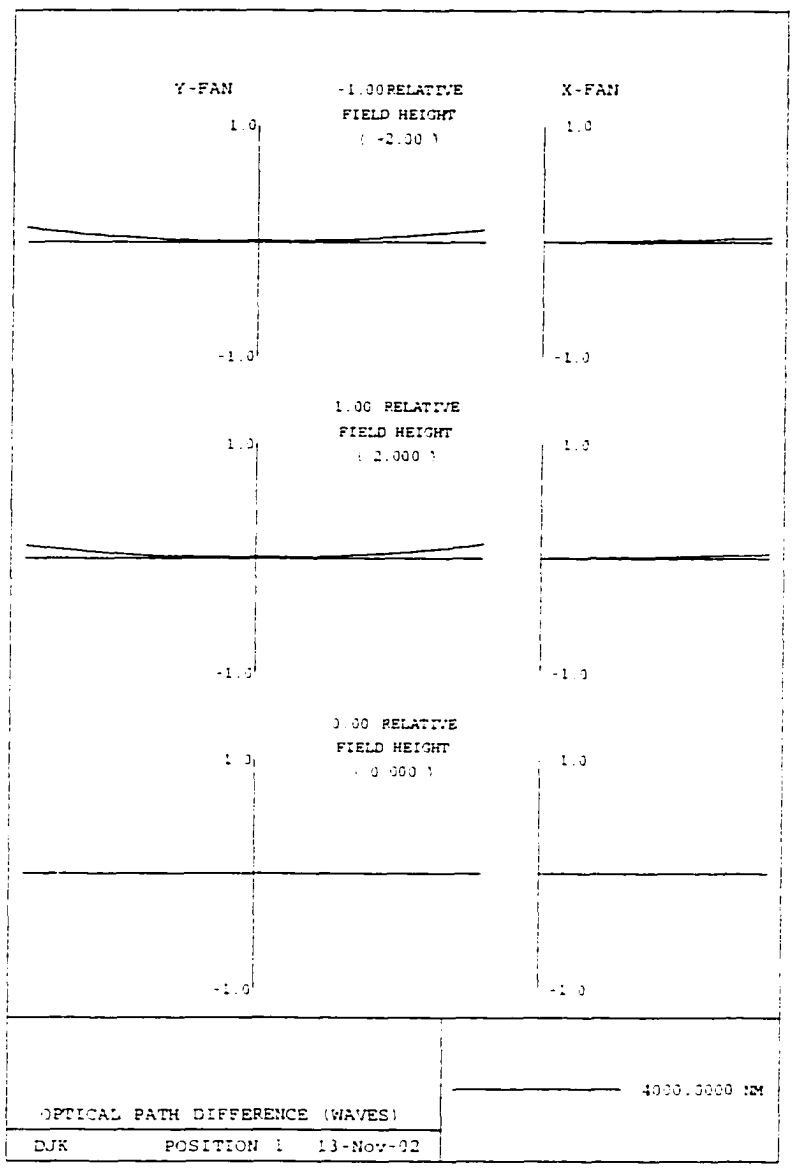

0 degree look angle. Scale: +/- 1 Wave

Figure 95. Wave aberration plot for front end system with perfect lens at 0 degree look angle

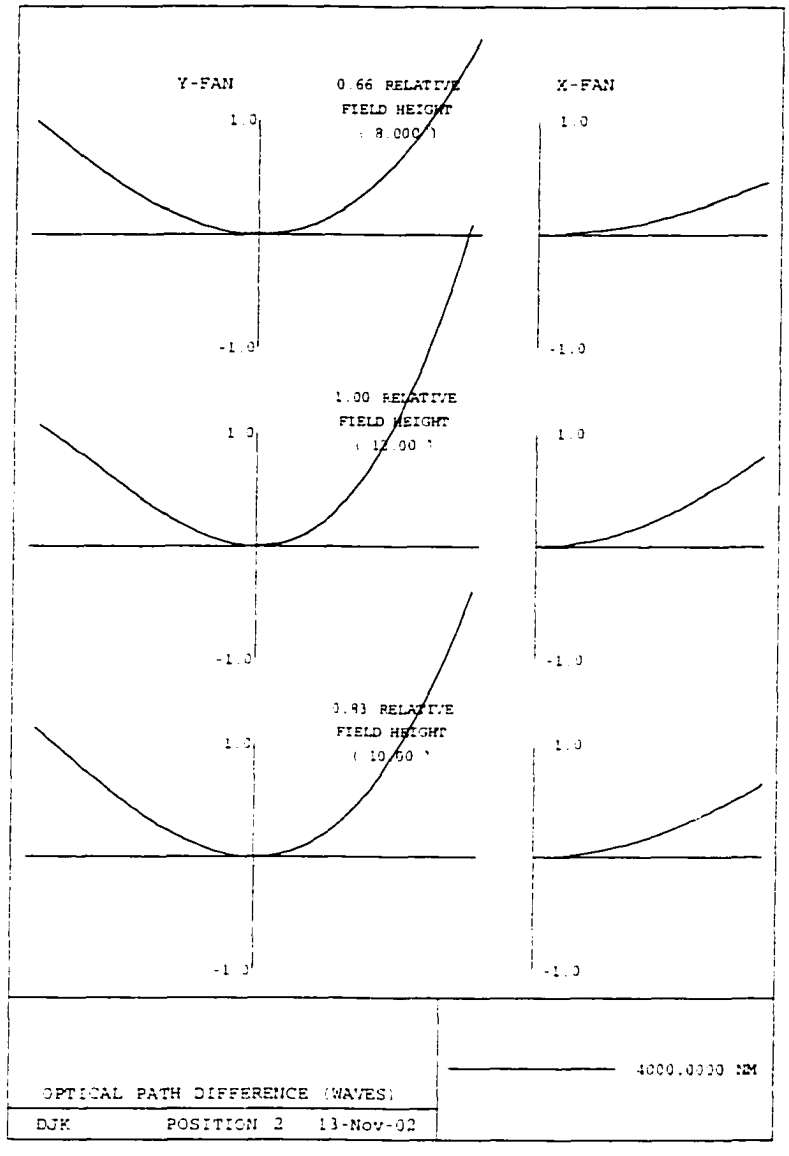

10 degree look angle. Scale: +/- 1 Wave

Figure 96. Wave aberration plot for front end system with perfect lens at 10 degree look angle

The performance for this front end design may be sufficient for this to be a final design. Alternatively, one may use optimization with a real imaging system behind the front end can further improve the design.

Summary

This chapter developed an understanding of the Wassermann-Wolf equations. Specifically, it focused on the constituent expressions that are used in deriving the Wassermann-Wolf equations. These expressions describe the passage of a tangential ray through a centered optical system. A pair of aspheric optical surfaces are used to control the ray so that it will have a desired position and direction at a tangent plane in image space. These relations form the basis for the Wassermann-Wolf equations. The Wassermann-Wolf equations relate the change in sag in the aspheric surfaces to a change in the parameter that defines the ray in a tangential ray fan. One may solve for the profile of the aspheric surfaces by integrating along the ray parameter. The aspheric surfaces make the tangential ray fan defined in object space transform into a desired ray fan in image space. By selecting the properties of the ray fan, one can make the optical system aplanatic. This is accomplished by ensuring that the ray fans focus at a specific point in image space and meet the Abbe Sine condition. This condition removes linear coma in an optical system by removing any variation in magnification over the aperture. The Wassermann-Wolf equations and Abbe Sine Condition are useful in the design of corrective optics for conformal domes. A technique is introduced for using the Wassermann-Wolf equations to generate a corrective element. Specifically, the Wassermann-Wolf equations are solved using an oversized ray fan. This creates a corrector element with a large defined area to accommodate off-axis ray bundles. One may stop down the fan, and add a field of regard and field of view to the system.

"The most overlooked advantage of owning a computer is that if they foul up there's no law against whacking them around a bit."
Eric Porterfield.

Chapter 3- Generalized Aspheric Design Equations

Introduction

The premise of conformal optics is to develop optical systems that are driven by non-optical constraints. This might imply optimizing a dome for increased missile performance. This might also mean blending a window in with the platform mold line to minimize an EO systems impact on aerodynamics. An outer optical surface might also be shaped in arbitrary ways for cosmetic reasons.

A challenge presents itself if the best window shape is not rotationally symmetric. In this situation, the axisymmetric solution forms of the arch and the wedge lose their applicability. To correct a non-rotationally symmetric conformal window, one may use an active aberration generator or a fixed corrector.

In rotationally symmetric systems, a fixed corrector may be automatically designed using a Wassermann-Wolf numerical approach. However, the classical Wassermann-Wolf algorithm does not work for systems that contain decentered or non-axisymmetric components. This dissertation presents a novel set of differential equations for the design of a fixed corrector design for non-rotationally symmetric systems. These equations are derived using the same approach as Wassermann and Wolf, but without the assumption of axial symmetry. Furthermore, a unique parameterization of a ray bundle is shown which allows a ray bundle to be defined using only one parameter. This parameterization allows one to numerically solve the general aspheric design equations

and generate two dimensional surfaces for the corrective surfaces. These corrective surfaces are typically not axisymmetric.

Review of the Wassermann-Wolf equations

At this point, it is helpful to review the essence of the classical Wassermann-Wolf. In the algorithm, the aspheric optic that is created allows one to control each ray's exit height from the axis and angle in image space. The designer defines the fans in object space and the desired conjugate fans in image space. Solving the Wassermann-Wolf equations creates the sag profile of two optical surfaces needed to make the ray fans conjugate. The ray fans may be defined at a tangent plane in image space and a tangent plane in object space. This tangent plane is not necessarily a pupil; it merely serves as a convenient plane of reference for defining a fan of rays in that space.

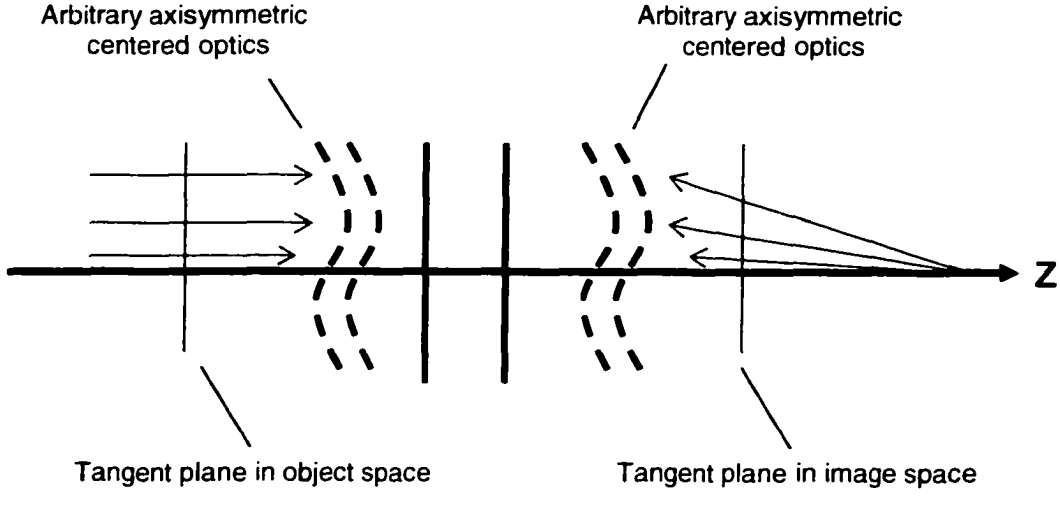

Figure 97. Planes tangent to the optical axis

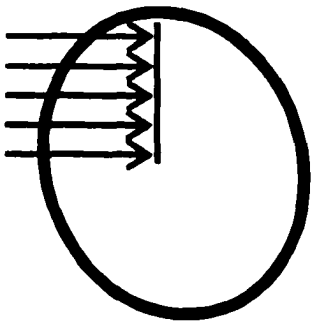

Figure 98. Ray fan in object space

Figure 98 shows a tangent plane in object space and the ray intersections. Figure 99 shows the image space tangent plane and the desired ray intersections.

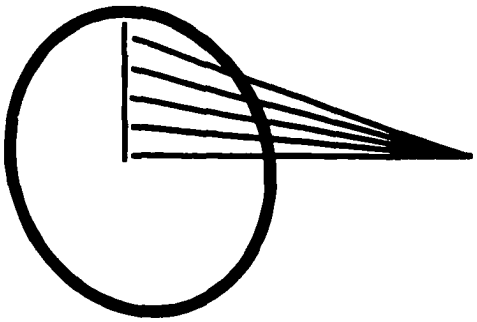

Figure 99. Tangent plane in image space shows desired conjugate ray fan

Asymmetric Case

In an asymmetric system, the optical surfaces are not necessarily symmetric around an axis Z. Consequently, to characterize the imaging behavior of a system for an on-axis object point, it is necessary to trace a bundle of rays.

In the Wassermann-Wolf case, the ray fans could be defined with respect to a pair of tangent planes in object and image space. In a non-rotationally symmetric system, the tangent planes are of greater use for defining desired ray bundles. Specifically, one may define a ray bundle with respect to the intersection coordinates (h_x, h_y) and direction cosines (L,M,N) of each ray at the tangent plane. Additionally, one may define an axis Z around which the ray bundle is centered. The optics in the system will not necessarily be symmetric about this Z axis. Figure 100 shows a layout of a non-rotationally symmetric system used with the generalized aspheric design equations.

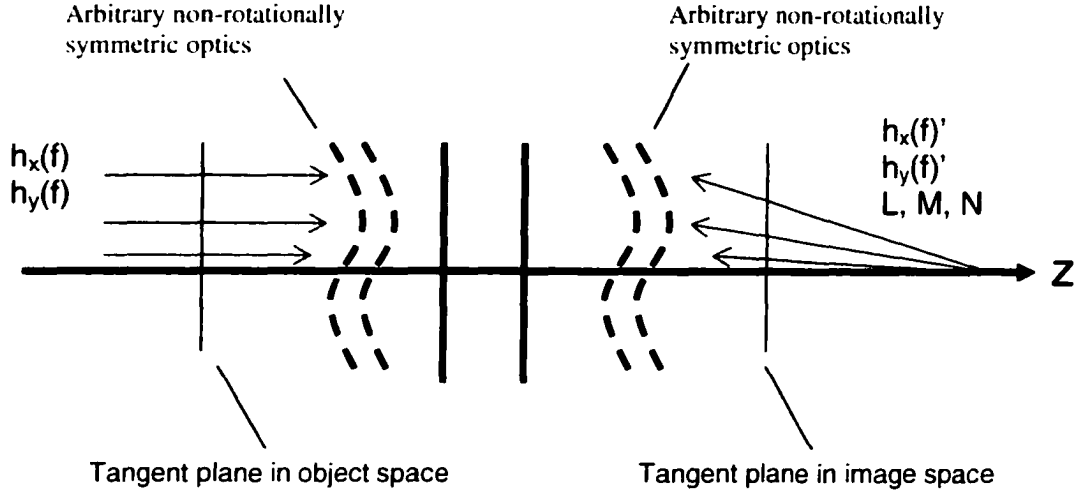

Figure 100. Layout of asymmetric system with desired ray bundle conjugates

The generalized aspheric design equations that are developed in this chapter solve for the two optical surfaces in the system to make the desired ray bundles conjugate to

each other, (i.e. each ray bundle in object space is 1:1 mapped to a defined ray bundle in image space). Figure 101 shows a ray bundle defined at a tangent plane in object space and Figure 102 shows the ray bundle at a tangent plane in image space.

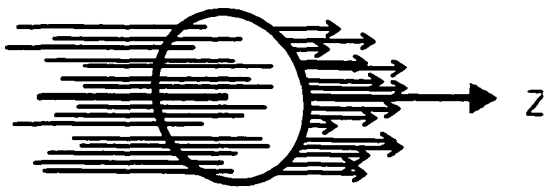

Figure 101. Ray bundle at object space tangent plane

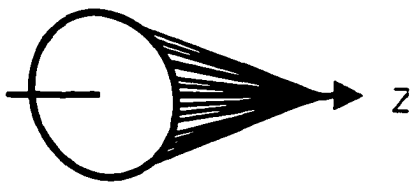

Figure 102. Desired ray bundle at image space tangent plane

One may use the Abbe Sine condition to define the direction and position of each ray in the bundle in image space and thereby guarantee aberration free imagery in the lateral area around the stigmatic point.

The generalized aspheric design equations create two tables of X-Y-Z points. These may be surface fit to an appropriate surface formula so that the surfaces may be modeled in a ray trace program. The generalized aspheric design equations provide a new tool for the design of aspheric surfaces to control a ray bundle.

The derivation for the generalized equations follows. Equations will also be shown for simultaneously correcting axial stigmatism and exact satisfaction of the sine condition.

Derivation of Generalized Aspheric Design Equations

The system where the new generalized equations are used is similar to the setup shown for the classical Wassermann-Wolf. Key differences are that parameterized ray bundles are specified rather than a tangential ray fan; the optical system may consist of elements that are tilted, decentered, or asymmetric; and the aspheric corrector surfaces generated by integration of the generalized equations may be non-axisymmetric. As mentioned previously, the ray bundles may be defined with respect to a pair of tangent planes in image and object space. Figure 103 shows a layout of a system used with the generalized aspheric design equations.

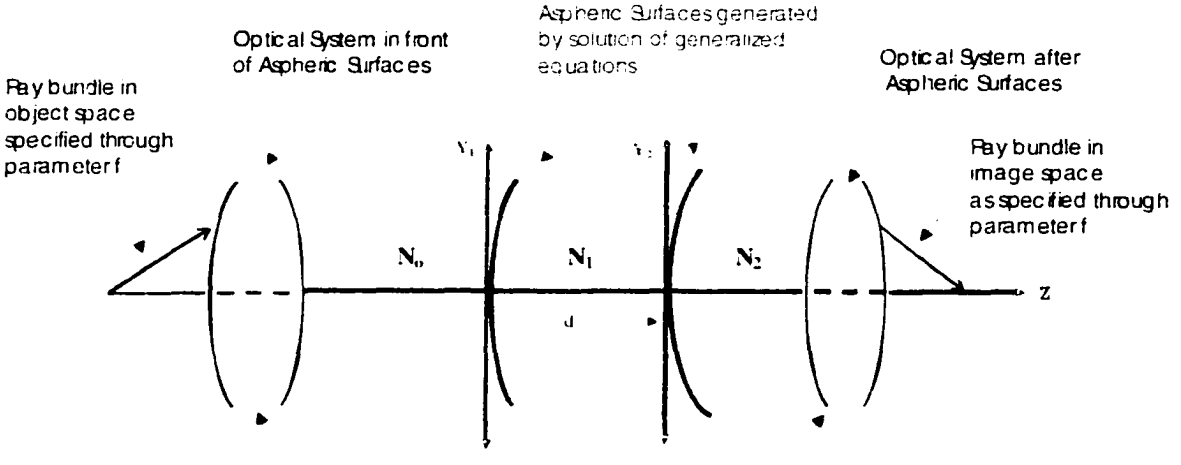

Figure 103. Layout of system

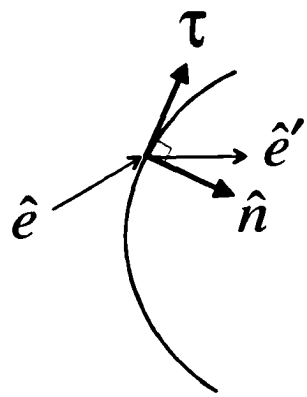

Figure 104. Skew ray intersecting a surface.

The first step of the derivation is to consider a skew ray in the bundle intersecting a surface. Figure 104 shows such a ray. The incident ray has a unit vector of $\hat{e}$ and after refraction the unit vector is $\hat{e}'$. The normal and tangent unit vectors are $\hat{n}$ and τ respectively.

By geometry, two intersecting lines ($\hat{n}$ and $\hat{e}$ for example) will always define a plane. By the law of refraction, the unit vector $\hat{e}'$ will be coplanar with $\hat{n}$ and $\hat{e}$. Using arbitrary constants, one may set up a summation using three known vectors and three unknown constants.

$$A \cdot \hat{e}' + B \cdot \hat{e} = \Gamma \cdot \hat{n}$$

Equation 17

Where

$\hat{n}$ - unit vector of surface normal
ê - unit vector of incident ray
ê′ - unit vector of refracted ray
τ - unit vector of surface tangent
A, B, Γ - constants

The summation of Equation 17 can be used to create a vector form of Snell's law in terms of the surface normal and ray vectors.

A non-vector form of Snell's law is

$$N' \cdot \sin I' = N \cdot \sin I$$

Equation 18

Equation 17 is with respect to angles I' and I contained in the plane of incidence. See Figure 105 below.

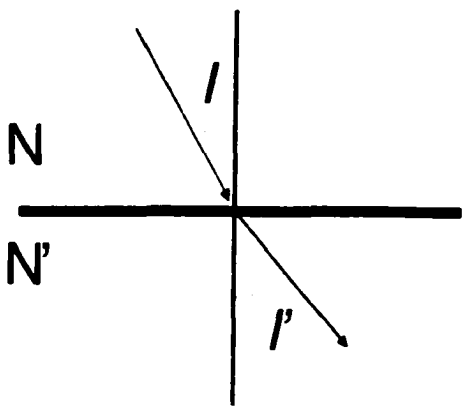

Figure 105. Snell's law

One may take the cross product of both sides of Equation 17 with the normal unit vector to yield:

$$A \cdot \hat{e}' \times \hat{n} + B \cdot \hat{e} \times \hat{n} = \Gamma \cdot \hat{n} \times \hat{n} = 0$$

Equation 19

Comparing with Equation 18 and solving for A and B produces:

$$A = N'$$
$$B = -N$$

Equation 20

This may be substituted back in to give:

$$N' \cdot \hat{e}' - N \cdot \hat{e} = \Gamma \cdot \hat{n}$$

Equation 21

The arbitrary constant Γ must still be dealt with. Applying the dot product of the surface tangent τ with the above equation removes $\Gamma \cdot \hat{n}$ as $\Gamma \cdot \hat{n} \bullet \tau = 0$. This gives the vector form of Snell's law in terms of the surface tangent, the indices of refraction on both sides of the surface, and the ray vectors.

$$(N' \cdot \hat{e}' - N \cdot \hat{e}) \bullet \tau = 0$$

Equation 22

The parts of this vector form will be used to construct a differential equation relating a change in the sag (delta z) of a surface with respect to a change in a ray parameter.

Looking at the surface tangent τ, this is at the point of incidence of a ray on the optical surface. At this stage, we will specify the optical surface coordinates as being parameterized with respect to a parameter f. In other words, x=x(f), y=y(f), and z=z(f). These coordinates represent the point of intercept of the ray defined by f. As one increments f, the surface is mapped out in terms of x, y, z coordinates. One may therefore represent the tangent at the point of incidence in terms of the derivatives of x, y, and z with respect to f:

$$\tau = \frac{\dot{x}}{\sqrt{\dot{x}^2 + \dot{y}^2 + \dot{z}^2}}, \frac{\dot{y}}{\sqrt{\dot{x}^2 + \dot{y}^2 + \dot{z}^2}}, \frac{\dot{z}}{\sqrt{\dot{x}^2 + \dot{y}^2 + \dot{z}^2}}$$

where $\dot{x}, \dot{y}, \dot{z}$ are derivatives with respect to a parameter f

Equation 23

Two other components of Equation 22 are the ray vectors. In terms of the direction cosines, the ray vectors are specified as

$$\hat{e} = \cos\theta_x, \cos\theta_y, \cos\theta_z$$
$$\hat{e}' = \cos\theta'_x, \cos\theta'_y, \cos\theta'_z$$

Equation 24

By placing Equation 24 into equation Equation 22, one obtains

$$\dot{z} = \frac{\dot{x} \cdot (N \cdot \cos\theta_x - N' \cdot \cos\theta'_x) + \dot{y} \cdot (N \cdot \cos\theta_y - N' \cdot \cos\theta'_y)}{-N \cdot \cos\theta_z + N' \cdot \cos\theta'_z}$$

Equation 25

Equation 25 describes the instantaneous change in the sag z of the refracting surface with respect to the parameter f for the ray that intersects the surface at this particular point. Furthermore, this equation relates the change in surface coordinates at the point of ray intersection to the direction cosines of the incident and refracted ray.

Now, consider the passage of an oblique ray through two adjacent surfaces separated by a distance d. This is shown in Figure 106.

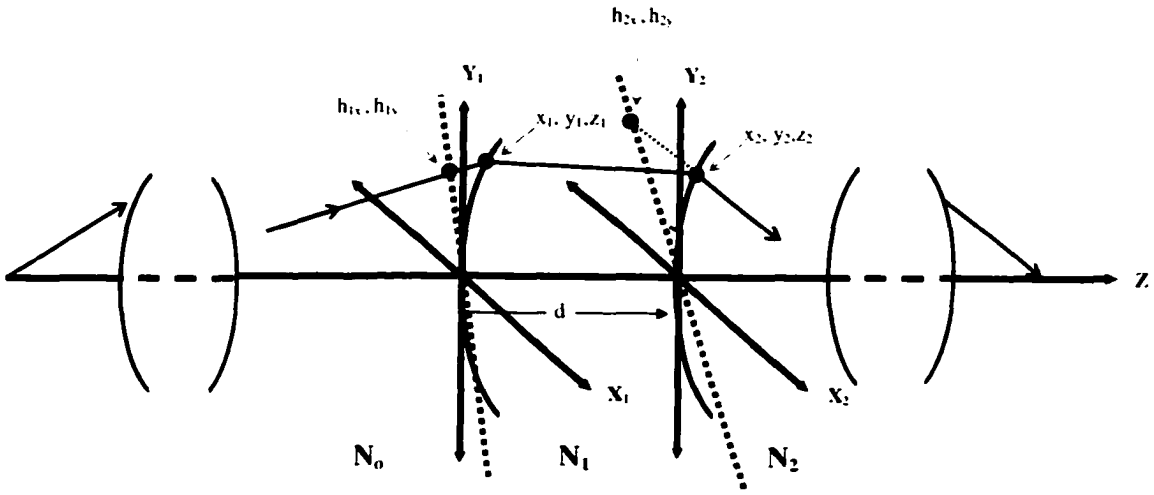

Figure 106. Passage of an oblique ray through two adjacent surfaces

The ray enters the system at the far left and passes through the optics in front of the two surfaces. The ray then intersects the tangent plane of the first surface at h_{1x}, h_{1y}.

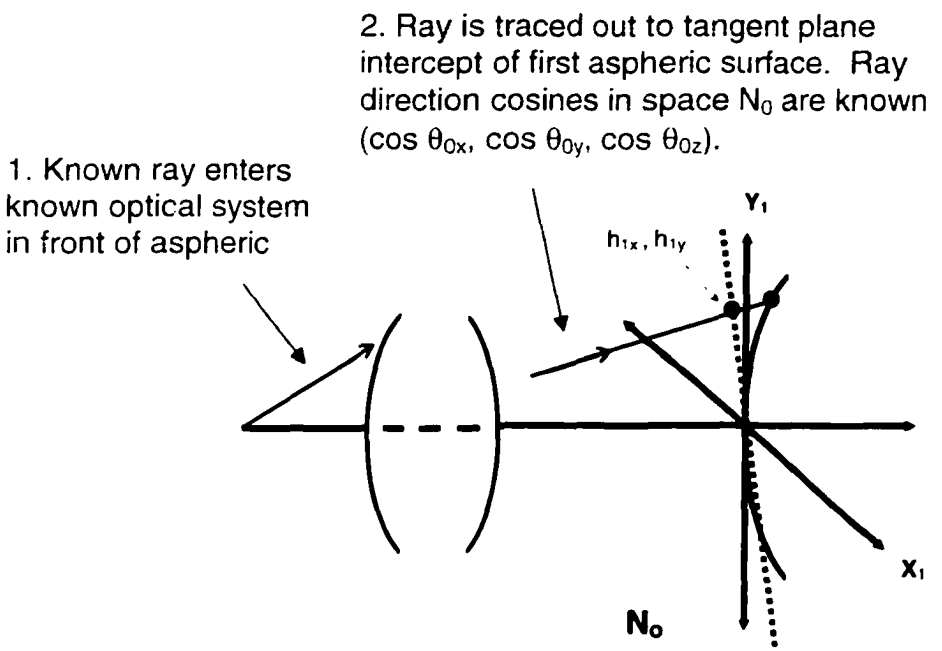

Figure 107. Ray trace to first tangent plane

The ray is refracted at point (x_1,y_1,z_1) and then travels to the point of intersection on the second surface (x_2,y_2,z_2).

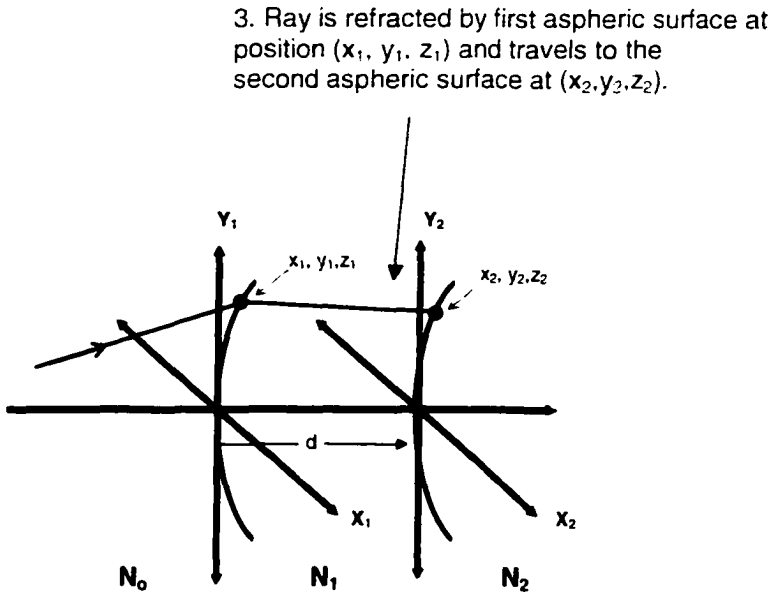

Figure 108. Ray refracted at first surface

By reverse ray tracing the refracted ray, one obtains the intercept of the refracted ray with the tangent plane of the second aspheric surface. The refracted ray enters the rest of the optical system after the aspheric surface and exits the system at the far right.

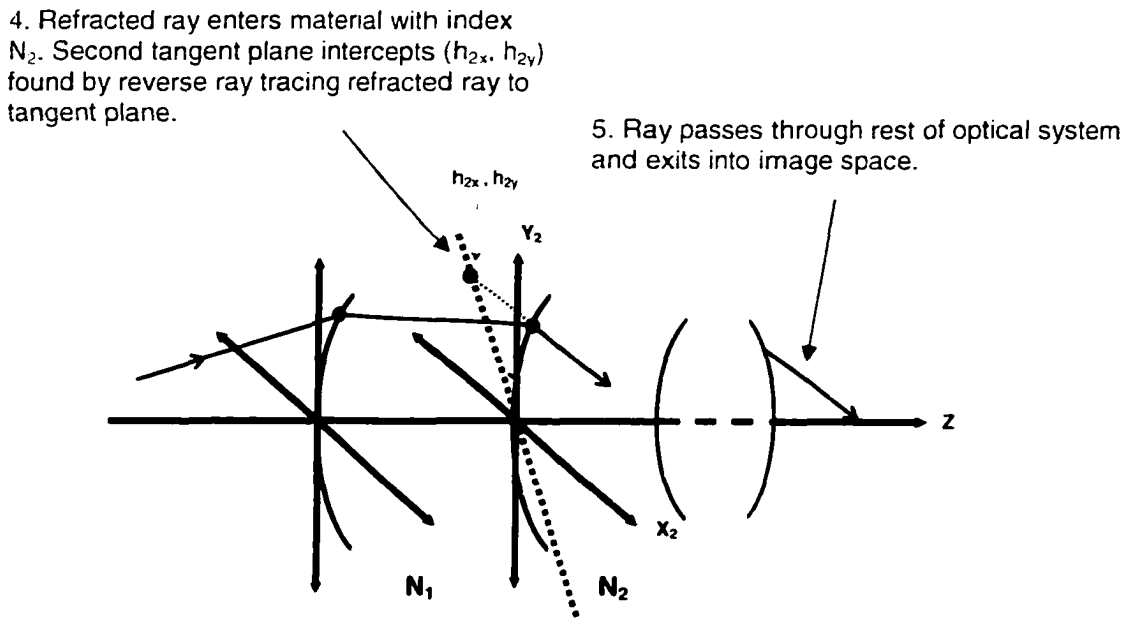

Figure 109. Ray refracted at second surface into rest of optical system

By using coordinates that are with respect to the local coordinate system of each of the two surfaces, one may obtain relations for the path length R of the ray and the R components in x, y, and z.

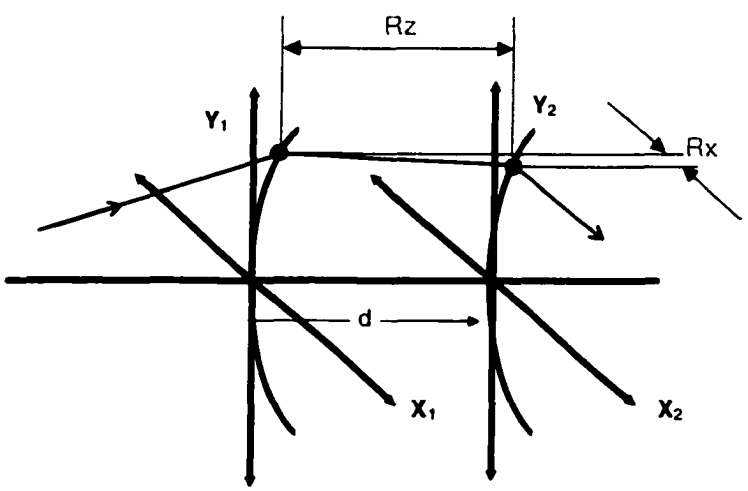

Equation 26. Rz and Rx

Let

$$R_y = y_2 - y_1$$

Equation 27

$$R_x = x_2 - x_1$$

Equation 28

$$R_z = d - z_1 + z_2$$

Equation 29

$$R = \sqrt{R_x^2 + R_y^2 + R_z^2}$$

Equation 30

As noted, R_x, R_y, and R_z are the path lengths parallel to the X, Y, and Z-axes respectively.

From the path lengths, one may obtain the direction cosines of the ray after the first surface refraction:

$$\cos\theta_{x1} = \frac{R_x}{R},$$
$$\cos\theta_{y1} = \frac{R_y}{R},$$
$$\cos\theta_{z1} = \frac{R_z}{R}$$

Equation 31

The direction cosines before the refraction are known from ray tracing through the optical system before the two neighboring optical surfaces.

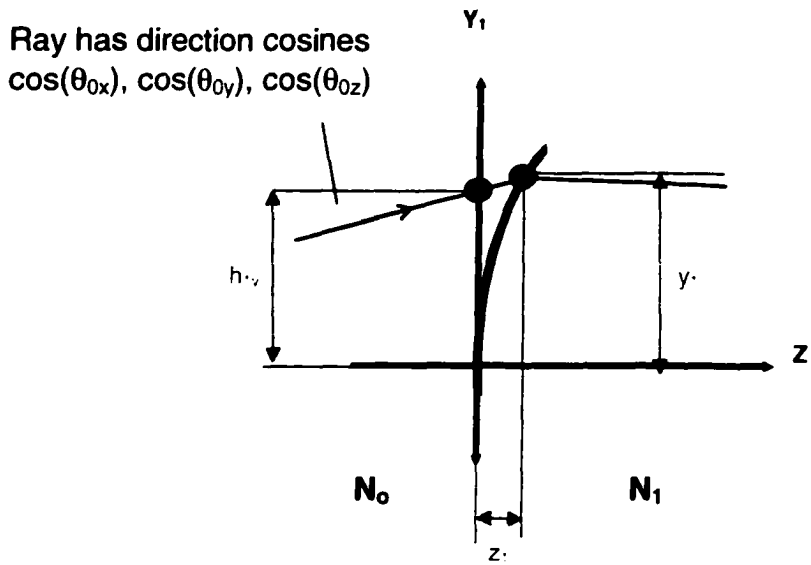

Figure 110. Y-Z view of first surface intersection

The x and y coordinates of the oblique ray on the first surface may be reformulated in terms of the direction cosines of the ray, $\cos(\theta_{0x})$, $\cos(\theta_{0y})$, $\cos(\theta_{0z})$, the tangent plane intercept coordinates, h_{1x}, h_{2y}, and the surface sag at the point of intersection on the aspheric surface, z. A similar expression can be found for the intercept coordinates on the last surface using the direction cosines of the ray in N_2.

$$y_1 = h_{y1} + z_1 \cdot \frac{\cos\theta_{0y}}{\cos\theta_{0z}}$$

$$x_1 = h_{x1} + z_1 \cdot \frac{\cos\theta_{0x}}{\cos\theta_{0z}}$$

$$y_2 = h_{y2} + z_2 \cdot \frac{\cos\theta_{2y}}{\cos\theta_{2z}}$$

$$x_2 = h_{x2} + z_2 \cdot \frac{\cos\theta_{2x}}{\cos\theta_{2z}}$$

Equation 32

Equation 32 shows the link between surface intercept coordinates, ray direction, and tangent plane intercept. This link can be used when the entering ray angles θ_o are known, and one wishes to find the surface contours of the two aspheric surfaces to cause the ray to exit the second surface with a desired θ_2.

Recasting Equation 25 in terms of the first surface results in:

$$\dot{z}_1 = \frac{\dot{x}_1 \cdot (N_0 \cdot \cos\theta_{x0} - N_1 \cdot \cos\theta_{x1}) + \dot{y}_1 \cdot (N_0 \cdot \cos\theta_{y0} - N_1 \cdot \cos\theta_{y1})}{-N_0 \cdot \cos\theta_{z0} + N_1 \cdot \cos\theta_{z1}}$$

Equation 33

This creates an equation relating the instantaneous change in surface coordinates of the first aspheric surface at the point of intercept of a particular ray. The coordinates at this surface are known by Equation 32. One can now take the derivative of the equations for x_1, y_1 and substitute out $\dot{x}_1$, $\dot{y}_1$.

The derivative of Equation 32 with respect to f yields:

$$\dot{y}_1 = \dot{h}_{y1} + z1 \cdot \frac{d(\frac{\cos(\theta_{y0})}{\cos(\theta_{z0})})}{df} + \dot{z}_1 \cdot (\frac{\cos(\theta_{y0})}{\cos(\theta_{z0})})$$

Equation 34

$$\dot{x}_1 = \dot{h}_{x1} + z1 \cdot \frac{d(\frac{\cos(\theta_{x0})}{\cos(\theta_{z0})})}{df} + \dot{z}_1 \cdot (\frac{\cos(\theta_{x0})}{\cos(\theta_{z0})})$$

Equation 35

$$\dot{y}_2 = \dot{h}_{y2} + z2 \cdot \frac{d\left(\frac{\cos(\theta_{y2})}{\cos(\theta_{z2})}\right)}{df} + \dot{z}_2 \cdot \left(\frac{\cos(\theta_{y2})}{\cos(\theta_{z2})}\right)$$

Equation 36

$$\dot{x}_2 = \dot{h}_{x2} + z2 \cdot \frac{d\left(\frac{\cos(\theta_{x2})}{\cos(\theta_{z2})}\right)}{df} + \dot{z}_2 \cdot \left(\frac{\cos(\theta_{x2})}{\cos(\theta_{z2})}\right)$$

Equation 37

Substituting Equation 34 and Equation 35 into Equation 33 results in:

$$\dot{z}_1 = \frac{\left[\dot{h}_{x1} + z1 \cdot \frac{d\left(\frac{\cos(\theta_{x0})}{\cos(\theta_{z0})}\right)}{df} + \dot{z}_1 \cdot \left(\frac{\cos(\theta_{x0})}{\cos(\theta_{z0})}\right)\right] \cdot (N_0 \cdot \cos\theta_{x0} - N_1 \cdot \cos\theta_{x1}) \ldots}{+\left[\dot{h}_{y1} + z1 \cdot \frac{d\left(\frac{\cos(\theta_{y0})}{\cos(\theta_{z0})}\right)}{df} + \dot{z}_1 \cdot \left(\frac{\cos(\theta_{y0})}{\cos(\theta_{z0})}\right)\right] \cdot (N_0 \cdot \cos\theta_{y0} - N_1 \cdot \cos\theta_{y1})}$$
$$- N_0 \cdot \cos\theta_{z0} + N_1 \cdot \cos\theta_{z1}$$

Equation 38

This expression is nearing a useful form. To make it useful, one must solve for $\dot{z}_1$. This will allow one to integrate z over the parameter f to calculate the change in surface sag as a function of that parameter. This effectively allows one to calculate a surface profile. The next steps are all basic algebra with large expressions.

$$\dot{z}_1 = \left[\dot{h}_{x1} + z1 \cdot \frac{d\left(\frac{\cos(\theta_{x0})}{\cos(\theta_{z0})}\right)}{df} + \dot{z}_1 \cdot \left(\frac{\cos(\theta_{x0})}{\cos(\theta_{z0})}\right) \right] \cdot \frac{(N_0 \cdot \cos\theta_{x0} - N_1 \cdot \cos\theta_{x1})}{-N_0 \cdot \cos\theta_{z0} + N_1 \cdot \cos\theta_{z1}} \cdots$$

$$+ \left[\dot{h}_{y1} + z1 \cdot \frac{d\left(\frac{\cos(\theta_{y0})}{\cos(\theta_{z0})}\right)}{df} + \dot{z}_1 \cdot \left(\frac{\cos(\theta_{y0})}{\cos(\theta_{z0})}\right) \right] \cdot \frac{(N_0 \cdot \cos\theta_{y0} - N_1 \cdot \cos\theta_{y1})}{-N_0 \cdot \cos\theta_{z0} + N_1 \cdot \cos\theta_{z1}}$$

Equation 39

In solving for $\dot{z}_1$, it is beneficial to make Equation 39 more compact through substitution.

Let

$$A = \frac{N_0 \cdot \cos\theta_{x0} - N_1 \cdot \cos\theta_{x1}}{-N_0 \cdot \cos\theta_{z0} + N_1 \cdot \cos\theta_{z1}}$$

$$B = \frac{N_0 \cdot \cos\theta_{y0} - N_1 \cdot \cos\theta_{y1}}{-N_0 \cdot \cos\theta_{z0} + N_1 \cdot \cos\theta_{z1}}$$

Equation 40

Equation 40 can be put in terms of R, R_x, and R_y. This removes the need to know the direction cosines of the ray after refraction by the first aspheric surface.

$$A = \frac{N_0 \cdot \cos\theta_{x0} - N_1 \cdot \frac{R_x}{R}}{-N_0 \cdot \cos\theta_{z0} + N_1 \cdot \frac{R_z}{R}} = \frac{R \cdot N_0 \cdot \cos\theta_{x0} - N_1 \cdot R_x}{-R \cdot N_0 \cdot \cos\theta_{z0} + N_1 \cdot R_z}$$

$$B = \frac{N_0 \cdot \cos\theta_{y0} - N_1 \cdot \frac{R_y}{R}}{-N_0 \cdot \cos\theta_{z0} + N_1 \cdot \frac{R_z}{R}} = \frac{R \cdot N_0 \cdot \cos\theta_{y0} - N_1 \cdot R_y}{-R \cdot N_0 \cdot \cos\theta_{z0} + N_1 \cdot R_z}$$

Equation 41

After substitution of A and B in Equation 41, the equation becomes

$$\dot{z}_1 = A \cdot \left[\dot{h}_{x1} + z1 \cdot \frac{d(\frac{\cos(\theta_{x0})}{\cos(\theta_{z0})})}{df} + \dot{z}_1 \cdot (\frac{\cos(\theta_{x0})}{\cos(\theta_{z0})}) \right] + B \cdot \left[\dot{h}_{y1} + z1 \cdot \frac{d(\frac{\cos(\theta_{y0})}{\cos(\theta_{z0})})}{df} + \dot{z}_1 \cdot (\frac{\cos(\theta_{y0})}{\cos(\theta_{z0})}) \right]$$

Equation 42

Collecting on the $\dot{z}_1$ coefficients yields

$$\dot{z}_1 \cdot \left[1 - A \cdot \frac{\cos(\theta_{x0})}{\cos(\theta_{z0})} - B \cdot \frac{\cos(\theta_{y0})}{\cos(\theta_{z0})} \right] = A \cdot \left[\dot{h}_{x1} + z1 \cdot \frac{d(\frac{\cos(\theta_{x0})}{\cos(\theta_{z0})})}{df} \right] + B \cdot \left[\dot{h}_{y1} + z1 \cdot \frac{d(\frac{\cos(\theta_{y0})}{\cos(\theta_{z0})})}{df} \right]$$

Equation 43

Dividing out separates the $\dot{z}$ onto one side of the equals sign.

$$\dot{z}_1 = \frac{A \cdot \left[\dot{h}_{x1} + z1 \cdot \frac{d(\frac{\cos(\theta_{x0})}{\cos(\theta_{z0})})}{df} \right] + B \cdot \left[\dot{h}_{y1} + z1 \cdot \frac{d(\frac{\cos(\theta_{y0})}{\cos(\theta_{z0})})}{df} \right]}{\left[1 - A \cdot \frac{\cos(\theta_{x0})}{\cos(\theta_{z0})} - B \cdot \frac{\cos(\theta_{y0})}{\cos(\theta_{z0})} \right]}$$

Equation 44

We now substitute back in the expressions for A and B.

$$\dot{z}_1 = \frac{\left[\frac{R\cdot N_0\cdot\cos\theta_{x0}-N_1\cdot R_x}{-R\cdot N_0\cdot\cos\theta_{z0}+N_1\cdot R_z}\cdot\left[\dot{h}_{x1}+z_1\cdot\frac{d(\frac{\cos(\theta_{x0})}{\cos(\theta_{z0})})}{df}\right]\cdots + \frac{R\cdot N_0\cdot\cos\theta_{y0}-N_1\cdot R_y}{-R\cdot N_0\cdot\cos\theta_{z0}+N_1\cdot R_z}\cdot\left[\dot{h}_{y1}+z_1\cdot\frac{d(\frac{\cos(\theta_{y0})}{\cos(\theta_{z0})})}{df}\right]\right]}{\left[1-\frac{R\cdot N_0\cdot\cos\theta_{x0}-N_1\cdot R_x}{-R\cdot N_0\cdot\cos\theta_{z0}+N_1\cdot R_z}\cdot\frac{\cos(\theta_{x0})}{\cos(\theta_{z0})}-\frac{R\cdot N_0\cdot\cos\theta_{y0}-N_1\cdot R_y}{-R\cdot N_0\cdot\cos\theta_{z0}+N_1\cdot R_z}\cdot\frac{\cos(\theta_{y0})}{\cos(\theta_{z0})}\right]}$$

Equation 45

A similar expression can be found for the second surface.

$$\dot{z}_2 = \frac{\left[\frac{N_1\cdot R_x-R\cdot N_2\cdot\cos\theta_{x2}}{-N_1\cdot R_z+R\cdot N_2\cdot\cos\theta_{z2}}\cdot\left[\dot{h}_{x2}+z_2\cdot\frac{d(\frac{\cos(\theta_{x2})}{\cos(\theta_{z2})})}{df}\right]\cdots + \frac{N_1\cdot R_y-R\cdot N_2\cdot\cos\theta_{y2}}{-N_1\cdot R_z+R\cdot N_2\cdot\cos\theta_{z2}}\cdot\left[\dot{h}_{y2}+z_2\cdot\frac{d(\frac{\cos(\theta_{y2})}{\cos(\theta_{z2})})}{df}\right]\right]}{\left[1-\frac{N_1\cdot R_x-R\cdot N_2\cdot\cos\theta_{x2}}{-N_1\cdot R_z+R\cdot N_2\cdot\cos\theta_{z2}}\cdot\frac{\cos(\theta_{x2})}{\cos(\theta_{z2})}-\frac{N_1\cdot R_y-R\cdot N_2\cdot\cos\theta_{y2}}{-N_1\cdot R_z+R\cdot N_2\cdot\cos\theta_{z2}}\cdot\frac{\cos(\theta_{y2})}{\cos(\theta_{z2})}\right]}$$

Equation 46

Equation 45 and Equation 46 relate a change in surface sag of two aspheric surfaces to a change in the parameter defining a ray in the bundle. Each ray corresponds to a set of x,y, and z coordinates on the two aspheric surfaces. As one varies the parameter f, the surfaces are traced out.

When integrating the generalized aspheric design equation, one must use the previously derived relations in Equation 32 to calculate the x and y coordinates of the ray f intercept on each general aspheric surface at sag point z. (The sag point z is calculated using the generalized equations.) For convenience, Equation 32 is repeated below.

$$y_1 = h_{y1} + z_1 \cdot \frac{\cos\theta_{0y}}{\cos\theta_{0z}}$$

$$x_1 = h_{x1} + z_1 \cdot \frac{\cos\theta_{0x}}{\cos\theta_{0z}}$$

$$y_2 = h_{y2} + z_2 \cdot \frac{\cos\theta_{2y}}{\cos\theta_{2z}}$$

$$x_2 = h_{x2} + z_2 \cdot \frac{\cos\theta_{2x}}{\cos\theta_{2z}}$$

Equation 47

The parameter f is used to define a ray bundle composed of rays that may vary both in an x,y position at a tangent plane in object space and in all three direction cosines. This is similar to the ray parameter used in the Wassermann-Wolf equations. In the Wassermann-Wolf equations, the ray parameter defined a ray fan composed of rays that varied in angle and height with respect to the optical axis.

Wassermann-Wolf Equations as a Special Case of the Generalized Equations

As a special case of the generalized aspheric design equations, one may constrain all the rays in the bundle to be contained in the Y-Z plane. If this is true, θ_x will always

be $\frac{\pi}{2}$. In other words, the angle that each ray makes with any local x axis will always be 90 degrees. Substituting $\theta_t = \frac{\pi}{2}$ into the generalized equations collapses the expressions into the classical 2-D Wassermann-Wolf equations. Unlike the generalized equations, the Wassermann-Wolf equations are used solely with a tangential ray fan that is contained in the Y-Z plane throughout the optical system. This is equivalent to saying that the surface normal at the point of intersection of each ray and the surface will be contained in the Y-Z plane. This is illustrated in Figure 111. If ray $\hat{e}$ is contained in the Y-Z plane, Snell's law forces the surface normal $\hat{n}$ to be coplanar with the incident ray if the refracted ray $\hat{e}'$ must also be in the Y-Z plane.

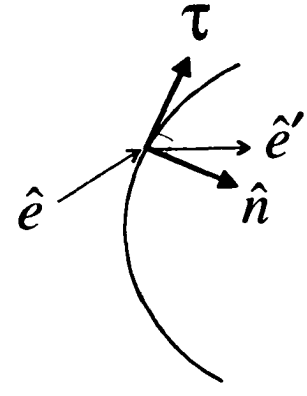

Figure 111. Intersection of a ray with a surface

The steps used in solving the generalized asphere design equations are similar to those used in solving the Wassermann-Wolf equations.

Steps in Solving Generalized Asphere Design Equations

1. Forward trace ray to first tangent plane starting from the optical axis (f=0) and moving up in the parameter f. The parameterization should be such that an entire ray bundle is defined.
2. Store data in array for h_{x1}, h_{y1} and direction cosines L_0, M_0, N_0 of ray
3. Reverse trace ray to second tangent plane starting from the optical axis (f=0) and moving up in the parameterization. Each ray should have a 1:1 mapping to a ray in the object space bundle.
4. Store data in array for h_{x2}, h_{y2} and direction cosines L_2, M_2, N_2 of ray
5. Solve Generalized Asphere Design equations using information from the ray just traced. (Solution is initiated at known aspheric sag values such as $x_1=0$, $y_1=0$, $z_1=0$ and $x_2=0$, $y_2=0$, $z_2=0$.) A method such as the Runge-Kutta method may be used.

6. The results from step 5 are two z values corresponding to points on the two aspheric surfaces. These z values are then related to corresponding x, y values using the equations:

$$y_1 = h_{y1} + z_1 \cdot \frac{\cos\theta_{0y}}{\cos\theta_{0z}}$$

$$x_1 = h_{x1} + z_1 \cdot \frac{\cos\theta_{0x}}{\cos\theta_{0z}}$$

$$y_2 = h_{y2} + z_2 \cdot \frac{\cos\theta_{2y}}{\cos\theta_{2z}}$$

$$x_2 = h_{x2} + z_2 \cdot \frac{\cos\theta_{2x}}{\cos\theta_{2z}}$$

7. The x, y, z values for the two surfaces are added to the list of calculated x, y,z points for the surfaces and used as a seed value for the next iteration.
8. Steps 1-7 are repeated as necessary until the edge of the aperture is reached.
9. Finally, a surface fit of x,y,z values to a surface representation is performed. This may be conveniently done by fitting with Zernike polynomials or performing a least squares fit to an x-y polynomial.

The solution generated by the new equations is dependent upon the rays selected. With the new equations, one defines a ray bundle in object space and a desired bundle in image space. Figure 112 shows a ray bundle defined about an axis Z for an optical system. The Z axis represents the center of the ray bundle.

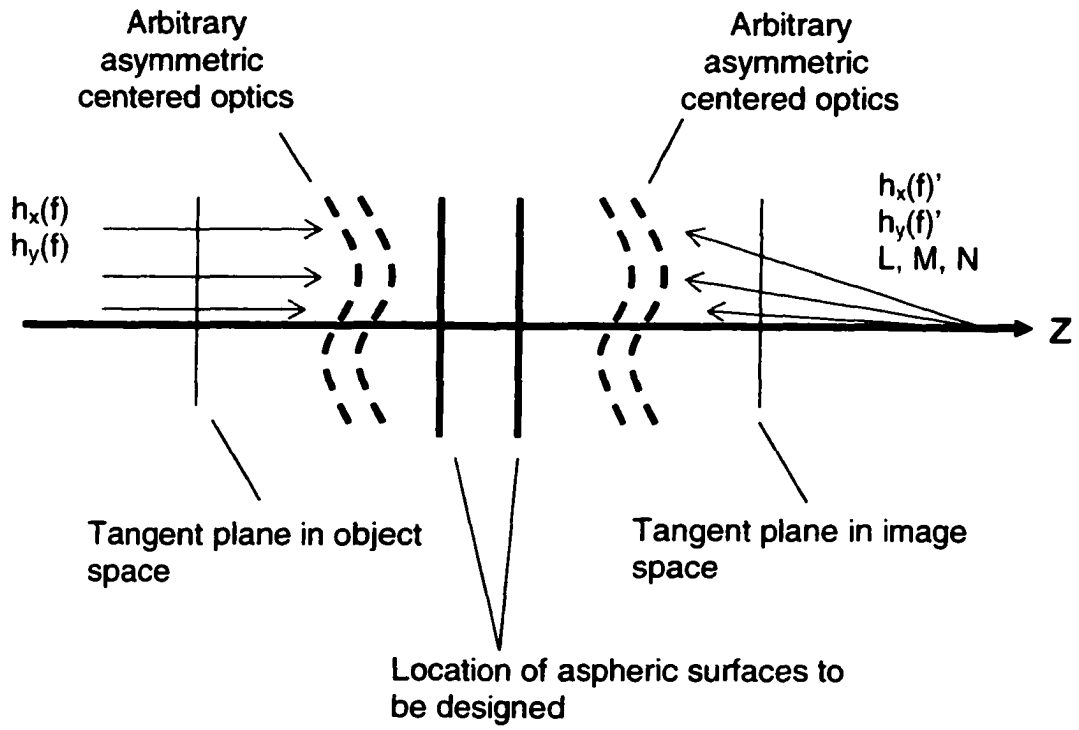

Figure 112. Layout of Asymmetric system

The optical elements contained in the asymmetric system may be tilted/decentered or non-rotationally symmetric. Rays in the bundle that are initially coplanar with the Z axis may be deviated out of plane. The ray bundle may also be displaced laterally, tilted, or have any variety of aberrations induced upon it. The generalized aspheric design equations are used to create the profiles of two aspheric optical surfaces to make the ray bundle defined in object space become the desired ray bundle in image space.

In addition to defining the ray bundles, the designer must select the location of the neighboring aspheric surfaces and the index of refraction between them. The ray bundles must be parameterized such that they fill the aperture of the system. This is performed with an aperture filling function.

Aperture Filling Functions

Te generalized asphere design equations describe the change in sag of two aspheric surfaces with respect to a change in a single ray parameter. In order to measure the sag of the aspheric element across two dimensions, one must parameterize the ray bundles so that a variation in the ray parameter also varies the ray in two dimensions. This section provides a method of defining the ray bundle through an aperture filling function.

The simplest function to conceptualize is one that contains sets of ray fans rotated about the optical axis. The intersection of the rays at the tangent plane object space is shown by the radial lines in Figure 113. The generalized equations are integrated for each ray fan starting from the optical axis. Along the axis, an initial sag of zero is assumed for both aspheric surfaces. This initial value of z1=0, and z2= 0 is necessary to solve the

equations for the next point along the blue line. Integrating the two equations along a fan of rays solves for a contour line of x,y,z values along each of the aspheric surfaces. This contour line corresponds to the intersection of the ray fan upon the aspheric surfaces needed to make the ray fan conjugate to the desired ray fan in image space. The equations are integrated repeatedly until there are enough x,y,z points across the aspheric surfaces to allow a surface fit.

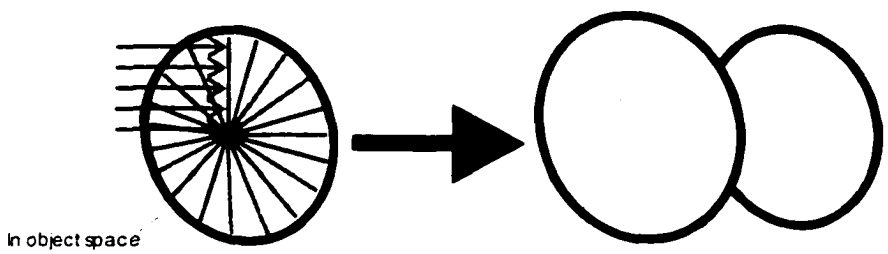

Figure 113. Tracing a single fan of rays creates a contour line on the two aspheric surfaces

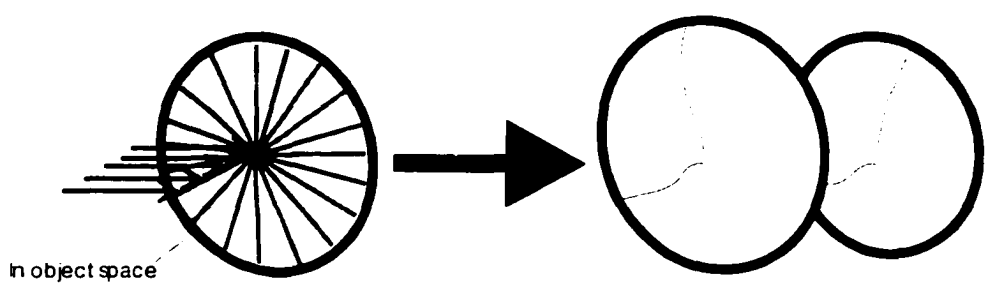

Figure 114. A ray fan in a different slice plane will trace out another contour line on the two aspheric surfaces

In the case of the radial aperture filling function, the equations are integrated out along fans of rays emanating from the optical axis.

Other aperture filling functions may be used. Different types are shown in Figure 115.

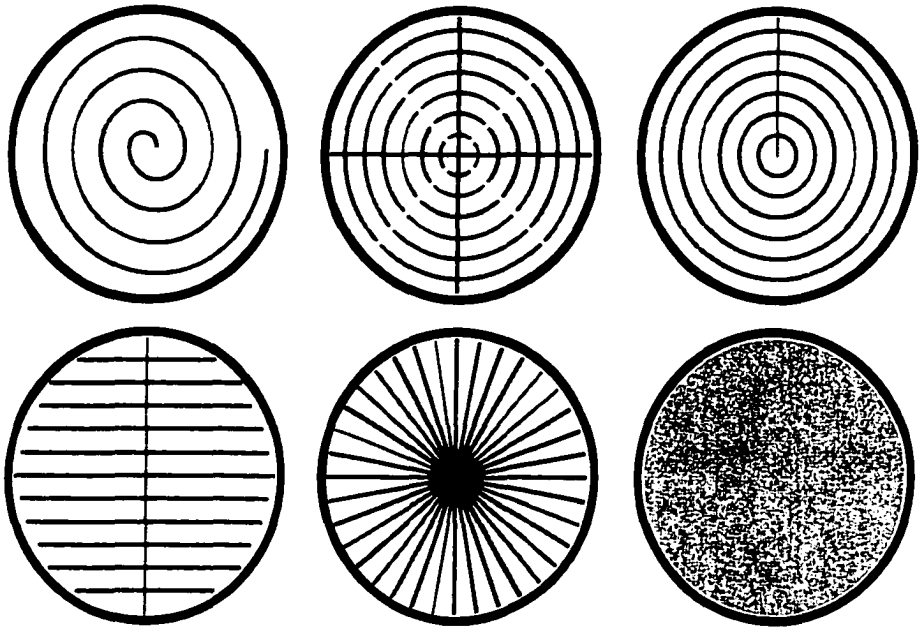

Figure 115. Examples of aperture filling functions. Rays are launched along the lines. The ideal aperture filling function fills in the aperture such that it is a solid color. I.e. the ray bundle samples the aperture to a very large density. In practice, one has to compromise due to computational limitations on the number of rays that may be traced in a reasonable amount of time.

Each aperture filling function defines a path along which rays are traced through the system to solve the coupled differential equations. Each ray in the aperture has a 1:1 mapping to a ray on the tangent plane in image space. At each tangent plane, the ray intersection coordinates and ray direction cosines must be defined.

The ideal aperture filling function will sample the aperture very densely and uniformly. This will produce a dense sampling of x,y,z points across the two aspheric

corrector surfaces. A surface fitting routine is then used to convert the two sets of points into surface coefficients so that they may be substituted into the design.

After the rays at the tangent planes in object and image space are defined, they are traced into the optical system and their coordinates and angles are recorded at the tangent planes of the aspheric surfaces. The coordinates and direction cosines at the aspheric surface tangent planes are then used in the solution of the generalized aspheric design equations.

$$L_1 = L_1(f) \qquad L_2 = L_2(f)$$
$$M_1 = M_1(f) \qquad M_2 = M_2(f)$$
$$N_1 = N_1(f) \qquad N_2 = N_2(f)$$
$$H_{x1} = H_{x1}(f) \qquad H_{x2} = H_{x2}(f)$$
$$H_{y1} = H_{y1}(f) \qquad H_{y2} = H_{y2}(f)$$

Figure 116. Direction cosines and coordinates at aspheric tangent planes

Abbe Sine condition revisited

One way of defining the ray bundles in the aperture filling function is to make them obey the Abbe Sine condition.

Previously, the Abbe Sine Condition was given for the finite conjugate case as

$$\frac{u}{u'} = \frac{\sin U}{\sin U'} = \text{constant}$$

Equation 48

and for the infinite conjugate case as

$$M' = -\sin(U') = -h / focal\_length$$

Equation 49

In the above equations, the angles and heights are with respect to the optical axis. The Abbe Sine condition is defined for rays contained in a plane defined by the optical axis and an orthogonal axis. In an axisymmetric system, a plane defined in this manner will have special properties.

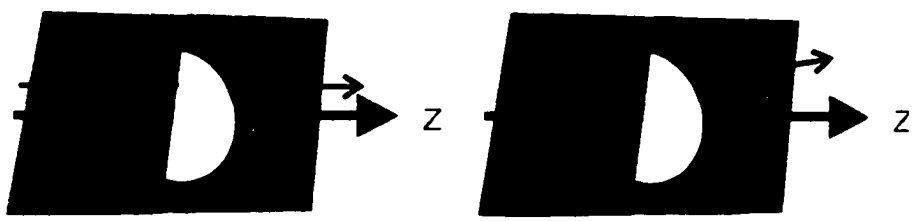

Figure 117. Rays in a plane passing through the axis of symmetry

By definition of axial symmetry, a ray fan contained in this plane in object space will remain in the plane throughout the system into image space. Put another way, every ray in the fan will only encounter surface normals that are contained in the plane. Rotating the fan of rays about the axis of symmetry produces no change in the rays. Accordingly, each ray in the fan may be specified by an angle with respect to the optical axis and the height of the ray in the direction orthogonal to the optical axis.

In a non-axisymmetric optical system, one may define a plane containing a desired optical axis passing through the system and an orthogonal axis. A ray fan contained in the plane in object space will not necessarily remain in the plane throughout the optical system. Due to the lack of an axis of symmetry in the plane, rays may encounter surface normals that are out of plane. Consequently, rays may be deviated out of the plane.

Unlike the axisymmetric case, rotating the fan of rays about the optical axis may change the fan of rays in image space. For instance, a cylindrical element with curvature in the X-Z plane will have no effect on the rays if the rays are incident along the Y-Z plane. However, if the ray fan is rotated about the axis such that it is incident on the cylindrical element at the X-Z plane, the ray fans will be refracted.

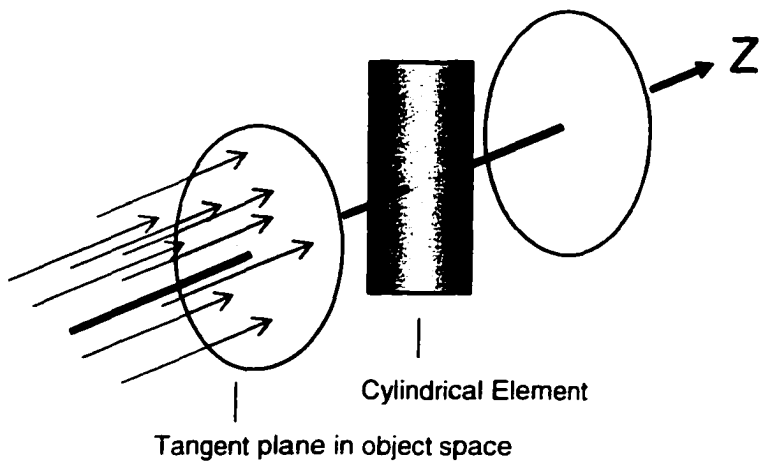

Figure 118. A cylindrical element will add anamorphic power

The desired behavior of the system may be that it acts like an axially symmetric system.

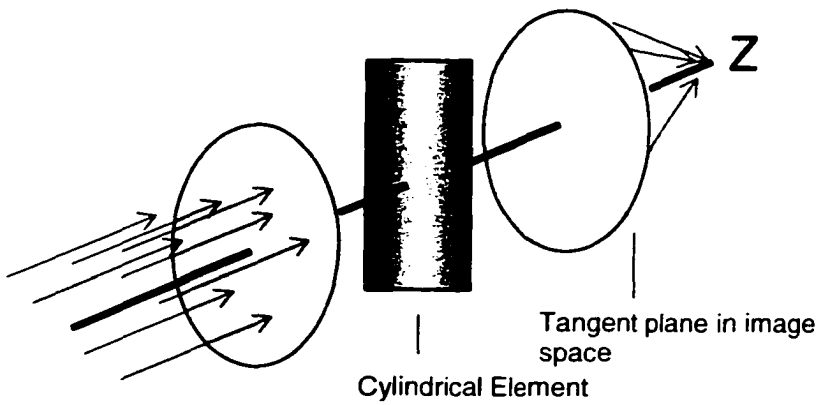

Figure 119. The preferred conjugate bundle in image space may be rotationally symmetric in image space.

Given this desire, one may formulate the Abbe Sine Condition for a non-axisymmetric system to provide a 1:1 mapping between a tangent plane in object space and one in image space.

Consider a plane slicing through the ray bundles which contains the optical axis Z. Conceptually, this plane will "slice" through an optical system. In terms of an X-Y-Z coordinate system, the plane will be rotated about the optical axis Z at some angle phi.

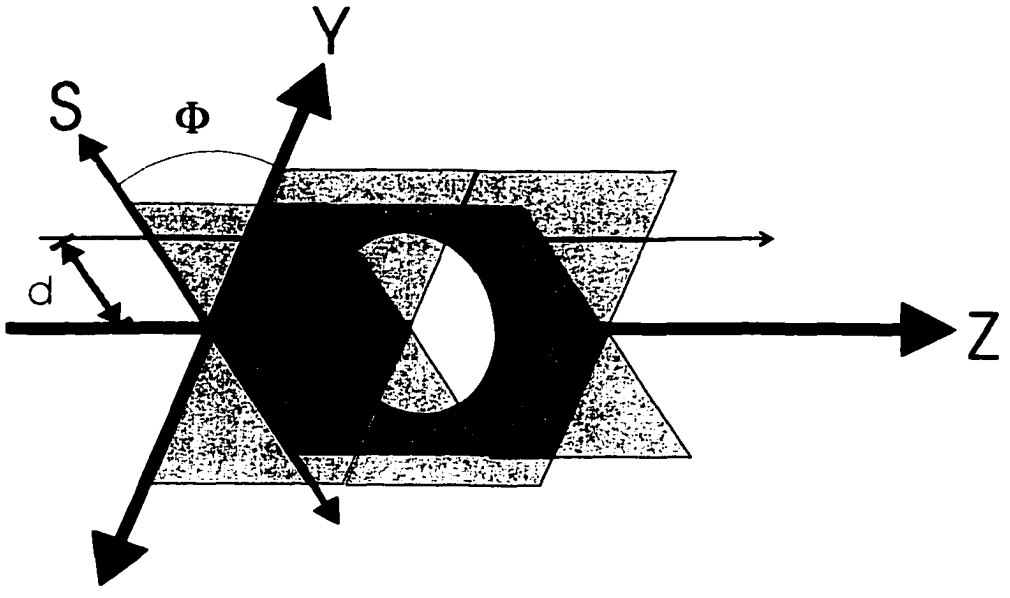

Figure 120. A slice plane containing a ray and the optical axis

One may define an axis S that is contained in the slice plane and rotated about the Z axis away from a Y axis. A ray contained in the slice plane will have a point along the S axis as seen in Figure 120. One may consider the slice plane to run through the optical system into image space. At the tangent plane in image space, one may define a conjugate ray with respect to a distance along the S axis and an angle along the slice plane. This is shown in Figure 121.

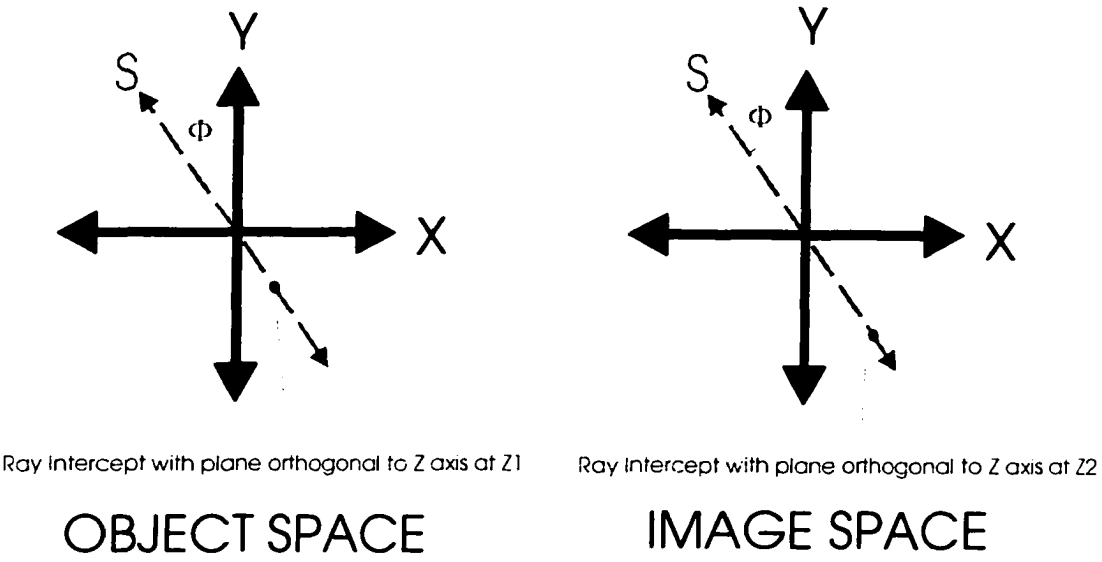

Figure 121. A ray contained in the Slice plane.

For the ray to be contained in the slice plane both in object and image space, the ratio of the x to y coordinates of each point along the ray in object and image space must be a constant. One may also specify a point along the ray in terms of the distance along the slice axis to the z axis. Let this distance be s.

Thus, for a particular plane:

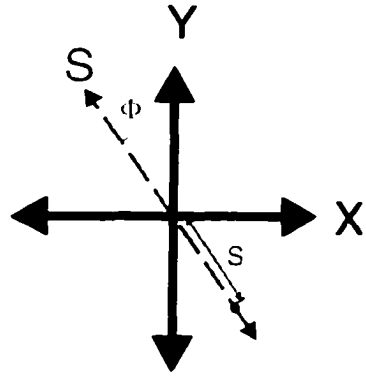

Figure 122. A point along the ray in object or image space

$$x = s \cdot \sin(\Phi)$$
$$y = s \cdot \cos(\Phi)$$
$$x : y = \text{constant}$$

Equation 50

To further uniquely define a ray in a slice plane, one may specify the angle of the ray with respect to the Z-axis in the Slice plane. One may now use the Abbe sine condition with respect to this angle.

$$\frac{u}{u'} = \frac{\sin U}{\sin U'} = \text{constant}$$

Equation 51

where u, u', U, and U' are all in the slice plane

For an infinite conjugate case, the sine condition is specified using the position along the S axis and the angle.

$$M' = -\sin(U') = -s / focal\_length$$

where U' is in the slice plane and s is the distance along the S axis in object space

Equation 52

Using these equations, one may define a ray in object space contained in a slice plane and calculate a corresponding ray in image space that satisfies the sine condition. This form of the Abbe Sine condition may be used in non-axisymmetric systems to define axial ray bundle behavior that makes it behave on-axis like a rotationally symmetric system. As before, the Abbe Sine Condition creates spherical principal surfaces that are centered about the object and image points. Each ray in the bundle that strikes the first

principal surface has a 1:1 mapping into a ray emanating from the second principal surface.

A ray bundle that satisfies the Abbe Sine Condition will have every ray in the bundle directed toward the image point. As a result, any on-axis aberration that was present before satisfaction of this condition will be removed. Furthermore, since there is a precise 1:1 scaling between the entrance pupil and the exit pupil, the Abbe Sine condition will be satisfied and linear coma corrected.

Summary

This chapter derived a set of generalized aspheric design equations for use in complex optical systems. These equations are derived using a general ray passing through an optical system. The position and direction cosines of this general ray is described by means of a pair of tangential planes, one in object space and one in image space. At each plane, the intersection position of the ray with the plane is defined along with the direction cosines of the ray at the point of intersection. A pair of adjacent general aspheric surfaces are used to control the passage of the ray such that the ray defined at a tangent plane in object space will have the desired position and direction cosines at a tangent plane in image space. The ray is considered to be contained in a bundle of rays defined through a parameter f. Varying the parameter f changes the ray selected in the bundle. The generalized aspheric design equations are derived to show the change in sag of the two general aspheric surfaces as a function of the change in the ray parameter. Integrating along the parameter produces the sag profiles of the two aspheric surfaces. The ray bundle must be parameterized such that all the rays intersect the aspheric surfaces at enough points to allow an accurate surface fit.

The generalized equations work for systems containing non-rotationally symmetric components, and/or tilted and decentered components. Solving these equations for a given optical system produces the three-dimensional profiles of two general aspheric surfaces that can be placed in the system to convert a specified ray bundle in object space into a desired ray bundle in image space. One may define the ray bundle such that it meets the Abbe Sine Condition and also focuses to a single point. The result is that the system will be free from coma and spherical aberration. Correcting

coma and spherical aberration creates a region of imagery near the center of the field that is relatively aberration free. At higher field angles, other aberrations such as astigmatism and field curvature will start to dominate. This system may be sufficient as a final design, or used as a starting point for interactive design.

"Example is not the main thing in influencing others. It is the only thing."
Albert Schweitzer

CHAPTER 4- Examples

This chapter looks at several examples to illustrate the operation of the Wassermann-Wolf design macro and General Asphere design Program (GAP) macro. The first example is a singlet design. This example illustrates a design approach with a conventional damped least squares (DLS) method versus a direct method using differential equations. The second example illustrates conformal dome design with the Wassermann-Wolf macro. This example shows the effectiveness of the Wassermann-Wolf macro for the design of rotationally symmetric systems. The third example is a prism. GAP is able to produce a single element with the functions of two conventional elements to correct tilt and decenter from the prism. The fourth example is a pair of cylindrical elements. GAP is used to correct coma and the on-axis aberrations induced by the elements. The fifth example is a conformal window design for an automotive application. GAP is used to create a corrector to cancel the aberrations from the window.

SINGLET

This example illustrates many of the basic attributes of a solution arrived via optimization versus a solution arrived at via a differential approach. The singlet designed with the Wassermann-Wolf equations is shown to be comparable to one created with an interactive design approach.

Conventional Design

To begin, one can examine an ordinary BK7 F/1 singlet with a design wavelength of 500 nm. With all spherical surfaces, the singlet will suffer from spherical aberration.

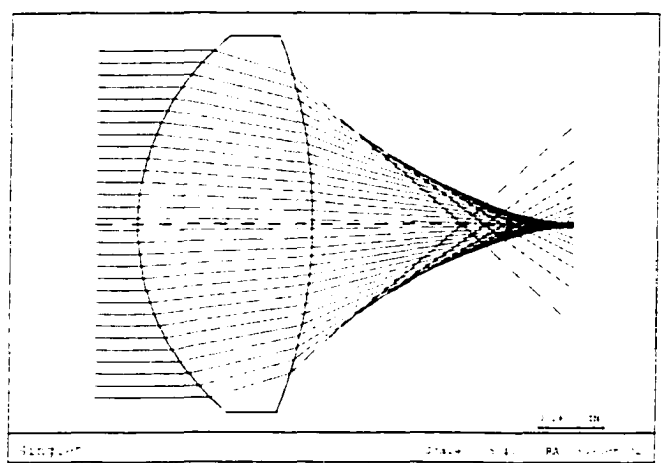

Figure 123. All-spherical BK-7 Singlet

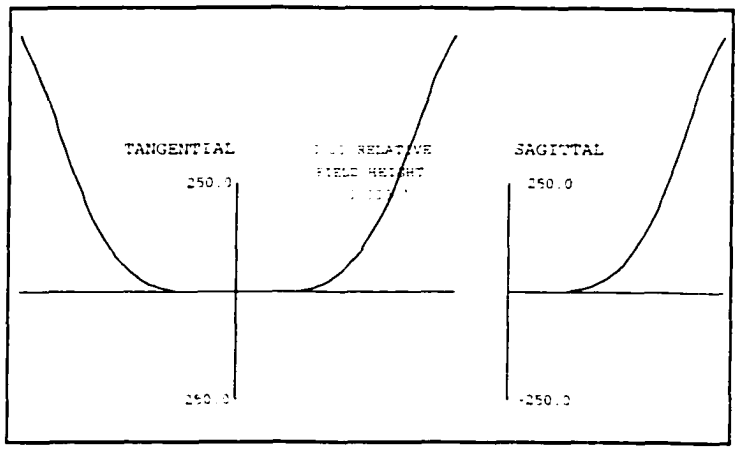

Figure 124. Wavefront aberration plot of all-spherical singlet

The all-spherical singlet shows a great amount of spherical aberration balanced by focus.

As is well-known, re-optimizing with a conic surface eliminates the spherical aberration. The system with a rear conic surface system is shown in Figure 125.

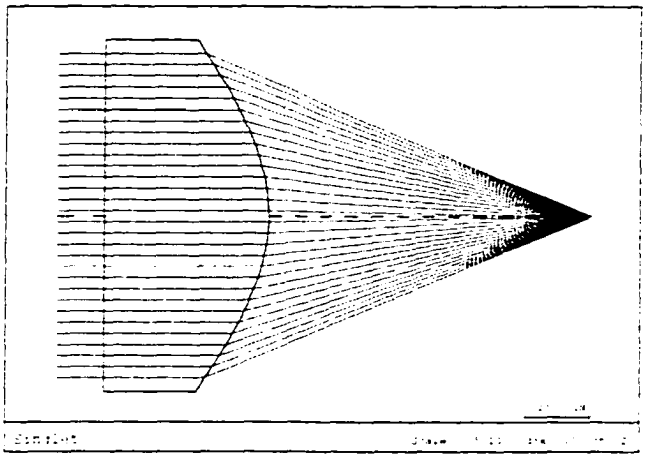

Figure 125. BK-7 Singlet with a Conic Surface

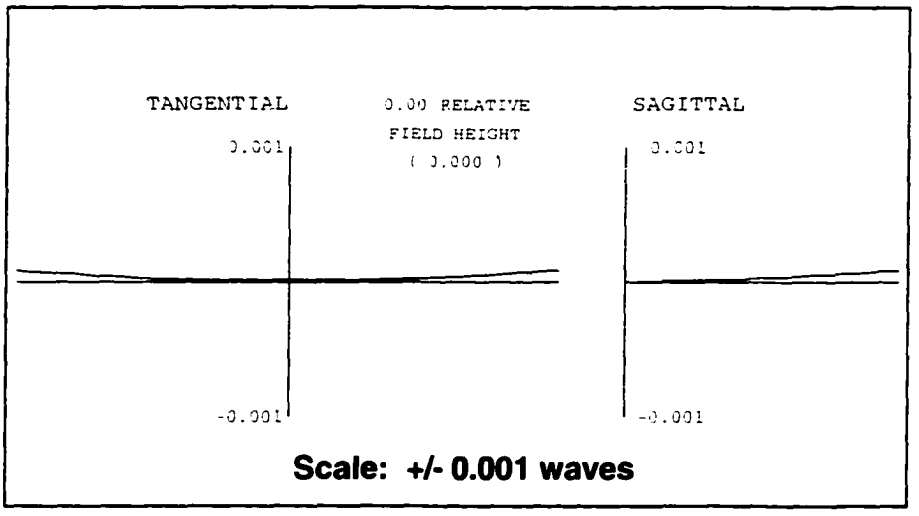

Figure 126. Wave aberration plot for lens with rear conic surface

The singlet shown in Figure 125 was optimized using Code V, the default merit function, and a zero degree field. It is insightful to plot offense against the sine condition (OSC) as a function of incident ray height. To meet the Abbe's Sine Condition, the

relationship between a ray at height h coming from an object at infinity, the focal length f, and the angle θ in image space should be: $\frac{h}{f} = \sin(\theta)$. The OSC may be plotted as a percentage difference from the ideal as a function of ray height. Percent difference is given by (Measured Value – Theoretical Value) X 100% / (Theoretical Value).

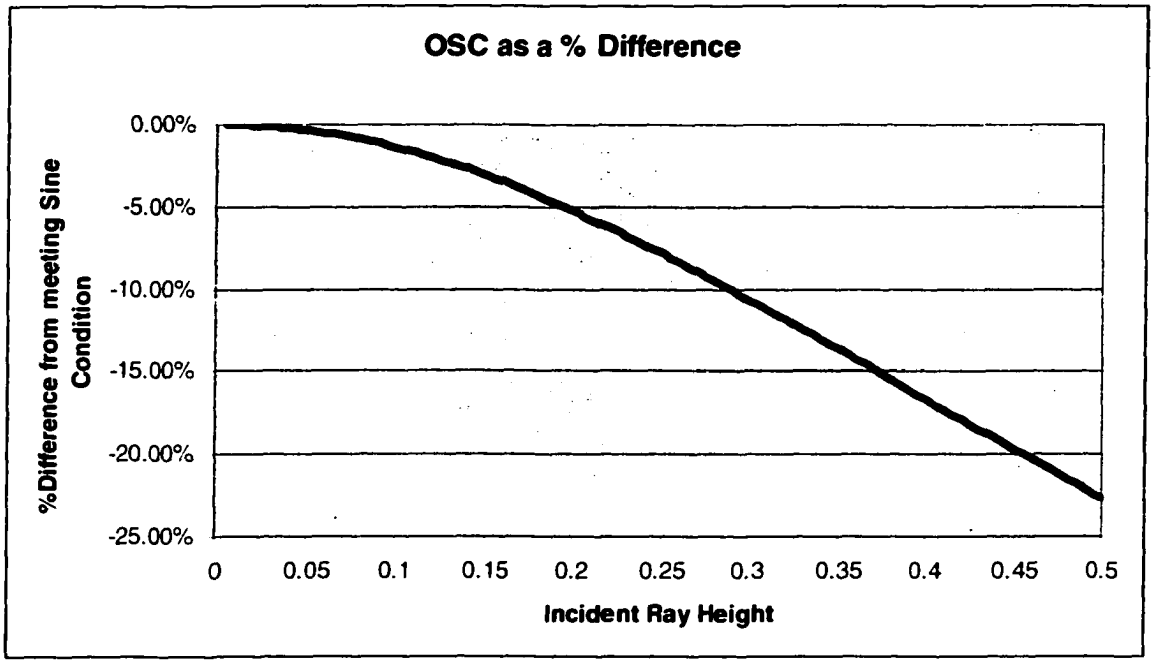

Figure 127. Plano-Conic Singlet has large OSC

Figure 127 shows that the sine-theta values for rays incident on the Plano-Conic singlet deviate significantly from the Abbe Sine Condition. As would be expected, this singlet has a substantial amount of coma for off-axis points.

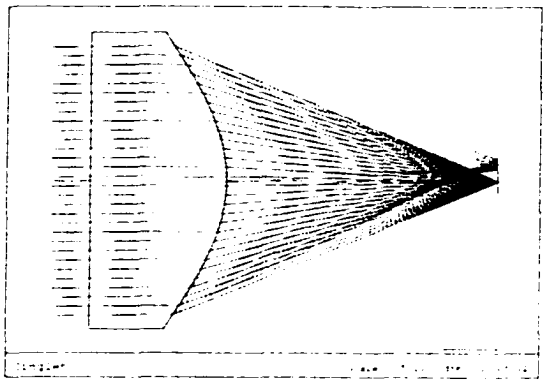

Figure 128. Plano-Conic Singlet with 2.5° field

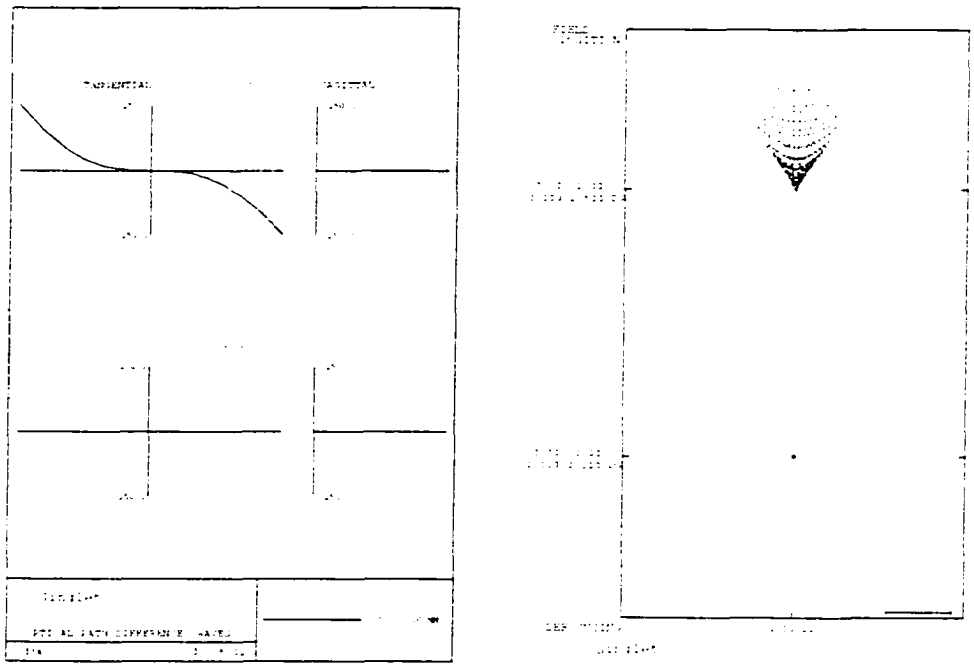

Figure 129. Wavefront Aberration and Spot Diagram of Plano-Conic Singlet

The singlet may be reoptimized with a 2.5° field, a variable back focal distance, and a constraint to fix the focal length to keep the singlet at F/1. This reoptimizaiton improves the aberrations in return for increased spherical aberration balanced by focus.

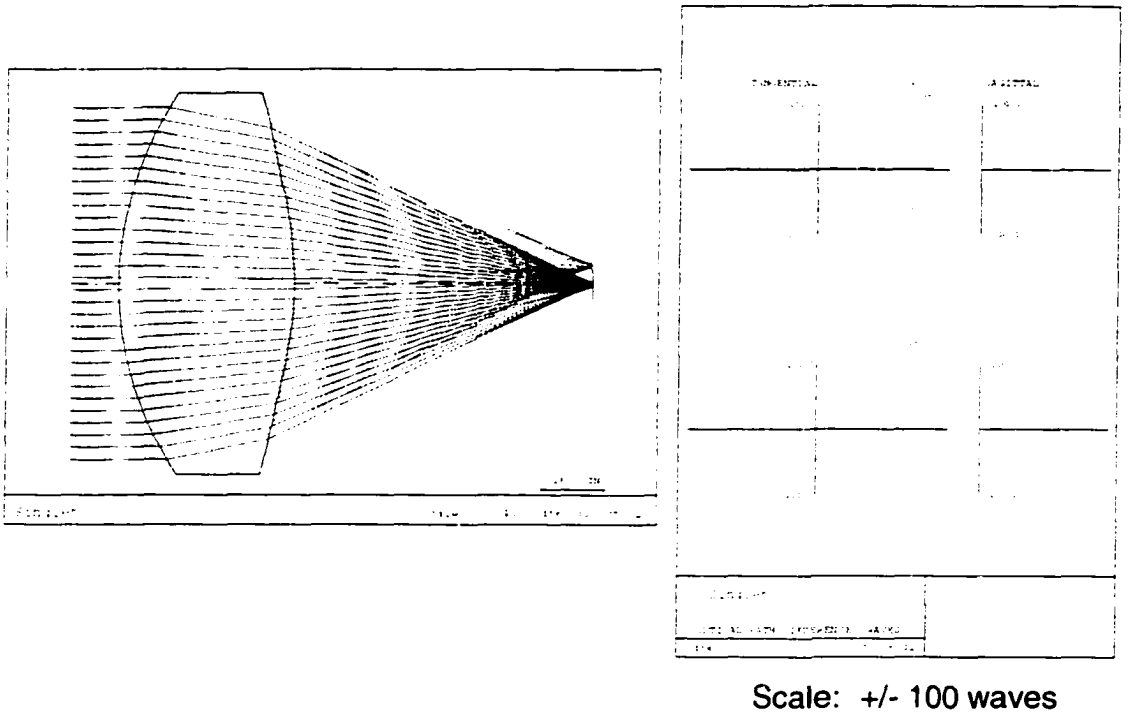

Figure 130. BK-7 Sphero-Conical Singlet

Allowing the both surfaces of the singlet to become aspheric, and reoptimizing with the previous constraints improves the performance even further. Each surface is converted into an even polynomial and the design is reoptimized beginning with low order coefficients and working to the higher order coefficients as needed.

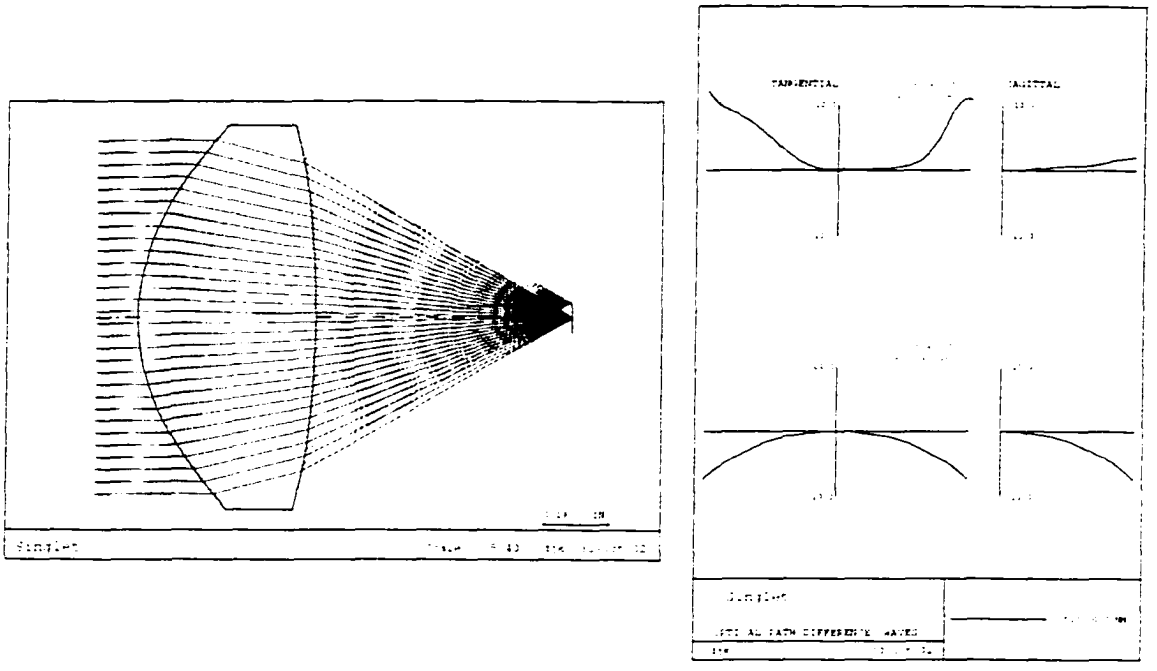

Figure 131. Double Aspheric BK-7 Singlet

Aberrations have dropped by an order of magnitude with the two aspheric surfaces. The polynomials used for the surfaces go out to the 10^{th} order. This design represents a typical local minimum in the solution space. Offense Against the Sine Condition (OSC) is also greatly reduced as shown in Figure 132.

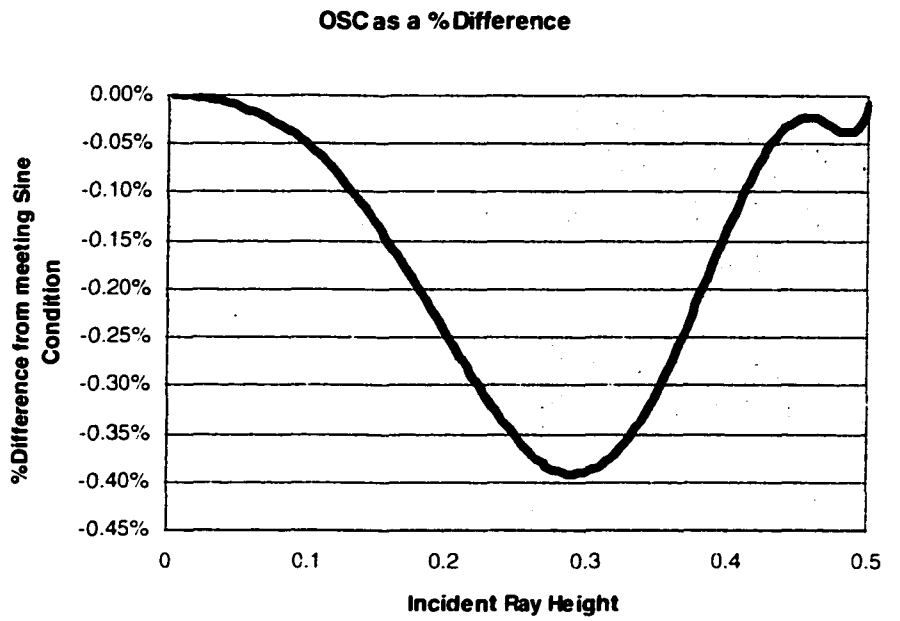

Figure 132. OSC for Aspheric-Aspheric BK7 Singlet

To improve performance, the designer might choose to perturb the design to kick it out of its local minimum, change the free parameters to alter the solution space landscape, or shift to a global optimization strategy to generate alternate starting points for further refinement.

Differential Design

The design of the singlet will now be approached using a differential design method.

Specifically, the Code V implementation of the Wassermann-Wolf equations will be used to generate an aplanatic F/1 singlet.

The initial lens is shown in Figure 133.

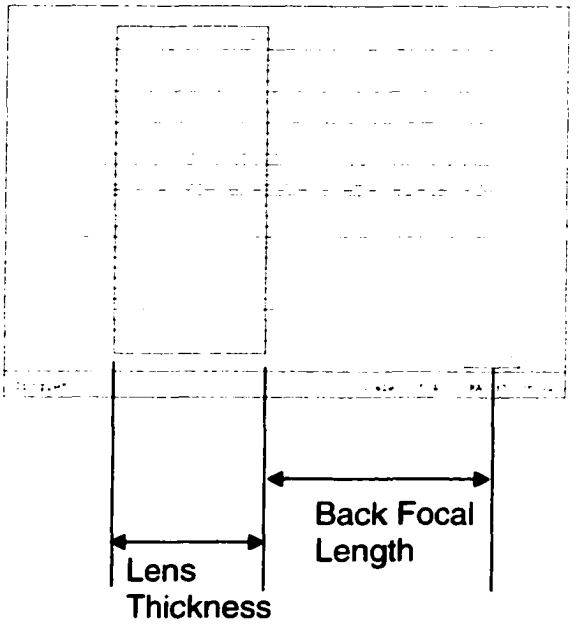

Figure 133. Initial Lens Setup

The inputs to the design program are the desired focal length, the number of points to use in the curve fit of the surfaces, and the number of additional points in between the points used on the curve fit. The material and thickness between the two aspheric surfaces is also selected as well as the back focal length. Since the object in this

configuration is at infinity, the entrance pupil diameter is defined by the designer. As the solution of the Wassermann-Wolf equations is through a numerical method, finite differences are used to approximate derivatives. Consequently, the smaller the step-size between points, the closer the finite differences will be to the true derivative.

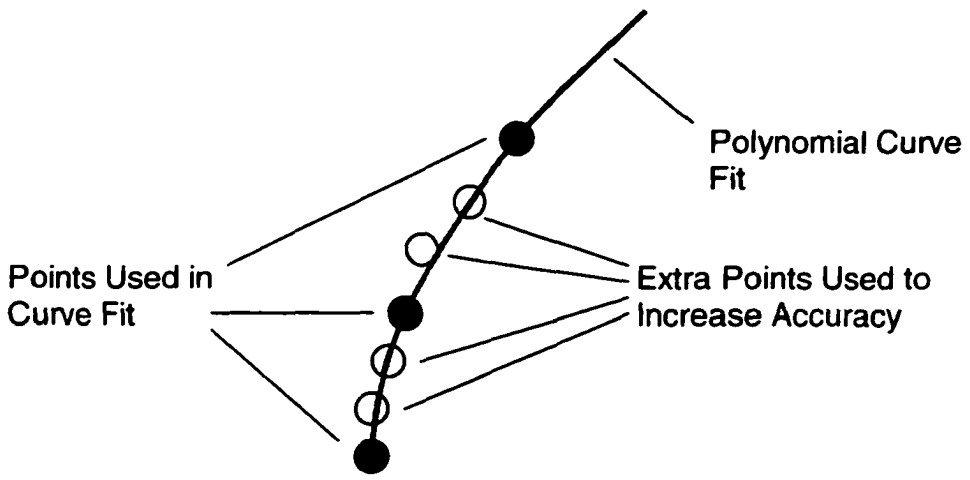

Figure 134. N*k steps are calculated, but only N steps are used in the curve fit.

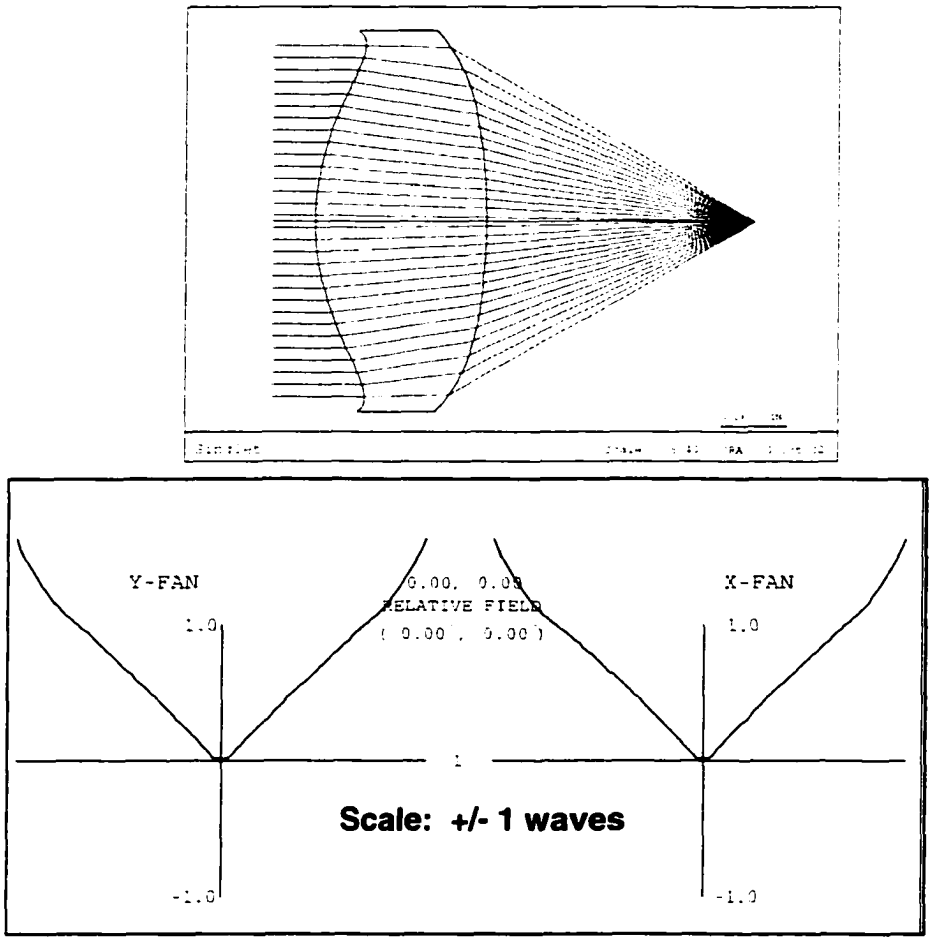

Figure 135. Result of Wassermann-Wolf Program used to create a singlet (50 * 50 sag points calculated for each surface, and 50 points are used in the curve fit)

The residual wavefront aberration shown on axis is error due to the integration of the Wassermann-Wolf equations. Using a large step-size results in a sizeable increase in error. Similarly, decreasing the step size decreases the error. Figure 136 shows the same configuration with a smaller step size.

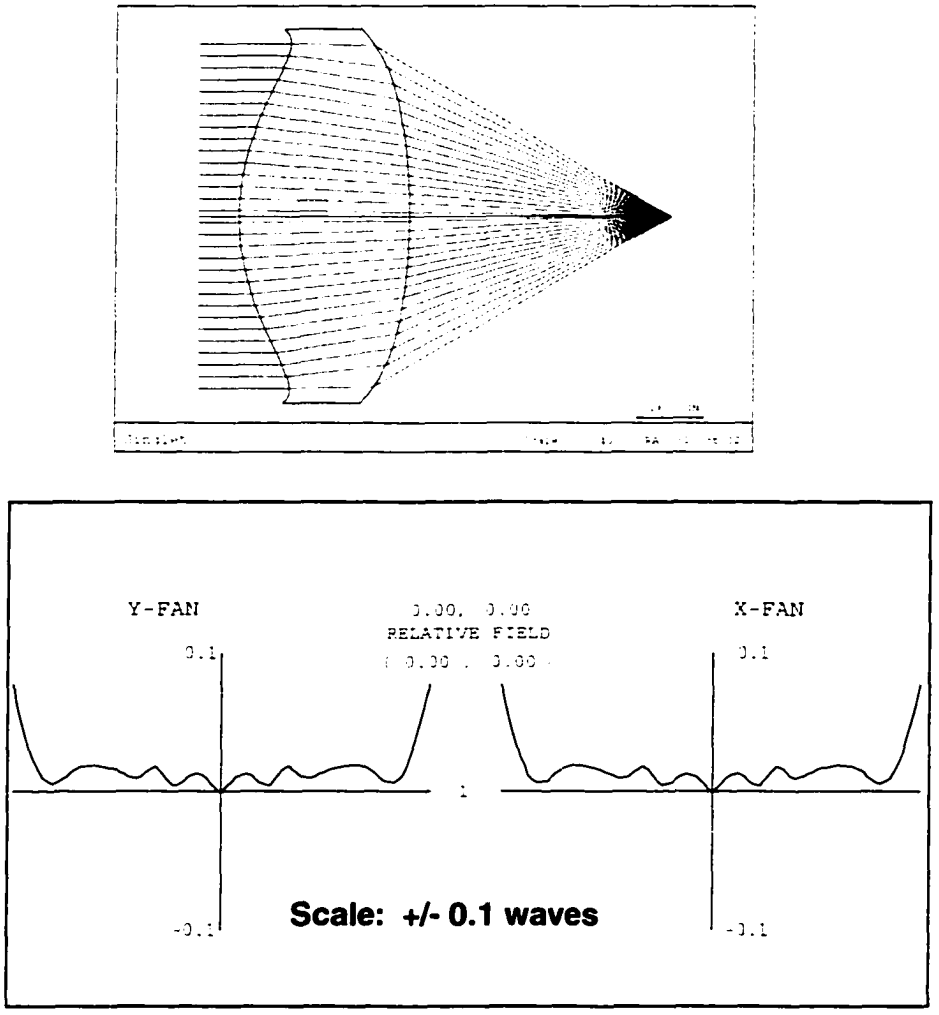

Figure 136. Result of Wassermann-Wolf Program used to create a singlet (300 * 3000 sag points calculated for each surface, but 300 points are used in the curve fit)

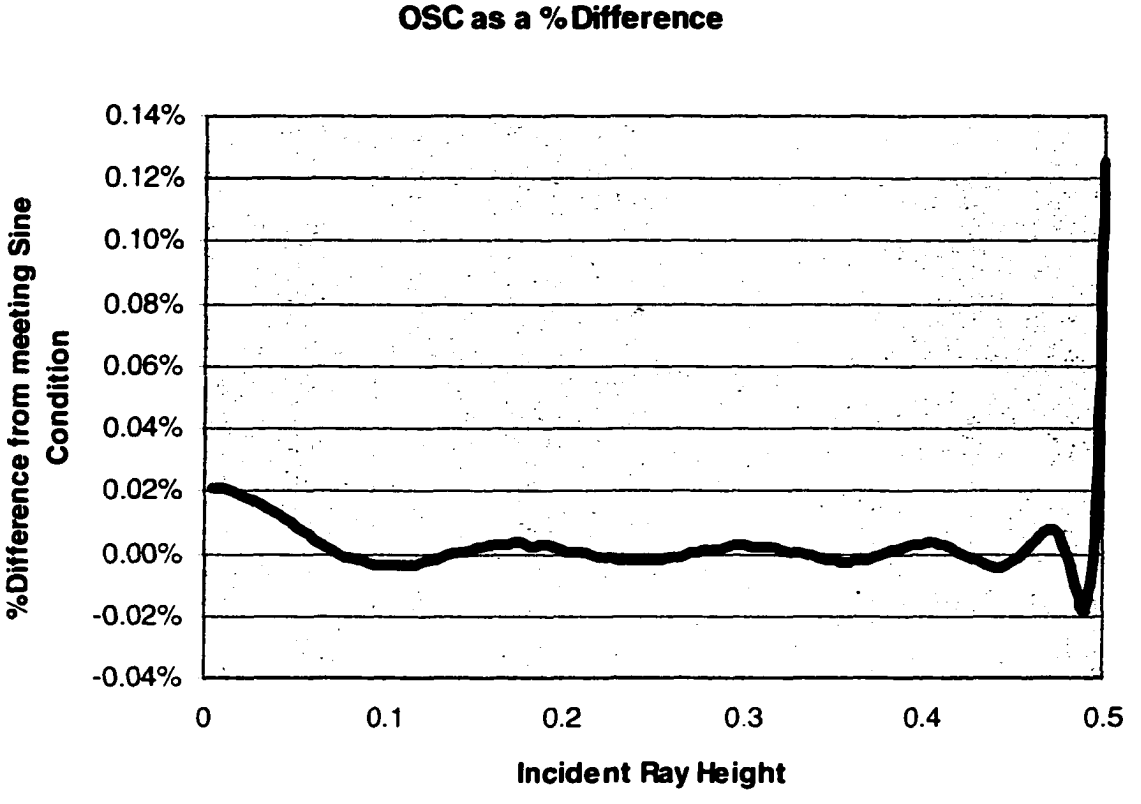

Figure 137. Offense Against the Sine Condition is Substantially Less for New Design. This chart also verifies the operation of the algorithm to prove that the Abbe Sine condition is met.

A 2.5° field may be added to the singlet designed by differential design. No other changes are made to the singlet. The 2.5 degree field shows a great deal of astigmatism. What is very interesting is that the relative magnitudes of the aberrations is about half of the aberrations for the asphere-asphere design arrived at via Damped Least Squares optimization and a default merit function.

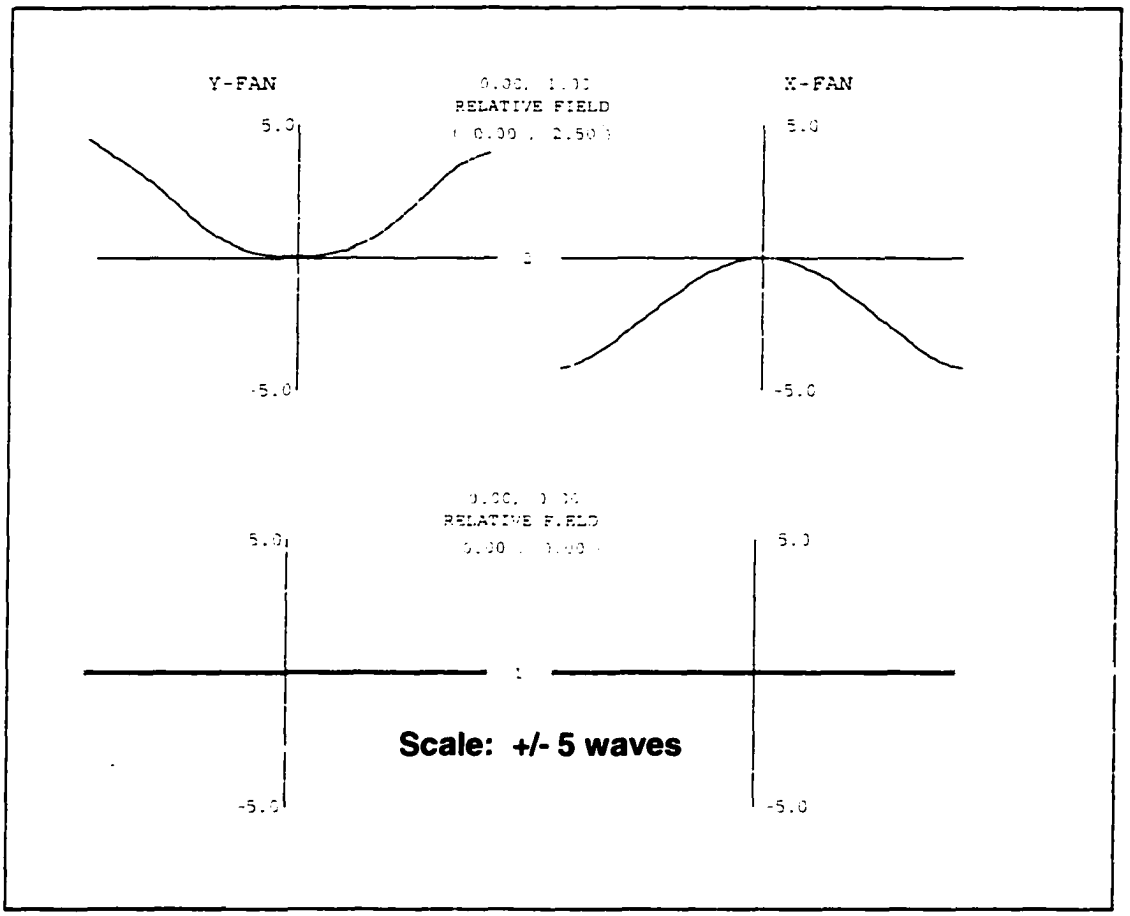

Figure 138. Wave Aberrations of Singlet

For comparison, the spot diagrams of the two designs may be placed side by side at the same scale. The spot sizes of the singlet arrived at via a differential design method is smaller. Clearly, there is much less coma in the design created via a differential equation method. This has an effect on the centroid position. The deviation of the centroid from the chief ray for the traditional design is 2.2 microns for the edge of the field. The deviation in the centroid from the chief ray for the differential design is -0.185 microns, an order of magnitude less. The RMS geometrical spot sizes for the traditional design at 0° and 2.5° are 24 and 32 microns respectively. The RMS geometrical spot sizes for the differential design at 0° and 2.5° are 2 and 12 microns respectively.

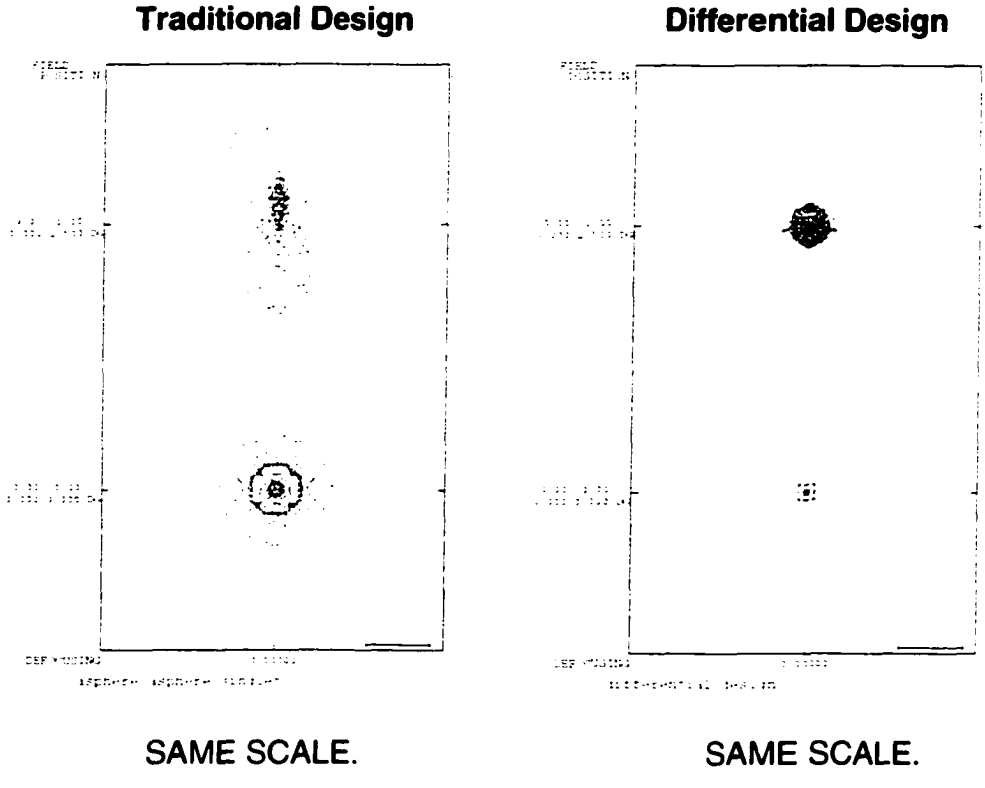

Figure 139. DLS vs. Differential Design Performance

The point of this comparison is not that a design arrived at via differential design methods will always be superior to a DLS design. Rather, the comparison shows that a differential design approach can produce a design comparable to a DLS design. It is quite conceivable that the DLS design could be made equal to the differential design. Indeed, the results from the Differential Design prove that it is theoretically possible to improve performance. However, the designer would have to change the merit function, use different surface types on the two surfaces, shift the stop, or use a global optimization technique.

The fascinating aspect of differential design is that the aspheric element is arrived at directly. The on-axis rays are controlled very precisely. Furthermore, a differential design method generates a sag table of values to any desired precision. The curve fit to the sag table tells the designer if the appropriate surface representation is being used and the parameters are useful. If the surface representation is invalid, it will show up as an RMS fitting error to the sag points. For example, trying to fit a spherical surface to a sag table with a large aspheric departure will create a huge RMS fitting residual. The designer would immediately know that the spherical formula will not work to represent the aspheric surface.

In his 1983 Ph.D. thesis, John Rogers looked for different aspheric formulas to solve various optical problems. Rogers found a striking correlation between equations that could be curve fit effectively to a Wassermann-Wolf sag table, and the ability of these equations to effectively cancel aberrations. Furthermore, parameters that were

significant in fitting a surface became effective design variables when the system created by the Wassermann-Wolf equations was optimized further.[64]

To reduce residual wavefront error, the designer can improve the sampling or solve the Wassermann-Wolf equations with a more accurate method. The designer may also choose to send the design into an interactive design method such as DLS, knowing that the starting point is near a useful point in design space.

By comparison, an aplanatic design arrived at via a traditional DLS method can take a significant amount of designer experience and interaction. The actual calculation of the solution via a differential approach can take substantially longer than a typical DLS run. (A differential approach can take from minutes to hours to complete. An optimization cycle can take from seconds to minutes to complete depending on the design complexity.)

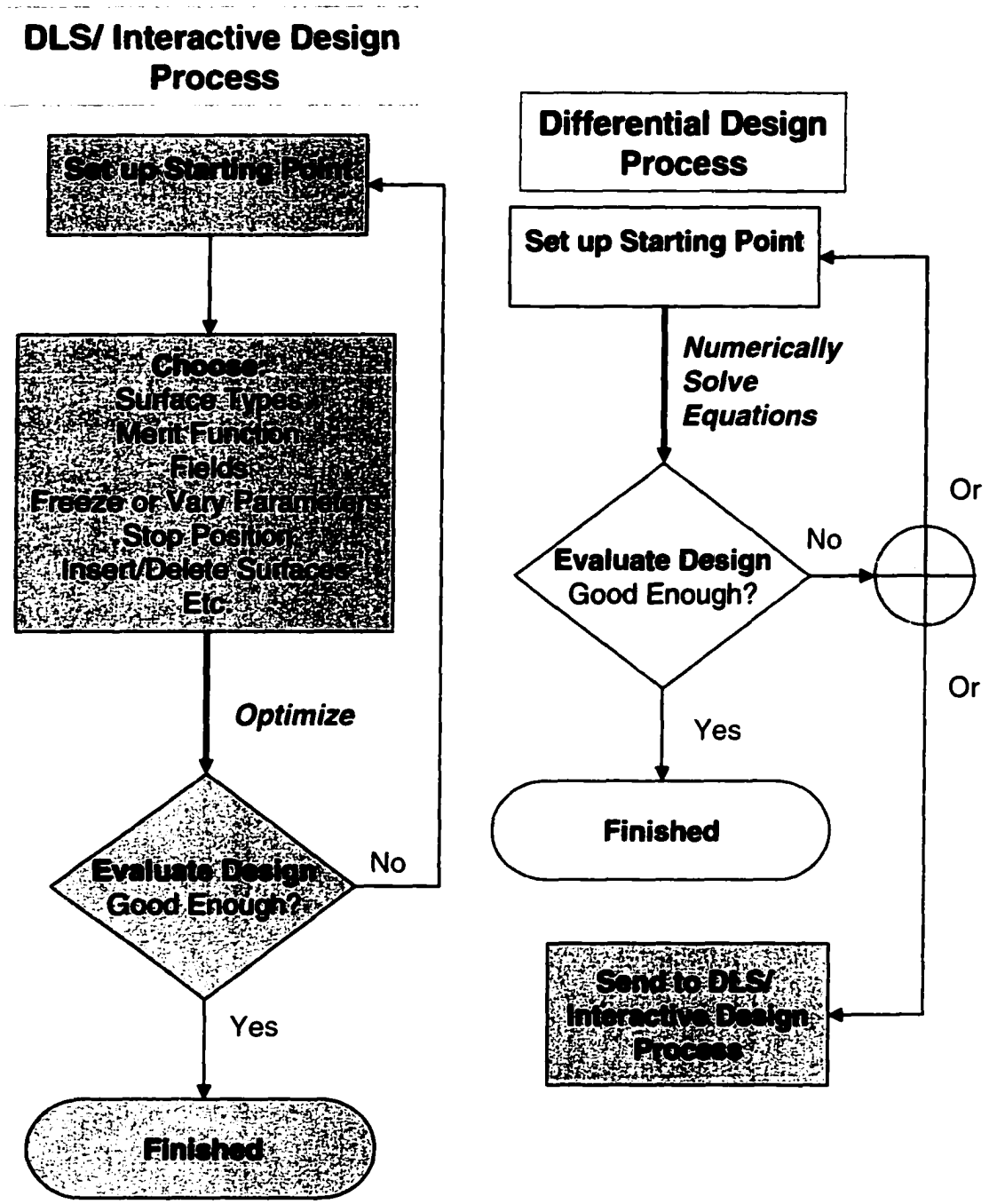

Figure 140. Comparison of Interactive vs. Differential Design Process

Conformal Dome

Another case of interest is the design of fixed correctors for conformal domes. Designing a corrector using Wassermann-Wolf is very straightforward. First, one defines the dome shape and material. Second, one defines the thickness, material, and position of the corrector. Third, one solves the Wassermann-Wolf equations to generate the corrector profile. In the solution of the Wassermann-Wolf equations, one must select the step size for the numerical solution. A high amount of sampling (lower step size) reduces the residual aberration.

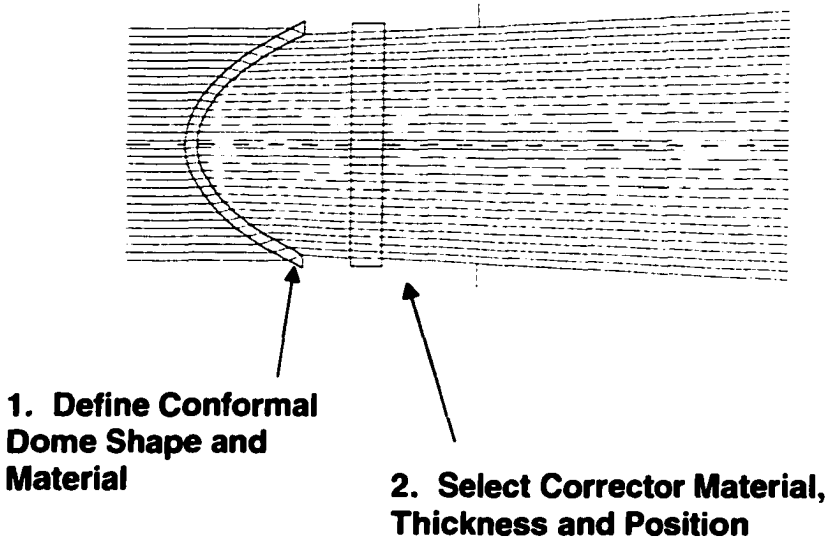

Figure 141. Layout of Conformal Dome

The layout of the dome system after application of the Wassermann-Wolf macro is shown in Figure 142. The dome is a fineness ratio 1.5 Magnesium Fluoride dome with a Magnesium Fluoride corrector. The initial aperture diameter is set to 1.5". The corrector creates a collimated wavefront in image space.

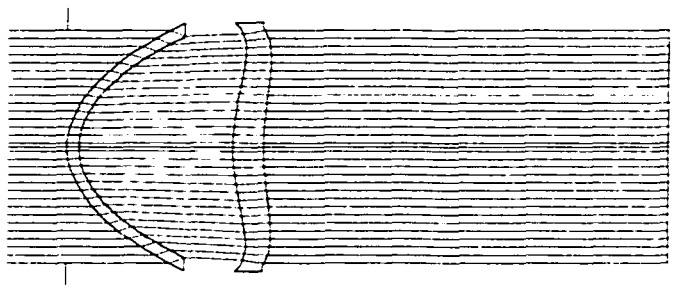

3. Select sampling density and Execute Wassermann-Wolf macro

Figure 142. Layout of Dome after WW Macro

The Wassermann-Wolf equations may be solved with 100,000 rays to create a system with less than 0.01 waves of residual aberration.

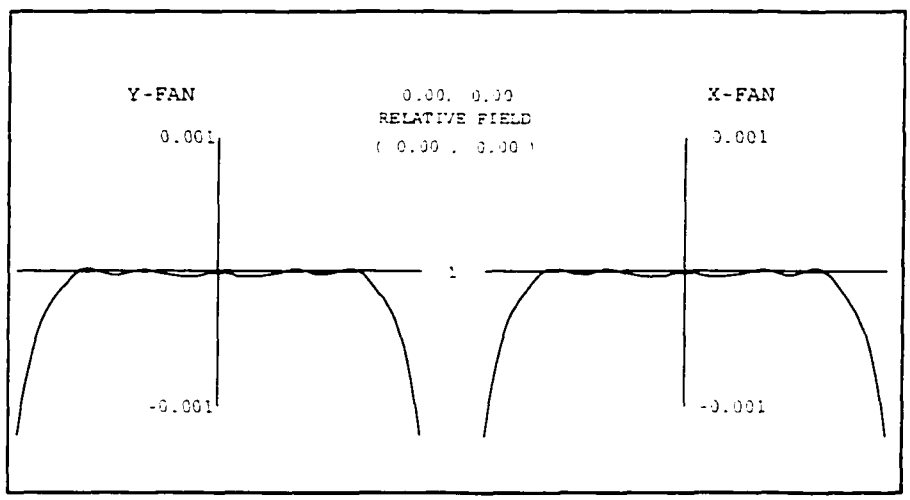

Figure 143. Wave Aberration Plot of system created with 100,000 rays
Scale +/- 0.001 Waves

Using only 10,000 rays in the calculation leaves residual aberration on the order of 0.1 waves.

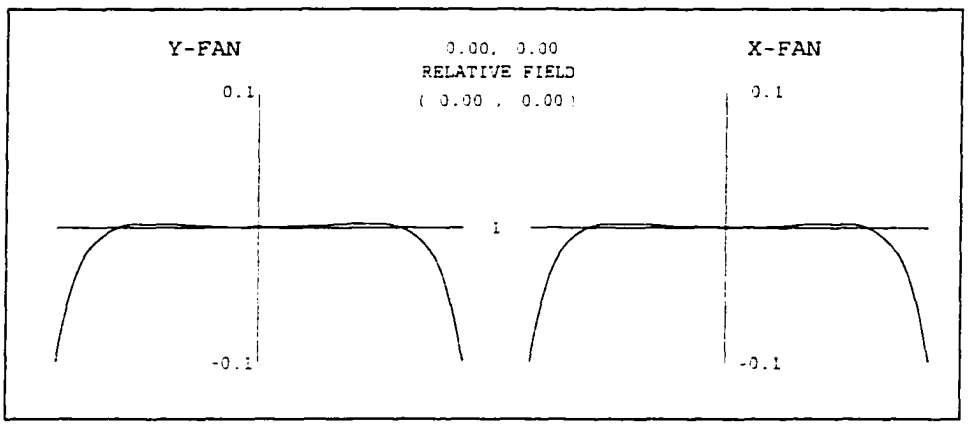

Figure 144. Wave Aberration Plot of system created with 10,000 rays
Scale +/- 0.1 Waves

Finally, one may stop down the system, add a field of view, add a field of regard, and add an imaging system.

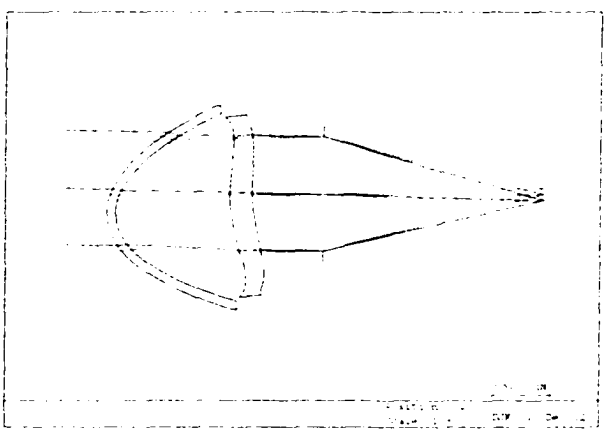

Figure 145. System with perfect lens added

Window with Wedge
Conventional Approach

In the layout shown below, a window with significant wedge is deviating a beam by 1.75°. The entrance pupil is set initially at 2". The initial wavelength of interest is 4 microns. To correct for this window, one may design a corrector optical element. A traditional approach to this problem might be to place another prism immediately behind the first prism of equal power, but opposite orientation. The double prism solution form will decenter the ray bundle with respect to the original optical axis.

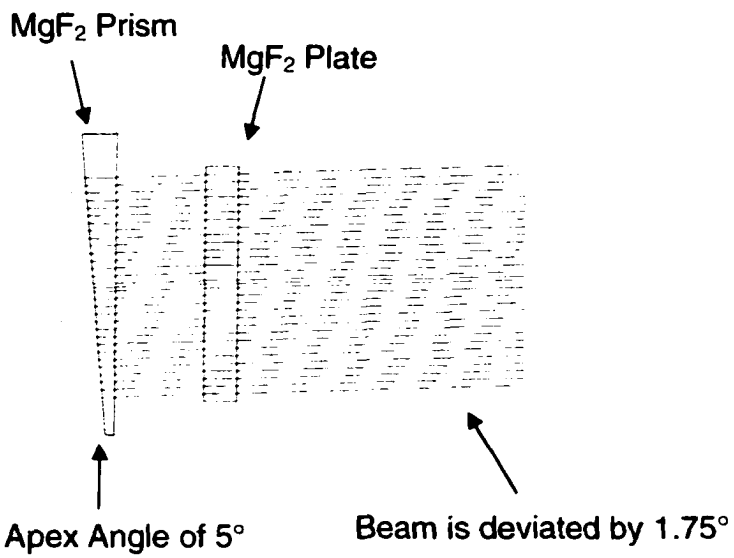

Figure 146. Initial Setup

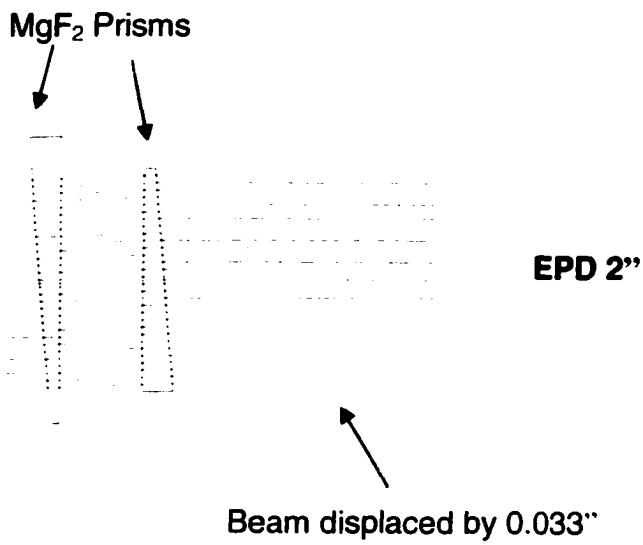

Figure 147. Window with wedge

The layout above shows the traditional solution to imaging through a window with non-parallel faces. Beam displacement can be corrected by tilting a plane parallel plate after the second prism. If the light remains collimated coming in, this nominal system imparts no aberrations to any optics that follow.

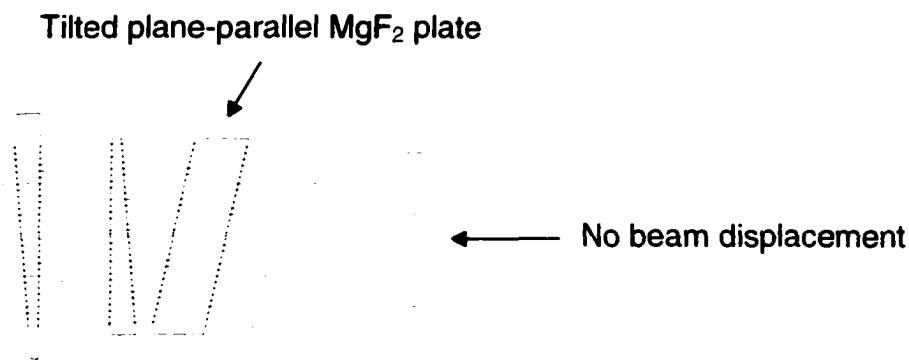

Figure 148. Adding a tilted plane parallel plate

GAP Approach

In the conventional approach, one element is used to correct the beam angle and a second element may be used to correct the beam displacement. Another solution approach would be to use the GAP program to design a single element that simultaneously corrects beam angle and displacement. The corrector element with its complex surface is directly generated by the GAP program. The magnification of the prism/corrector combination is set to one. The EPD on this system may be set to 1" and the field increased to more than +/- 10 degrees with a slight amount of induced astigmatism induced. Decreasing the EPD ensures that the beam footprints fall on useable portions of the corrector.

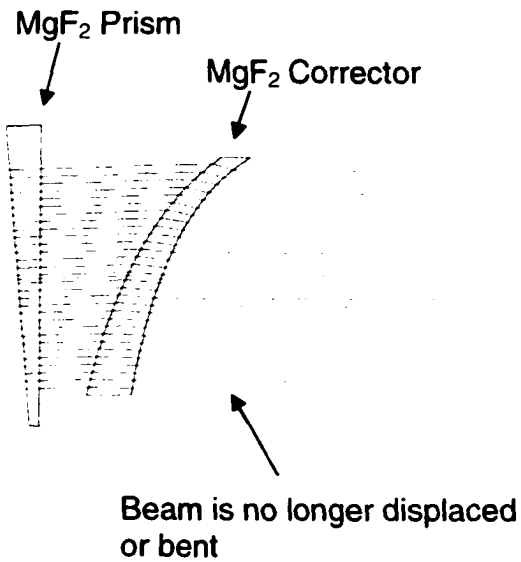

Figure 149. Corrector created using
Differential Design Appraoch

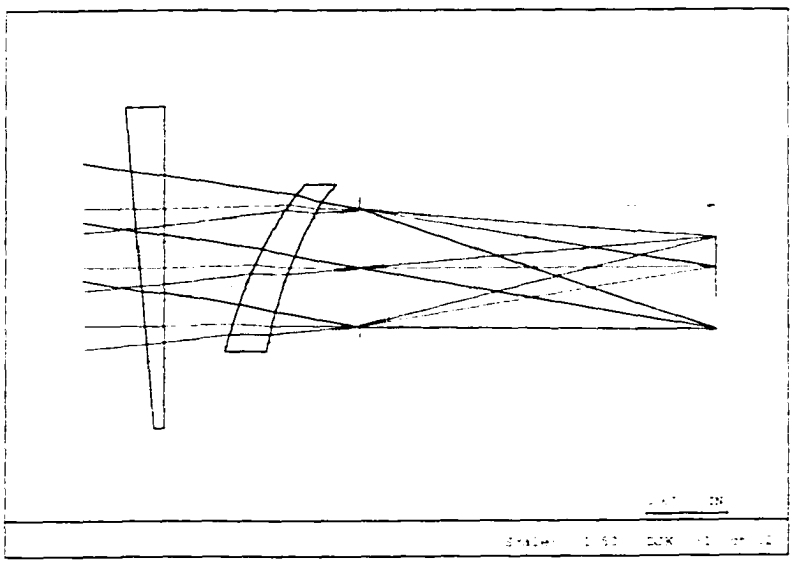

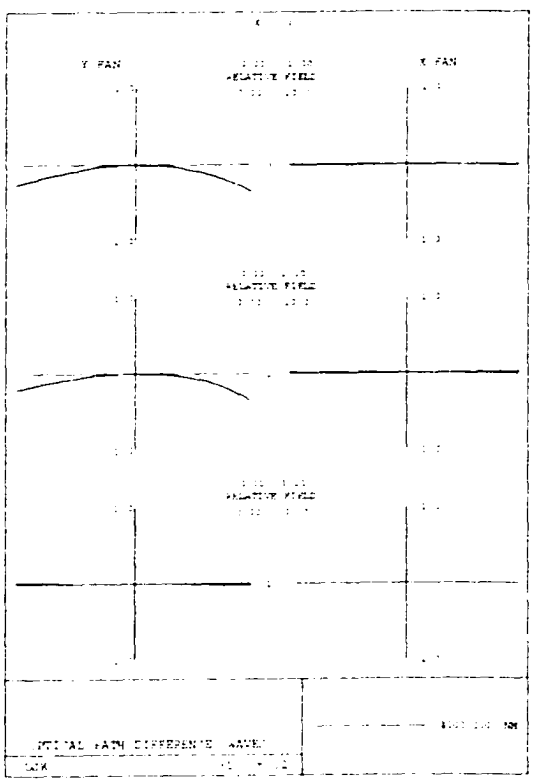

Scale: +/- 1 waves

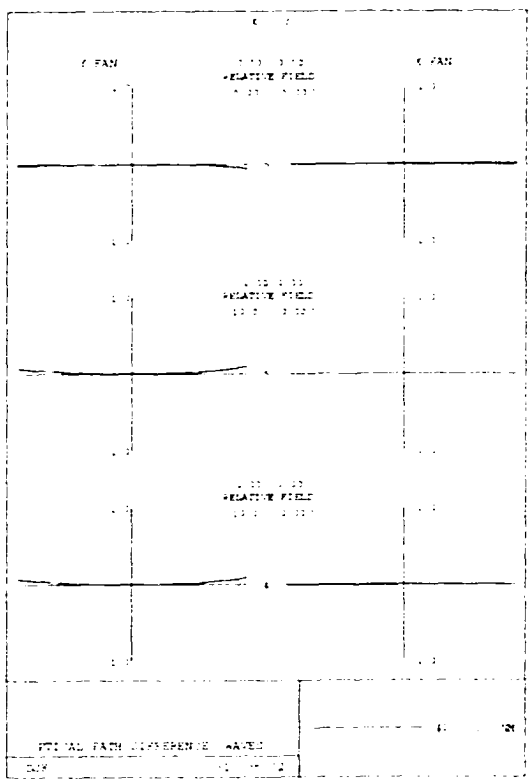

Scale: +/- 1 waves

Figure 150. Design Supports Large FOV

A similar single element design created by a conventional method would involve writing a merit function to control the ray angles and locations in the exit pupil. Additionally, the designer would need to select an appropriate surface type and attempt to find the parameters with the most leverage to meet the performance criteria. In contrast, the differential design approach directly reaches the solution with little designer involvement beyond the initial setup and the final analysis.[‡‡]

Another general insight can be seen in this example. When the beam incident on the aspheric corrector is tilted with respect to the optical axis, the corrector tilts in the opposite direction to remove beam decenter. This is a similar action to the tilted plane parallel plate seen in the conventional approach. If one has a conformal window, one may introduce a slight wedge in the window to bend the corrector in a desired direction.

[‡‡] On the other hand, the computer had lots of involvement with this problem. The calculation took approximately one hour on a 1.6 GHz Pentium Xeon.

Cylindrical Windows

The previous example showed the generalized aspheric design program operating on a window with wedge in it. In this example, a pair of MgF_2 cylindrical windows will be placed upstream from the corrector lens. The second cylindrical window is rotated by 45° about the z axis. The system wavelength is set at 4 microns and the Entrance Pupil Diameter is initially set at 2". A plate of germanium is converted into a corrector by GAP.

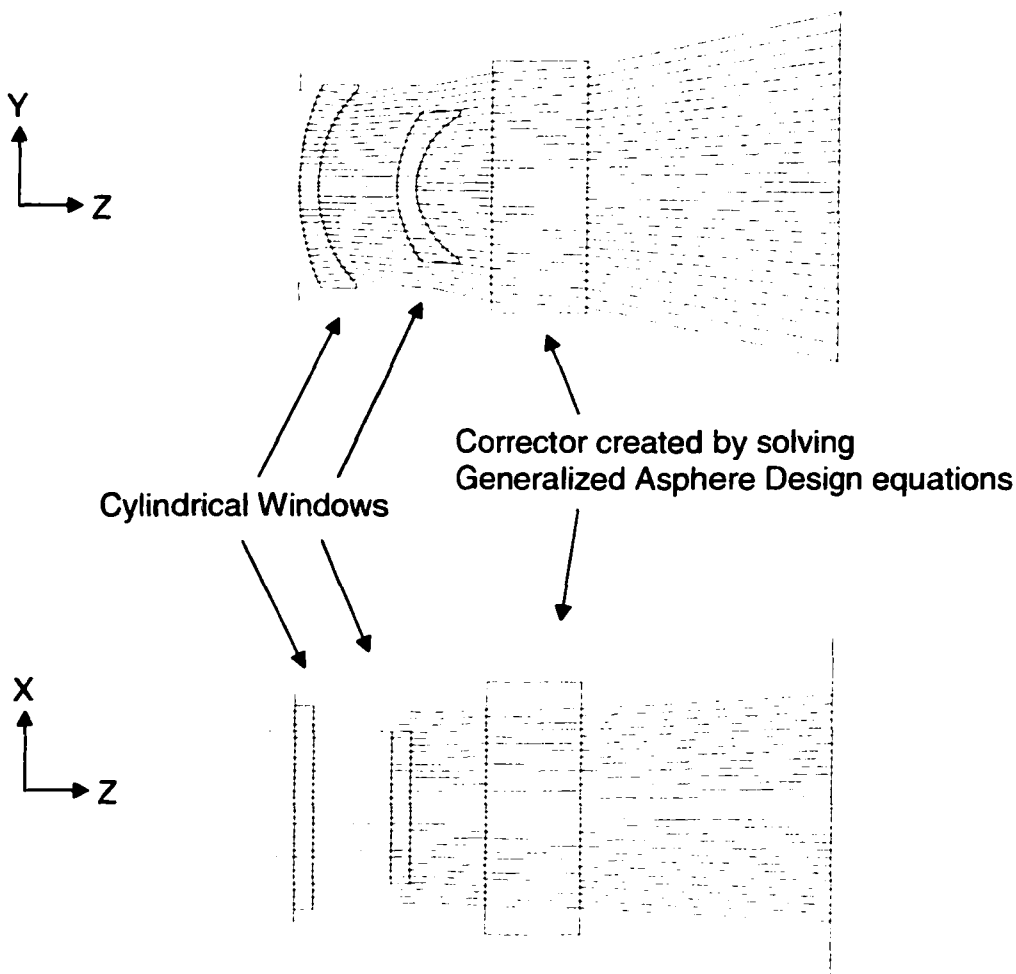

Figure 151. Before application of the GAP program

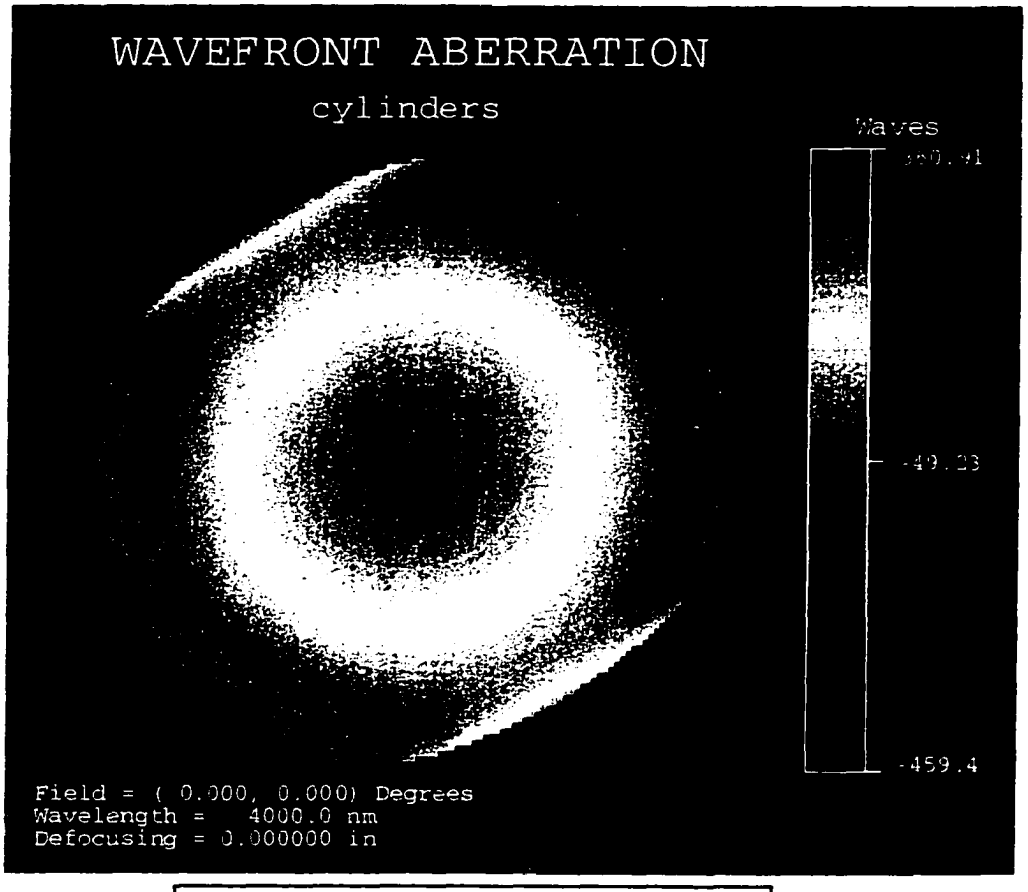

Figure 152. Exit pupil map of wavefront aberration minus power and tilt

Before correction, the system has a significant amount of aberration due to the astigmatism from the cylindrical elements. A Zernike decomposition of the exit pupil wavefront yields approximately 193 waves of Zernike astigmatism oriented at 0° and 223 waves of Zernike astigmatism oriented at 45°.

To design the corrector shape, the GAP program is executed with 36 spokes, 100 sampled points for each spoke, and 2000 extra points in between the sampled points. The

3600 points were surface fit to a Zernike polynomial as the default fit used by GAP. The surface fitting residual on both surfaces was less than 0.025 microns RMS.

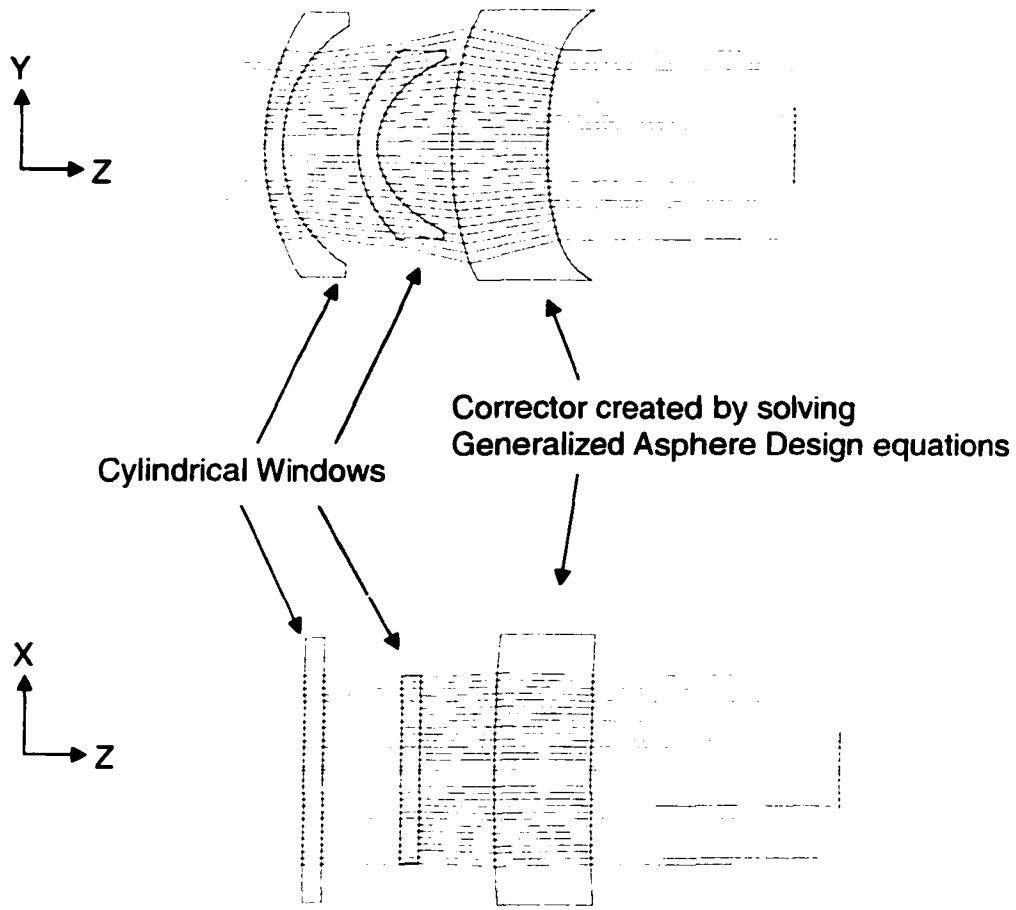

Figure 153. After application of the GAP program

The corrector generated by the GAP program substantially corrects for the on-axis aberrations. This can be seen by once again looking at the exit pupil with focus taken out.

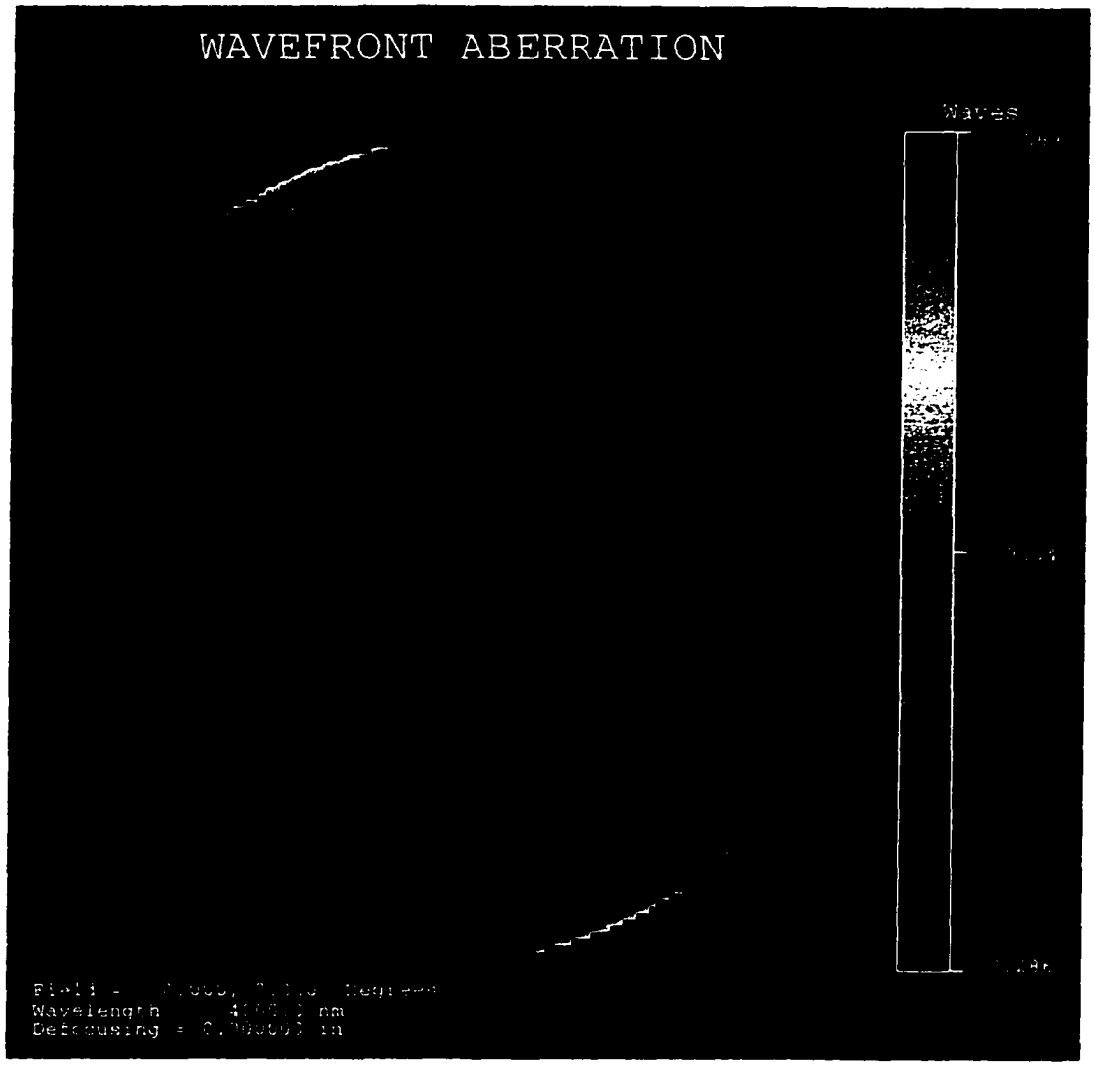

Figure 154. Exit pupil map of wavefront aberration minus power

The numerical integration of the generalized asphere design equations was not perfect. There is residual aberration at the edge of the pupil. This also shows up in a wavefront aberration plot, which is shown in Figure 155.

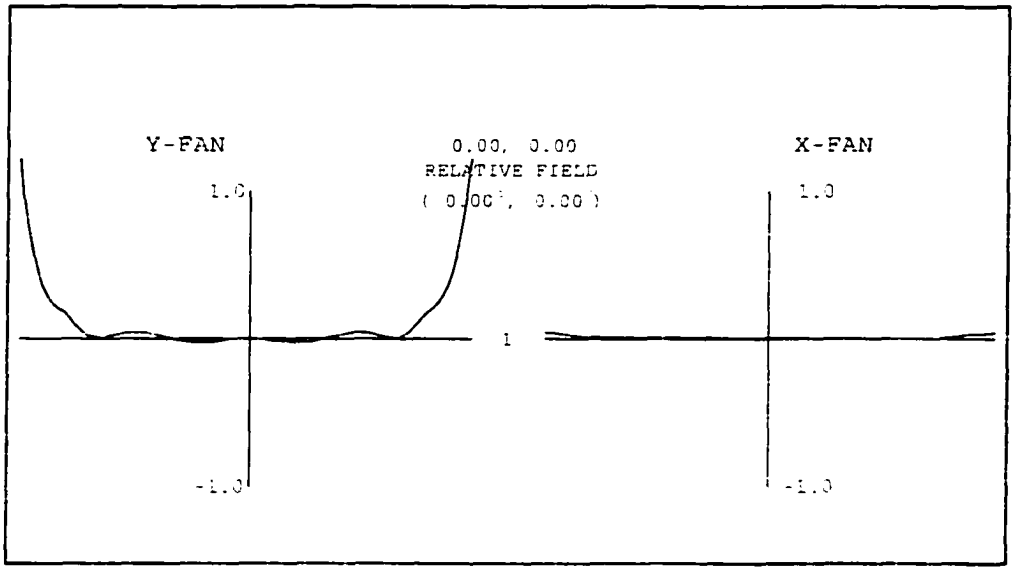

Figure 155. Wavefront aberration.
Scale: +/- 1 Waves

The design process could be repeated at a higher sampling density and/or smaller step size to increase the accuracy and knock down the aberration at the edge of the pupil. Or, the entrance pupil can be reduced to 1" to use the most accurate portion of the corrector. A 4" focal length perfect lens is used to represent the imaging system and decouple the problem of the window design from the imager design. To evaluate image quality over field of view, the field was analyzed out to 10°. The dominant aberration is determined to be astigmatism followed by elliptical coma.

At a zero degree field angle, the wavefront aberration is on the order of 0.1 waves.

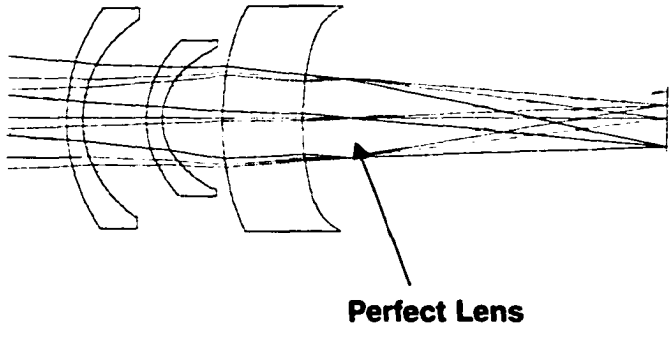

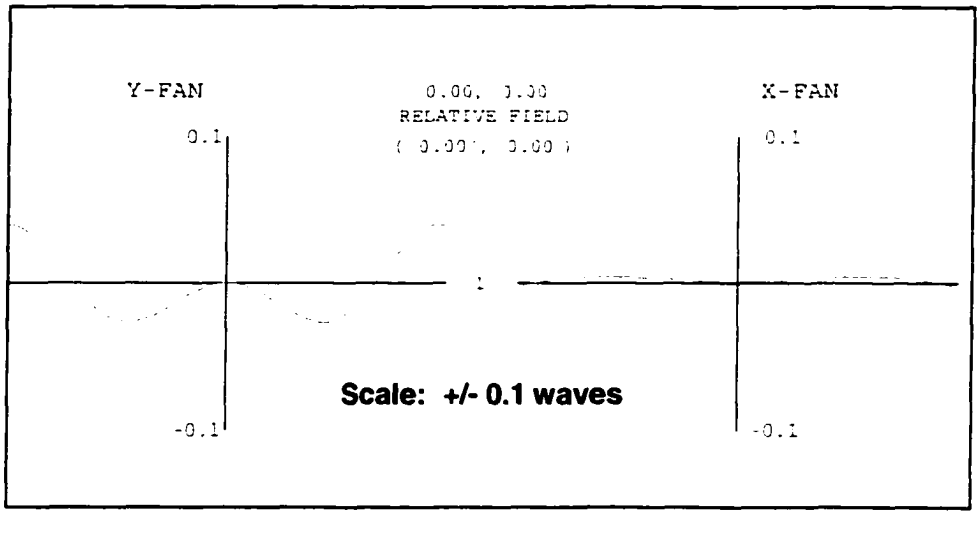

Figure 156. Reduced aperture of 1", a 10° field, and a perfect lens

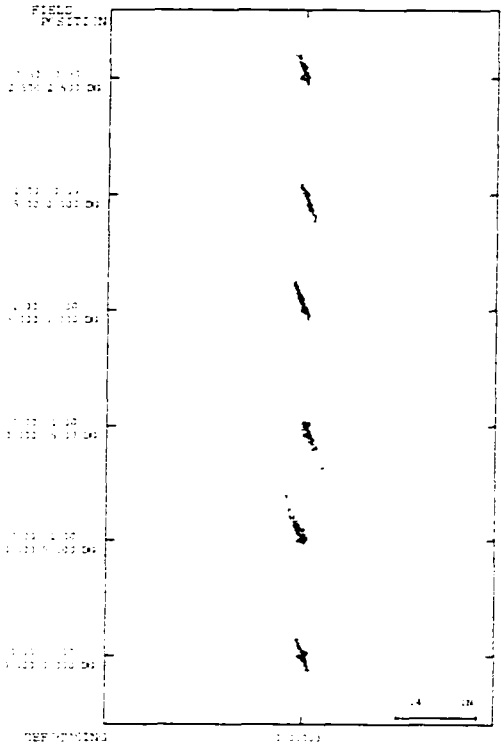

Figure 157. Spot diagram across field

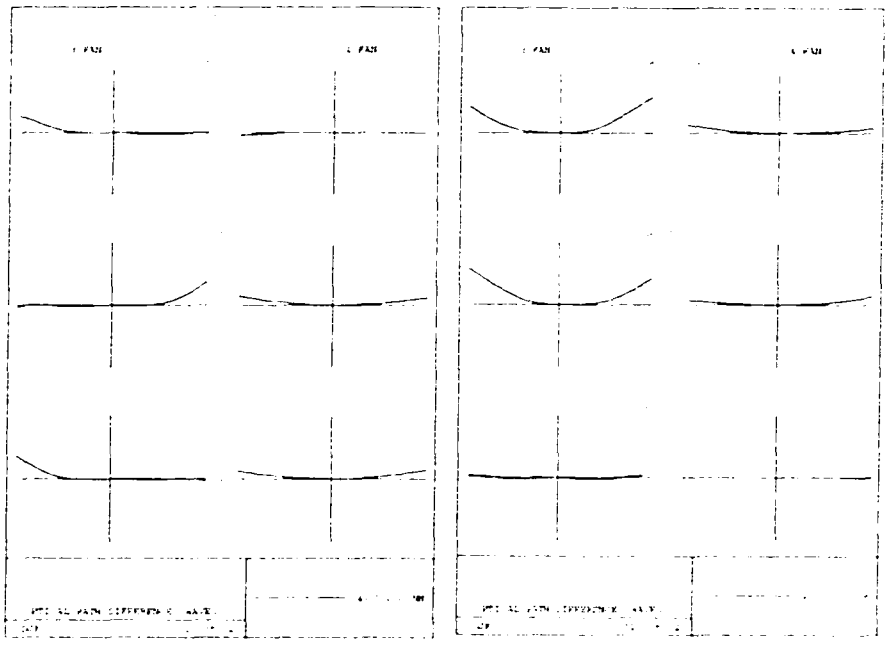

Figure 158. Wavefront aberration across field
Scale: +/- 1 Wave

This exercise showed that a window or windows with arbitrary aberration content may be corrected numerically to meet the Abbe Sine Condition. The generalized aspheric design equations do not depend on axial symmetry to achieve aplanatic performance. Furthermore, this exercise shows that on-axis aberrations that arise from non-rotationally symmetric elements can be corrected with the generalized aspheric design equations.

Mustang Camera

As a final design example, the utility of the generalized asphere design equations will be shown for a conformal window design for an automotive application. The imager is a fixed camera offset and looking through a quarter section of a toroidal window.

To begin, we assume that we want to design an uncooled infrared viewer for a Ford Mustang. It is assumed that the camera will be contained in a quarter section of a streamlined toroidal bubble mounted on the hood. The location of the window is shown in Figure 159.

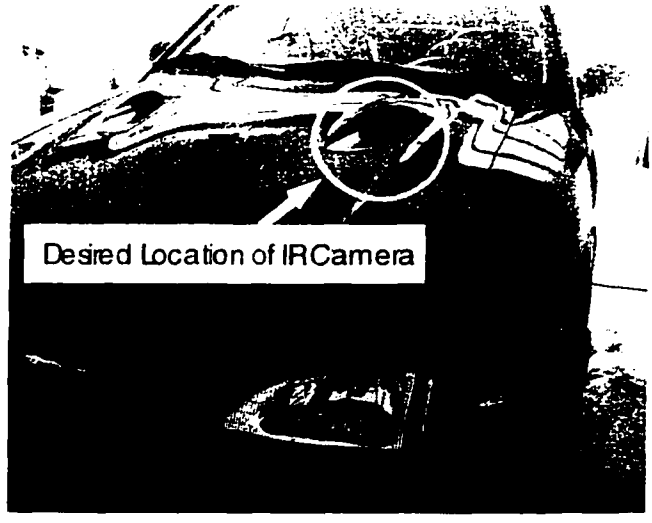

Figure 159. Location on Vehicle

In order to blend in with a hood, the assumption is made that a quarter toroid shape is desired with a height of 4", a half width of 6", and a length from base to tip of 8". This gives fineness ratios of 1 and 0.67 for the toroid cross-sections along the Y-Z and X-Z planes respectively. The conic constants and radii of curvature of an appropriate toroid may now be calculated. The formula used for the toroid is given in Equation 53.

$$z = \frac{CUX \cdot x^2 + CUY \cdot y^2}{1 + \sqrt{1 - (1 + KX) \cdot CUX^2 \cdot x^2 - (1 + KY) \cdot CUY^2 \cdot y^2}}$$

Equation 53

if x=y, this formula collapses into a conic equation.

Given a fineness ratio for an ellipsoidal dome, the conic constant K may be obtained by the formula:

$$K = \left(\frac{1}{4 \cdot F^2} \right) - 1$$

Equation 54

where F is the fineness ratio. Furthermore, the radius of curvature is given by:

$$R = \frac{y}{2 \cdot F}$$

Equation 55

where y is the semi-diameter given by:

$$y = \frac{D}{2}$$

Equation 56

From this the following values for the conic constants and radii of curvature for the desired quarter ellipsoid are obtained:

Bubble Height:	4	"
Bubble Half-width:	6	"
Bubble Length:	8	"

	F	Rdy	K
Y-Z	1.00	2	-0.75
X-Z	0.67	4.5	-0.4375

A fixed corrector plate is placed behind the window to compensate for the aberrations.

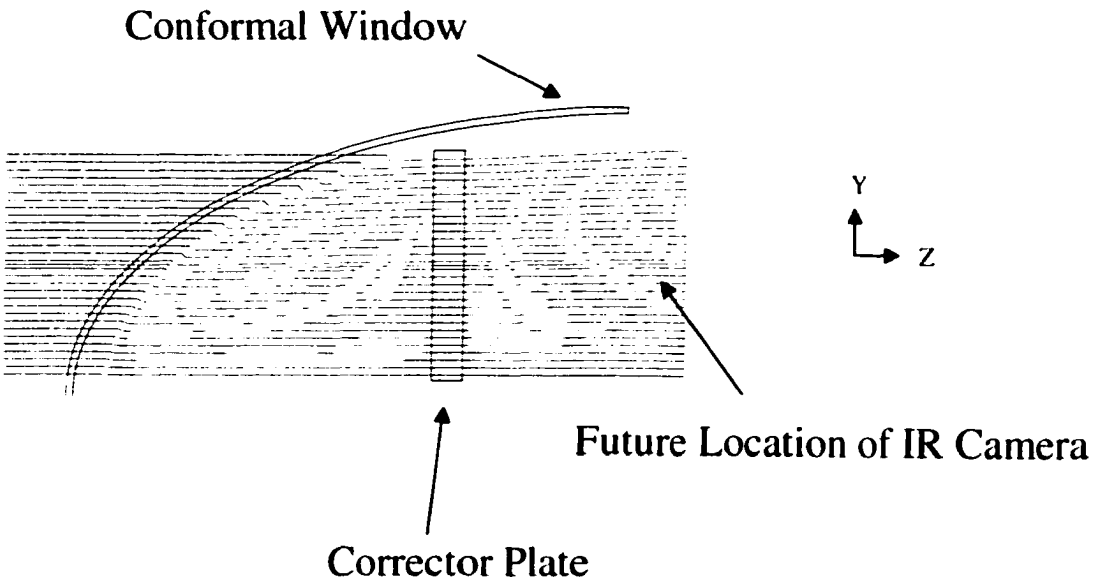

For the detector array, a 128X128 pixel micro-bolometer array is assumed with 50 micron square pixels. This places the maximum image corner at 0.178" from the optical axis. A 5° full field of view is desired for the camera.

$$\tan(HFOV) = \frac{image\_height}{efl}$$

Equation 57

The equation above may be used to calculate the corresponding effective focal length (efl). This yields a focal length of 4". Assuming an F/2 imaging system, the final entrance pupil diameter will need to be 2". The detector is sensitive to radiation in the

Figure 160. Layout of window and corrector plate

waveband from 3.8 microns to 4.5 microns. A center wavelength of 4.2 microns is selected for use with the GAP program.

The camera is set at a position to where it is approximately in the center of the window clear aperture. The location is shown in Figure 161.

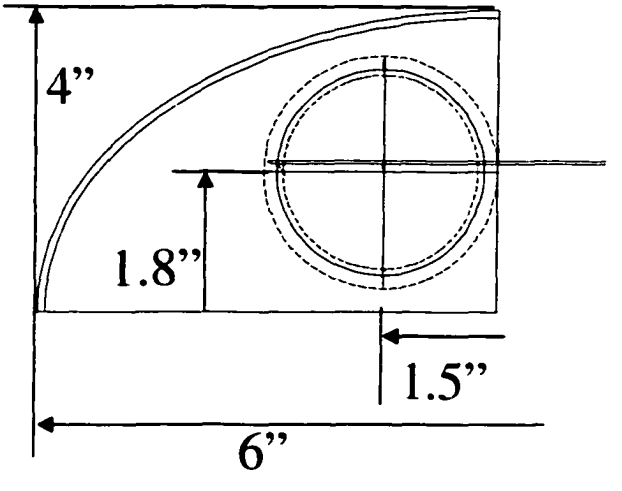

Figure 161. X-Y Cross-Section of Layout

Silicon is chosen for the window and corrector materials. Silicon offers relatively low dispersion in the Mid-IR. The aperture of the system is set to be 2.5" to allow it to be stopped down for the configuration with field. Next, the GAP program is executed on the system with 500 sample points, 500 extra points in between the sample points, and 36 spokes. After GAP, a perfect lens is used to represent the imaging system for analysis of the window and corrector perofrmance. The results are shown in Figure 162.

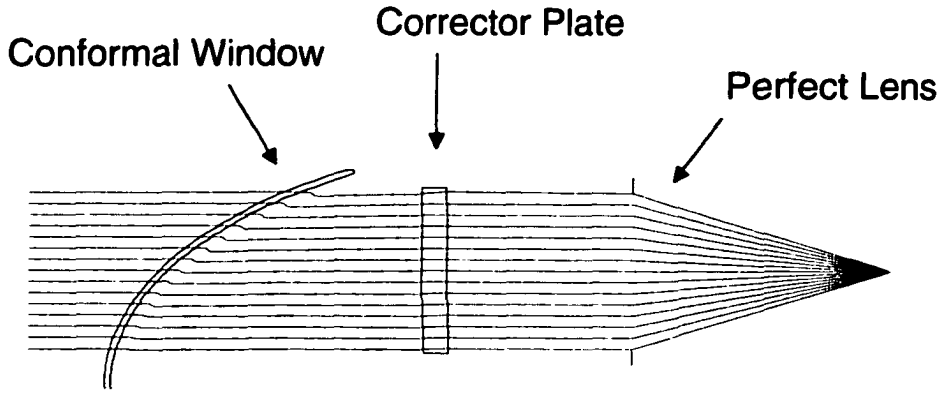

Figure 162. System after execution of the GAP macro

The wave fans show a small amount of residual aberration at the corner of the system. The geometrical spot size is well below the diffraction limited spot size.

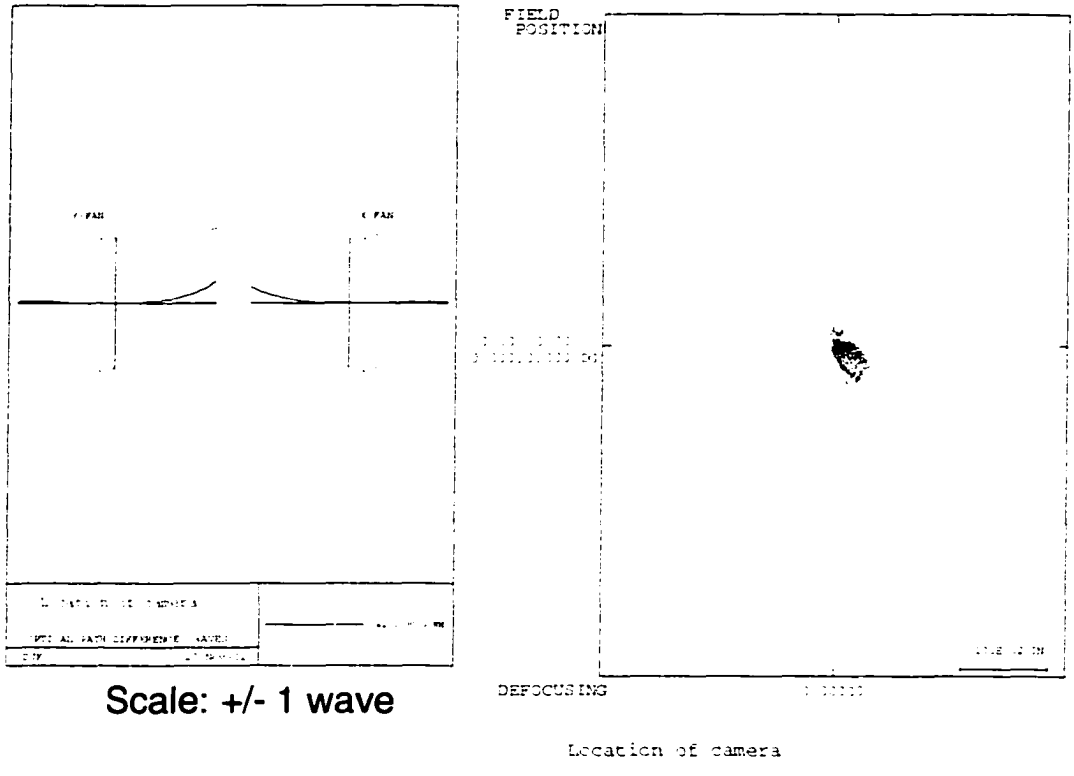

Figure 163. Wave aberration fans and spot diagram

Next, the system is stopped down to an entrance pupil diameter of 2", and a 5° full-field of view is added. The wavelengths at 3.8 microns and 4.5 microns are added to the system. The resulting system is shown in Figure 164.

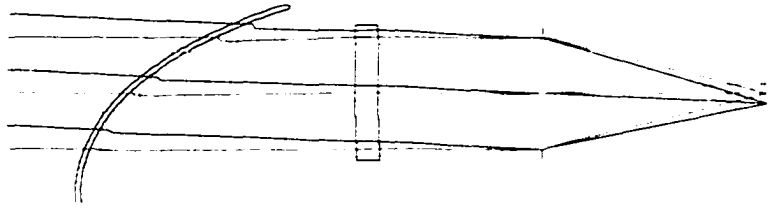

Figure 164. F/2 system with 5° full field of view

The window and corrector do not appear to introduce significant chromatic aberration. Astigmatism is the dominant residual aberration.

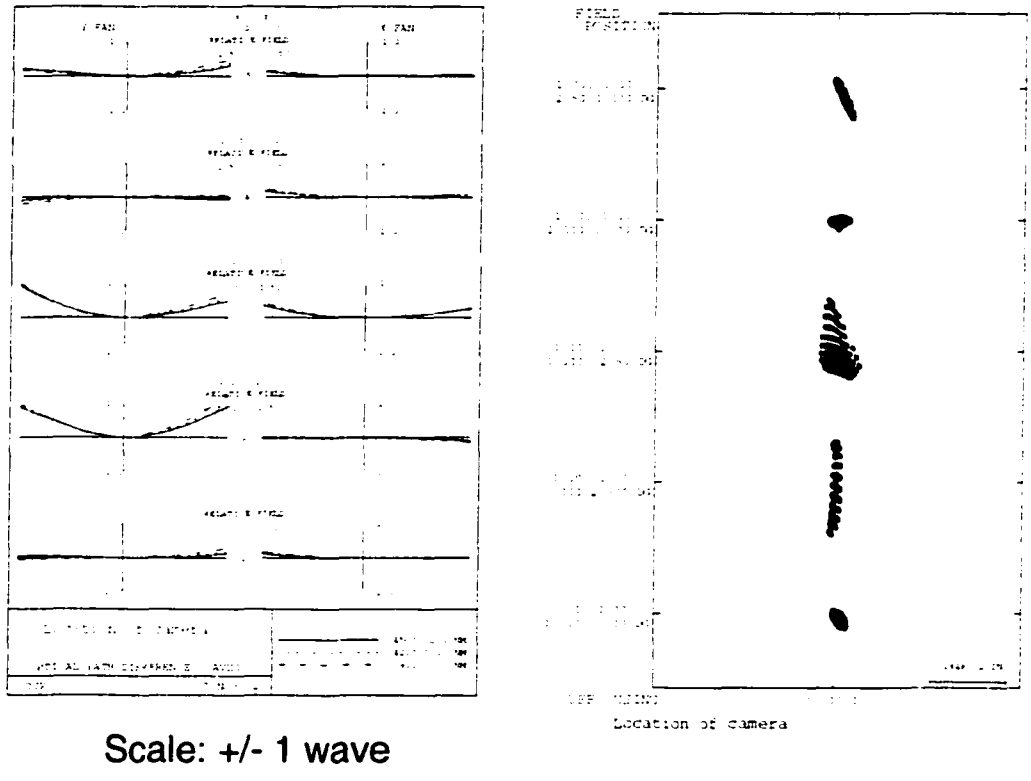

Figure 165. Wave fans and spot diagrams for full bandwidth and full field of view

The diffraction limited spot size for an F/2 system operating at 4.2 microns is 20.5 microns. The RMS spot sizes for the field angles are shown in Table 4.

	Field (x°, y°)				
	(0,0)	(0,2.5)	(0,-2.5)	(2.5,0)	(-2.5,0)
RMS Spot Size (microns)	6.35	34.77	28.96	6.51	13.40

Table 4. RMS Spot Sizes

By optimizing the focus, one may balance the image quality across the field of view. The rebalanced spot sizes are shown in Table 5.

	Field (x°, y°)				
	(0,0)	(0,2.5)	(0,-2.5)	(2.5,0)	(-2.5,0)
RMS Spot Size (microns)	9.40	28.02	18.94	13.18	9.84

Table 5. RMS Spot Size with Optimized Focus

These results show that the image quality is diffraction limited except toward the bottom of the image plane. The spot sizes are well below the pixel size of 50 microns.

Summary

This chapter illustrated the operation of a macro implementing the Wassermann-Wolf equations and a macro implementing the new generalized aspheric design equations, GAP. Both macros are members of the family of design tools that operate by solving differential equations.

"A design is what the designer has when time and money run out."
James Poole (1952 - ____) English novelist
In "The Fifth 637 Best Things Anybody Ever Said," ed. Robert Byrne, 1993.

CHAPTER 5- Discussion

A design created with the traditional DLS approach requires a significant amount of designer involvement. The designer must interact with the design program to establish a merit function, define free variables, set surface types, insert or delete surfaces, and shepherd the lens through solution space. After optimization, a design will be settled into a local minimum from which it must be coaxed. Ultimately, the designer must use intuition, analysis, trial and error, global optimization, or pure chance to determine when the lens performance has reached the maximum. In contrast, a design created with GAP directly lands on a useful region in design space with no coma or spherical aberration. If these aberrations are not sufficiently minimized, the process is straightforward. A higher density of sampling may be used to bring down coma and spherical aberration further. One does not have to guess at whether the proper surface type is being used. An improper surface type reveals itself through a high RMS residual in the sag fitting step of the solution.

Unfortunately, GAP has limitations. First, GAP takes a long time to arrive at a solution. Whereas the Wassermann-Wolf macro typically operates on a single ray fan containing perhaps 100's to 1000's of rays, the generalized design equations often require ray bundles containing one to two orders of magnitude more rays. Adding to the calculation time, the generalized design equations contain a large number of terms. This problem can be mitigated with a faster computer or a more efficient differential equation

solving algorithm. Second, chromatic aberrations are not addressed by the GAP program. Correcting a system for spherical aberration and coma can still leave large amplitudes of axial color uncorrected. This can be addressed by experimenting with different corrector material choices to find a natural balance. One might also use low dispersion conformal window and corrector materials to minimize the inherent chromatic variation. Third, GAP can only produce results permissible by the laws of physics. Very thin correctors do not support large clear apertures for many configurations. The ray bundles defined for GAP must trace through the system if one does not want vignetting. In an experimental sense, one can easily determine when GAP is being driven toward an impossible corrector shape when it produces erratic surfaces that do not trace. Common sense coupled with basic optical design theory and patience allow one to get reasonable solutions from GAP.

Accomplishments

There have been many accomplishments in this dissertation. First, an extensive review of the patent literature was conducted. This review showed a number of intriguing solutions for conformal optics. Second, a methodology for the design of conformal optical systems was synthesized. Initial design considerations were given and a special emphasis placed on the value of three important resource categories. Those categories were solution forms, surface types, and design tools. Members from each category were explained in detail. Third, the Wassermann-Wolf equations were explained in great detail. The components of these equations were illustrated and the procedure for solving the equations outlined. These equations are limited to

axisymmetric systems and tangential ray fans. The equations were implemented in a Code V macro. Four, a new set of equations was derived that could be used with non-rotationally symmetric systems and arbitrary ray bundles. These equations may be solved to create two surface profiles that make a ray bundle in object space be transformed by the optical system into a desired ray bundle in image space. When a stigmatic ray bundle is made to also meet the Abbe Sine Condition, the resulting system will be free of coma. These generalized equations were implemented in a Code V macro called the Generalized Aspheric design Program (GAP). Six, a series of examples was discussed that illustrated the operation of the Wassermann-Wolf macro and the GAP program. These examples show that an aberration free image field may be obtained for a variety of optical systems. Specifically, the GAP program is shown to produce a diffraction limited field of view for a system containing cylindrical elements and a system with a conformal window.

Problems Areas that Benefit from Generalized Equations

Besides systems containing conformal windows, there are other applications that could benefit from the generalized aspheric design equations.

First, one might apply the equations to the general class of systems containing tilted and decentered elements. For example, one might use the generalized aspheric design equations to design a corrector to compensate for optics with extremely loose tolerances. The final surface shape of a corrector element might be fabricated with magnetorheological finishing (MRF) after an initial measurement of the system was conducted.

Second, one might use the equations to design a null test optic for a non-rotationally symmetric element. By properly defining the ray bundles, one could control the spacing of rays over the optic under test as well as correct the aberrations. The drawback to this application is that a null test might be required to test the GAP null optics.

Summary

Overall the generalized aspheric design equations work and are well suited for a variety of problems.

"I think and think for months and years. Ninety-nine times, the conclusion is false. The hundredth time I am right."
Albert Einstein (1879 - 1955) Swiss-German-US physicist
Recalled on his death, 18 Apr 1955

CHAPTER 6- Conclusions

Summary

The purpose of this dissertation is to advance the state of the art in the design of conformal optical systems. The biggest achievement has been the development of a new design tool. The tool allows one to directly generate two optical surfaces that correct for coma and spherical aberration in a system containing non-rotationally symmetric elements. Correcting these aberrations is sufficient to create a region of aberration free imagery around the center of the field of view. The resulting system may be considered a final design or be used as a starting point for further optimization. Beyond the corrected region of imagery, other aberrations such as astigmatism and field curvature will begin to dominate the system and increase the spot size of a point object. These residual aberrations may be reduced using conventional methods such as adding an additional corrector optic to the system and using damped least squares optimization.

Chapter 1 developed an understanding of the prior art of conformal optics. As much of the early work in conformal optics is not available in the open literature, the best source of information was found to be in the patent literature. The patent literature showed a variety of solutions for conformal optics. The second half of Chapter 1 presented a synthesis of conformal optical design methodology. Three categories of resources were shown to be valuable in conformal optical design: solution forms, surface types, and design tools.

Chapter 2 developed the theory behind the Wassermann-Wolf equations. A series of relations was developed for a tangential ray traversing a centered rotationally symmetric optical system containing a pair of adjacent optical surfaces. The Wassermann-Wolf equations describe the change in sag of two adjacent optical surfaces with respect to a change in the parameter defining the ray. The surfaces have the property that a defined object space ray fan was made conjugate to a desired image space ray fan. The ray fans may be selected such that the system is stigmatic and meets the Abbe Sine Condition. This makes the system free form spherical aberration and coma. This type of system is called aplanatic. An aplanatic system has a finite lateral region of aberration-corrected imagery about the center of the field of view. Beyond this region, other aberrations will begin to dominate. The Wassermann-Wolf equations are well suited for rotationally symmetric systems such as those encountered in conformal dome design.

Chapter 3 developed the theory behind a pair of generalized aspheric design equations. These new equations were derived using a ray traversing through an optical system. The ray was not required to be contained in the Y-Z plane. Furthermore, the

optical system could contain non-rotationally symmetric surfaces. A pair of general differential equations was derived that related a change in the parameter defining the ray to a change in the sag of the adjacent aspheric surfaces. The surfaces have the property that a defined object space ray bundle is made conjugate to a desired image space ray bundle. Similar to the Wassermann-Wolf equations, the ray bundle can be selected such that the system is stigmatic and meets the Abbe Sine Condition. This makes the system aplanatic. Of particular significance is the fact that the system may be non-rotationally symmetric. This opens the door to applying the generalized aspheric design equations to conformal window systems.

Chapter 4 provided design examples for the Code V implementations of the Wassermann-Wolf and generalized aspheric design equations. The first example was a singlet design. This example illustrated how the Wassermann-Wolf macro could produce a solution comparable to that produced with a DLS method. The second example was a conformal dome design. This example showed the usefulness of the Wassermann-Wolf macro for correcting conformal dome aberrations. The third example was prism design. The generalized aspheric design equations produced a novel solution that corrected angular deviation and beam decenter simultaneously. The fourth example consisted of a pair of cylindrical elements creating on-axis astigmatism. GAP corrects the on-axis astigmatism in addition to the spherical aberration and coma. The fifth example was a conformal window design for an infrared camera. GAP directly generates a corrector for the system that allows a reasonably aberration free field of view. In all cases, the Wassermann-Wolf and GAP macros performed as predicted.

Suggestions for Future Work

Improving GAP

The macro implementing the generalized aspheric design equations is adequate for many design problems. However, there is ample room for improving it.

First, the method for solving the differential equations could be enhanced. GAP uses the Runge-Kutta method, which is simple to implement but offers only moderate performance in terms of speed and accuracy. This is due to the fixed integration step size. One might incorporate an adaptive step size algorithm to improve the accuracy and speed of GAP. This would allow the sampling of the corrector surfaces to be tuned to the portions of greatest change.

Second, additional choices could be created for the surface fit. GAP currently fits the surface points to a Zernike polynomial surface. Fitting to other surfaces such as anamorphic aspheres and X-Y polynomial expansions might provide a better fit.

Third, GAP could be more tightly integrated with Code V. Specifically, one might create a GAP solve in Code V so that the profile of a corrector could be calculated at every DLS optimization cycle. This would allow one to automatically solve for coma and spherical aberration while driving the system toward the solution of other aberration with degrees of freedom from other elements. Essentially, this capability would be the non-rotationally symmetric design equivalent to OSLO's Wassermann-Wolf solve capability for rotationally symmetric systems.

Fourth, more aperture filling functions could be implemented. GAP currently uses a function consisting of radial spokes. This samples the corrector surfaces more densely toward the center at the expense of the outer zones. As described in Chapter 3, an

assortment of other aperture filling functions could be implemented with a more uniform sampling across the corrector surfaces.

Fifth, other ray bundle parameterizations could be used. GAP uses a parameterization of ray bundles to correspond to the Abbe Sine Condition and make a system aplanatic. However, other ray bundle parameterizations could be explored to create other effects. For instance, one might want a novel distribution of rays in image space such as triangle shape. This could be achieved by mapping a new ray bundle in image space.

Exploring Solution Space

The GAP and Wassermann-Wolf macros are well suited for methodically exploring parameter space for conformal windows and domes. One could measure the performance of various dome and window shapes in terms of the diffraction limited field of view created by the macros. This would give one a comparison of the basic limitations of one shape over another using a single corrector.

Conclusion

The design of conformal optics is made much easier by a robust set of tools and techniques. The tool presented in this dissertation does not claim to be the all-powerful solution to every problem that a conformal designer might encounter. However, it should be a useful addition. When used in conjunction with other tools such as DLS and global optimization, conformal designs should be easier to create.

Increasingly, the spread of conformal optics technology will be limited more by the difficulty of manufacturing and testing complex aspheric surfaces rather than by the difficulty of designing them.

APPENDIX A- GAP Macro

```
!  Generalized Aspheric design Program (GAP)
!  Implements generalized aspheric design equations.
!  (Note: uses raytra instead of raysin for speed improvements.)
!
!   David Knapp
!   11/27/02
!
!   "Photon enslavement resources for the new millennium."
!
!  Modified for an infinite conjugate in image space.
!
!
!  Syntax:
!  In GAP [location of corrector surface] [# of points per radial]
[multiplier to increase sampling] [Normalized XP Height]
rfd 3 50 100

gbl num ^d ^outd ^sint ^pi
num ^x ^f ^zv1(2000000) ^zv2(2000000) ^df ^yv1(2000000)
num ^yv2(2000000) ^xv1(2000000) ^xv2(2000000) ^zrnco1(100) ^zrnco2(100)
gbl num ^y1 ^y2 ^zz ^in0 ^in1 ^in2
num ^m1 ^m2 ^m3 ^m4 ^rr ^w ^order ^even ^num_pts  ^ok
num ^err ^sum2 ^sum ^mlt ^rad ^theta ^hy1 ^hx1 ^hy2 ^hx2
str ^odd_even
num ^z1 ^z2 ^fx ^fy ^i ^j ^rad ^dfx ^dfy ^df ^mm1 ^mm2 ^mm3 ^mm4
num ^h1x ^h1y ^h2x ^h2y ^l1 ^n1 ^m1 ^l2 ^n2 ^m2 ^lng ^s
num ^x1 ^x2 ^th
num ^input(4) ^output(8)
str ^filename
gbl num ^scl

chk n
afi n

ver n
bnd y
!in test2   ! define test system
vie;fan yz 30;go

!  Define Constants
^order == 12          ! order of fit
^odd_even == 'o'      ! even or odd order (e/o)
^mlt ==#3             ! multiplier to increase sampling density
^num_pts==#2          ! number of points to use on the curve fit
^pi == 4*atanf(1.0)
^outd==(epd)*1        ! can be modified to change XP diameter
^zz==(thi s#1+1)      !  define focal point
^rr==^outd/2
^w==-atanf(0)
^sint==sinf(^w)
if ((^mlt*^num_pts)>10000000)
      wri "too many points!"
      goto END
```

```
end if


^in0 == (ind s#1-1)
^in1 == (ind s#1)
^in2 == (ind s#1+1)
^d == (thi s#1)

if (^odd_even = 'e')
    ^even == 2
else
    ^even == 1
end if

! reset two targeted surfaces  (They will be replaced soon anyway.)
! (Also speeds up ray tracing)
sph s#1
rdy s#1 0
sph s#1+1
rdy s#1+1 0
sto s1
sav
ins s#1   ! Dummy surface


del s#1+1..i-1    ! delete surfaces after the dummy surface


^scl==(epd)/2
!!!!!!!!!!!!!!!!!!!!!!!!!!!!!!!!!!
FCT @f1(num ^fx, num ^fy,num ^z1,num ^z2,num ^dfx,num ^dfy)
num ^lng ^ok
num ^hx1 ^hx2 ^hy1 ^hy2
num ^hx12 ^hx22 ^hy12 ^hy22
num ^x1 ^x2 ^y1 ^y2
num ^rx ^ry ^r ^rz
num ^dhx1 ^dhy1 ^dhx2 ^dhy2
num ^l1 ^m1 ^n1 ^l2 ^m2 ^n2 ^s ^s2
num ^l12 ^m12 ^n12 ^l22 ^m22 ^n22
num ^dccxz1 ^dccyz1 ^dccxz2 ^dccyz2
num ^a ^b ^numerator ^denominator ^dz ^df
num ^input(4) ^output(8)

^lng==sqrtf(^fx**2+^fy**2)     ! Length to optical axis
^df==sqrtf(^dfx**2+^dfy**2)
^dlng==sqrtf((^fx+^dfx*.0001)**2+(^fy+^dfy*.0001)**2)


^input(1)==^fx*^scl
^input(2)==^fy*^scl
^input(3)==0
^input(4)==0
^ok==raytra(1,0,0,^input,^output)      ! Trace original ray
^hy1==^output(2)
^hx1==^output(1)
```

```
^l1==^output(4)                    ! Optical direction cosines with x, y, z
axes
^m1==^output(5)                       !  (Note: the index is assumed to be
1)
^n1==^output(6)


^input(1)==^fx*^scl+^dfx*^scl*.0001
^input(2)==^fy*^scl+^dfy*^scl*.0001
^ok==raytra(1,0,0,^input,^output)       ! Trace original ray
^hy12==^output(2)
^hx12==^output(1)
^l12==^output(4)                   ! Optical direction cosines with x, y, z
axes
^m12==^output(5)                      !  (Note: the index is assumed to be
1)
^n12==^output(6)



^hy2==^fy*^scl
^hx2==^fx*^scl
^l2==0
^m2==0
^n2==1


!!!!!!!!
^hy22==^fy*^scl+^dfy*^scl*.0001
^hx22==^fx*^scl+^dfx*^scl*.0001
^l22==0
^m22==0
^n22==1


^dhy1== (^hy12-^hy1)/(^df*.0001)
^dhy2== (^hy22-^hy2)/(^df*.0001)
^dhx1== (^hx12-^hx1)/(^df*.0001)
^dhx2== (^hx22-^hx2)/(^df*.0001)

^dccxz1==(^l12/^n12-^l1/^n1)/(^df*.0001)
^dccyz1==(^m12/^n12-^m1/^n1)/(^df*.0001)
^dccxz2==(^l22/^n22-^l2/^n2)/(^df*.0001)
^dccyz2==(^m22/^n22-^m2/^n2)/(^df*.0001)

^rz ==^d-^z1+^z2
^y1==^hy1+(^z1*^m1/^n1)
^x1==^hx1+(^z1*^l1/^n1)
^y2==^hy2+(^z2*^m2/^n2)
^x2==^hx2+(^z2*^l2/^n2)
^ry==^y2-^y1
^rx==^x2-^x1
^r==sqrtf(^rx**2+^ry**2+^rz**2)
```

```
!!!!!!!!!  the following will change depending on whether this is the
first or last diff eq
^a== (^in0**r*^l1-^in1**rx)/(-^in0**r**n1+^in1**rz)
^b== (^in0**r**m1-^in1**ry)/(-^in0**r**n1+^in1**rz)

^numerator==^a*(^dhx1+^z1*^dccxz1)+^b*(^dhy1+^z1*^dccyz1)
^denominator==1-^a*(^l1/^n1)-^b*(^m1/^n1)

^dz==^numerator/^denominator


END FCT ^dz
!!!!!!!!!!!!!!!!!!!!!!!!!!!!!!!!!!!!

!!!!!!!!!!!!!!!!!!!!!!!!!!!!!!!!!!!!
FCT @f2(num ^fx, num ^fy,num ^z1,num ^z2, num ^dfx, num ^dfy)
num ^lng ^ok
num ^hx1 ^hx2 ^hy1 ^hy2
num ^hx12 ^hx22 ^hy12 ^hy22
num ^x1 ^x2 ^y1 ^y2
num ^rx ^ry ^r ^rz
num ^dhx1 ^dhy1 ^dhx2 ^dhy2
num ^l1 ^m1 ^n1 ^l2 ^m2 ^n2 ^s ^s2
num ^l12 ^m12 ^n12 ^l22 ^m22 ^n22
num ^dccxz1 ^dccyz1 ^dccxz2 ^dccyz2
num ^a ^b ^numerator ^denominator ^dz ^df
num ^input(4) ^output(8)

^lng==sqrtf(^fx**2+^fy**2)      ! Length to optical axis
^df==sqrtf(^dfx**2+^dfy**2)
^dlng==sqrtf((^fx+^dfx*.0001)**2+(^fy+^dfy*.0001)**2)


^input(1)==^fx*^scl
^input(2)==^fy*^scl
^input(3)==0
^input(4)==0
^ok==raytra(1,0,0,^input,^output)       ! Trace original ray
^hy1==^output(2)
^hx1==^output(1)
^l1==^output(4)                 ! Optical direction cosines with x, y, z
axes
^m1==^output(5)                    !  (Note: the index is assumed to be
1)
^n1==^output(6)


^input(1)==(^fx+^dfx*.0001)*^scl
^input(2)==(^fy+^dfy*.0001)*^scl
^ok==raytra(1,0,0,^input,^output)       ! Trace original ray
^hy12==^output(2)
^hx12==^output(1)
^l12==^output(4)                ! Optical direction cosines with x, y, z
axes
^m12==^output(5)                    !  (Note: the index is assumed to be
1)
```

```
^n12==^output(6)


^hy2==^fy*^scl
^hx2==^fx*^scl
^l2==0
^m2==0
^n2==1


!!!!!!!!
^hy22==^fy*^scl+^dfy*^scl*.0001
^hx22==^fx*^scl+^dfx*^scl*.0001
^l22==0
^m22==0
^n22==1

^dhy1== (^hy12-^hy1)/(^df*.0001)
^dhy2== (^hy22-^hy2)/(^df*.0001)
^dhx1== (^hx12-^hx1)/(^df*.0001)
^dhx2== (^hx22-^hx2)/(^df*.0001)

^dccxz1==(^l12/^n12-^l1/^n1)/(^df*.0001)
^dccyz1==(^m12/^n12-^m1/^n1)/(^df*.0001)
^dccxz2==(^l22/^n22-^l2/^n2)/(^df*.0001)
^dccyz2==(^m22/^n22-^m2/^n2)/(^df*.0001)

^rz ==^d-^z1+^z2
^y1==^hy1+(^z1*^m1/^n1)
^x1==^hx1+(^z1*^l1/^n1)
^y2==^hy2+(^z2*^m2/^n2)
^x2==^hx2+(^z2*^l2/^n2)
^ry==^y2-^y1
^rx==^x2-^x1
^r==sqrtf(^rx**2+^ry**2+^rz**2)


!!!!!!!!!  the following will change depending on whether this is the
first or last diff eq
^a== (^in2*^r*^l2-^in1*^rx)/(-^in2*^r*^n2+^in1*^rz)
^b== (^in2*^r*^m2-^in1*^ry)/(-^in2*^r*^n2+^in1*^rz)

^numerator==^a*(^dhx2+^z2*^dccxz2)+^b*(^dhy2+^z2*^dccyz2)
^denominator==1-^a*(^l2/^n2)-^b*(^m2/^n2)

^dz==^numerator/^denominator


END FCT ^dz
!!!!!!!!!!!!!!!!!!!!!!!!!!!!!!!!!!!


! Meat of the routine

^df==1/(^num_pts*^mlt)
```

```
^theta == 0
^rad == 0
^fx==0
^fy==0
^arms==36   ! Change to increase/decrease number of arms
^ptr==1
   wri "max arms:" ^arms
for ^th 0 ^arms-1
   wri "arm:" ^th
  ^theta==^th*360*^pi/(^arms*180)
  ^rad == 0
  ^fx==-(1/(^num_pts*^mlt))*sinf(^theta)
  ^fy==-(1/(^num_pts*^mlt))*cosf(^theta)
   ^z1==0
   ^z2==0
   for ^i 1 ^num_pts
   for ^j 1 ^mlt

    ^rad == ((^i-1)*^mit+^j)/(^num_pts*^mlt)   ! normalized radius by
the number of points
    ^dfx==^rad*sinf(^theta)-^fx
    ^dfy==^rad*cosf(^theta)-^fy
    ^df==sqrtf(^dfx**2+^dfy**2)
    ^fx==^rad*sinf(^theta)
    ^fy==^rad*cosf(^theta)

   ^m1==^df*@f1(^fx,^fy,^z1,^z2,^dfx, ^dfy)
   ^mm1==^df*@f2(^fx,^fy,^z1,^z2,^dfx, ^dfy)

   ^m2==^df*@f1((^fx+^dfx/2),(^fy+^dfy/2),(^z1+^m1/2),(^z2+^mm1/2),^dfx,
^dfy)
   ^mm2==^df*@f2((^fx+^dfx/2),(^fy+^dfy/2),(^z1+^m1/2),(^z2+^mm1/2),^dfx,
^dfy)

   ^m3==^df*@f1((^fx+^dfx/2),(^fy+^dfy/2),(^z1+^m2/2),(^z2+^mm2/2),^dfx,
^dfy)
   ^mm3==^df*@f2((^fx+^dfx/2),(^fy+^dfy/2),(^z1+^m2/2),(^z2+^mm2/2),^dfx,
^dfy)

   ^m4==^df*@f1((^fx+^dfx),(^fy+^dfy),^z1+^m3,^z2+^mm3,^dfx, ^dfy)
   ^mm4==^df*@f2((^fx+^dfx),(^fy+^dfy),^z1+^m3,^z2+^mm3,^dfx, ^dfy)

   ^z1==^z1+(1/6)*(^m1+2*^m2+2*^m3+^m4)
   ^z2==^z2+(1/6)*(^mm1+2*^mm2+2*^mm3+^mm4)

      ^input(1)==^fx*^scl
      ^input(2)==^fy*^scl
      ^input(3)==0
      ^input(4)==0
      ^ok==raytra(1,0,0,^input,^output)      ! Trace original ray
      ^hy1==^output(2)
      ^hx1==^output(1)
      ^l1==^output(4)                    ! Optical direction cosines with
x, y, z axes
```

```
      ^m1==^output(5)                    !  (Note: the index is assumed
 to be 1)
      ^n1==^output(6)

    ^lng==sqrtf(^fx**2+^fy**2)


    ^hy2==^fy*^scl
    ^hx2==^fx*^scl
    ^l2==0
    ^m2==0
    ^n2==1

    ^y1==^hy1+(^z1*^m1/^n1)
    ^x1==^hx1+(^z1*^l1/^n1)
    ^y2==^hy2+(^z2*^m2/^n2)
    ^x2==^hx2+(^z2*^l2/^n2)


!!!!!!!!!!!!
end for

   ^zv1(^ptr)==^z1
   ^zv2(^ptr)==^z2
   ^yv1(^ptr)==^y1
   ^yv2(^ptr)==^y2
   ^xv1(^ptr)==^x1
   ^xv2(^ptr)==^x2
!     wri ^z1 ^z2 ^fy ^fy ^fx ^fx
^ptr==^ptr+1
end for
end for

res

!!!!!!!!!!!!
^ptr==^ptr-1
^rad1==sqrtf(^y1**2+^x1**2)
^rad2==sqrtf(^y2**2+^x2**2)

!!!!!!!!!!!!!!!!!!!!!!!!!!!!!!
!  Normalize x and y points
!!!!!!!!!!!!!!!!!!!!!!!!!!!!!!
for ^i 1 ^ptr
   ^yv1(^i)==^yv1(^i)/^rad1
   ^yv2(^i)==^yv2(^i)/^rad2
   ^xv1(^i)==^xv1(^i)/^rad1
   ^xv2(^i)==^xv2(^i)/^rad2
!     wri ^yv1(^i) ^xv1(^i)
end for
!!!!!!!!!!!!!!!!!!!!!!!!!!!!!!

ver n
^err1==ZRNFIT(^ptr,^xv1,^yv1,^zv1,66,^zrnco1)
^err2==ZRNFIT(^ptr,^xv2,^yv2,^zv2,66,^zrnco2)
```

```
wri "zrn coefficients"
for ^i 1 66
      wri ^zrnco1(^i) ^zrnco2(^i)
end for
wri "rms errors are" ^err1 ^err2

sps zrn s#1
sps zrn s#1+1
rdy s#1 0
rdy s#1+1 0
for ^i 2 67
      sco c^i s#1 ^zrnco1(^i-1)
      sco c^i s#1+1 ^zrnco2(^i-1)
end for
sco c1 s#1 0
sco c1 s#1+1 0
sco c69 s#i ^rad1
sco c69 s#1+1 ^rad2
sco c68 s#1 66
sco c68 s#1+1 66

!wri "rms errors are" ^err1 ^err2


!!!!!!!!!!!!!!
! perform cleanup
lbl END
wri "end!"
dro fct f1 f2
dro gbl num ^d ^outd ^sint ^n0 ^n1 ^n2 ^pi
dro gbl num ^y1 ^y2 ^sc1


vie;fan yz 30;go
rim;wfr;go

wri "mlt" ^mlt "order" ^order "num pts of fit:" ^num_pts
wri "total number of points:" ^ptr
ver n
vie;fan yz 30;go;vie;fan xz 30;plc xz;go
```

APPENDIX B- Wassermann-Wolf Macro

```
! Wassermann-Wolf Design Macro
!
!infinitewolf.seq
!
!  Fast wolf macro revised for infinite object AND infinite image
!
!   David Knapp
!   5/10/01
!
!   "Photon enslavement resources for the new millenium."
!
!
rfd 0 50 100 0.85 2

gbl num ^d ^outd ^sint ^n0 ^n1 ^n2 ^pi
num ^x ^f ^zv1(100000) ^zv2(100000) ^df ^yv1(100000) ^yv2(100000)
gbl num ^y1 ^y2
num ^m1 ^m2 ^m3 ^m4 ^xx ^yy ^w ^order ^even ^num_pts ^vec(4) ^ok
num ^err ^sum2 ^sum ^mlt
str ^odd_even
gbl num ^scl ^thick2
num ^input(4) ^output(8)

sav tmp

if (#1 =  0)           ! No input trap
    wri "syntax:  in fastwolf surface sample_points multiplier aperture
odd(1)/even"
   goto END
end if

ver n
!in test2   ! define test system
vie;fan yz 30;go

!  Define Constants
^order == 20         ! order of fit
^odd_even == 'o'     ! even or odd order (e/o)
^mlt ==#3            ! multiplier to increase sampling density
^num_pts==#2         ! number of points to use on the curve fit
^pi == 4*atanf(1.0)
^outd==(epd)*#4       !  exit face diameter  - change this to desired
diameter...just not = epd.
^xx==(thi s#1+1)       !  define focal point
^yy==^outd/2
^w==-atanf(^yy/^xx)
^sint==sinf(^w)
!if (^num_pts>100000)
!     wri "too many points!"
```

```
!     goto END
!end if


^n0 == (ind s#1-1)
^n1 == (ind s#1)
^n2 == (ind s#1+1)
^d == (thi s#1)

if (^odd_even = 'e')
    ^even == 2
else
    ^even == 1
end if


! reset two targeted surfaces  (They will be replaced soon anyway.)
! (Also speeds up ray tracing)
sph s#1
rdy s#1 0
sph s#1+1
rdy s#1+1 0

^thick2==(thi s#1+1)
^scl==(epd)/2
sav
ins s#1   ! Dummy surface
del s#1+1..i-1



!!!!!!!!!!!!!!!!!!!!!!!!!!!!!!!!
FCT @f1(num ^f,num ^z1,num ^z2,num ^df)
num ^h1 ^h2 ^rz ^ry ^r ^dz ^w1 ^w2 ^w12 ^w22 ^h12 ^h22 ^y1 ^y2 ^dtan1
^dtan2 ^vec(4) ^ok
num ^input(4) ^output(8)

!!!!!!!!!!!!!!!!!!!!!!!!!!!!!!!!

^input(1)==0
^input(2)==^f*^scl
^input(3)==0
^input(4)==0
^ok==raytra(1,0,0,^input,^output)       ! Trace original ray
^h1==^output(2)
^w1==-acosf(^output(5))+^pi/2

^input(2)==^f*^scl+^df*^scl*.0001
^ok==raytra(1,0,0,^input,^output)       ! Trace original ray
^h12==^output(2)
^w12==-acosf(^output(5))+^pi/2

^w2==0
^w22==0
^h2==^f*^outd/2
^h22==^f*^outd/2+^df*^outd/2*.0001
```

```
^dh1==(^h12-^h1)/(^df*.0001)
^dh2==(^h22-^h2)/(^df*.0001)

^dtan1==(tanf(^w12)-tanf(^w1))/(^df*.0001)
^dtan2==(tanf(^w22)-tanf(^w2))/(^df*.0001)

^rz ==^d-^z1+^z2
^y1 == ^h1+^z1*tanf(^w1)
^y2 == ^h2+^z2*tanf(^w2)
^ry==^y2-^y1
^r==sqrtf(^ry**2+^rz**2)

^dz ==-(^dh1+^z1*^dtan1)&
/(&
 (^n1*^rz-^n0*^r*cosf(^w1))&
/(^n1*^ry-^n0*^r*sinf(^w1))&
+tanf(^w1)&
)
END FCT ^dz
!!!!!!!!!!!!!!!!!!!!!!!!!!!!!!!!!!

!!!!!!!!!!!!!!!!!!!!!!!!!!!!!!!!1
FCT @f2(num ^f,num ^z1,num ^z2,num ^df)
num ^h1 ^h2 ^rz ^ry ^r ^dz ^y1 ^y2 ^w1 ^w2 ^w12 ^w22 ^h12 ^h22 ^dtan1
^dtan2 ^vec(4) ^ok
num ^input(4) ^output(8)

^input(1)==0
^input(2)==^f*^scl
^input(3)==0
^input(4)==0
^ok==raytra(1,0,0,^input,^output)      ! Trace original ray
^h1==^output(2)
^w1==-acosf(^output(5))+^pi/2

^input(2)==^f*^scl+^df*^scl*.0001
^ok==raytra(1,0,0,^input,^output)      ! Trace original ray
^h12==^output(2)
^w12==-acosf(^output(5))+^pi/2

^w2==0
^w22==0
^h2==^f*^outd/2
^h22==^f*^outd/2+^df*^outd/2*.0001

^dh1==(^h12-^h1)/(^df*.0001)
^dh2==(^h22-^h2)/(^df*.0001)

^dtan1==(tanf(^w12)-tanf(^w1))/(^df*.0001)
^dtan2==(tanf(^w22)-tanf(^w2))/(^df*.0001)

^rz ==^d-^z1+^z2
^y1 == ^h1+^z1*tanf(^w1)
^y2 == ^h2+^z2*tanf(^w2)
^ry==^y2-^y1
```

```
^r==sqrtf(^ry**2+^rz**2)

^dz ==-(^dh2+^z2*^dtan2)&
/(&
 (^n1*^rz-^n2*^r*cosf(^w2))&
/(^n1*^ry-^n2*^r*sinf(^w2))&
+tanf(^w2)&
)
END FCT ^dz
!!!!!!!!!!!!!!!!!!!!!!!!!!!!!!!!!!!!

! Meat of the routine

^df==1/(^num_pts*^mlt)
^z1==0
^z2==0

for ^i 1 ^num_pts
for ^j 1 ^mlt
    ^x == (^i-1)*^mlt+^j
    ^f==^x/(^num_pts*^mlt)

   ^m1==^df*@f1(^f,^z1,^z2,^df)
   ^mm1==^df*@f2(^f,^z1,^z2,^df)

   ^m2==^df*@f1((^f+^df/2),(^z1+^m1/2),(^z2+^mm1/2),^df)
   ^mm2==^df*@f2((^f+^df/2),(^z1+^m1/2),(^z2+^mm1/2),^df)

   ^m3==^df*@f1((^f+^df/2),(^z1+^m2/2),(^z2+^mm2/2),^df)
   ^mm3==^df*@f2((^f+^df/2),(^z1+^m2/2),(^z2+^mm2/2),^df)

   ^m4==^df*@f1((^f+^df),^z1+^m3,^z2+^mm3,^df)
   ^mm4==^df*@f2((^f+^df),^z1+^m3,^z2+^mm3,^df)

   ^z1==^z1+(1/6)*(^m1+2*^m2+2*^m3+^m4)
   ^z2==^z2+(1/6)*(^mm1+2*^mm2+2*^mm3+^mm4)


      ^input(1)==0
      ^input(2)==^f*^scl
      ^input(3)==0
      ^input(4)==0
      ^ok==raytra(1,0,0,^input,^output)      ! Trace original ray
      ^h1==^output(2)
      ^w1==-acosf(^output(5))+^pi/2

   ^w2==0
   ^h2==^f*^outd/2
   ^y1 == ^h1+^z1*tanf(^w1)
   ^y2 == ^h2+^z2*tanf(^w2)

!!!!!!!!!!!!
end for

   ^zv1(^i)==^z1
   ^zv2(^i)==^z2
```

```
    ^yv1(^i)==^y1
    ^yv2(^i)==^y2
 end for

 del s#1

 res

 !!!!!!!!!!!!!!!!!!!!!!!!!!
 !  Fit points to surface
 !!!!!!!!!!!!!!!!!!!!!!!!!!

   buf put b1 i1 j1 0
   buf put b1 i1 j2 0
 for ^x 1 ^num_pts
       buf put b1 i^x+1 j1 ^yv1(^x)
       buf put b1 i^x+1 j2 ^zv1(^x)
 end for
 in polyfit b1 ^order $odd_even (^num_pts+1)
 !buf lis b1
 buf del b1

 !  Input new coefficients into surface.
 ^even==1
 sps odd s#1
 for ^i 1 ^order
       ^j == (^i*^even)+1
       sco c^j s#1 ^coeff(^i)
 end for

 !  Convert polynomial into a base paraboloid + the aspheric terms
 rdy s#1 0.5/(sco c3 s#1)
 sco c1 s#1 -1
 sco c3 s#1 0


 !!!!!!!!!!!!


   buf put b1 i1 j1 0
   buf put b1 i1 j2 0
 for ^x 1 ^num_pts
       buf put b1 i^x+1 j1 ^yv2(^x)
       buf put b1 i^x+1 j2 ^zv2(^x)
 end for
 in polyfit b1 ^order $odd_even (^num_pts+1)
 buf del b1


 !  Input new coefficients into surface.
 ^even==1
 sps odd s#1+1
 for ^i 1 ^order
       ^j == (^i*^even)+1
       sco c^j s#1+1 ^coeff(^i)
 end for
```

```
!  Convert polynomial into a base paraboloid + the aspheric terms

rdy s#1+1 0.5/(sco c3 s#1+1)
sco c1 s#1+1 -1
sco c3 s#1+1 0

^sum==0
for ^x 1 ^num_pts
      ^err==(^zv1(^x)-sagf(#1,1,0,^yv1(^x)))**2
      ^sum==^err+^sum
      ^err==(^zv2(^x)-sagf(#1+1,1,0,^yv2(^x)))**2
      ^sum2==^err+^sum2
end for
^sum2==^sum2/(^num_pts-1)
^sum==^sum/(^num_pts-1)
^sum==sqrtf(^sum)
^sum2==sqrtf(^sum2)



! perform cleanup
lbl END
wri "end!"
dro fct f1 f2
dro gbl num ^d ^outd ^sint ^n0 ^n1 ^n2 ^pi
dro gbl num ^y1 ^y2 ^sc1

vie;fan yz 30;go
rim;wfr;go

wri "rms errors:"^sum ^sum2
wri "mlt" ^mlt "order" ^order "num pts of fit:" ^num_pts
wri "total number of points:" ^mlt*^num_pts
```

REFERENCES

1. Schaefer, J. and R. Eichholtz, "Fabrication Challenges Associated with Conformal Optics," Window and Domes Technologies and Materials VII, SPIE Orlando April 2001

2. Goela, J.S. "Precision Replication by Chemical Vapor Deposition Process" US Patent #6,042,758 (March 28, 2000).

3. Fess, E. and J. Ruckman, "Deterministic Contour Grinding of Conformal Optics," Technical Digest, Optical Society of America, OF&T 2000, Quebec City, Canada (June 18-21, 2000). TOPS Vol. 42, pages 5-7.

4. Jacobs, S., Arrasmith, S., Kozhinova, I., Gregg, L., Shorey, A., Romanofsky, H.,Golini,D., Kordonski, W., Dumas, P., and Hogan, S. "MRF: Computer-Controlled Optics Manufacturing," Ceramic Bulletin, December 1999, Vol. 78, No 12.

5. Hegg, R.G. and C.W. Chen, "Testing Conformal Windows with Null Optics," Proc. Of the 8th Electromagnetic Windows Symposium, U.S. Air Force Academy, April 2000.

6. Greivenkamp, J.E., D.G. Smith, G.A. Williby, R.O. Gappinger, P.H. Marushin, A. Gupta, S.R. Clark, J. Lee, S.A. Lerner and J.M. Sasian, "Transmitted Wavefront Testing of Conformal Windows," Proceedings of the 8th DoD Electromagnetic Windows Symposium, U.S. Air Force Academy, CO, April 2000.

7. Clark, S.R., Optical Reference Profilometry, Ph.D. Dissertation, Optical Sciences, University of Arizona (2000).

8. Funded by DARPA/TTO, Agreement No. MDA 976-96-9-0800

9. Fischer, R.E., L.R. Siegel , R.J. Korniski, E.J. Boudreaux, Jr., "New developments in optical correction for non-spherical windows and domes," SPIE 2286

10. Sparrold, S.W., Correcting Dynamic Third-order Astigmatism in Conformal Missile Domes with Gimbaled Seekers, Master's Thesis, Department of Optical Sciences, University of Arizona, 1997.

11. Sparrold, S. W., Knapp, D. J., Manhart, P. K., Elsberry, K. W., "Capabilities of an Arch Element for Correcting Conformal Optical Domes," presented at SPIE Optical Science, Engineering and Instrumentation Meeting, July 21, 1999, Denver Colorado.

12. Novak, M.J., Analysis and Correction of Wavefront Deformation Introduced by Conformal Aspheric Surfaces, Master's Thesis, Department of Optical Sciences, University of Arizona, 1997.

13. Chen, C.B., "Aircraft Conformal Window Shapes in Current and Near Term operational Systems," Invited Paper in 1997 OSA Annual Meeting, Long Beach, CA, Oct. 13, 1997.

14. Crowther, B.G., McKenney, D.B. and J.P. Mills, "Aberrations of Optical Domes," Technical Digest of the 1998 International Optical Design Conference, SPIE, Kailua-Kona, Hawaii, pp. 11-13, 1998.

15. Palusinski, I.A., Sasian, J.M.and Greivenkamp, J.E. "Lateral-Shift Variable Aberration Generators," Applied Optics 38, 86-90 (1999).

16. Mills, J.P., Sparrold, S.W., Mitchell, T.A., Ellis, K.S., Knapp, D.J. and Manhart, P.K., "Conformal dome aberration correction with counter-rotating phase plates," Proceedings of the SPIE International Symposium on AeroSense, Window and Dome Technologies and Materials VI, Orlando, FL, April 1999.

17. Sparrold, S.W., J.P. Mills, D.J. Knapp, K.E. Ellis, T.A. Mitchell and P.K. Manhart, "Conformal Dome Correction With Counter rotating Phase Plates," Optical Engineering, Vol. 39(7), 2000.

18. Mitchell, T.A., Aberration Generation With Axially Translating Aspheric Plates, Master's Thesis, Department of Optical Sciences, University of Arizona, 1998.

19. Whalen, M.R., A Technique for Correcting Variable Third Order Astigmatism Introduced by Conformal Aspheric Surfaces, Master's Thesis, Department of Optical Sciences, University of Arizona, 1997.

20. Marushin, P.H., J.M. Sasian, T.Y. Lin, B. Robinson, J. Ashkenazi and J. G. Greivenkamp, "Demonstration of a Conformal Window Imaging System: Design, Fabrication and Testing," Window and Domes Technologies and Materials VII, SPIE Orlando April 2001.

21. Ellis, K.S., The Optics of Ellipsoidal Domes, Ph.D. Dissertation, Department of Optical Sciences, University of Arizona, 1999

22. Lerner, S.A., and J.M. Sasian, "The Use of Implicitly Designed Optical Surfaces for the Design of Imaging and Illumination Systems," Opt. Eng. 39, 7 (2000)

23. Lerner, S.A., Optical Design Using Novel Aspheric Surfaces, Ph.D. Dissertation, Department of Optical Sciences, University of Arizona (2000)

24. Chase, H., Optical Design With Rotationally Symmetric NURBS, Master's Thesis, Department of Optical Sciences, University of Arizona, 2001.

25. Mills, J.P., D.J. Knapp, C.B. Smith, E.M. Ek, R.G. Hegg and J. Schafer, "Conformal Optics Proof of Concept," Proceedings of the 8th DoD Electromagnetic Windows Symposium, U.S. Air Force Academy, CO pp. 260-266, April 2000

26. Knapp, D.J. "Fundamentals of Conformal Dome Design", Proceedings of the IODC, Tucson, Arizona, June 2002

27. Engineering Sciences Data (Aeronautical Series) Item Number 80021.

28. Sparrold, Scott W.; Mills, James P.; Knapp, David J.; Ellis, Kenneth S.; Mitchell, Thomas A.; Manhart, Paul K., "Conformal dome correction with counterrotating phase plates," Optical Engineering 39(07), 1822-1829, Roger A. Lessard; Ed., Publication Date: 7/2000.

29. Roland Shack, Class notes, Optics 514.

30. Sparrold, S.W., "Correcting Dynamic Third-order Astigmatism in Conformal Missile Domes with Gimbaled Seekers ", Master's Thesis, Department of Optical Sciences, University of Arizona, 1997.

31. Manhart, Paul K.; Knapp, David ; Ellis, Scott; Sparrold, Scott W., "Optical system with zernike-shaped corrector," US Patent Number 6,313,951. November 6, 2001.

32. Knapp, David J.; Sparrold, Scott W., "Optical system with asymmetric optical corrector," US Patent Number 6,310,730. October 30, 2001.

33. Sparrold, Scott W., "Arch corrector for conformal optical systems," Proc. SPIE Vol. 3705, p. 189-200, Window and Dome Technologies and Materials VI, Randal W. Tustison; Ed., 7/1999.

34. Sparrold, Scott W.; Knapp, David J.; Manhart, Paul K.; Elsberry, Kevin W., "Capabilites of an arch element for correcting conformal optical domes," Proc. SPIE Vol. 3779, p. 434-444, Current Developments in Optical Design and Optical Engineering VIII, Robert E. Fischer; Warren J. Smith; Eds., Publication Date: 10/1999.

35. Sparrold, Scott W.; Mills, James P.; Knapp, David J.; Ellis, Kenneth S.; Mitchell, Thomas A.; Manhart, Paul K., "Conformal dome correction with counter-rotating phase plates," Optical Engineering 39(07), 1822-1829, Roger A. Lessard; Ed., Publication Date: 7/2000.

36. Sparrold, Scott W. ; Mills, James P. ; Paiva, Richard A.; Arndt Thomas D.; Ellis, Kenneth S. ; Knapp, David J., "Beam steering optical arrangement using Risley prisms with surface contours for aberration correction," US Patent Number 6,344,937, February 5, 2002.

37. Sparrold, Scott W. : Mills, James P. ; Paiva, Richard A.; Arndt Thomas D.; Knapp, David J. : Ellis, Kenneth S., "Missile seeker having a beam steering optical arrangement using risley prisms."US Pat. Number 6,343,767, February 5, 2002.

38. Mitchell, Thomas A., and J. Sasian, "Variable aberration correction using axially translating phase plates", Proc. SPIE Vol. 3705, p. 209-220, Window and Dome Technologies and Materials VI, Randal W. Tustison; Ed., July, 1999.

39. Whalen, Michael, "Dynamic aberration correction of conformal/aspheric domes and windows for missile and airborne fire control applications", US Patent Number 5,946,143, August 31, 1999

40. McDonald: Mark, "Apparatus for adjustable spherical aberration correction," US Patent Number 6,115,192, September 5, 2000.

41. Kunick: Joseph M; Chen: Chungte W.; Cook: Lacy G.; Lau: Anthony S.; "Dynamic aberration corrector for conformal windows", US Patent Number 5,526,181, June 11, 1996

42. Sparrold, S.W., Correcting Dynamic Third-order Astigmatism in Conformal Missile Domes with Gimbaled Seekers , Master's Thesis, Department of Optical Sciences, University of Arizona, 1997.

43. Knapp, David J.; Mills, James P.; Hegg, Ronald G.; Trotta, Patrick A.; Smith, Christopher B., "Conformal optics risk reduction demonstration," Proc. SPIE Vol. 4375, p. 146-153, Window and Dome Technologies and Materials VII, Randal W. Tustison; Ed., 9/2001.

44. Manhart, Paul; Knapp, David; Moore, Ken, "Conformal Optical Design with NURBS," Raytheon Engineering Notebook, August 2000.

45. Lerner, Scott, personal correspondence, 2000.

46. Robert A. Gonsalves, "Phase Retrieval and Diversity in Adaptive Optics," Optical Engineering 21 (5), 829-832. September/October, 1982.

47. "Form follows function." -Louis Henri Sullivan, "Lippincott's Magazine", March, 1896

48. Chase, Holden, "NURBS Surface Description in Optical Design," in International Optical Design Conference, OSA 2002.

49. Gregory K. Hearn, "The evolution of optimization algorithms," Critical Review Vol. CR41, Lens Design, ed. Warren J. Smith (Jan 1992) Copyright SPIE.

50. Texas Instruments, "Wassermann-Wolf Algorithm", Texas Instruments Technical Report on Conformal Optics, Section 3, p. 22, 1997.

51. G. Wassermann and E. Wolf, "On the Theory of Aplanatic Aspheric Systems," Proc. Phys. Soc. 62B, p.2, 1949.

52. Trotta, Pat, correspondence on derivation of Wassermann-Wolf equations.

53. Born, Max; Wolf, Emil, Principles of Optics, 7th Edition, 1999 Cambridge University Press

54. Gerald, Curtis; Wheatley, Patrick, Applied Numerical Analysis, 5th Edition, 1994 Addison-Wesley Publishing Company.

55. Molecular Expressions: Science, Optics and You, Ernst Abbe biography. http://micro.magnet.fsu.edu/optics/timeline/people/abbe.html

56. E. Abbe, "Beitrage zur Theorie des Mikroskops und der mikroskopischen Wahmehmung," Archiv fuer mikroskopische Anatomie 9, pp. 413-468, 1873.

57. Kidger, Michael, "Principles of Lens Design," Critical Review Vol. CR41, Lens Design, ed. Warren J. Smith (Jan 1992).

58. Kidger, Michael, "Principles of Lens Design," Critical Review Vol. CR41, Lens Design, ed. Warren J. Smith (Jan 1992).

59. Smith, Warren G., Modern Optical Engineering, Second Edition, 1990 McGraw-Hill, Inc.

60. Hecht, Eugene, Optics, Third Edition, 1998 Addison Wesley.

61. Mansuripur, Masud, Classical Optics and Its Applications, 2002 Cambridge University Press

62. E. Vaskas, "Note on the Wassermann-Wolf method for designing aspheric surfaces," J. Opt. Soc. Am. 47, p. 669, 1957.

63. Texas Instruments, "Wassermann-Wolf Algorithm", Texas Instruments Technical Report on Conformal Optics, Section 3, p. 22, 1997.

64. Rogers, J.M. "Nonstandard Representations of Aspheric Surfaces in Optical Design", Ph.D. Dissertation, Optical Sciences Center, University of Arizona, 1984